SEISMIC RESPONSE OF NORMAL AND HIGH-STRENGTH CONCRETE MEMBERS

by

Stuart Bristowe

March 2000

Department of Civil Engineering and Applied Mechanics
McGill University, Montréal

A THESIS SUBMITTED TO THE FACULTY OF GRADUATE STUDIES AND RESEARCH IN PARTIAL FULFILMENT OF THE DEGREE OF DOCTOR OF PHILOSOPHY

0-612-69857-2

SEISMIC RESPONSE OF NORMAL AND HIGH-STRENGTH CONCRETE MEMBERS

Abstract

A series of full-scale, reversed cyclic tension and compression tests was conducted to aid in the development of constituitive relationships for predicting the seismic response of concrete elements. These specimens were constructed using normal and high-strength concrete and contained varying amounts of transverse reinforcement consistent with both beam and column detailing requirements for different ductility levels. The influence of several parameters was investigated, including the effect of confinement, bar buckling and concrete strength.

Reversed cyclic loading tests were carried out on conventionally reinforced nominally ductile and ductile coupling beams constructed with normal and high-strength concrete. These tests investigated the effect of the design and detailing of the transverse reinforcement, as well as the strength of the concrete.

Analytical models for the prediction of the reversed cyclic loading response of concrete and steel are presented and used to predict the reversed cyclic tension-compression response of the axially loaded specimens tested. These tension-compression models were used to develop a plane sections analysis program, which was capable of evaluating the reversed cyclic moment-curvature response of concrete members. These models were very effective at predicting the reversed cyclic responses of the axially loaded specimens, the coupling beams and a flexural wall.

RÉPONSE SISMIQUE DE COMPOSANTS EN BÉTON
NORMAL ET À HAUTE RÉSISTANCE

Sommaire

L'auteur a développé des relations constitutives d'éléments en béton afin de prédire leur réponse sismique. À cet effet, un programme d'essais a été réalisé sur échantillons pleine grandeur soumis à des charges cycliques inversées en traction/compression . Les échantillons ont été construits en utilisant du béton normal et du béton à haute résistance, avec des quantités variables d'armature transversale et des détails conformes aux exigences de ductilité des poutres et colonnes. L'auteur a également étudié l'influence de paramètres tels l'effet du confinement du béton, le flambage des barres d'armature et la résistance du béton.

Des essais cycliques ont aussi été réalisés sur des poutres de ductilité nominale avec armature conventionnelle et des poutres ductiles, avec béton normal et béton à haute résistance. Ces essais ont ainsi permis d'étudier l'influence de la conception et des détails de l'armature transversale ainsi que de la résistance du béton.

L'auteur propose des modèles analytiques pour prédire le comportement cyclique du béton et de l'armature en acier, lesquels il applique pour prédire la réponse des éléments chargés uniaxialement. Ces modèles constitutifs ont ensuite été utilisés pour développer un modèle d'analyse de sections planaires qui a permis d'évaluer la réponse cyclique "moment-courbure" d'éléments fléchis. Les modèles proposés se sont avérés très efficaces pour prédire le comportement des échantillons chargés uniaxialement, des poutres ainsi que d'un mur flexionnel.

Acknowledgements

The author would like to express his gratitude to Professor Denis Mitchell for his skillful guidance and encouragement during this research programme. The encouragement and assistance of Dr. William D. Cook was also greatly appreciated.

The experimental research programme presented in this thesis was conducted in the Jamieson Structures Laboratory at McGill University. The assistance of Ron Sheppard, John Bartczak, Damon Kiperchuk and Marek Przykorski was invaluable. Special thanks is extended to Kent Harries, Jay McHarg, Glenn Marquis, David Dunwoodie, Bryce Tupper, Pierre Koch, Rob Zsigo and Nick Vannelli for their helpful suggestions and assistance during this study. The French translation of the abstract by Professor Ghyslaine McClure is greatly appreciated.

The completion of this project would not have been possible without the patience and valuable help of the secretaries of the Department of Civil Engineering and Applied Mechanics, particularly Sandy Shewchuk-Boyd, Lily Nardini, Ann Bless and Anna Dinolfo.

Finally the author would like to thank his family and friends for their support, constant encouragement and understanding throughout his stay at McGill University.

Stuart Bristowe
March, 2000.

Table of Contents

List of Figures

Chapter 1

Chapter 2

Chapter 3

Chapter 4

Chapter 5

Chapter 6

Chapter 7

List of Tables

List of Symbols

A	parameter for modified Ramberg-Osgood function
A_{ch}	area of confined concrete core
A_e	area of effectively confined concrete core
A_g	gross column area
A_s	area of transverse reinforcement
A_{sh}	cross-sectional area of transverse reinforcement
A_{sx}	total area of transverse reinforcement in x-direction
A_{sy}	total area of transverse reinforcement in y-direction
b	core dimension
b_c	larger core dimension
b_{cx}	core dimension in x-direction
b_{cy}	core dimension in y-direction
B	parameter for modified Ramberg-Osgood function
c_x	core dimension in x-direction
c_y	core dimension in y-direction
C	end restraint coefficient
C	parameter for modified Ramberg-Osgood function
d	distance from extreme compression fibre to centroid of tensile steel
d	diameter of the tie wire or bar
d_b	diameter of longitudinal reinforcement
d_b	diameter of the tie reinforcement
d_c	smaller core dimension
d_t	diameter of longitudinal bar
D	diameter of longitudinal bar
E	elastic modulus of steel
E_b	tangent modulus of the longitudinal steel at buckling
E_c	tangent modulus of elasticity of concrete
E_h	strain hardening modulus
E_{sec}	secant modulus of concrete
E_{sh}	strain hardening modulus
E_t	tangent modulus of elasticity
E_u	initial concrete modulus at commencement of unloading
f'_c	peak compressive stress of concrete
f_{cl}	closing stress in concrete
f_{cr}	critical stress
f'_{cc}	peak compressive stress of confined concrete
f'_{cc2}	reduced peak compressive stress
f_{ch}	characteristic stress of steel
f'_{co}	peak compressive stress of unconfined concrete
f_{cr}	tensile cracking stress of concrete
f_f	stress at focal point
f_{hcc}	stress in transverse reinforcement
f_l	confining pressure
f_{le}	effective lateral confining pressure
f_{lex}	effective lateral confining pressure in x-direction
f_{ley}	effective lateral confining pressure in y-direction
f_{new}	reduced concrete stress at reloading point corresponding to ε_{un}

f_r rupture stress of concrete
f_{re} stress at return point at which reloading curve rejoins the concrete stress-strain envelope
f_{ro} compressive stress in concrete at reloading reversal
f_s stress in transverse reinforcement
f_{sp} splitting tensile stress of concrete
f_{ult} ultimate stress of steel
f_{un} stress at concrete compressive uloading
f_y yield stress steel
f_{yh} yield stress of the transverse reinforcement
h_c cross-sectional dimension of the concrete core
k shape function based on the degree of lateral confinement
k decay factor for descending branch of compressive stress-strain response of concrete
k_1 confinement coefficient
k_2 confinement coefficient
k_3 confinement coefficient
k_e confinement effectiveness coefficient
l unsupported length, tie spacing
l_d development length of steel
L_b spacing of the stirrups
L_t unsupported length of stirrup tie leg
m numerical coefficient based on the configuration of the ties
M moment
n number of longitudinal bars
N total axial force
P_{cr} tensile cracking load for axially loaded specimens
q number of tie legs that cross the side of the core
r Ramberg-Osgood parameter
R Ramberg-Osgood parameter
R force modification factor
s spacing of transverse reinforcement
s' clear distance between adjacent hoops
S_e unloading strain ratio
s_l spacing of laterally supported longitudinal reinforcement
S_r returning strain ratio
V applied shear
w_i' clear distance between adjacent longitudinal bars
α angle between transverse reinforcement and b_c
α peak-to-peak stiffness
α_1 factor accounting for bond characteristics of reinforcement
α_2 factor accounting for sustained or repeated loading
β hysteretic damping coefficient
β confinement coefficient
ΔN equivalent axial tension corresponding to shear force
Δ_y tensile yield deformation for axially loaded specimens
Δ_y yield deflection for coupling beam specimens
ε strain
ε_{35} strain corresponding to 0.35 f_c'
ε_a common strain at intersection of initial tangent and plastic unloading slopes
ε_c strain in concrete

ε'_c	strain corresponding peak compressive stress of concrete
ε_{C50C}	strain in confined concrete when stress drops to 0.5 f'_{cc}
ε_{C50U}	strain in unconfined concrete when stress drops to 0.5 f'_{co}
ε_{cc}	strain corresponding to peak compressive stress of confined concrete
ε_{cc2}	reduced strain, corresponding to peak reduced compressive stress f'_{cc2}
ε_{cf}	strain causing stress in concrete
ε_{ch}	characteristic strain of steel
ε_{co}	strain corresponding to peak compressive stress of unconfined concrete
ε_{cr}	critical strain
ε_f	strain at focal point
ε_h	strain at commencement of strain hardening
ε_{hcc}	strain in the transverse reinforcement
ε_{pl}	plastic strain offset in concrete
ε_{plcr}	critical plastic strain offset in concrete
ε_{re}	strain at return point at which reloading curve rejoins the concrete stress-strain envelope
ε_{ro}	strain in concrete at reloading reversal
ε_{rupt}	rupture strain of steel
ε_s	steel strain
ε_{sh}	strain at commencement of strain hardening of steel
ε_{sp}	strain at spalling of concrete
ε_t	strain at tensile cracking of concrete
ε_{un}	strain at concrete compressive unloading
ε_y	yield strain of steel
ε^*	strain ratio with respect to strain corresponding to the peak concrete compressive stress
ε^*	strain ratio with respect to yield strain of steel
θ	angle of inclination of the principal compressive stresses measured from the longitudinal axis of the member, degrees
ρ_c	ratio of total area of transverse reinforcement in two orthogonal directions to the corresponding concrete area
ρ_{cc}	ratio of the area of longitudinal reinforcement to the area of the concrete core
σ	stress
σ_h	ultimate stress in steel
σ_y	yield stress of steel
σ^*	stress ratio with respect to the peak concrete compressive stress
σ^*	stress ratio with respect to yield stress of steel
ν	Poisson's ratio

Chapter 1

Introduction and Literature Review

High-strength concrete is becoming more popular due to its increased strength, improved durability and the availability of ready-mix concrete with a peak compressive strength of up to 100 MPa. In North America, most applications of high-strength concrete have been in columns of high-rise structures, where the reduction in member sizes due to the higher concrete strength results in a lighter structure and an increase in the rentable area.

While some research has been done on the monotonic behaviour of high-strength concrete members, little research is available on the reversed cyclic loading response of such members. This lack of experimental evidence forced some codes of practice to limit the peak compressive strength of concrete used in seismic design of structural systems. In the CSA A23.3 Standard (1994) this limit is conservatively chosen as 55 MPa, in the New Zealand Standard (SANZ, 1995) a specified limit of 70 MPa is used, while the ACI Code (1995) does not specify an upper limit on the peak concrete compressive strength used in seismic design.

Although the limitation of the CSA Standard was judged to be necessary in 1994, it severely limits the use of high-strength concrete in high-rise buildings located in significant seismic regions. This research programme investigates the influence of high strength concrete on the behaviour of lateral load resisting elements subjected to reversed cyclic loading. Emphasis is placed on developing constituitive relationships for the prediction of the reversed cyclic loading responses of high-strength and normal-strength concrete sections.

1.1 Previous Research

1.1.1 Seismic Behaviour of High-Strength Concrete Columns

Higher strength concrete exhibits a less ductile post peak response in compression than normal strength concrete. This, together with the tendency for splitting cracks to form, can result in a reduction of the compressive capacity of columns and has led to greater confinement requirements for high strength concrete columns (Cusson and Paultre, 1992, ACI Committee 363, 1992 and Collins et al, 1993). The 1994 CSA Standard was modified to provide a more conservative approach for determining the capacities and to provide an increased the amount of confinement reinforcement for high-strength concrete columns.

A number of studies have been performed to evaluate the seismic performance of high-strength concrete columns. Azizinamini et al (1994) examined the reversed cyclic loading response of two-thirds scale square high-strength concrete columns. These tests indicated that the ACI Code (1989) needed to be more conservative in determining the capacity of high-strength columns and they showed the need to examine the details of the confinement reinforcement and the spacing limits of the hoops required to prevent the buckling of the vertical bars.

Légeron and Paultre (1996a and 1996b) constructed six large-scale high-strength concrete columns and tested them under reversed cyclic loading conditions. It was determined that the spacing of the ties and the applied constant axial load level significantly influenced the flexural behaviour of the high-strength concrete columns. It was concluded that with proper detailing high-strength concrete columns could behave in a ductile manner.

Tests were conducted by Zhu et al (1996) to evaluate the reversed cyclic loading performance of concrete columns. They studied the influence of the axial load level, the amount and configuration of transverse reinforcement and the ratio of the core area to gross cross-sectional area. It was concluded that while the ductility of the columns decreased with increasing concrete strength, the seismic design requirements could be met provided that the axial load level is limited and with the provision of proper confinement of the concrete.

Tests on large-scale high-strength and ultra high-strength concrete columns were conducted at the University of Toronto (Bayrak and Sheikh, 1996 and 1998). These specimens were subjected to reversed cyclic loading under moderate to high axial loads. The test results showed that with proper detailing of the confinement reinforcement these specimens behaved in a ductile manner. It was also observed that an increase in the constant axial load reduced the column's ductility and accelerated the deterioration of the strength and stiffness of the section with each loading cycle. The configuration of the confinement reinforcement also played an important role in the response of these specimens. Improved deformability and energy absorption characteristics were observed when all longitudinal bars were supported by tie bends. It was therefore suggested that the level of axial loading and tie configuration parameters be included in the design of the confinement reinforcement.

1.1.2 Seismic Behaviour of Concrete Frames

The key design philosophy of ductile reinforced concrete frames is to achieve a minimum level of ductility and to dissipate a significant amount of energy. This is achieved by detailing the column, beam and joint regions to ensure a desirable hierarchy of yielding of the various elements and providing the system with the ability to undergo large displacements without a significant loss of capacity. This is accomplished by designing the columns and joint regions with sufficient strength to ensure that yielding of the beams occurs first. This produces a beam sidesway mechanism which results in larger ductility levels being achieved and a greater level of energy dissipation compared with a column sidesway mechanism, where the yielding of the columns and/or joint regions occurs first.

Ma et al (1976) and Bertero and Popov (1977) presented the results of several tests on normal-strength concrete beam-column sub-assemblages, constructed with and without slabs. These tests were conducted at the University of California at Berkeley and had a major impact on North American seismic design codes. The observed failure of these specimens occurred due to either the buckling of the bottom longitudinal beam reinforcement or the loss of shear capacity of the beam due to the opening of cracks over the full height of the beam. The presence of the slab was found to increase the negative moment capacity of the beam, thus enhancing the energy dissipation. However the presence of the slabs elevated the compressive and shear forces resulting in the premature buckling of the bottom longitudinal beam reinforcement. By decreasing the spacing of the ties in the critical region of the beam, thus providing improved support for the compressed longitudinal reinforcement, there was an improvement in the energy dissipation capacity of the sub-assemblage. Furthermore, it was also concluded that the amount of compressive reinforcement affected the energy dissipation of the system and they suggested a minimum ratio of 0.75, for the area of bottom to top reinforcement in beams.

Park (1977) suggested that the spacing of the ties supporting longitudinal beam bars in compressive regions should not exceed six times the diameter of the longitudinal bar, to prevent the buckling of this reinforcement in regions of plastic hinging. It was also recommended that each of these longitudinal bars be supported laterally by the corner of a tie.

Rattray (1986), Paultre (1987), Paultre et al (1989) and DiFranco (1993) investigated the seismic performance of normal-strength concrete frame members. A number of full-scale exterior beam-column connections with transverse spandrel beams and slabs were tested under reversed cyclic loading, with reinforcement detailing corresponding to various levels of ductility. It was found that the specimens with nominally ductile details failed due to yielding of the joint region and hinging in the columns, while the responses of the ductile specimens exhibited flexural yielding of the beam. These specimens were detailed using the 1984 CSA Standard and reached ductility levels of 4.0 and 11.8 for the nominally ductile and ductile specimens, respectively. For the ductile specimen, the small spacing of the beam ties in the plastic hinge region effectively restrained the compressed longitudinal bars from buckling, even after the spalling of the beam cover concrete. The focus of this research was to aid in the development of design and detailing requirements for ductile and nominally ductile frame members for the 1994 CSA Standard.

Research has also been conducted on the seismic response of high-strength concrete frame members, with some of the initial work being conducted by Ehsani et al (1987). These test results were compared with normal strength-concrete specimens reported by Ehansi and Wight (1985). It was found that if the high-strength concrete specimens were properly designed and detailed, they exhibited a ductile hysteretic response similar to that of the normal-strength concrete specimens. The main focus of this research program was the influence of the joint shear stress and it was concluded that the maximum allowable shear stress should be a function of the peak compressive strength of the concrete.

Ehsani and Alameddine (1991) investigated the main parameters on the cyclic response of high-strength concrete beam-column corner joints. Twelve specimens with concrete strengths ranging between 55 MPa and 93 MPa were constructed. It was found that the recommendation of ACI-ASCE Committee 352 (1995), which is used in the 1994 CSA Standard (see Equation 1.1), for evaluating the total cross-sectional area of transverse reinforcement, A_{sh}, gave large values when used for high-strength concrete joints.

$$A_{sh} = 0.3 s h_c \frac{f'_c}{f_{yh}} \left(\frac{A_g}{A_{ch}} - 1 \right) \geq 0.09 s h_c \frac{f'_c}{f_{yh}} \tag{1.1}$$

where

s	=	spacing of the transverse reinforcement
h_c	=	cross-sectional dimension of the core
f_{yh}	=	yield stress of the transverse reinforcement
A_g	=	gross column area
A_{ch}	=	area of the confined core

The authors concluded that the while an increase in the amount of transverse reinforcement in high-strength concrete joints is required, the increased amount required was not proportional to f'_c. It was also suggested that the benefit of using higher strength steel in the joint region should not be a linear relationship, suggesting that 600 MPa confinement steel is not 1.5 times more effective than 400 MPa confinement steel.

Shin et al (1992) conducted an experimental program on beam-column joints evaluating the effect of parameters including the concrete strength, the amount of joint reinforcement and the column-to-beam flexural strength ratio. From these tests it was concluded that the amount of transverse reinforcement required by Equation 1.1, seemed to be suitable for high-strength concrete, since specimens failed in the beam-column joint core if a lower amount of transverse reinforcement, than suggested by Equation 1.1, was used. It was also found that energy dissipation capacity of the system improved as the column-to-beam flexural ratio was increased.

Marquis (1997) evaluated the reversed cyclic response of a ductile high-strength beam-column connection constructed with transverse spandrel beams and a slab. This specimen was designed using the provisions of the 1994 CSA Standard for ductile frames, but assuming a concrete compressive strength of 70 MPa. The specimen performed in a ductile manner, with energy dissipation characteristics similar to that of a ductile normal-strength concrete beam-column connection. It was also concluded that the code provisions for the amount of confinement reinforcement in the joint region could be modified for high-strength concrete because the provisions provide excessive amounts of confinement reinforcement.

1.1.3 Seismic Behaviour of Coupling Beams

The flexural resistance of coupled wall systems arises from the moment resistance of each of the walls together with the couple formed by the axial forces induced in the walls by the shear in coupling beams. In the 1994 CSA Standard a force modification factor, R, of 3.5 or 4 is permitted for coupled walls, depending on the degree of coupling of the system (ACNBC, 1990). The degree of coupling of a coupled system indicates the percentage of the base overturning moment which is resisted by the couple formed by the axial tension and compression in the walls.

Guidelines for the design of concrete coupling beams were developed at the University of Canterbury. Initial studies of flexure dominated concrete coupling beams (Paulay, 1971) led to the design philosophy of preventing a shear failure by providing sufficient shear reinforcement to develop plastic hinges at the ends of the beams.

It was found that conventionally reinforced coupling beams with small span-to-depth ratios tend to fail in sliding shear at the beam-wall interface. This failure mechanism led to the development of diagonally reinforced concrete coupling beams (Paulay and Binney, 1974). This well confined diagonal reinforcement is designed to transmit alternating tension and compression forces which provide the shear and moment resistance in the beams. For coupling beams with small span-to-depth rations the diagonal reinforcement improved the energy absorption and ductility characteristics to more than that observed in conventionally reinforced coupling beams.

Conventionally and diagonally reinforced concrete coupling beams of span to depth ratios of 2.5 and 5 were tested by the Portland Cement Association (Shiu et al, 1978). Failure of the conventionally reinforced beams resulted from shear sliding within the plastic hinge region for both cases. The use of diagonal reinforcement within the beam improved the seismic response of the short span beams as was found by Paulay. They concluded that the long span beams showed little improvement in their response with diagonal reinforcement due to the shallow inclination of the reinforcement.

1.1.4 Stress-Strain Response of Confined Concrete

The load carrying ability of concrete members subjected to large deformations is primarily dependent on the response of the confined concrete core. There are various analytical models for the confinement of concrete. Early work performed by Richart et al (1928) found that lateral confining pressures increased both the concrete compressive strength and the strain at which this peak strength was reached. The following relationships for an active confining pressure were suggested:

$$f'_{cc} = f'_{co} + k_1 f_l \tag{1.2}$$

$$\varepsilon_{cc} = \varepsilon_{co}\left(1 + k_2 \frac{f_l}{f'_{co}}\right) \tag{1.3}$$

where

f'_{cc} and ε_{cc}	= confined peak compressive stress and strain, respectively
f'_{co} and ε_{co}	= unconfined peak compressive stress and strain, respectively
f_l	= confining pressure
k_1 and k_2	= coefficients

Richart et al chose average values for k_1 and k_2 of 4.1 and $5k_1$, respectively. Although these expressions for the increase in concrete strength were derived for an active confining pressure, it was determined that the increase in concrete strength with the passive confinement of spiral reinforcement, providing a similar confining pressure, was the same (Richart et al, 1929). This defining work has been the starting point for the modeling of passively confined concrete.

There have been many concrete confinement models suggested over the years by several researchers. The stress-strain relationships developed by Kent and Park (1971), which was modified by Park et al (1982), Vallenas et al (1977) and Sheikh and Uzumeri (1980) are given in Fig. 1.1. The analytical model developed by Sheikh and Uzumeri (1980) for concrete confined by rectilinear ties introduced the concept of an effectively confined concrete core. Several variables were included in this model including: the ratio of the lateral steel area to the area of the concrete core, the spacing and configuration of the ties, the distribution of the longitudinal steel and the properties of both the tie steel and the unconfined concrete. These variables were used to evaluate the stress-strain relationship of the confined concrete as illustrated in Fig. 1.1d. The stress-strain relationship for the confined concrete was applied to the effectively confined core concrete which is less than the area of concrete within the centreline perimeter of the ties. The effectively confined core for two different tie and longitudinal bar configurations is shown as the shaded areas in Fig. 1.2. In this figure, the gross core area of each section is identical but one can see the increased area of the effectively confined core when the steel configuration of the cross section is adjusted. The minimum effectively confined core area is located at the midpoint between ties, since the arching action is assumed to occur horizontally between the longitudinal bars and vertically between the transverse ties. The arc, between adjacent longitudinal bars in plan and adjacent hoops in elevation, is defined by a second degree parabola with an initial tangent angle, θ, of 45 degrees. Sheikh (1982) performed a comparative study which evaluated various confinement models for rectilinearly confined concrete. The model proposed by Sheikh and Uzumeri proved to be the most accurate for the prediction of the experimental results of the selected specimens which were tested under either axial loading or axial loading and moment.

Mander et al (1988a) suggested the following equation, which is based on the equation suggested by Popovics (1973), to define the complete stress-strain relationship of confined concrete (see Fig. 1.3):

$$f_c = \frac{f'_{cc} x r}{r - 1 + x^r} \tag{1.4}$$

where

f'_{cc}	= peak compressive strength of the confined concrete
x	= $\varepsilon_c / \varepsilon_{cc}$, ratio of the compressive strain to strain corresponding to f'_{cc}
r	= $E_c / (E_c - E_{sec})$
E_c	= $5000\sqrt{f'_c}$, tangent modulus of elasticity for the unconfined concrete
E_{sec}	= $f'_{cc} / \varepsilon_{cc}$

The calculation of the peak compressive stress of concrete confined by two lateral confining pressures, as is the case with rectilinear ties, was done graphically using Fig.1.4 and the corresponding peak compressive strain was determined from:

$$\varepsilon_{cc} = \varepsilon_{co}\left[1 + 5\left(\frac{f'_{cc}}{f'_{co}} - 1\right)\right] \tag{1.5}$$

Assuming that the confining reinforcement yields at the peak confined stress, the effective lateral confining pressures, in the x and y directions are calculated as follows:

$$f_{lex} = k_e \frac{A_{sx}}{s d_c} f_{yh} \tag{1.6}$$

$$f_{ley} = k_e \frac{A_{sy}}{s b_c} f_{yh} \tag{1.7}$$

where

f_{lex} and f_{ley}	= effective lateral confining pressure in the x and y directions
k_e	= confinement effectiveness coefficient
A_{sx} and A_{sy}	= total area of transverse reinforcement in the x and y directions
s	= centreline to centreline spacing of the transverse reinforcement
b_c and d_c	= core dimensions to the centrelines of the perimeter hoop, $b_c \geq d_c$
f_{yh}	= yield stress of the confinement reinforcement

The confinement effectiveness coefficient, k_e, is a ratio of the area of the effectively confined concrete core to the area of concrete in the core, which is defined by the perimeter of the centreline of the confinement reinforcement. This coefficient is calculated as follows:

$$k_e = \frac{\left(1 - \sum_{i=1}^{n} \frac{(w_i')^2}{6b_c d_c}\right)\left(1 - \frac{s'}{2b_c}\right)\left(1 - \frac{s'}{2d_c}\right)}{(1 - \rho_{cc})} \quad (1.8)$$

where

w_i' = clear distance between adjacent longitudinal bars

n = number of longitudinal bars

s' = clear vertical distance between adjacent hoops

ρ_{cc} = ratio of the area of the longitudinal reinforcement to the area of the core

Figure 1.5 shows the effectively confined core for a rectangular cross section, in plan and elevation illustrating the terms used in Equation 1.8. This analytical model performed well in predicting the response of several normal-strength concrete specimens confined by rectilinear ties of various configurations. The improved strength and ductility of the confined concrete was also accurately predicted (Mander et al, 1988b).

Fafitis and Shah (1985) proposed a model for the stress-strain relationship for confined high-strength concrete. It consisted of two expressions defining the ascending and descending branches, with both meeting at the peak with zero slope at this location. The mathematical expressions for each branch are as follows:

for $0 \le \varepsilon_c \le \varepsilon_{cc}$

$$f_c = f'_{cc}\left[1 - \left(1 - \frac{\varepsilon_c}{\varepsilon_{cc}}\right)^A\right] \quad (1.9)$$

for $\varepsilon_c \ge \varepsilon_{cc}$

$$f_c = f'_{cc} \exp\left(-k(\varepsilon_c - \varepsilon_{cc})^{1.15}\right) \quad (1.10)$$

where

A = $(E_c\, \varepsilon_{cc}) / f'_{cc}$

k = shape function based on the degree of lateral confinement

The value of k increases as the effective confinement pressure increases. As the value of k approaches zero the post-peak behaviour becomes more brittle and as k approaches infinity the behaviour becomes more plastic. The authors compared analytical results from this proposed model with experimental data and they concluded that it performed well in predicting the ultimate loads, curvatures and rotations of circular and square columns which were subjected to cyclic loading.

Li (1994) derived the following equation for the compressive strength of confined high-strength concrete to be used for both circular and rectilinear confinement:

$$f'_{cc} = f'_{co}\left(-0.413 + 1.413\sqrt{1 + 11.4\frac{f_{le}}{f'_{co}} - 2\frac{f_{le}}{f'_{co}}}\right) \qquad (1.11)$$

where

$f_{le} = 0.5\,(f_{lex} + f_{ley})$, for rectilinear confinement

The calculation of the effective lateral confining pressures in the x and y directions, f_{lex} and f_{ley} respectively, is the same as indicated in the model proposed by Mander et al (1988a). The axial strain at the maximum confined concrete stress, f'_{cc}, for high-strength concrete with rectilinear ties and having an unconfined compressive strength between 60 MPa and 80 MPa, is defined by the following equation:

$$\frac{\varepsilon_{cc}}{\varepsilon_{co}} = 1.0 + 11.3\left(\frac{f_{le}}{f'_{co}}\right)^{0.7} \qquad (1.12)$$

The stress-strain relationship for confined high-strength concrete proposed by Li, consists of three branches as given below:

for $0 \le \varepsilon_c \le \varepsilon_{co}$

$$f_c = E_c\varepsilon_c + \frac{\left(f'_{co} - E_c\varepsilon_{co}\right)}{\left(\varepsilon_{co}\right)^2}\left(\varepsilon_c\right)^2 \qquad (1.13)$$

for $\varepsilon_{co} \le \varepsilon_c \le \varepsilon_{cc}$

$$f_c = f'_{cc} - \frac{\left(f'_{cc} - f'_{co}\right)}{\left(\varepsilon_{cc} - \varepsilon_{co}\right)^2}\left(\varepsilon_c - \varepsilon_{cc}\right)^2 \qquad (1.14)$$

for $\varepsilon_c \geq \varepsilon_{cc}$

$$f_c = f'_{cc} - \beta \frac{f'_{cc}}{\varepsilon_{cc}}(\varepsilon_c - \varepsilon_{cc}) \geq 0.4 f'_{cc} \tag{1.15}$$

where for rectilinear confinement

$$\beta = \left(0.048 f'_{co} - 2.14\right) - \left(0.098 f'_{co} - 4.57\right)\left(\sqrt[3]{\frac{f_{le}}{f'_{co}}}\right) \tag{1.16}$$

The value of β, for the tests performed by Li, ranged from 0.05 to 0.9. The larger values of β occurred when the effective confining pressure was small. Li performed numerous monotonic tests on columns with concrete strengths up to 82.5 MPa and varying tie configurations. This proposed model performed well in the prediction of these experimental results.

Further work on the modeling of confined high-strength concrete was performed by Cusson and Paultre (1995). They suggested the following expressions for the evaluation of the peak confined compressive stress and corresponding strain:

$$\frac{f'_{cc}}{f'_{co}} = 1.0 + 2.1\left(\frac{f_{le}}{f'_{co}}\right)^{0.7} \tag{1.17}$$

$$\varepsilon_{cc} = \varepsilon_{co} + 0.21\left(\frac{f_{le}}{f'_{co}}\right)^{1.7} \tag{1.18}$$

For sections confined with rectilinear ties the effective lateral confinement pressure, f_{le}, is calculated using the following expression:

$$f_{le} = \frac{k_e f_{hcc}}{s}\left(\frac{A_{sx} + A_{sy}}{c_x + c_y}\right) \tag{1.19}$$

where

k_e	= confinement effectiveness coefficient (see Equation 1.8)
f_{hcc}	= stress in the transverse reinforcement
s	= centre-to-centre spacing of the transverse reinforcement
A_{sx} and A_{sy}	= area of transverse reinforcement in the x and y directions
c_x and c_y	= dimensions of the core in the x and y directions

It was observed by Cusson and Paultre (1995) that the yield stress of high-strength steel ties was only developed in well confined concrete specimens. For lightly confined sections the peak strain, ε_{cc} is small and thus the concrete expansion is lower resulting in a smaller strain in the confining steel, possibly lower than the steel yield strain. The relationship for the strain in the transverse reinforcement, assuming a Poisson's ratio, ν, of 0.5 was given as:

$$\varepsilon_{hcc} = 0.5\varepsilon_{cc}\left(1 - \left(f_{le}/f'_{cc}\right)\right) \tag{1.20}$$

For the evaluation of ε_{cc} and f'_{cc}, the following iterative procedure was suggested to ensure the estimated stress in the transverse reinforcement was compatible with that assumed initially:

1. compute the f_{le} assuming the yield of the transverse reinforcement, $f_{hcc} = f_{yh}$;
2. estimate the value of the ε_{cc} and f'_{cc} ;
3. estimate the value of ε_{hcc} and calculate the corresponding f_{hcc} ;
4. if $f_{hcc} < f_{yh}$ then re-evaluate f_{le} using the new transverse steel stress ; and
5. repeat steps 2 to 4 until convergence .

The stress-strain relationship for confined high strength concrete proposed by Cusson and Paultre is comprised of two curves. The ascending branch is the stress strain relationship proposed by Popovics (1973) as used by Mander et al (1988a). The descending branch is a modified version of the relationship proposed by Fafitis and Shah (1985). The stress-strain relationship proposed is:

for $0 \leq \varepsilon_c \leq \varepsilon_{cc}$

$$f_c = f'_{cc}\left[\frac{r\left(\varepsilon_c/\varepsilon_{cc}\right)}{r - 1 + \left(\varepsilon_c/\varepsilon_{cc}\right)^r}\right] \tag{1.21}$$

for $\varepsilon_c \geq \varepsilon_{cc}$

$$f_c = f_{cc} \cdot \exp\left(k_1\left(\varepsilon_c - \varepsilon_{cc}\right)^{k_2}\right) \tag{1.22}$$

where the coefficients are:

$$r = \left(\frac{E_c}{E_c - f'_{cc}/\varepsilon_{cc}}\right) \tag{1.23}$$

$$k_1 = \frac{\ln 0.5}{\left(\varepsilon_{C50C} - \varepsilon_{cc}\right)^{k_2}} \tag{1.24}$$

$$k_2 = 0.58 + 16\left(\frac{f_{le}}{f'_{co}}\right)^{1.4} \tag{1.25}$$

$$\varepsilon_{C50C} = \varepsilon_{C50U} + 0.15\left(f_{le}/f'_{co}\right)^{1.1} \tag{1.26}$$

The value of ε_{C50U} is taken from experimental data for the stress-strain relationship of the unconfined concrete and is equal to the strain at which 50% of the peak compressive strength has been lost.

This confined high strength concrete model predicted the monotonic axial response of specimens tested by Cusson and Paultre, (1995), very accurately. These specimens included columns with four different confinement steel configurations, using normal and high-strength steel and unconfined concrete strengths of up to 96 MPa. The approach taken by Cusson and Paultre (1995) is presented in some detail because it is the method used in Chapter 4 to define the envelope of the stress-strain response of the high-strength concrete in compression.

Saatcioglu and Razvi (1992) suggested an analytical procedure for the modeling of confined normal-strength concrete and modified this model to include high-strength concrete (Razvi and Saaticoglu, 1999). The model suggested for both normal and high-strength concrete is presented and is based on an equivalent uniform confinement pressure taking into account variations in the confining pressures in two orthogonal directions. The evaluation of the peak compressive stress of confined concrete in square columns is as follows:

$$f'_{cc} = f'_{co} + k_1 f_{le} \tag{1.27}$$

where

f_{le} = $k_2 f_l$; equivalent uniform pressure

f_l = average lateral pressure

k_1 = $6.7(f_{le})^{-0.17}$

The evaluation of the average lateral pressure, f_l, and the parameter k_2 are as follows:

$$f_l = \frac{\sum_{i=1}^{q}(A_s f_s \sin\alpha)_i}{s b_c} \tag{1.28}$$

where

q	= number of tie legs that cross the side of the core
A_s	= area of transverse reinforcement
f_s	= stress in transverse reinforcement
α	= angle between the transverse reinforcement and b_c
b_c	= core dimension, measured centre-to-centre of perimeter hoop

$$k_2 = 0.15\sqrt{\left(\frac{b_c}{s}\right)\left(\frac{b_c}{s_l}\right)} \leq 1.0 \tag{1.29}$$

where

s	= transverse hoop spacing
s_l	= spacing of laterally supported longitudinal reinforcement

The stress in the transverse hoop reinforcement can be estimated using the following:

$$f_s = E_s\left(0.0025 + 0.04\sqrt[3]{\frac{k_2\rho_c}{f'_{co}}}\right) \leq f_{yh} \tag{1.30}$$

f_{yh} = yield stress of hoop reinforcement

The maximum yield stress of the hoop reinforcement was limited to 1400 MPa since that was the maximum yield strength used in the experimental data considered for the calculation of Equation 1.30. The value of ρ_c is calculated by dividing the total area of transverse steel in two orthogonal directions by the corresponding area of concrete.

If the cross-section is rectangular the calculation of the equivalent uniform pressure, f_{le}, is as follows:

$$f_{le} = \frac{f_{lex}b_{cx} + f_{ley}b_{cy}}{b_{cx} + b_{cy}} \tag{1.31}$$

where

f_{lex}	= effective lateral pressure acting perpendicular to b_{cx}
f_{ley}	= effective lateral pressure acting perpendicular to b_{cy}
b_{cx}, b_{cy}	= core dimensions

The strain corresponding to the peak compressive confined stress is evaluated using:

$$\varepsilon_{cc} = \varepsilon_{co}(1 + 5k_3K) \tag{1.32}$$

where

$k_3 = 40 / f'_{co} \leq 1.0$

$K = (k_1 f_{le}) / f'_{co}$

The stress-strain relationship for confined concrete that was suggested by Razvi and Saatcioglu (1999) comprised of two branches. The ascending branch was defined by the relationship suggested by Popovics (1973), see Equation 1.4. The descending branch was defined by a linear line which originated at the peak, passing through the point defined by the strain corresponding to 85% of the peak stress. At a compressive stress of 20% of the maximum, the assumed compressive response of the confined concrete becomes horizontal. This model was used to predict a wide range of experimental tests with various levels of confinement. The analytical results correlated very well with the experimental data. A comprehensive experimental programme, which included tests on square and circular columns, different levels of confinement as well as investigating the influence of concrete strength was conducted (Saatcioglu and Razvi, 1998, and Razvi and Saatcioglu, 1999).

1.1.5 Cyclic Loading Response of Concrete

Early investigations into the cyclic behaviour of concrete resulted in the concept that the envelope curve of the cyclic stress-strain relationship coincides with that obtained from a monotonic loading test (Sinha et al, 1964 and Karsan and Jirsa, 1969). Shin et al termed the intersection point between the reloading branch and the initial unloading branch as the "common point". When the concrete was cyclically loaded several times to the initial unloading branch, stability of the intersection point occurred and the stress strain history went into a closed loop, indicating no further loss of compressive capacity at a given strain, as shown in Fig. 1.6. By connecting the first common point for each increase in compressive strain a curve representing the reloading stress strain relationship is produced and was called the common point limit. Karsan and Jirsa (1969) suggested that this curve could be represented by the equation for the concrete compressive envelope by multiplying the peak compressive stress, f'_c and the corresponding strain, ε'_c, by a value β. The suggested value of β was 0.9 according to the tests performed by Karsan and Jirsa.

Menegotto and Pinto (1973) presented a method for the analysis of cyclically loaded reinforced concrete frame members. This included a representation of the cyclic response of the reinforcing steel which is presented in Section 1.1.7. The compressive envelope of the concrete was described by two curves joining at the peak compressive stress with the unloading and reloading branches being parallel to the initial tangent of the loading curve. The formulas for the envelope curve are given below:

for $\varepsilon^* \leq 1$

$$\sigma^* = \varepsilon^* (2 - \varepsilon^*) \tag{1.33}$$

for $\varepsilon^* > 1$

$$\sigma^* = \sigma^* (1 - \alpha\varepsilon^* + \alpha) \tag{1.34}$$

where

σ^* $= \sigma / f'_c$, stress ratio with respect to the peak stress

ε^* $= \varepsilon / \varepsilon'_c$, strain ratio with respect to the strain at peak stress

α $= (1 - \alpha) f'_c$ is the stress corresponding to $2\,\varepsilon'_c$

Mander et al (1988a) suggested a stress strain relationship for the cyclic loading of concrete assuming that the monotonic and cyclic stress-strain envelopes are identical. Figure 1.7 illustrates the compressive unloading branch from the unloading point, (ε_{un} , f_{un}) which is based on the evaluation of the plastic offset strain, ε_{pl}, of the concrete. The value of the plastic strain is given by:

$$\varepsilon_{pl} = \varepsilon_{un} - \frac{(\varepsilon_{un} + \varepsilon_a) f_{un}}{(f_{un} + E_c \varepsilon_a)} \tag{1.35}$$

where

ε_a $= a\sqrt{\varepsilon_{un}\varepsilon_{cc}}$

a $=$ maximum of either $\dfrac{\varepsilon_{cc}}{\varepsilon_{cc} + \varepsilon_{un}}$ or $\dfrac{0.09\varepsilon_{un}}{\varepsilon_{cc}}$

The unloading branch is defined by:

$$f_c = f_{un} - \frac{f_{un} x r}{r - 1 - x^r} \tag{1.36}$$

where

x	$= (\varepsilon_c - \varepsilon_{un}) / (\varepsilon_{pl} - \varepsilon_{un})$
r	$= E_u / (E_u - E_{sec})$
E_{sec}	$= f_{un} / (\varepsilon_{un} - \varepsilon_{pl})$
E_u	$= bcE_c$
b	$= f_{un} / f'_{co} \geq 1$
c	$= \left(\varepsilon_{cc}/\varepsilon_{un}\right)^{0.5} \leq 1$
E_c	= initial tangent modulus of the concrete

If the reversal strain, ε_{un}, is lower than the maximum strain reached on the previous loop then the previously calculated ε_{pl} should be used for the evaluation of the unloading curve.

The compressive reloading branch is illustrated in Fig. 1.8 with the important points indicated. It should be noted that if the strain in the concrete, after reloading in compression, does not reach the plastic strain, ε_{pl}, then there is no compressive stress in the concrete. The compressive reloading branch is assumed to be linear between the reloading point, (ε_{ro}, f_{ro}), and the point with a strain equal to the unloading strain, ε_{un}, with a corresponding stress, f_{new}, which is reduced to account for cyclic softening and calculated using the following formula:

$$f_{new} = 0.92 f_{un} + 0.08 f_{ro} \tag{1.37}$$

The strain at which the reloading branch rejoins the envelope curve is calculated from:

$$\varepsilon_{re} = \varepsilon_{un} + \frac{f_{un} - f_{new}}{E_r \left(2 + \frac{f'_{cc}}{f'_{co}} \right)} \tag{1.38}$$

where

$$E_r = \frac{f_{ro} - f_{new}}{\varepsilon_{ro} - \varepsilon_{un}}$$

Mander et al (1988a) also derived a parabolic transition curve connecting the linear portion of the reloading branch to the envelope curve.

Tensile loading and unloading of the concrete was assumed to follow the tensile modulus of the concrete calculated by dividing the cracking stress by the cracking strain. However, if the concrete was preloaded in compression a reduction of the tensile strength is assumed as shown in Fig. 1.9. It was assumed in this model that once the tensile strength of the concrete was exceeded, the concrete no longer had any tensile capacity.

Further work on the cyclic modeling of confined concrete was done by Martinez-Rueda and Elnashai (1997). This model was a modified version of that proposed by Mander et al (1988a). These modifications included the evaluation of the unloading and reloading stiffness since at large strains the model proposed by Mander et al predicted an increase in these values. Furthermore, Mander et al proposed a uniform degradation of the strength of the concrete independent of the maximum strain reached (i.e., $f_{new} = 0.92\ f_{un} + 0.08f_{ro}$). Experimental evidence suggests that the strength and stiffness degradation were a function of the accumulated damage and thus depended of the magnitude of the reversal strain, (Karsan and Jirsa, 1969). The calculation of the plastic strain consisted of three rules based on the level of damage that had occurred in the concrete as given by:

$0 \le \varepsilon_{un} \le \varepsilon_{35}$

$$\varepsilon_{pl} = \varepsilon_{un} - \frac{f_{un}}{E_c} \tag{1.39}$$

$\varepsilon_{35} \le \varepsilon_{un} \le 2.5\varepsilon_{cc}$

$$\varepsilon_{pl} = \varepsilon_{un} - \frac{(\varepsilon_{un} + \varepsilon_a)f_{un}}{(f_{un} + E_c\varepsilon_a)} \tag{1.40}$$

$2.5\varepsilon_{cc} \le \varepsilon_{un}$

$$\varepsilon_{pl} = \frac{f_{cr}\varepsilon_{un} - |\varepsilon_f|}{f_{cr} + f_{un}} \tag{1.41}$$

where

ε_{35}	= strain corresponding to $0.35f'_c$
ε_a	= see Equation 1.35
ε_f and f_f	= location of the focal point

$|\varepsilon_f| \quad = \dfrac{f_{cr}\varepsilon_{plcr}}{E_c(\varepsilon_{cr}\varepsilon_{plcr}) - f_{cr}}$

$|f_f| \quad = E_c\,|\varepsilon_f|$

ε_{cr} and f_{cr} = critical stress and strain, $\varepsilon_{cr} = 2.5\ \varepsilon_{cc}$ and f_{cr} = corresponding stress

ε_{plcr} = plastic strain corresponding to ε_{cr}

It is noted that Equation 1.40 is the same as Equation 1.35, proposed by Mander et al (1988a). Figure 1.10 illustrates the evaluation of the plastic strain if the compressive strain, ε_c, is greater that $2.5\varepsilon_{cc}$,with the critical points labeled. This formulation for the calculation of the plastic strain produces an increasing level of decay in the response of the concrete at large strain levels. The unloading curve is a second order parabola having zero slope at (ε_{pl} , 0) and is defined by the following equation:

$$f_c = \left(\frac{\varepsilon_c - \varepsilon_{pl}}{\varepsilon_{un} - \varepsilon_{pl}}\right)^2 \tag{1.42}$$

The reloading branch consists of two linear lines, the first drawn between the reloading point (ε_{ro}, f_{ro}) and the degraded strength point (ε_{un}, f_{new}) and the second connecting this point to the monotonic envelope at the reentry point (ε_{re}, f_{re}) and Fig. 1.8 shows the location of these key points. The reduced stress, f_{new} corresponding to the previous maximum strain is given by:

$$f_{new} = \frac{f'_{cc2}\,xr}{r - 1 + x^r} \tag{1.43}$$

where

$f'_{cc2} \quad = 0.9\ f'_{cc}$

$x \quad = \varepsilon_c / \varepsilon_{cc2}$

$\varepsilon_{cc2} \quad = 0.9\varepsilon_{cc}$

This approach is similar to that suggested by Karsan and Jirsa (1969), assuming that ε_{un} lies on the curve of common points allowing for this calculation of f_{new}. This allows for an increase in the degradation of the strength of the concrete relative to its loading history.
The evaluation of the returning strain, ε_{re}, is as follows with the returning strength, f_{re}, being evaluated based on the monotonic envelope:

$$\varepsilon_{re} = \frac{\varepsilon_{re}^{'} + \varepsilon_{un}}{2} \tag{1.44}$$

where

$\varepsilon_{re}^{'}$ $= S_r \varepsilon_{un}$

S_r $= 0.00273 + 1.2651 S_e$, returning strain ratio

S_e $= \varepsilon_{un} / \varepsilon_{cc}$, unloading strain ratio

This cyclic model for concrete was used in a finite element analysis program and was used to predict column tests performed by Park et al (1982). The model performed well but was unable to predict the pinching of the hysteretic loops.

1.1.6 Buckling of Reinforcing Bars Under Monotonic Loading

Bresler and Gilbert (1961) performed an analytical investigation into the requirements of ties in reinforced concrete columns. Tie spacing and size were examined based on the buckling of the longitudinal reinforcement, assuming the spalling of the concrete cover. The derivation of the equation for tie spacing was based on Euler's buckling formula, solving for the unsupported length, assuming that the critical buckling stress is equal to the yield stress of the longitudinal reinforcement.

$$\frac{l}{D} = \left(\frac{C\pi^2 E_t}{f_y} \right)^{1/2} \tag{1.45}$$

where

l = unsupported length, tie spacing

D = diameter of longitudinal bar

C = end restraint coefficient

E_t = tangent modulus of elasticity corresponding to f_{cr} ($f_{cr} = f_y$ thus $E_t = E$)

f_y = yield stress of the longitudinal reinforcement

From this formulation it is evident that the spacing of the ties decreases as the yield strength of the longitudinal reinforcement increases. The underlying assumption to this derivation is the fact that the ties are sufficiently stiff to prevent lateral movement at their location, which leads to the sizing of the ties based on longitudinal buckling. The deflected shape of the bar was defined by the sum of two functions describing the first two buckling modes of the bar, as shown in Fig. 1.11. The potential energy of the system was calculated, summing the energy stored in the elastic spring and the energy due to the shortening of the column. Minimizing the potential energy with respect to the amplitude of each buckling mode, resulted in equations for the buckling load, P and the spring constant, k. There were two types of lateral support of the longitudinal reinforcement considered in this study. The first arising from the direct tensile support of a tie, (support from the corner of a tie), therefore the stiffness, k, previously calculated was equated to that of an equivalent elastic rod, resulting in Equation 1.46. Lateral support also results from the flexural stiffness of the tie if the longitudinal bar is located at the middle of a leg of the tie. For this possibility, the stiffness, k, previously calculated was equated to the stiffness of a beam fixed at both ends with a concentrated load at mid span, resulting in Equation 1.47.

from direct tensile restraint:

$$\frac{d}{D} = \frac{D}{l}\left(\frac{4.56b}{ml}\right)^{1/2} \qquad (1.46)$$

from flexural stiffness:

$$\frac{d}{D} = 0.785\left(\frac{b}{l}\right)^{3/4} \qquad (1.47)$$

where

d	= diameter of the tie wire or bar
D	= diameter of the longitudinal reinforcing bar
l	= tie spacing
b	= core dimension
m	= numerical coefficient based on the configuration of the ties

For restraint due to flexural stiffness, it is clear that if the core dimension and the tie spacing are the same, (b/l = 1.0), then the calculated tie diameter would be approximately 75% of the longitudinal bar diameter.

Scribner (1986) developed an analytical model to evaluate the size of ties required to prevent buckling of the longitudinal reinforcement in flexural members. The buckling of the longitudinal bar was assumed to span three tie intervals and was modeled assuming fixed conditions at both ends with springs located at the one-third points to simulate the ties effect at those locations. Using the same analysis as that used by Bresler and Gilbert (1961), the required spring stiffness to prevent buckling was calculated. The lateral support for the longitudinal bar was assumed to come from the flexural stiffness of the tie, resulting in Equation 1.48.

$$\left(\frac{d_b}{d_t}\right)^4 = 3.74\frac{E_t}{E_b}\left(\frac{L_b}{L_t}\right)^3 \tag{1.48}$$

where

d_b and d_t	= the diameter of the tie and the longitudinal bar respectively
E_t	= modulus of elasticity of the tie steel
E_b	= tangent modulus of the longitudinal steel at buckling
L_b	= spacing of the stirrups
L_t	= unsupported length of stirrup tie leg

This analysis was also performed for cases assuming that the buckling of the longitudinal bar spanned two tie spaces and four tie spaces. By making some approximations for the stiffness and length ratios, the calculated ratio of the longitudinal bar diameter to the tie bar diameter were 1.69, 1.85, 2.11 for the two span, three span and the four span configurations, respectively. Therefore it was assumed appropriate to use a tie diameter half that of the longitudinal bar to prevent the buckling of the longitudinal bars. Experimental tests were also performed to evaluate this analytical model. It was determined that large ties did prevent the type of buckling assumed in the analytical study, but were unable to prevent other types of longitudinal bar buckling.

Papia et al (1988) developed a model for the buckling of reinforcing bars resulting in the evaluation of the critical buckling load and the length, L, of the section of the bar that buckles. The length of the buckle in the longitudinal bar can occur across the tie location if the tie is not sufficiently stiff, therefore the length could be a multiple of the tie spacing, *l*. The modeled bar rests on elastic supports representing the tie locations and the ends are allowed to translate along the length of the beam only. A schematic of the model is given in Fig. 1.12 with the core concrete shown as the thatched area. The value δ_j is the lateral displacement at tie j, α is the stiffness of the tie and F_j is the resulting restraining force of the tie at that location. From comparisons with experimental results it was concluded that the model predicted the maximum load of the longitudinal reinforcement accurately and the predicted length of the buckled region was consistent with observations made at the end of testing. Papia et al also concluded that the failure of a reinforced concrete column would be affected by the buckling of the longitudinal reinforcement even for small spacings of the transverse reinforcement. The suggested sequence of failure started with the buckling of the longitudinal bars, which involved straining of the hoops, resulting in a local loss of confinement, consequently causing the crushing of the concrete.

Mau and El-Mabsout (1989) developed a finite element model to predict the stress-strain response of reinforcing bars in the presence of buckling. The model was constructed using beam column elements with the following assumptions:

1. the cross section of the element was circular;
2. the beam was initially straight and was loaded concentrically;
3. plane sections remain plane before and after buckling;
4. the square of the slope of the deflected shape is much less than unity;
5. shear deformations were negligible; and
6. the axial strain is small compared to unity.

This model was used to predict the inelastic response of bars with varying L/r ratios, (length to radius of gyration or slenderness ratio). This ratio is exactly double that of the tie spacing to diameter ratio, s/d, for circular reinforcing bars. Two different stress-strain diagrams were used for the steel. The first was an elastic perfectly plastic response and the second was an elastic-plastic response, with a distinct yield plateau represented, including strain hardening. The plots for these analyses are given in Fig. 1.13 for slenderness ratios ranging from 10 to 30. Mau and El-Mabsout (1989) concluded that for an elastic perfectly plastic material, the load capacity of the section decreases once buckling occurs at the yield load in all cases. Also, the post-buckling behaviour of the bar is dominated by the formation of a plastic hinge early in the post-buckling history, thus strain hardening of the material dictates the post-buckling path. They found that for a strain hardening material the peak capacity in the post buckling range could be higher, equal to or lower than the capacity at initial buckling and is dependent on the slenderness ratio of the bar.

Mau (1990) performed a parametric study, evaluating the effect of the post-yielding stress-strain curve of the steel on the critical spacing limit for ties. For this investigation, the yield stress was a constant value of 476 MPa (69 ksi), with the post-yield stress-strain curve being represented by three dimensionless parameters:

1. the hardening ratio, a = hardening strain / yield strain ($\varepsilon_h / \varepsilon_y$)
2. the peak stress ratio, b = ultimate stress / yield stress (σ_h / σ_y)
3. the hardening modulus ratio, α = strain hardening modulus / yield modulus (E_h / E)

Figure 1.14 indicates the variation of the stress-strain curve considered in this parametric study. The same finite element model as Mau and El-Mabsout (1989) was used for this study and various tie spacing to diameter ratios, s/d, were evaluated. It was concluded that the critical s/d ratio was between 5 and 7 for Grade 60 steels, ($f_y = 414$ MPa). This ratio was most sensitive to the hardening modulus ratio, α, while the least sensitive parameter was the peak stress ratio, b. If the s/d ratio is smaller than the critical s/d ratio, assuming the ties are sufficiently stiff, the steel bar response would closely follow the material stress-strain curve.

Monti and Nuti (1990 and 1992) developed a numerical model for steel bars that included the effect of bar buckling. It was developed for the cyclic behaviour of steel bars and will be discussed in the following section.

1.1.7 Cyclic Loading Behaviour of Reinforcing Bars

Singh et al (1965) performed a series of reversed cyclic loading tests on reinforcing bars to investigate the Bauschinger effect, which is illustrated in Fig. 1.15. After the first yield excursion the linearity between stress and strain is no longer valid. This dependence on previous strain history is termed the Bauschinger effect and is characterised by the reduction of the reversed yield strength. Several tests were performed and resulted in the following numerical expression for the reloading branch of reinforcing steel subjected to reversed loading, with variables for the steel strain, ε, and resulting stress, σ. These exponential expressions are for a particular type of steel and thus are not universally applicable. The steel stress is given as:

$$|\sigma|(\mathrm{ksi}) = 64.5 - 52.7(0.838)^{1000\varepsilon} \tag{1.49}$$

$$|\sigma|(\mathrm{MPa}) = 444 - 363(0.838)^{1000\varepsilon} \tag{1.50}$$

Further work on the reversed cyclic behaviour of reinforcing steel, was performed by Kent and Park (1973). The suggested expression for the cyclic behaviour of the reinforcing steel is given below and is a version of the Ramberg-Osgood function (see Fig. 1.16):

$$\varepsilon_s = \frac{f_s}{E_s}\left(1 + \left(\frac{f_s}{f_{ch}}\right)^{r-1}\right) \tag{1.51}$$

where

ε_s and f_s	= steel strain and stress, respectively
E_s	= modulus of elasticity
ε_{ch} and f_{ch}	= characteristic strain and stress of the steel, respectively
r	= Ramberg-Osgood parameter

The variation of the value of the parameters f_{ch} was evaluated for the tests performed by Kent and Park (1973) and it was concluded that the ratio of f_{ch} / f_y was dependent on the amount of plastic strain incurred during the previous loading cycle. This equation represented the loading curve, while the unloading branch, was defined by a line parallel to the initial elastic slope. The problem with this formulation is that for a given strain, the corresponding stress must be found by trial and error, thus increasing computational effort.

Menegotto and Pinto (1973) suggested the following version of the Ramberg-Osgood function to represent the initial loading and reloading branches of the reinforcing steel subjected to cyclic loading:

$$\sigma^* = (1-b)\left(\frac{\varepsilon^*}{\left(1+\left(\varepsilon^*\right)^R\right)^{1/R}}\right) + b\varepsilon^* \qquad (1.52)$$

where

σ^*	= σ / f_y, stress ratio with respect to the yield stress
ε^*	= $\varepsilon / \varepsilon_y$, strain ratio with respect to the yield strain
b	= defines the slope of the strain hardening line
R	= coefficient defining the curvature of the transition curve

The value of the parameter R was taken as 20 for the initial loading branch but decreased rapidly to values close to 3, after several post-yield strain reversals. As the value of R decreases the transition curve becomes smoother. The unloading branches were again assumed to be parallel to the initial stiffness of the steel. Equation 1.52 was modified by Mattock (1979) to the form given below, which was used to represent the stress strain response of prestressing strand:

$$f_s = E\varepsilon_s\left\{A + \frac{1 - A}{\left(1 + (B\varepsilon_s)^C\right)^{1/C}}\right\} \tag{1.53}$$

Figure 1.17 shows this function with the parameters A and B illustrated on the graph. The parameter C is consistent with R in the previous equation, with smaller values giving a smoother transition. This equation is used in Chapter 4 for the shape of the envelope stress-strain response for reinforcing bars under reversed cyclic loading.

A numerical model for the stress-strain response of steel bars under cyclic loading which included the effects of buckling, was developed by Monti and Nuti (1990 and 1992). The branch connecting two load reversal points is defined by a finite stress-strain relationship. This relationship is updated after each load reversal using four hardening rules, which are the kinematic, isotropic, memory and saturation rules. Four parameters are required to evaluate each of the rules and these are the steel yield stress, elastic modulus, hardening ratio and a weighting function (which varies between 0 and 1). This model was also expanded to include the effect of inelastic buckling of the reinforcing bar. The critical s/d ratio was taken as five, therefore buckling was assumed to occur if the spacing to diameter ratio, s/d > 5. Additional parameters, which are analytical relations of the s/d ratio, are incorporated into the model to account for buckling of the longitudinal bar. This analytical model predicted the experimental results of tests on reinforcing bars performed by Monti and Nuti (1992), very accurately. These tests were conducted on bars, with three different s/d ratios (5, 8 and 11), subjected to symmetrical and unsymmetrical loading reversed cyclic histories.

1.2 Research Programme Objectives

The objectives of this research programme are divided into two sections. The first section relates to the experimental investigations and the second to the analytical programme, which compliments the experimental results.

1.2.1 Experimental Programme

In the experimental programme the objectives are to investigate the following behavioural aspects:

(i) the influence of tie spacing on the reversed cyclic loading response of reinforcing bars, including load history effects;

(ii) the influence of crack closing on the compressive response of concrete for both normal-strength and high-strength concrete;

(iii) the reversed cyclic axial loading response (tension–compression) of confined concrete elements with the following parameters:

- the effect of normal-strength and high-strength concrete;
- the influence of hoop spacing on bar buckling; and
- the influence of confinement on the concrete response.

(iv) reversed cyclic loading response of coupling beams to determine:

- the effect of normal-strength and high-strength concrete;
- the influence of nominally ductile and ductile design detailing;
- the shear contribution from residual tensile stresses in the concrete under reversed cyclic loading; and
- the influence of cover spalling and bar buckling.

1.2.2 Analytical Programme

The objectives for the analytical research programme are the following:

(i) to develop a reversed cyclic loading model for concrete including the following effects:

- crack closing
- confinement
- cover spalling
- strain history

(ii) to develop a reversed cyclic loading model for reinforcing bars including the following:

- complete stress-strain response including yielding, strain hardening and the Bauschinger effect
- hoop and tie spacing influence on bar buckling and the stress-strain response

(iii) to develop a reversed cyclic loading model for reinforced concrete elements subjected to flexure and axial loading

In order to assess the accuracy of the behavioural models developed, the predictions from these models will be compared with the reversed cyclic responses of axially loaded specimens, coupling beams and a flexural wall specimen.

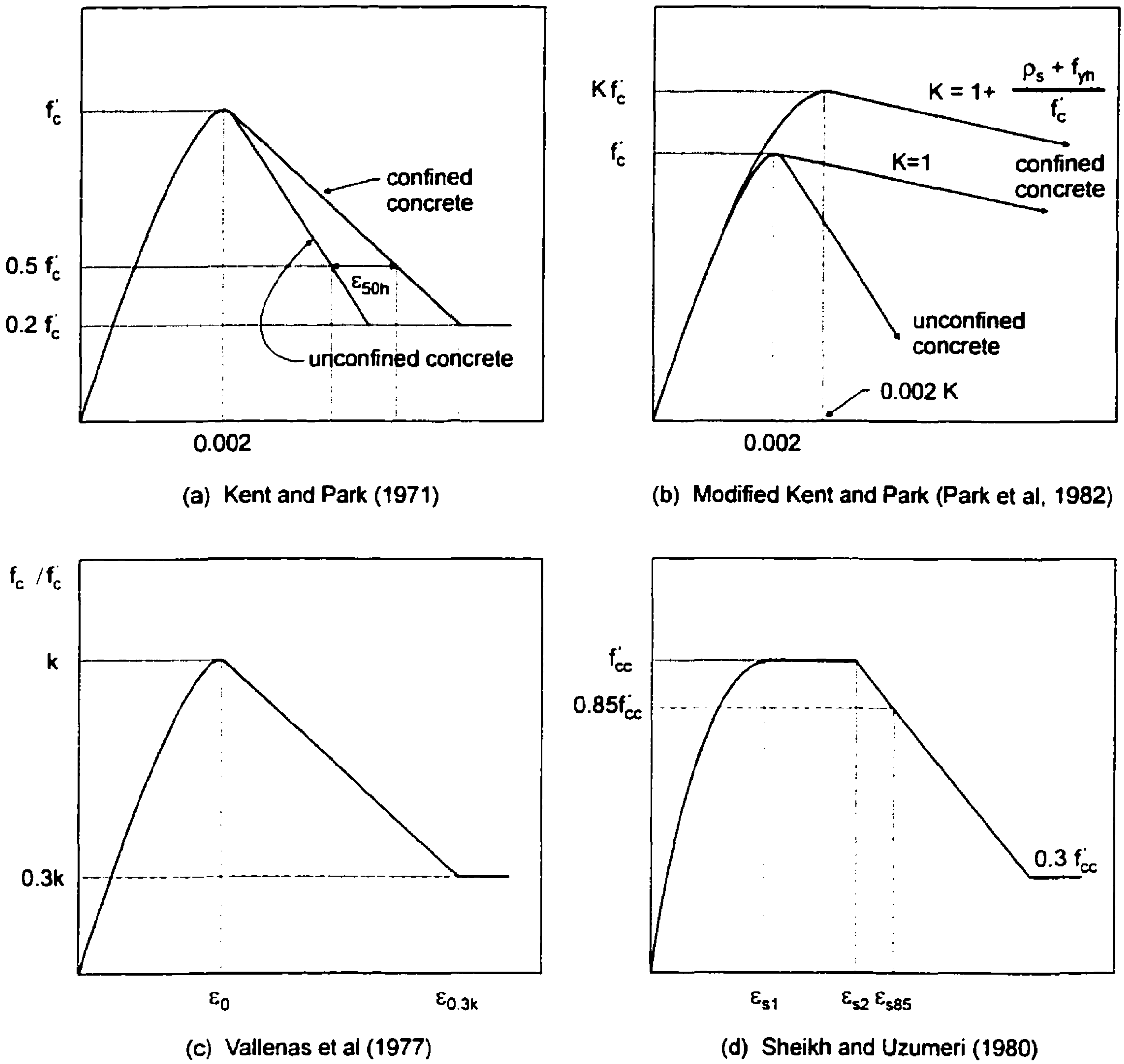

Figure 1.1 Stress-strain response models for confined concrete

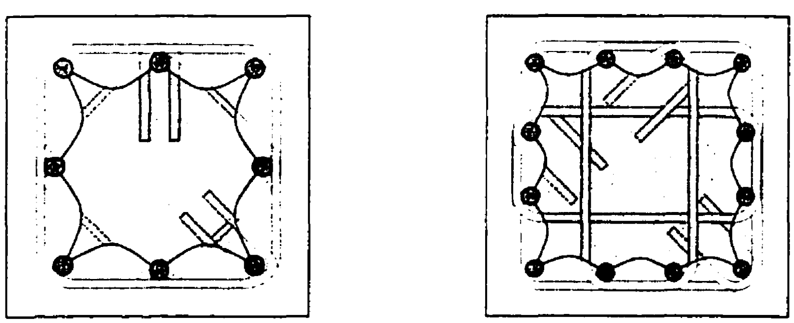

Figure 1.2 Effectively confined concrete core for two reinforcement configurations

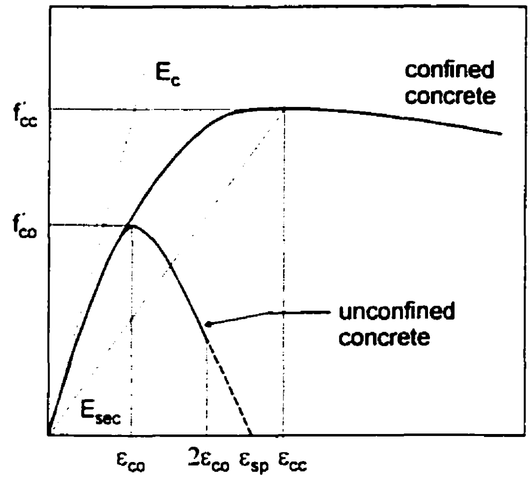

Figure 1.3 Stress-strain relationship for confined concrete proposed by Mander et al (1988a)

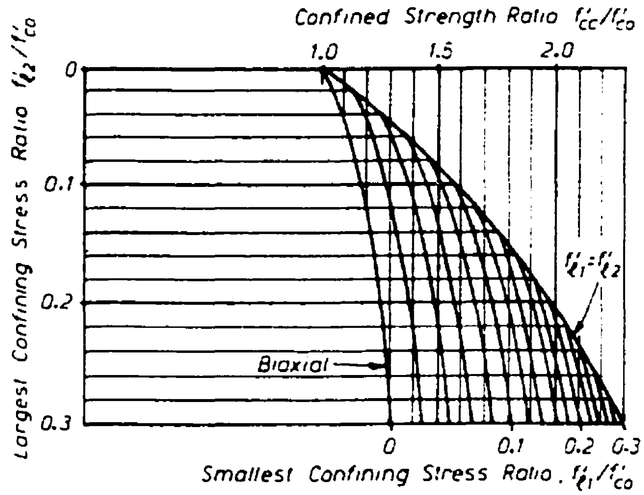

Figure 1.4 Confined concrete strength evaluation for two confining pressures (Mander et al, 1988a)

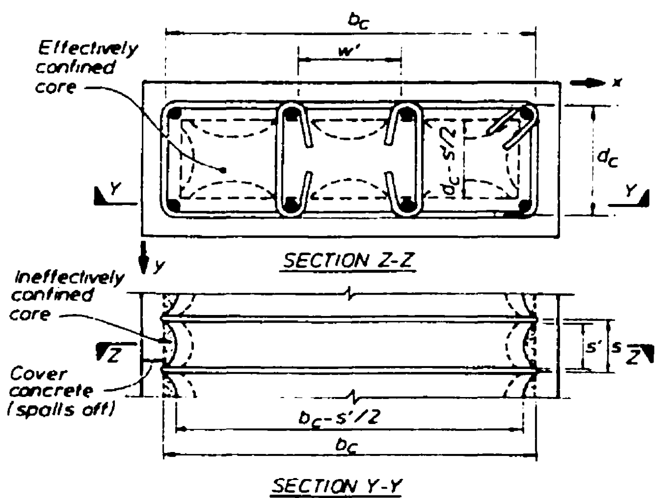

Figure 1.5 Terms used for the evaluation of the effectively confined core (Mander et al, 1988a)

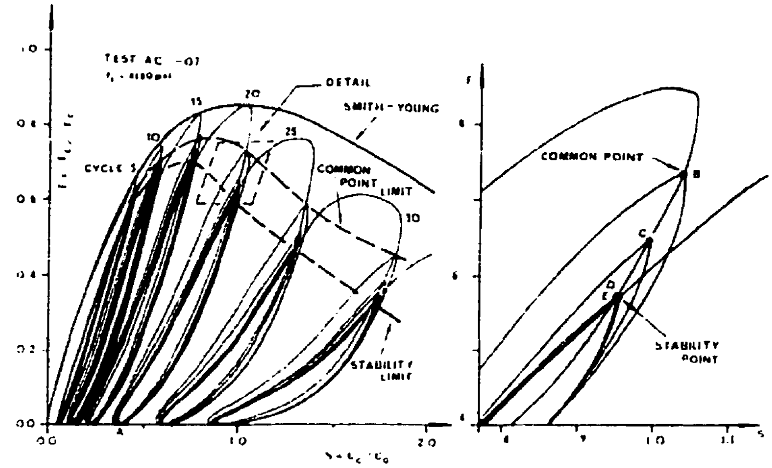

Figure 1.6 Determination of common and stability points for cyclic loading of concrete (Karsan and Jirsa, 1969)

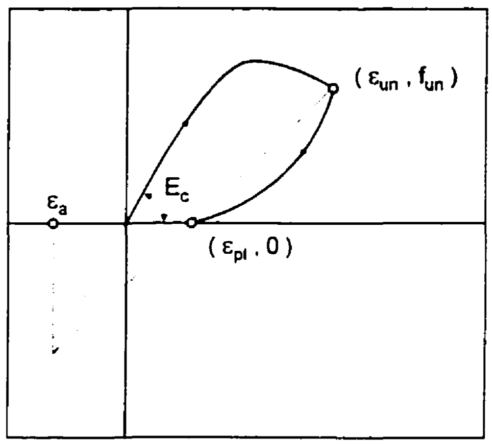

Figure 1.7 Concrete plastic offset strain, ε_{pl} (Mander et al, 1988a)

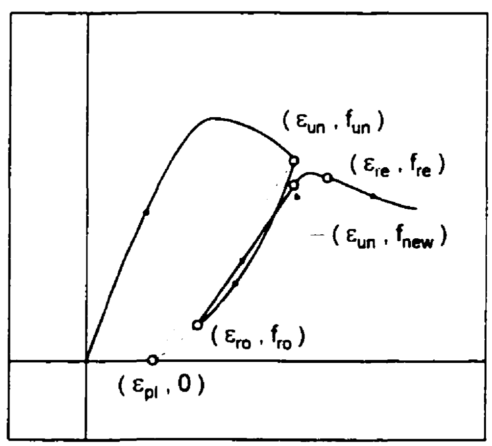

Figure 1.8 Key points on reloading branch of concrete (Mander et al, 1988a)

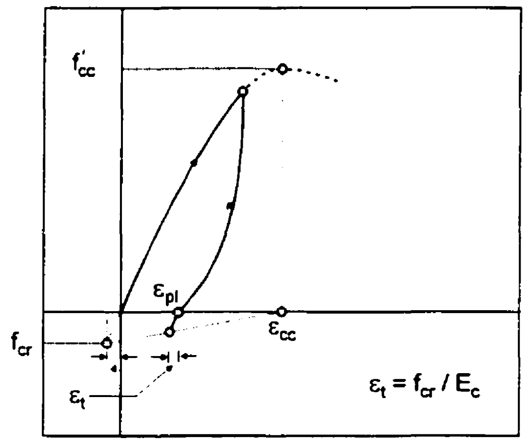

Figure 1.9 Reduction of tensile strength of concrete due to previous compressive loading (Mander et al, 1988a)

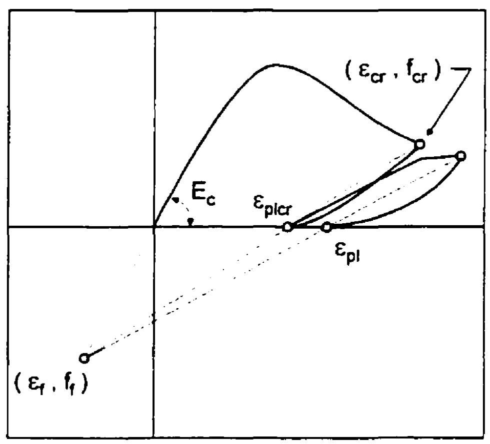

Figure 1.10 Concrete plastic offset strain, ε_{pl} for $\varepsilon_c > 2.5\varepsilon_{cc}$ (Martinez-Rueda and Elnashai, 1997)

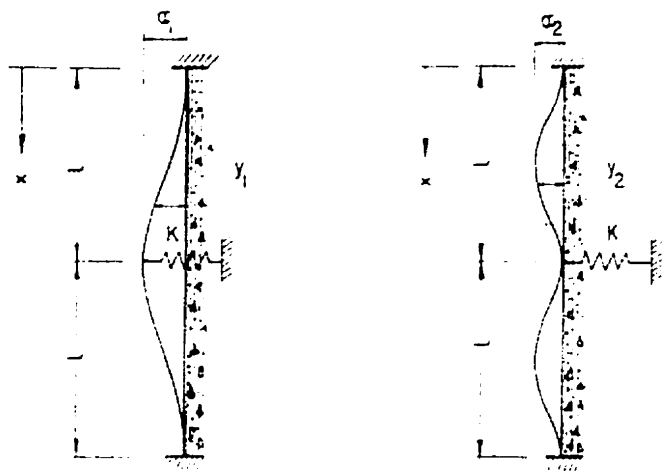

Figure 1.11 Possible buckling modes used by Bresler and Gilbert (1961)

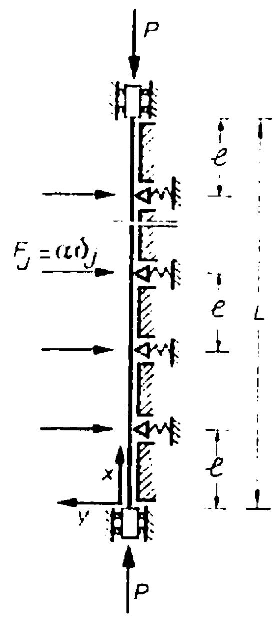

Figure 1.12 Analysis model for longitudinal bar used by Papia et al (1988)

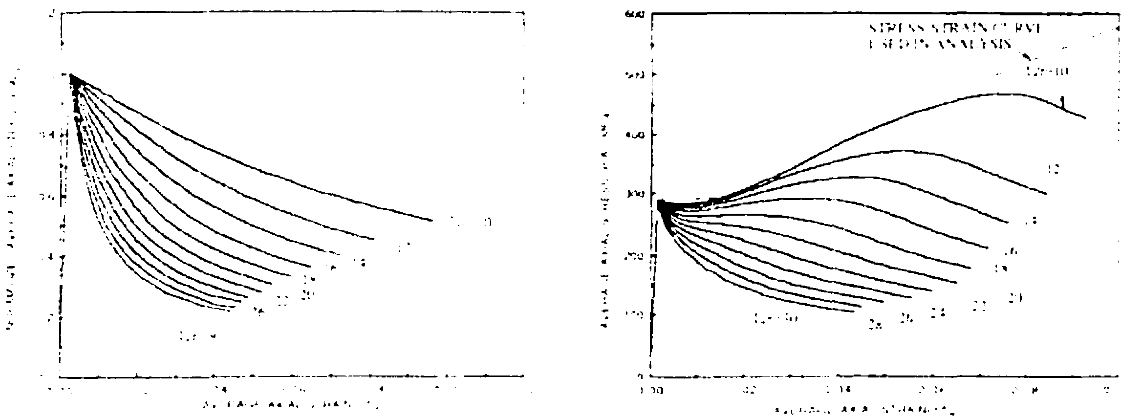

(a) Elastic perfectly plastic steel (b) Elastic plastic steel with strain hardening

Figure 1.13 Stress-strain relationship for steel bars with various L/r ratios (Mau and El-Mabsout, 1989)

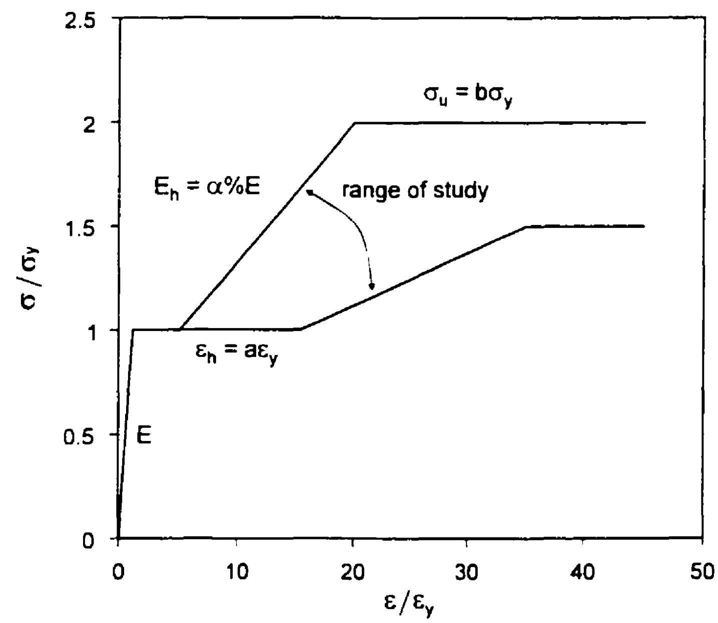

Figure 1.14 Stress and strain ranges studied by Mau (1990)

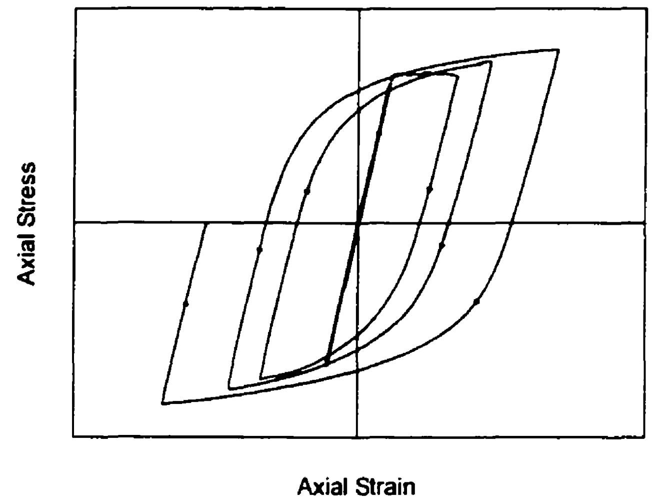

Figure 1.15 Cyclic stress-strain curve for steel including the Bauschinger Effect

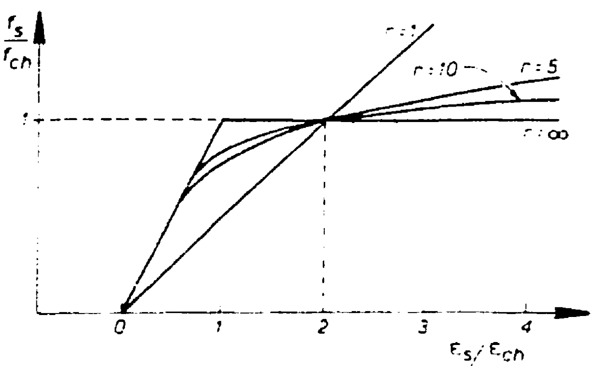

Figure 1.16 Ramberg-Osgood function for various values of r (Kent and Park, 1973)

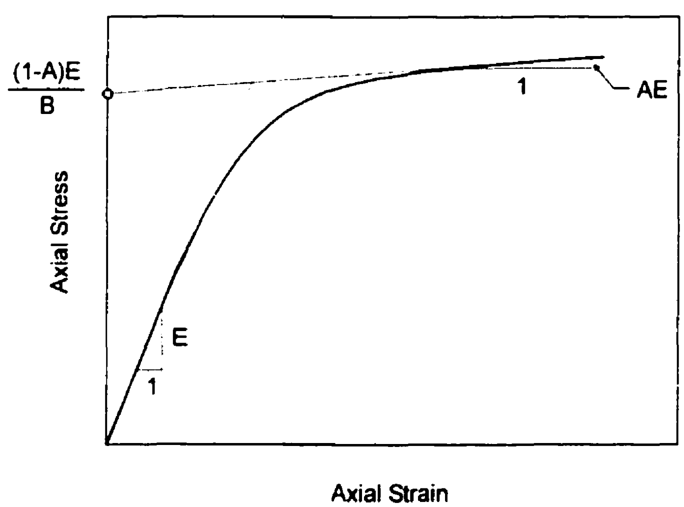

Figure 1.17 Parameters of modified Ramberg-Osgood function (Mattock, 1979)

Chapter 2

Description of Axially Loaded Specimens

A testing programme was conducted to investigate the effect of high-strength concrete on the response of members subjected to reversed cyclic tension and compression. The specimens contained varying amounts of transverse reinforcement consistent with both beam and column detailing requirements for different ductility levels. Structural members are not typically subjected to pure axial loading, but in beams and columns portions of the member are subjected to reversals of tension and compression. The behaviour of these specimens is presented in Chapter 3.

2.1 Axial Specimens

A series of full scale, reversed cyclic loading tests, were conducted to evaluate the seismic response of axially loaded members constructed using high-strength concrete. The specimens were constructed using normal (30 MPa) and high-strength (70 MPa) concretes. For each concrete strength three specimens were constructed; one detailed as a beam (R = 2 and 4), the second as a nominally ductile column (R = 2) and the third as a ductile column (R = 4). The cross-section was taken to be 350 mm, square. This dimension was chosen based on the axial load capacity of the testing machine. The clear span of the specimen was taken as four times the cross-sectional width, b. Uniform axial loading was assumed to occur over a length of 3b in the central portion of the specimen. Prototype beams and columns were designed using Clause 21, Special Provisions for Seismic Design, of the CSA Standard A23.3-M94, and the transverse reinforcement details required for these prototypes were used in the test specimens. The seismic design limit of 55 MPa for the specified concrete compressive strength, f'_c, in Clause 21.2.3.1 of the standard, was ignored.

At each end of all specimens, a corbel was designed to allow connection to the testing machine, see Section 2.1.4. Table 2.1 summarizes the details of the specimens tested.

Table 2.1 Details of the axially loaded specimens

Specimen	f'_c	Hoop Details	Hoop Spacing	Description
N1	30 MPa	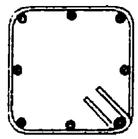	156 mm	- normal-strength concrete - "beam" details for nominally ductile and ductile member
N2	30 MPa	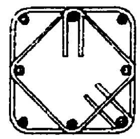	156 mm	- normal-strength concrete - "column" details for nominally ductile member
N3	30 MPa	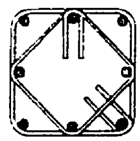	82 mm	- normal-strength concrete - "column" details for ductile member
H1	70 MPa	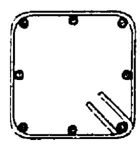	156 mm	- high-strength concrete - "beam" details for nominally ductile and ductile member
H2	70 MPa	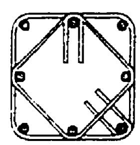	117 mm	- high-strength concrete - "column" details for nominally ductile member
H3	70 MPa	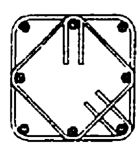	58 mm	- high-strength concrete - "column" details for ductile member

2.1.1 Nominally Ductile and Ductile Beams

Figure 2.1 shows the dimensions and reinforcing details of a specimen with typical "beam details". The clear cover thickness of these specimens was taken as 30 mm, which satisfies the interior exposure conditions for a beam. The longitudinal reinforcement consisted of 8 No. 20 bars, which were embedded into the corbel for its full height (600 mm). The development length, l_d, of a No. 20 bar in 30 MPa concrete is 526 mm, with a reduced required length when high-strength concrete is used. To ensure full tensile development of these longitudinal bars at the interface between the corbel and the specimen, square plates were welded to each end of all of the longitudinal bars.

The confinement details of the transverse reinforcement for the "beam" specimens are based on considerations of required shear capacity, as well as confinement requirements. In choosing the details for the prototype beams it was assumed that the confinement requirements controlled the choice of the transverse reinforcement. A ductile beam is designed to develop the probable moment capacity of the section, while a nominally ductile beam is designed to develop the nominal moment capacity of the cross-section. Thus, since strength considerations are assumed not to govern, the confinement detailing for the ductile and nominally ductile beams constructed using normal and high-strength concrete are identical. Furthermore, it was assumed that the prototype beam was sufficiently deep such that the effective depth over four, (d/4), spacing limit did not control the design of the confinement hoops. The spacing, s, of the No. 10 hoops was governed by the bar buckling requirements, resulting in a required spacing of 156 mm (8 d_b) for both the normal (30 MPa - N1) and the high-strength concrete (70 MPa - H1) specimens. These square hoops were fabricated from No. 10 reinforcing bars including a seismic hook at each end for anchorage in the confined core of the specimen. The hoops were extended into the corbel to ensure similar transverse restraint over the full height of the test specimens.

2.1.2 Nominally Ductile Columns

The reinforcement details of a specimen with typical "column details" are given in Fig. 2.2. The overall dimensioning and longitudinal reinforcement of these specimens were chosen to be the same as that of the specimens with "beam details". The cover thickness for these elements had to be increased to 40 mm to provide a two hour fire rating.

Square and diamond-shaped No. 10 hoops, with seismic hooks were provided to ensure support of each longitudinal bar, resulting in an effective area of confinement reinforcement of 341 mm^2 in each principal direction of the section. For a nominally ductile column, the confinement requirements are determined by using 50% of the spacing limits given by Clause 7.6.5.2, of CSA A23.3-M94. The resulting spacing, s, for the normal-strength concrete specimen (N2) was 156 mm ($8d_b$). For concrete strengths greater than 50 MPa, Clause 7.6.5.2 reduces the above spacing by 25%, resulting in a required confinement spacing of 117 mm for the high-strength concrete specimen, (H2). These transverse reinforcement details were extended into the corbels to ensure adequate restraint of the longitudinal reinforcement.

2.1.3 Ductile Columns

The detailing of these specimens, representing ductile prototype columns, was the same as the nominally ductile columns, (see Fig. 2.2). However the design of the confinement reinforcement was governed by Clause 21.4.4.2, of CSA A23.3-M94. The amount of transverse reinforcement must not be less than the larger of the amounts given by Equations 2.1 and 2.2.

$$A_{sh} = 0.3sh_c \frac{f_c'}{f_{yh}}\left(\frac{A_g}{A_{ch}} - 1\right) \tag{2.1}$$

$$A_{sh} = 0.09sh_c \frac{f_c'}{f_{yh}} \tag{2.2}$$

where

A_{sh}	=	total cross-sectional area of transverse reinforcement
s	=	spacing of transverse reinforcement
h_c	=	cross-sectional dimension of the core
f'_c	=	specified compressive strength of concrete
f_{yh}	=	specified yield strength of transverse reinforcement
A_g	=	gross area of section
A_{ch}	=	cross-sectional area of the core

Thus the spacing of the hoops is a function of the member dimensions, the cross-sectional area of transverse reinforcement and material properties of the concrete and the hoop steel. The resulting confinement spacing for the normal-strength concrete specimen, (N3), was 82 mm. If 400 MPa, No. 10 hoop reinforcement was used as the transverse reinforcement for the high-strength concrete specimen, (H3), the centreline-to-centreline spacing of the hoops would be 46 mm. This would result in a clear spacing between the hoops of 26 mm, which is extremely difficult to construct and thus unrealistic. Therefore, high-strength steel, (500 MPa), was used for the confinement of the 70 MPa specimen. The resulting spacing of the hoops was 58 mm. Again this transverse reinforcement was extended over the full height of the corbel.

2.1.4 Corbel Details

The dimensions of the corbels at each end of the specimens were chosen to be 350 mm thick, 900 mm wide and 600 mm long. These dimensions were selected for ease of construction and connection to the testing machine. The corbels were designed using the strut and tie method for the critical tension loading case. For the tension tie, three double No. 10 hoops were supplied, resulting in an area of reinforcement of 1200 mm^2. Additional reinforcement was placed within the corbel to ensure that cracking was well controlled during the entire testing procedure. There were four sleeves, with an interior diameter of 57 mm, in each corbel to allow for anchorage of the specimens to the testing machine.

2.2 Material Properties

2.2.1 Concrete

In order to ensure consistency between the specimens constructed using the same concrete strength, all three of the specimens were cast from the same batch of ready-mix concrete. A minimum specified compressive strength of 30 MPa and 70 MPa was used for the normal-strength and high-strength specimens, respectively. The mix designs for these concretes are given in Table 2.2.

Table 2.2 Concrete mix proportions

Component	30 MPa	70 MPa
cement, (kg/m^3)	355	480
fine aggregate, (kg/m^3)	790	850
coarse aggregate, (kg/m^3)	1040	1015
water, (L/m^3)	178	135
water-cement ratio	0.50	0.25
water reducing agent, (L/m^3)	1.11	1.63
superplasticizer, (L/m^3)	-	13.0
air entraining agent, (L/m^3)	0.18	-
retarding agent, (L/m^3)	-	0.78
slump, (mm)	95	130
air content	7.5 %	-
density, (kg/m^3)	2364	2494

All six of the specimens remained in the formwork and were moist cured for a total of five days after casting. Before each test, a set of three 150 x 300 mm cylinders, was tested to determine the average compressive strength of the concrete, f'_c, and another set was tested to measure the average splitting tensile stress, f_{sp}. The average modulus of rupture, f_r, was determined by conducting a third point flexural test on a set of three 100 x 100 x 400 mm beams spanning 300 mm. The shrinkage strain of the concrete over time was also measured for each of the concrete batches. Table 2.3 summarizes the measured concrete properties. The stress-strain relationship and the shrinkage strain over time, for each batch of concrete, are shown in Fig. 2.3 and Fig. 2.4, respectively.

Table 2.3 Concrete properties

Concrete	f'_c, MPa (std. dev.)	ε'_c (std. dev.)	f_{sp}, MPa (std. dev.)	f_r, MPa (std. dev.)
30 MPa	39.0 (1.16)	0.0024 (0.00004)	2.91 (0.150)	5.05 (0.170)
70 MPa	76.5 (2.58)	0.0031 (0.00010)	5.26 (0.032)	6.74 (0.145)

2.2.2 Reinforcing Steel

The properties of the reinforcing steel are given in Table 2.4. For a member designed for a force modification factor, R, greater than 2, the reinforcing steel must conform to CSA Standard G30.18 and be of weldable grade. For consistency, all of the specimens were constructed using the same weldable grade steel. Tension tests were performed on three random specimens for each bar size and an extensometer with gauge lengths of 50 and 150 mm, for the No. 10 and No. 20 bars respectively, was used to determine the steel strains. The high-strength No 10 bars did not exhibit a distinct yield plateau, therefore a strain offset of 0.002 was used to determine the yield stress. Figure 2.5 shows the typical stress-strain relationships for the reinforcement.

Table 2.4 Reinforcing steel properties

Bar Description	f_y, MPa (std. dev.)	ε_y (std. dev.)	ε_{sh} (std. dev.)	f_{ult}, MPa (std. dev.)	ε_{rupt} (std. dev.)
No. 10 W	428 (11.3)	0.0023 (0.00016)	0.0165 (0.00211)	587 (6.5)	0.183 (0.0241)
No. 10 H-S	648 (2.5)	0.0055 (0.00026)	- -	672 (5.3)	0.031 (0.0008)
No. 20 W	444 (5.0)	0.0023 (0.00017)	0.0112 (0.00093)	614 (1.6)	0.152 (0.0028)

2.3 Test Setup

The axially loaded specimens were all tested using a 11 400 kN capacity MTS testing machine (see Fig. 2.6).

Each specimen was post-tensioned to the base plate of the testing machine using four 50 mm diameter high-strength steel threaded rods which were reacted against 50 mm thick bearing plates on the top of the bottom corbel. An 89 mm thick high-strength steel plate, with four 50 mm threaded holes, was bolted to the main piston of the testing machine. Once the bottom corbel had been post-tensioned, the piston was lowered until contact was made with the top corbel. Four 50 mm high-strength steel threaded rods were threaded into the steel plate and post-tensioned against the 50 mm bearing plates identical to those used for the lower corbel (see Fig. 2.7). Each specimen was rotated 45° in plan, due the orientation of the circular bolt pattern on the base plate of the MTS machine.

2.4 Instrumentation

The overall applied load and axial deformation of each specimen was measured by the load cell and extensometer of the MTS testing machine.

Linear voltage differential transducers (LVDT's) were used to measure the axial deformation at each corner in the central 1500 mm of each specimen. Five additional LVDT's, having gauge lengths of 300 mm, were used to record the local deformations on the back face of the specimen (see Fig. 2.8).

Electrical resistance strain gauges with a 5 mm gauge length were glued to selected longitudinal bars at their mid-height and gauges with a 2 mm gauge length were installed on selected hoops to measure the strains in the steel (see Fig. 2.9). Selected longitudinal bars were instrumented with pairs of strain gauges as shown in Fig. 2.9 in an attempt to capture the onset of bar buckling. The instrumented hoop was located directly above the mid-height of the specimen and the gauge locations were selected to give a complete strain picture of the transverse reinforcement. Electrical resistance strain gauges with a 30 mm gauge length were also glued to the surface of the concrete on three sides of each specimen, at mid-height in a vertical orientation, to measure axial strains in the concrete.

2.5 Loading Procedure

Under the action of reversing loads the extreme fibres of beams and columns experience alternating compressive and tensile strains.

A prototype beam was designed and the full monotonic flexural response was calculated using the programe RESPONSE, (Collins and Mitchell, 1997). For these calculations the actual material properties of the test specimen were input into the program. At selected ductilities of the monotonic response, the strain distribution over the depth of the beam was determined assuming that plane sections remain plane. At each of these ductility levels the strains in the tensile steel (ε_s) and the extreme compressive fibre (ε_c) were determined (see Fig. 2.10a). This analysis gave target strains for the axially loaded specimens. As shown in Fig. 2.10b, the specimens were subjected to a uniform tensile strain, ε_s, during the tension cycle and the corresponding compressive strain, ε_c, during the compression cycle, to simulate the reversed cyclic loading effects in a typical beam specimen.

A prototype column was also designed and the full monotonic flexural response was determined for a constant applied compressive load using the program RESPONSE. This compressive load corresponded to $0.2A_g f'_c$ (735 kN for the normal-strength concrete specimens and 1715 kN for the high-strength concrete specimens). The column specimens were loaded using the strains determined in a similar manner to that of the beam specimens, (see Figs. 2.10c and 2.10d)

For each cycle, the selected tensile strain, ε_s was measured during testing by using the strain gauges on the longitudinal bars and the LVDT's attached to the back of the specimen. The corresponding compressive strain, ε_c was reached by applying a calculated compressive load. This compressive load corresponded to the sum of the concrete and steel contributions. These contributions were evaluated by determining the stress in each material at the given strain, ε_c, using the stress-strain relationships for each material and multiplying by the respective areas. After yielding of the longitudinal reinforcement had occurred, the strain used in the calculations for the steel contribution accounted for strain offsets due to cyclic loading effects.

The typical loading histories of the specimens are shown in Fig. 2.11. The ductility levels shown in these figures refer to the peak tensile strain reached in each cycle. Tensile loads and elongation were considered to be positive. For each load level, the specimens were cycled three times; one cycle included a tensile peak and a compressive peak.

For each of the beam specimens, load levels reflecting one-half of the cracking load, cracking, half of the yield load and the yield load were imposed. The specimens were then subjected to multiples of the tensile yield deformation, Δ_y. For each of these increments in the tensile deformation, the compressive load corresponding to the target compressive strain was calculated. This calculated compressive load was used as the target load for the compressive cycle.

For the specimens with the column details the assumed axial load of $0.2A_g f_c'$ was first applied and this was considered the "zero" position for these specimens. The loading histories for these specimens were the same as the specimens with beam details up to the yield of the longitudinal reinforcement. Multiples of the tensile yield deformation were applied to the specimens and the corresponding compressive load was calculated and was used as the target compressive load for the compressive cycle.

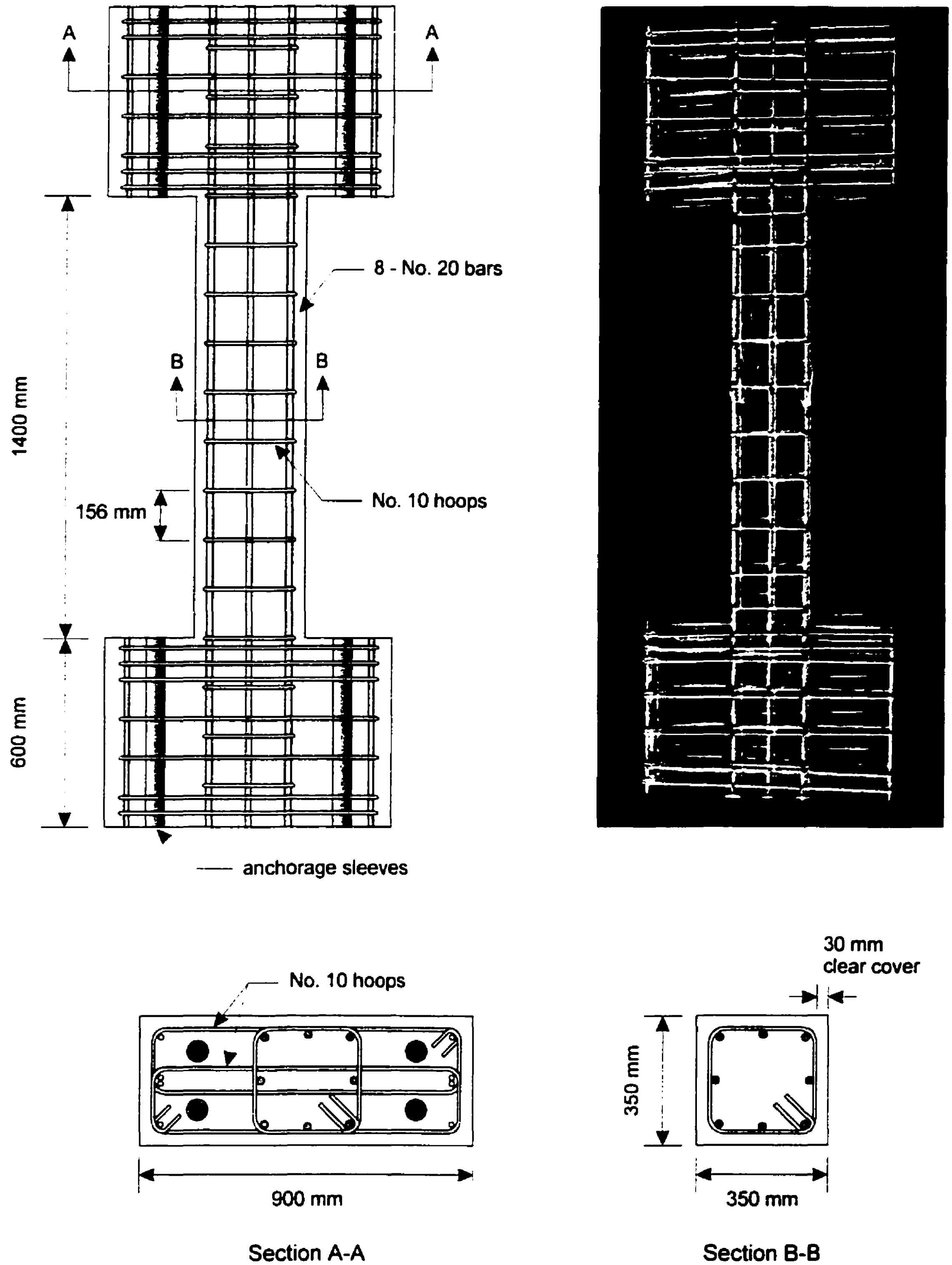

Figure 2.1 Specimens N1 and H1 with "beam" reinforcing details

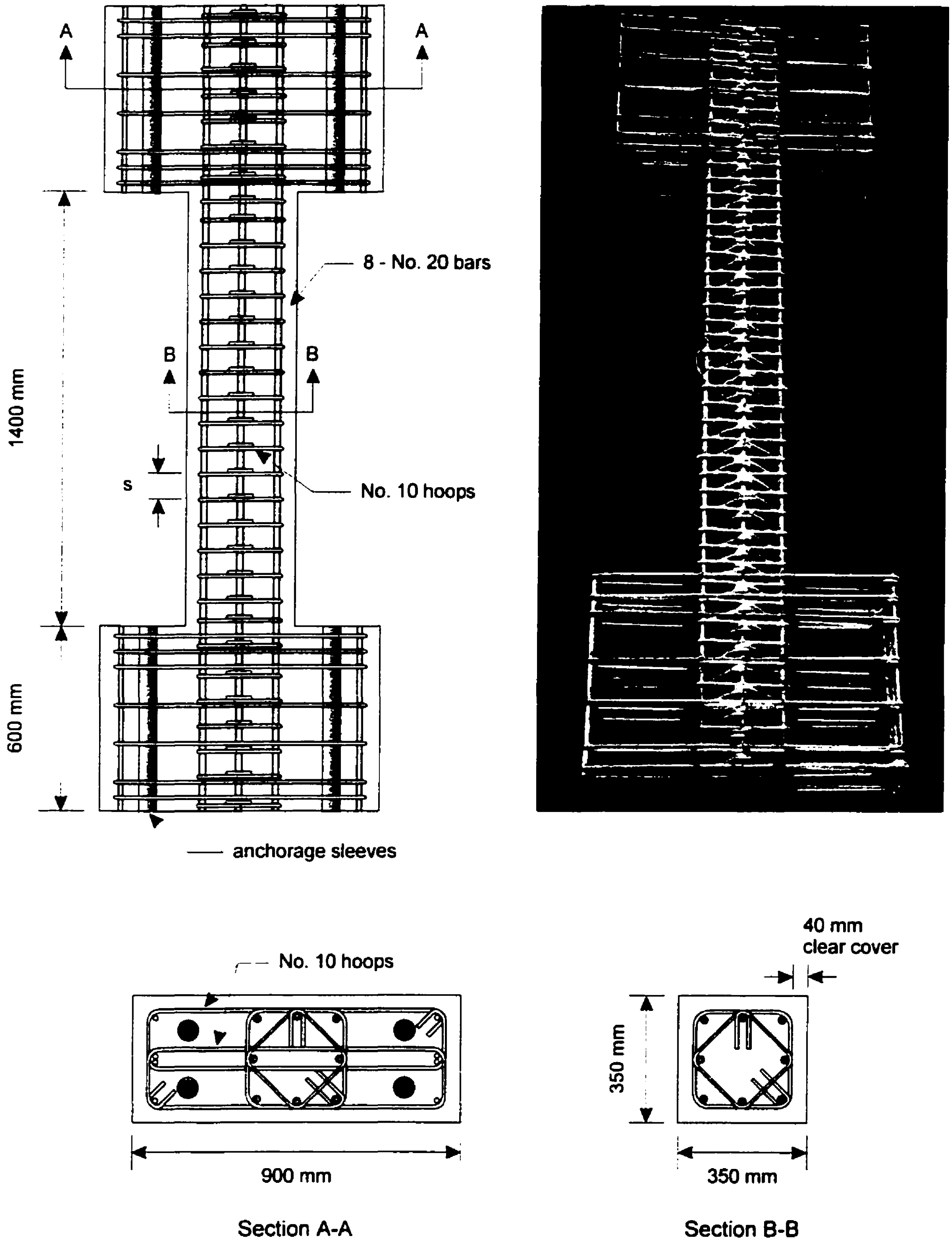

Figure 2.2 Specimens N2, H2, N3 and H3 with "column" reinforcing details and the reinforcing cage of Specimen H3

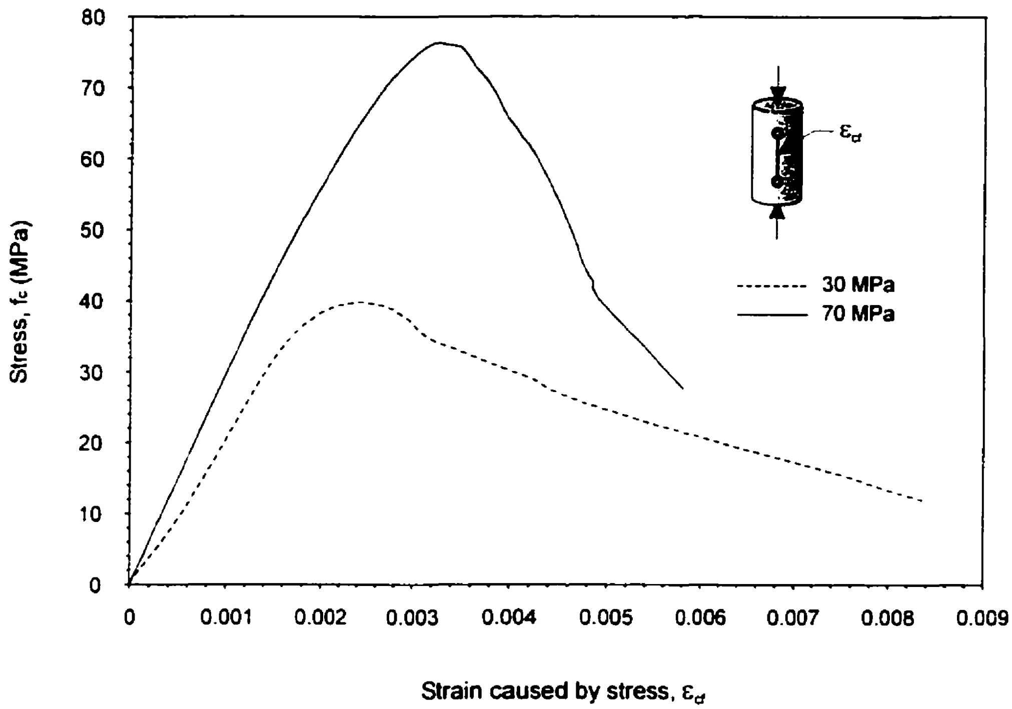

Figure 2.3 Typical compressive stress-strain responses for concrete

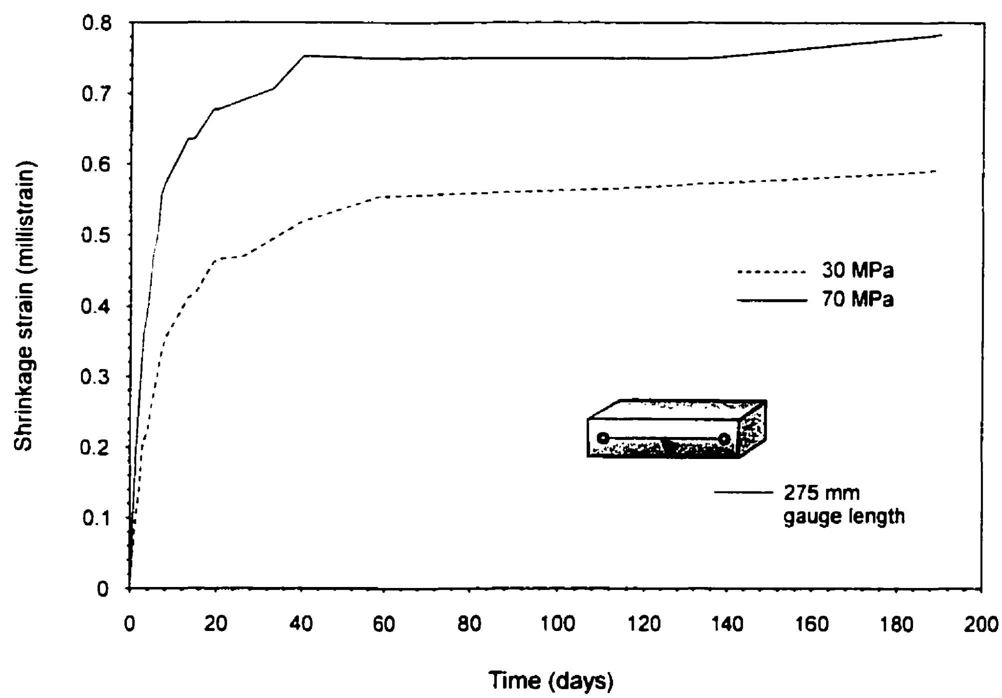

Figure 2.4 Average shrinkage strains measured in concrete prisms

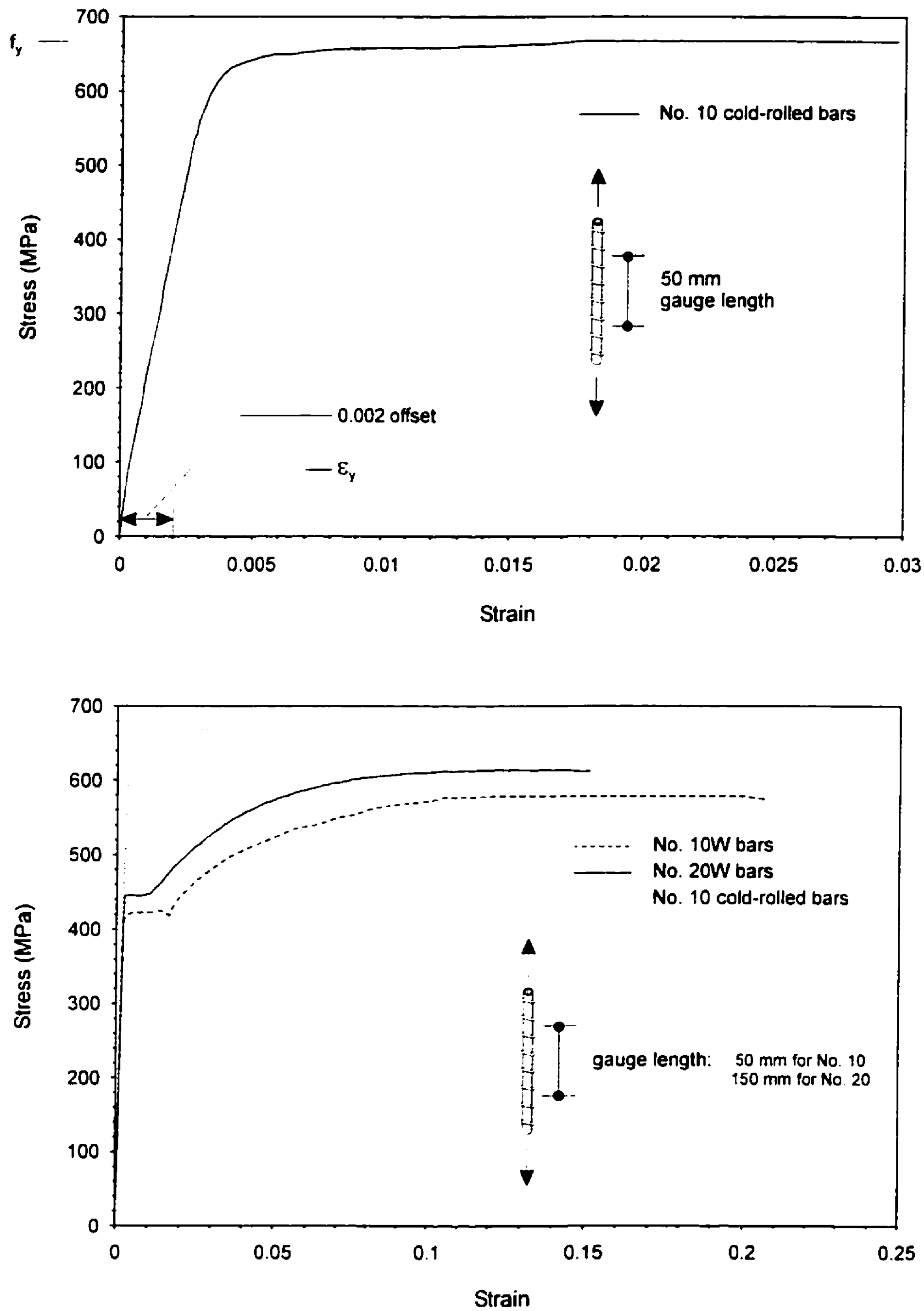

Figure 2.5 Typical stress-strain responses for reinforcing steel

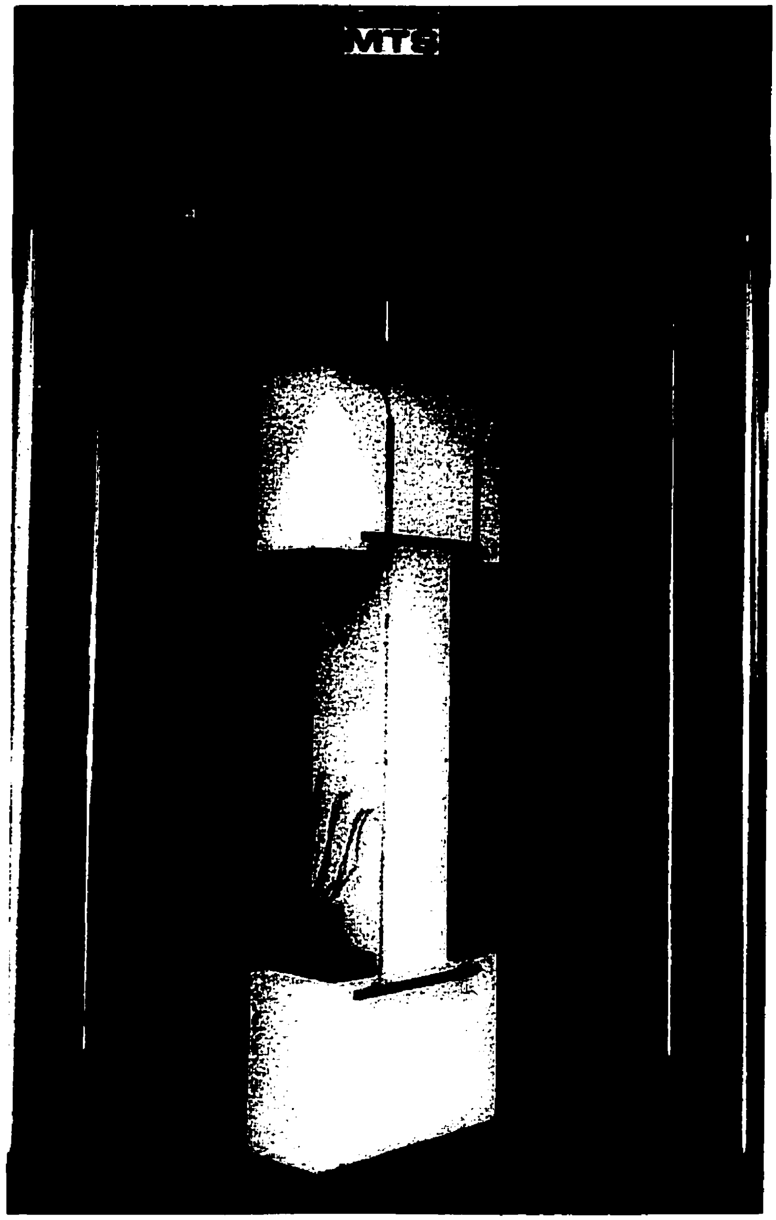

Figure 2.6 Axially loaded specimen prior to testing

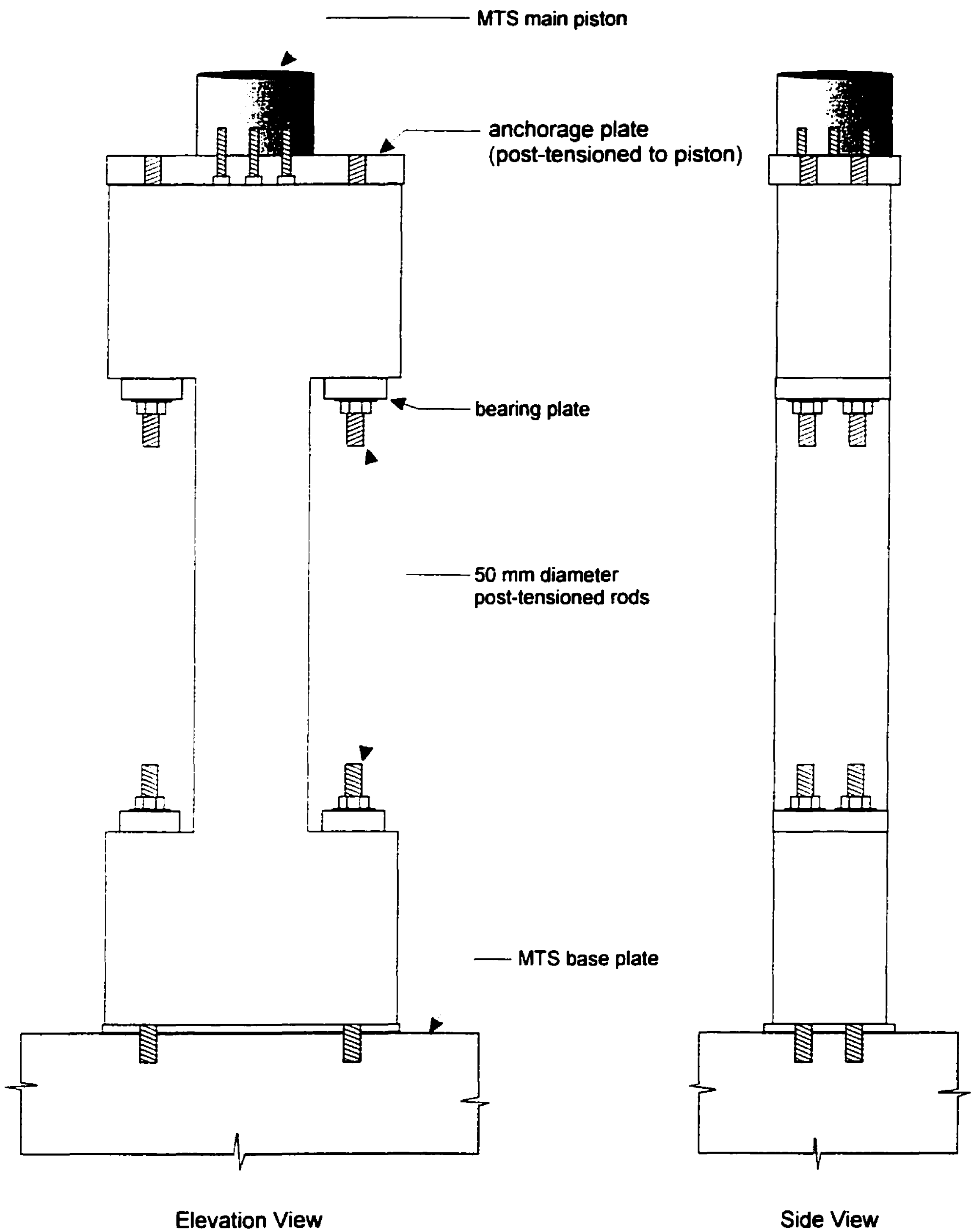

Figure 2.7 Loading apparatus for axially loaded specimens

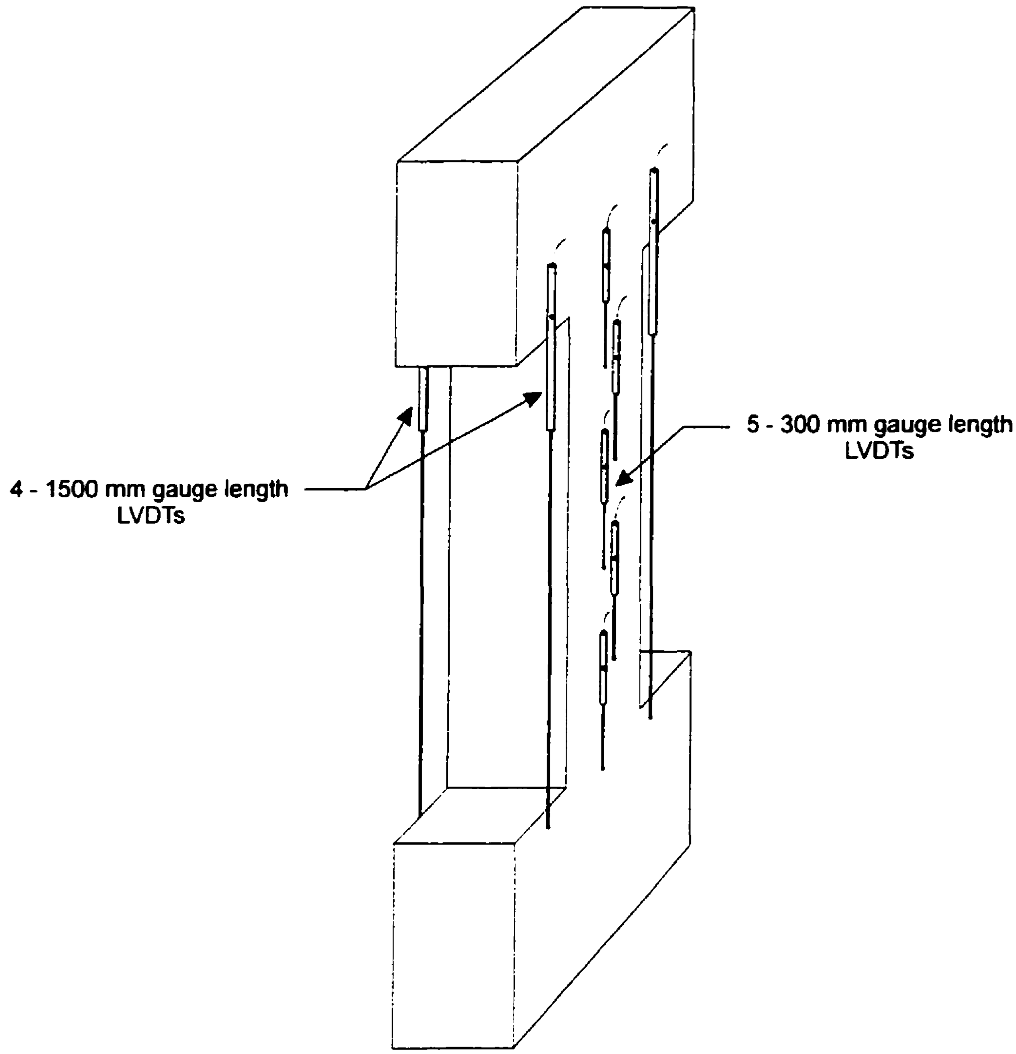

Figure 2.8 Locations of LVDTs for axially loaded specimens

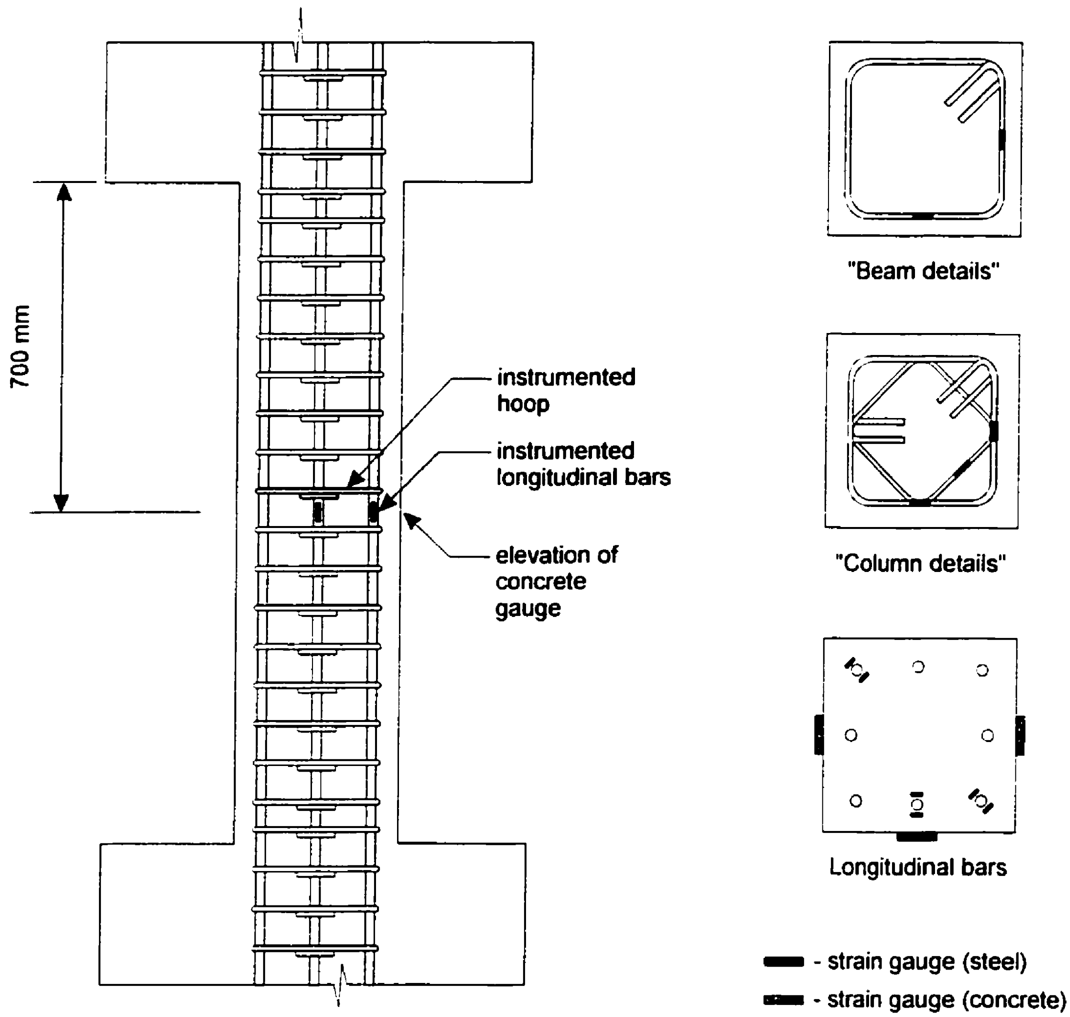

Figure 2.9 Locations of electrical resistance gauges

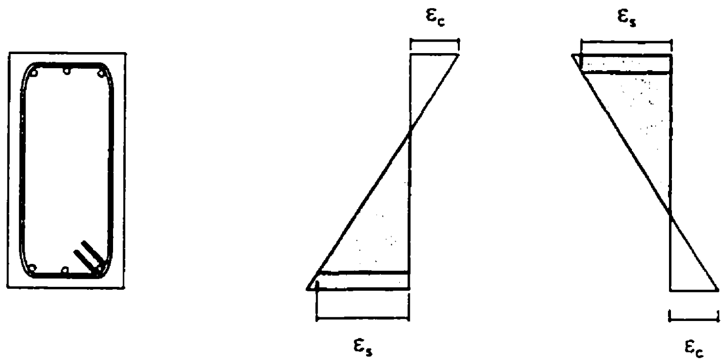

(a) Strain distributions of prototype beam under reversed cyclic loading at a given ductility

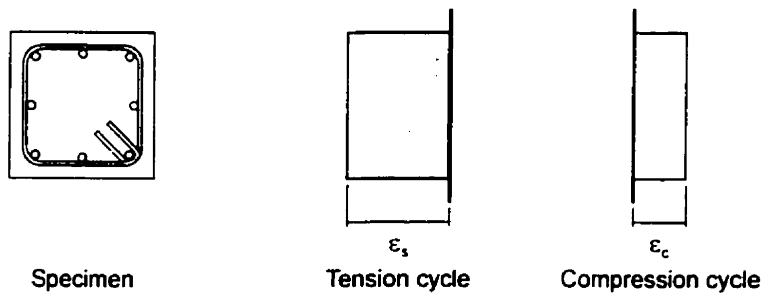

(b) Simulating strain reversals on axially loaded "beam" specimen

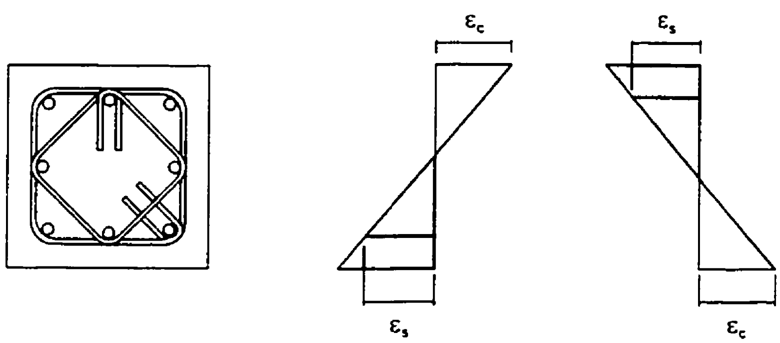

(c) Strain distributions of prototype column under reversed cyclic loading at a given ductility

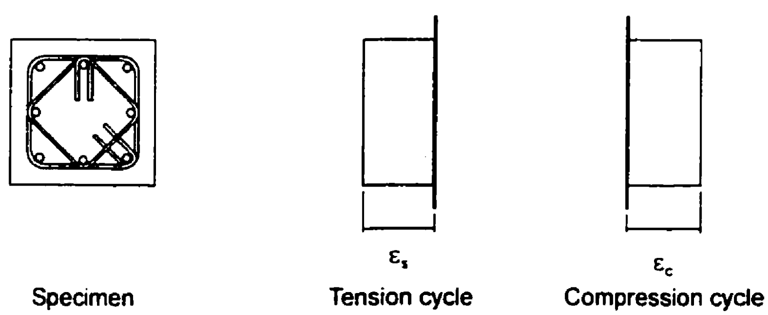

(d) Simulating strain reversals on axially loaded "column" specimen

Figure 2.10 Simulation of reversing strains for axially loaded specimens

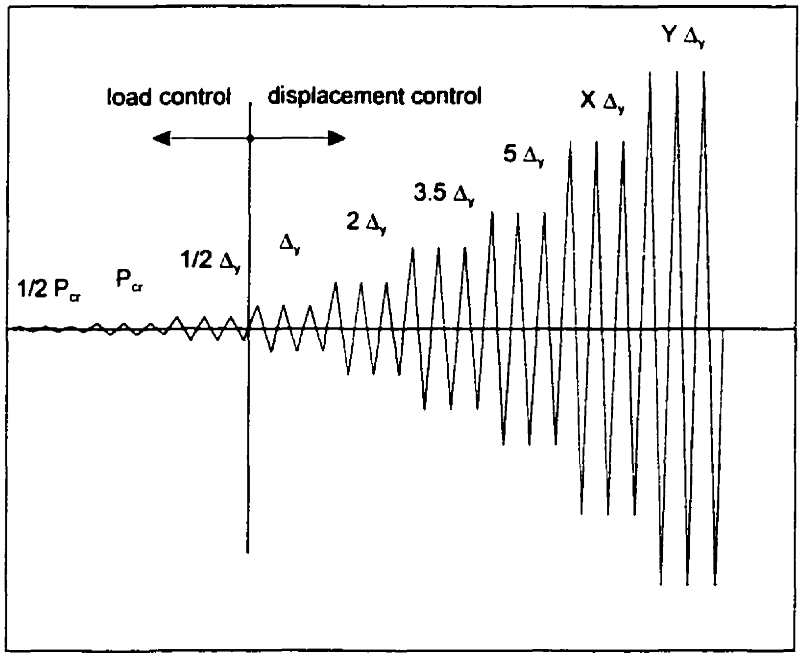

(a) Specimens N1 and H1

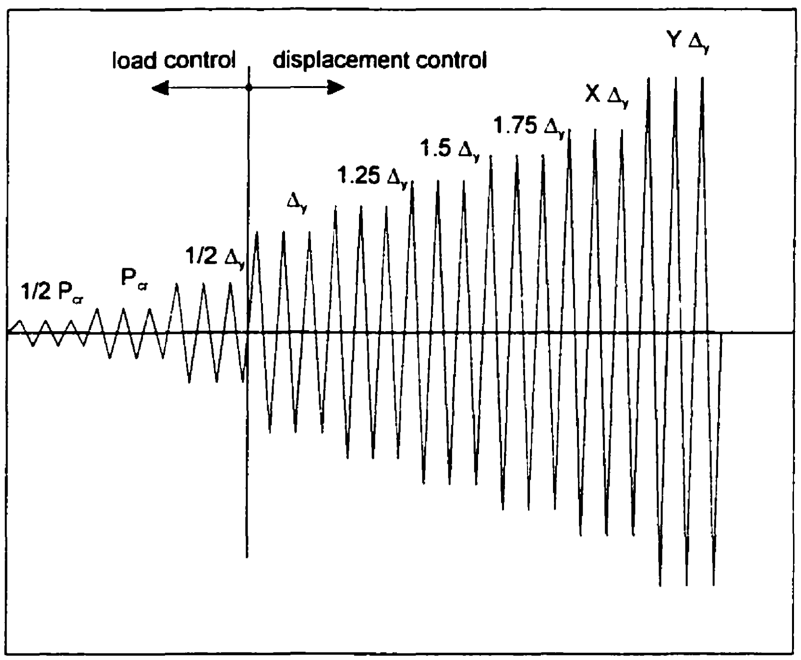

(b) Specimens N2, N3, H2 and H3

Figure 2.11 Schematic representation of loading histories for axially loaded specimens

Chapter 3

Behaviour of Axially Loaded Specimens

This chapter presents a description of the observed experimental behaviour of the axially loaded specimens and compares their reversed cyclic loading responses.

For the load-deformation plots; the load corresponds to the axial load applied to the cross section and the deformation represents the axial deformation of the central 1500 mm region.

Summaries of the peak loads and deformations for the first cycle of key load stages are given in Tables 3.1 through 3.6. All of the peak loads and deformations for each of the specimens are given in Appendix A.. The load stage designations A and B represent positive (tensile) and negative (compressive) loads and deformations, respectively, with the level of ductility of each load stage described by the increase in the tensile deformation.

3.1 Observed Behaviour of Specimens with "Beam Details"

3.1.1 Specimen N1

Specimen N1 was constructed using normal-strength concrete and was designed with typical "beam details". The spacing of the transverse hoops was assumed to be controlled by the design requirements for buckling of the longitudinal bars, resulting in a hoop spacing of 156 mm. Figure 3.1 gives the applied load versus deformation of this specimen. The load stages, peak loads and deformations are presented in Table 3.1.

This specimen was accidentally cracked during adjustment of the loading head and therefore the true cracking load was not determined. The tensile load used for the first three cycles was the calculated tensile load assuming the cracking stress was 65% of the splitting stress, f_{sp}, of the test cylinders (calculated P_{cr} = 240.9 kN). At the completion of the first three cycles, the hairline cracks had formed at the locations of the transverse reinforcement and thus were spaced at approximately 160 mm, over the full height of the specimen. These cracks increased uniformly in width to 0.1 mm and 0.3 mm during the $0.5\Delta_y$ and Δ_y loading cycles, respectively. The first hairline cracks formed in the corbel region during loading cycles to half yield, while the first vertical splitting cracks, propagating from the previously formed horizontal cracks, started forming during the first tensile cycle at $\sim 2\Delta_y$. During this first series of cycles

Table 3.1 Key load stages for Specimen N1

Load Stage	Tensile (A) Cycle		Compressive (B) Cycle		Notes (Δ_y based on tensile cycle)
	Applied Load (kN)	Axial Deformation (mm)	Applied Load (kN)	Axial Deformation (mm)	
1	241	0.90	-274	0.08	first cracking
4	528	2.14	-1903	-1.28	$\cong 0.5\Delta_y$
7	1053	4.77	-2580	-1.84	$1.06\Delta_y$
10	1119	8.03	-3258	-2.05	$1.78\Delta_y$
13	1145	13.88	-4435	-3.10	$3.08\Delta_y$
16	1177	19.81	-4995	-3.81	$4.40\Delta_y$
19	1269	31.36	-5599	-4.59	$6.97\Delta_y$
22	1318	42.24	-5801	-5.82	$9.39\Delta_y$

after yield of the longitudinal reinforcement, the crack widths varied from a maximum of 1.4 mm down to 0.25 mm, indicating that some localized straining of the longitudinal steel was taking place. The number of splitting cracks continued to increase during the subsequent cycles with the horizontal cracks reaching widths of 3.5 mm on the final cycle at $\sim 7\Delta_y$. A photograph of Specimen N1 at $\sim 7\Delta_y$ is given in Fig. 3.2a. At the first compressive peak at $\sim 9\Delta_y$, which corresponded to a peak strain of 0.0039, the cover concrete showed signs of crushing. The spalling of the cover concrete occurred as the specimen was loaded towards the next tensile peak, exposing the longitudinal and transverse steel (see Fig. 3.2b). This specimen was further cycled at these positive and negative peak deflections to evaluate the reduction in the compressive capacity of the section. The peak compressive load was 5801 kN and the residual capacity after spalling was 1204 kN, which is almost an 80% drop in the load. During the final loading cycles, the longitudinal bars straightened during the tensile cycle and severely buckled during the compressive cycle. The core concrete in the central region had severely deteriorated and the exposed hoop had lost anchorage within the concrete core. The legs of the hoop had bent dramatically due to the severe buckling of the mid-side longitudinal bars as shown in Fig. 3.2c.

Figure 3.3 shows the applied load versus axial strain responses of the 5 regions of the specimen that were instrumented on the back face, with the overall curve shown in the top left corner. The central three regions represent the true behaviour of the cross section, since the regions just above and below the corbels could be considered disturbed regions.

It is clear from Fig. 3.3 that all of the central regions performed similarly until the peak compressive load was reached. At this point the second region from the bottom experienced a sudden increase in compressive strain accompanied by a drop in load as the concrete cover separated from the core. This resulted in the release of the compressive strain in the central region (see Fig. 3.3). Figure 3.4 shows strains recorded in the longitudinal reinforcement versus the applied axial load at six locations at the mid-height of the section. The shaded area indicates the elastic range of the longitudinal reinforcement. The offsets in the strains under compressive loading are due to the closing of the cracks. The strain in the hoop reinforcement versus the applied load is given in Fig. 3.5. The hoop, which was the hoop just below mid-height, did not yield until the peak applied load was reached. This indicates that once the cover concrete crushed, the confining force provided by this concrete was transferred to the hoop reinforcement, resulting in the increase in strain.

3.1.2 Specimen H1

Specimen H1 was constructed using high-strength concrete and was designed with typical "beam details". As with Specimen N1, the spacing of the transverse hoops was controlled by the buckling requirement for the longitudinal reinforcement, therefore the same spacing of 156 mm was used. The applied load versus axial deformation of this specimen is given in Fig. 3.6. The load stages, peak loads and deformations are presented in Table 3.2.

Table 3.2 Key load stages for Specimen H1

Load Stage	Tensile (A) Cycle		Compressive (B) Cycle		Notes (Δ_y based on tensile cycle)
	Applied Load (kN)	Axial Deformation (mm)	Applied Load (kN)	Axial Deformation (mm)	
1	82	0.15	-28	0.14	elastic
4	189	0.22	-225	-0.03	first cracking
7	541	2.15	-1603	-0.70	$\cong 0.5\Delta_y$
10	1078	4.67	-2726	-1.13	$1.08\Delta_y$
13	1126	9.16	-4201	-1.79	$2.12\Delta_y$
16	1145	13.73	-5102	-2.00	$3.18\Delta_y$
19	1186	19.77	-5890	-2.29	$4.58\Delta_y$
22	1264	28.33	-7221	-2.83	$6.56\Delta_y$
25	1329	39.79	-8457	-3.40	$9.21\Delta_y$

The first series of loading cycles for this specimen were elastic. The cracking load was calculated for this specimen using the method described in Section 3.1.1 resulting in a predicted cracking load of 456.7 kN. The measured cracking load was 189 kN when three horizontal hairline cracks formed in the section. Cracking over the full height of the section occurred during the first cycle at $0.5\Delta_y$, at the locations of the transverse hoops and these cracks had an average width of 0.15 mm. The cracks increased in width to 0.33 mm and the first signs of vertical splitting cracks occurred during the tensile yielding cycles. There was a wide range in the crack widths, from 1.1 mm to 0.1 mm during the first cycles at $\sim 2\Delta_y$. Figure 3.7a shows the Specimen H1 at a tensile deformation of $\sim 3\Delta_y$. The number of splitting cracks continued to increase and width of the transverse cracks continued to grow during the subsequent cycles. The horizontal cracks reached maximum widths of 4 mm during the first loop at $\sim 9\Delta_y$. For this cycle a corresponding peak compressive strain of 0.0024 was reached which is about 74% of the experimental strain at peak stress for this concrete. On the second compressive loop at this deflection there was evidence of separation of the cover concrete from the core. Just as the peak strain for this loading cycle was about to be reached there was sudden spalling of the concrete cover and buckling of the longitudinal reinforcement. Figure 3.7b shows Specimen H1 at the completion of testing. During these last three cycles the peak compressive capacity of the cross section deteriorated from 8457 kN on the first cycle to 7175 kN on the third cycle, which corresponds to a 15% loss of compressive load. This early spalling of the concrete could have been a result of the splitting cracks located in this region. These cracks reduced the restraint on the longitudinal bars provided by the cover concrete, thus allowing these bars to buckle. The buckling of the bars could have also instigated the premature spalling of the concrete cover of this specimen.

Figure 3.8 shows the applied load versus axial strain for the 5 regions instrumented on the specimen. The three central regions performed similarly until the spalling of the concrete cover with the central region showing an increase in compressive strain once this event had occurred. The applied load versus the strain in the longitudinal steel is given in Fig. 3.9 and again shows the shift of the reloading strain due to the closing of the cracks. The strain in the hoop reinforcement versus the applied load is given in Fig. 3.10. It is clear that one of the instrumented legs of the hoop yielded during the second cycle at the peak compressive strain. This is probably due to the buckling of the longitudinal reinforcement. The applied load versus the strain in the concrete cover, between cracks is shown in Fig. 3.11. With each successive cycle at a particular deformation the decrease in compressive capacity from the previous cycle diminishes. It also shows that the peak strain reached in the cover concrete was approximately

0.0027 at this location, which again is lower than the strain corresponding to the peak stress for this high-strength concrete.

3.2 Observed Behaviour of Specimens with "Nominally Ductile Column Details"

3.2.1 Specimen N2

Specimen N2 was constructed using normal-strength concrete and was designed with "nominally ductile column details". At each level of transverse reinforcement there was a square and a diamond hoop providing lateral restraint of each longitudinal bar with a hoop bend. The spacing of these hoops was 156 mm. Figure 3.12 gives the applied load versus axial deformation of this specimen. The load stages, peak loads and deformations are presented in Table 3.3.

Table 3.3 Key load stages for Specimen N2

Load Stage	Tensile (A) Cycle		Compressive (B) Cycle		Notes (Δ_y based on tensile cycle)
	Applied Load (kN)	Axial Deformation (mm)	Applied Load (kN)	Axial Deformation (mm)	
0	-	-	-735	-0.40	$0.2A_gf'_c$ (dead load)
1	-476	-0.31	-1177	-0.67	elastic
4	147	0.25	-1961	-1.17	first cracking
7	526	2.20	-4071	-2.43	$\cong 0.5\Delta_y$
10	1039	4.65	-5385	-3.40	$0.98\Delta_y$
13	1094	6.96	-5713	-4.07	$1.47\Delta_y$
16	1109	9.01	-5760	-4.40	$1.90\Delta_y$
19	1124	10.61	-6437	-5.87	$2.23\Delta_y$
22	1102	12.51	-4333	-7.98	$2.63\Delta_y$
25	1178	16.47	-3028	-10.43	$3.47\Delta_y$

This specimen was initially loaded to an assumed dead load of $0.2A_gf'_c$, which was equivalent to 735 kN. The first three cycles were elastic, with two hairline cracks forming during the fourth cycle at a load of 147 kN. This is 61% of the cracking load calculated for Specimen N2. Tensile cracks formed at the transverse steel locations during the first cycle at $0.5\Delta_y$ and had uniform widths of 0.1 mm, which increased to 0.4 mm during the yield cycles. The first signs of some vertical cracking also occurred during the tensile yield loading cycles. There was again a disparity in the crack widths at the peaks of the first loop at $\sim 1.5\Delta_y$, with the widths of the horizontal cracks ranging from 1.25 mm down to 0.4 mm. Figure 3.13a shows Specimen N2 at a tensile deformation of ~$1.5\Delta_y$. This difference in crack widths decreased during subsequent cycles at the same deflection level. There was no great increase in the cracks widths during the cycles just below and above $2\Delta_y$. The crushing of the concrete cover occurred at a compressive strain of 0.0039 during the first cycle at $2.2\Delta_y$ (see Fig. 3.13b). Buckling of the vertical bars was not noticeable until the third cycle at $2.6\Delta_y$, after which the compressive capacity of the cross section diminished quickly. This specimen was capable of resisting over 67% of the peak compressive load after the crushing of the cover concrete. At the end of testing there was buckling of the longitudinal bars between the locations of the hoop reinforcement as shown in Figs. 3.13c and 3.13d.

The applied load versus strain responses are given in Fig. 3.14 for this specimen. Again it is clear that one region underwent severe compressive straining, while there was added tensile straining in other regions. Figure 3.15 shows the applied load versus the strain in the vertical bars at mid-height of the specimen. The bars at this location just reached tensile yielding during the extent of the test, however once the cover concrete crushed these bars had a large increase in their compressive strain. The strain in the hoop steel is given in Fig. 3.16 and these plots indicate that the strain within this reinforcement was approximately 70% of yield until the peak compressive cycle when there was a jump in the tensile strain. The compressive strain in the cover concrete between cracks is given in Fig. 3.17, again showing the reduction in the applied load at the same compressive strain upon reloading of the specimen.

3.2.2 Specimen H2

Specimen H2 was constructed using high-strength concrete and was designed with "nominally ductile column details". Due to the use of high-strength concrete in this specimen the hoop spacing of the transverse reinforcement was taken as 75% of that for Specimen N2, resulting in a spacing of 117 mm. The applied axial load versus relative deformation of this specimen is given in Fig. 3.18. The load stages, peak loads and deformations are given in Table 3.4.

The superimposed dead load was again taken as $0.2A_g f'_c$, which is equivalent to a load of 1715 kN. This specimen was initially cycled in the elastic range with first cracking occurring at a tensile load of 206 kN, which is 45% of the calculated cracking load for Specimen H1. Horizontal cracking occurred over the full height of the specimen during the first $0.5\Delta_y$ loading cycle, resulting in crack widths of 0.1 mm spaced at approximately 120 mm. These widths

Table 3.4 Key load stages for Specimen H2

Load Stage	Tensile (A) Cycle: Applied Load (kN)	Tensile (A) Cycle: Axial Deformation (mm)	Compressive (B) Cycle: Applied Load (kN)	Compressive (B) Cycle: Axial Deformation (mm)	Notes (Δ_y based on tensile cycle)
0	-	-	-1658	-0.93	$0.2A_gf'_c$ (dead load)
1	-1399	-0.87	-3384	-1.65	elastic
4	206	0.63	-4041	-1.89	first cracking
7	546	2.29	-7206	-3.16	$\cong 0.5\Delta_y$
10	1056	4.75	-9424	-4.38	$1.07\Delta_y$
13	1092	5.80	-9763	-4.76	$1.30\Delta_y$
16	1082	7.45	-10066	-5.28	$1.67\Delta_y$
19	1100	8.13	-9772	-5.54	$1.83\Delta_y$
22	1148	9.72	-3225	-9.41	$2.18\Delta_y$
25	1149	12.30	-3144	-11.07	$2.76\Delta_y$

increased uniformly to 0.33 mm during the cycles at tensile yielding. The first evidence of vertical splitting occurred during the cycles at approximately $1.3\Delta_y$, with crack widths ranging from 0.7 mm down to 0.3 mm. During the first cycle (19B), at a compressive strain of 0.0037 the cover concrete spalled abruptly. The peak compressive capacity of this specimen had occurred three cycles earlier and the cover spalling occurred at 97% of the previous peak capacity. There was also evidence of buckling of the longitudinal reinforcement. Photographs of this specimen at the tensile peak before cover spalling and the compressive peak after cover spalling are given in Figs. 3.19a and 3.19b, respectively. The photograph before spalling indicates that there was very little damage to the specimen during the loading cycles between yielding and cover spalling. A total of eight loading loops were performed after the spalling of the concrete cover. The compressive capacity of this specimen after cover spalling was a maximum of 3252 kN during the first cycle and diminished to 2662 kN during the final cycle. These loads are equivalent to 32% and 26% of the peak compressive load. The loss of capacity was due to the deterioration of the concrete core resulting from loss of confinement and buckling of the longitudinal bars. Figure 3.19c shows this specimen at the completion of testing.

Figure 3.20 shows the applied load versus the axial strains for the instrumented regions on the back of the specimen. The central region did not undergo as much tensile straining as the others, but did see a large compressive strain increase once the cover concrete had spalled. Due to the abrupt spalling of the cover the LVDTs located on the back of the specimen were unable to capture the post-peak response of this specimen. The recorded strains in the longitudinal bars are given in Fig. 3.21. All of the bars had yielded in both tension and compression over the course of testing with the maximum compressive strain exceeding 3 times the yield strain at the peak load. The three instrumented locations on the hoop reinforcement indicate that this steel had only just reached or was very close to the yield strain once the peak applied load was reached, as shown in Fig. 3.22. The strains recorded in the cover concrete between cracks, up to the spalling of the cover concrete are given in Fig. 3.23.

3.3 Observed Behaviour of Specimens with "Ductile Column Details"

3.3.1 Specimen N3

Specimen N3 was constructed using normal-strength concrete and was designed with "ductile column details". The transverse reinforcement spacing was 82 mm, following the provisions of Clause 21 of the 1994 CSA Standard. The applied load versus axial deformation of this specimen is given in Fig. 3.24. The load stages, peak loads and deformations are presented in Table 3.5.

This specimen was loaded to the same dead load (735 kN) and initially cycled in the elastic range as was done with Specimen N2. The experimental cracking load was 142 kN which is 59% of the calculated load, but is very similar to that recorded for Specimen N2. The spacing of the hairline horizontal cracks which formed during the $0.5\Delta_y$ tensile cycle varied between approximately 80 and 160 mm, since the spacing of the hoop reinforcement was very small for this specimen. As for the other normal-strength concrete specimens the first signs of vertical splitting cracks formed during the yield loading cycles. The widths of the cracks at this loading stage varied between 0.1 and 0.45 mm due to the non-uniform crack spacing. These cracks reached a maximum width of 1.5 mm during the $2.23\Delta_y$ tensile cycle. During the compressive loop at this loading level (stage 19B) the concrete cover crushed at a compressive strain of 0.0037, with a small amount of spalling occurring on the back face. On the next compressive cycle, at approximately the same strain the load capacity of the cross section decreased to 4659 kN, which is 73% of the peak capacity. The compressive load capacity continued to increase as the compressive strain in the system was increased, reaching a maximum compressive load of 5453 kN at a compressive strain of 0.0068. This load equates to 85% of the peak compressive load. Further cycling of this specimen promoted continued spalling of the cover

Table 3.5 Key load stages for Specimen N3

Load Stage	Tensile (A) Cycle Applied Load (kN)	Tensile (A) Cycle Axial Deformation (mm)	Compressive (B) Cycle Applied Load (kN)	Compressive (B) Cycle Axial Deformation (mm)	Notes (Δ_y based on tensile cycle)
0	-	-	-738	-0.42	$0.2A_g f'_c$ (dead load)
1	-476	-0.34	-1176	-0.68	elastic
4	142	0.18	-1913	-1.11	first cracking
7	523	2.25	-4070	-2.39	$\cong 0.5\Delta_y$
10	1062	4.93	-5358	-3.37	$1.08\Delta_y$
13	1102	6.60	-5697	-4.10	$1.45\Delta_y$
16	1098	8.25	-5716	-4.64	$1.81\Delta_y$
19	1114	10.16	-6407	-5.48	$2.23\Delta_y$
22	1109	11.68	-5117	-7.79	$2.57\Delta_y$
25	1155	15.22	-5453	-10.27	$3.35\Delta_y$
28	1210	18.65	-5261	-12.67	$4.10\Delta_y$
31	1254	25.71	-4329	-17.71	$5.65\Delta_y$
34	1330	32.38	-3406	-23.16	$7.12\Delta_y$

concrete and Fig. 3.25a shows this specimen at the compressive peak at $3.35\Delta_y$. In the third cycle of loading towards a peak tensile strain of $7.12\Delta_y$ a longitudinal reinforcing bar ruptured due to low-cycle fatigue. Seventeen loading cycles after the initial crushing of the concrete cover the compressive capacity of Specimen N3 was 2735 kN or 43% of the peak compressive load. Figure 3.25b shows this specimen at the completion of testing showing the degree of spalling of the concrete cover. The deterioration of the core concrete can be seen towards the top of the specimen with some minor buckling of the longitudinal bars visible. The core below this region appears to be completely intact. Figure 3.25c shows a close up of the ruptured longitudinal bar which is indicated by an arrow.

Figure 3.26 shows the breakdown of the axial strains with respect to the applied load for Specimen N3. The region second from the top underwent a large amount of compressive straining with the level increasing dramatically during the final compressive loop. This confirms the visual observations of the deterioration of the core concrete in this area, as was shown in Fig. 3.25b. It is also clear that different regions underwent varying degrees of both tensile and compressive straining during testing. The strain in the longitudinal bars is given in Fig. 3.27 and shows the degree of compressive straining of these bars, confirming the excellent restraint provided by the transverse hoops. Figure 3.28 gives the strains in the transverse reinforcement. The two instrumented legs of the square hoop almost reached their yield strain at the peak compressive load, but the diamond shaped hoop was at less than 20% of its yield strain. The measured strains in the cover concrete between cracks are given in Fig. 3.29. As was the case for the previous specimens the applied load drops on each successive cycle at the same strain but at a decreasing rate. This loss of capacity seems to increase as the peak compressive strain in the concrete increases.

3.3.2 Specimen H3

Specimen H3 was constructed using high-strength concrete and was designed with "ductile column details". The hoop spacing was dependent on variables including the concrete compressive strength and the yield stress of the hoop steel resulting in a transverse hoop spacing of 58 mm. The applied load versus relative deformation of this specimen is given in Fig. 3.30. The load stages, peak loads and deformations are presented in Table 3.6.

As with Specimen H2, an initial dead load equal to 1715 kN was applied to this specimen and the first three cycles were in the elastic range. The cracking load for this specimen was equal to 195 kN which is very close to those observed for the two previously tested high-strength concrete specimens. The spacing and widths of the horizontal cracks varied over the height of the specimen. The spacing ranged from 50 to 200 mm and some of the cracks were hairline and increased in width to 0.15 mm, during the cycles at $0.5\Delta_y$. During the tensile yield cycles some small vertical splitting cracks developed in the specimen. The widths of the cracks increased over the following cycles to a maximum of 1.1 mm at $2.2\Delta_y$. On the compressive portion of this cycle (stage 22B) the cover concrete crushed at a compressive strain of 0.0038 and there was some minor spalling on the back face. It should be noted that there was no abrupt spalling of the cover as was the case with the previous high-strength concrete specimens. Figure 3.31a shows the specimen at this compressive peak. The compressive capacity of Specimen H3 decreased to 8010 kN, which is 76% of the peak load, during the first compressive cycle after crushing of the cover concrete. During the following cycles, at an increase in compressive strain the peak compressive load increased to 8460 kN, which is 81% of the peak capacity. Figure 3.31b shows this specimen after two cycles at a tensile deflection of $2.8\Delta_y$. Failure of the specimen was due to the rupture of some of the transverse hoop reinforcement. Figure 3.31c shows this specimen at

Table 3.6 Key load stages for Specimen H3

Load Stage	Tensile (A) Cycle Applied Load (kN)	Tensile (A) Cycle Axial Deformation (mm)	Compressive (B) Cycle Applied Load (kN)	Compressive (B) Cycle Axial Deformation (mm)	Notes (Δ_y based on tensile cycle)
0	-	-	-1710	-0.86	$0.2A_g f'_c$ (dead load)
1	-1404	-0.86	-3389	-1.63	elastic
4	195	0.36	-4041	-1.91	first cracking
7	513	2.50	-7193	-2.95	$\cong 0.5\Delta_y$
10	1043	4.72	-9457	-4.20	$1.00\Delta_y$
13	1072	6.35	-9767	-4.74	$1.35\Delta_y$
16	1087	7.28	-10095	-4.92	$1.54\Delta_y$
19	1092	9.10	-10235	-5.27	$1.93\Delta_y$
22	1095	10.31	-10471	-5.65	$2.18\Delta_y$
25	1104	13.36	-8460	-7.85	$2.83\Delta_y$
28	1164	15.68	-8205	-9.46	$3.32\Delta_y$
31	1219	20.81	-5699	-12.87	$4.41\Delta_y$
34	1273	25.83	-5203	-15.63	$5.47\Delta_y$

the completion of the test indicating the extent of the spalling of the concrete cover. One of the ruptured hoops is shown in Fig. 3.31d. From this photograph the deterioration of the core concrete evident.

Figure 3.32 shows the applied load versus the axial strain for the multiple regions instrumented over the height of the specimen. The central region underwent the most compressive straining, which is clear considering that the cover concrete had spalled primarily from this area. The strain in the longitudinal bars is given in Fig. 3.33 and these plots indicate that some of the bars were experiencing compressive strains up to 10 times that of yield. Figure 3.34 gives the plot of the strain recorded in the transverse reinforcement. The strain in the transverse steel had not reached half of the yield strain at the peak compressive load, but after the crushing of the cover concrete the strain started to increase at a greater rate.

3.4 Comparison of Reversed Cyclic Responses of the Axially Loaded Specimen

The peak compressive loads and strains for all of the axially loaded specimens are summarized in Table 3.7.

Table 3.7 Peak compressive loads and strains for the axially loaded specimens

Specimen	Peak Load (kN)	Post Peak		Peak Load Strain	Maximum Strain
		Load (kN)	% of Peak Load		
N1	5801	-	-	0.00388	-
N2	6437	4333	67.3	0.00391	0.00709
N3	6407	5453	85.1	0.00365	0.01570
H1	8457	-	-	0.00239	-
H2	10066	3252	32.3	0.00369	0.00769
H3	10471	8460	80.8	0.00377	0.01091

For both the normal and high-strength concrete specimens, there was an improvement in both the post-peak capacity and maximum strain reached as the confinement of the concrete core was increased. Both of the highly confined specimens were able to reach over 80% of the peak load capacity after the spalling of the cover concrete had occurred. The strain at which the peak load was reached was approximately the same for all of the specimens, except for the high-strength concrete specimen with "beam details". It should be noted that this strain is approximately 60% higher than the strain corresponding to the peak compressive stress for the normal-strength concrete. In comparison, the strain at peak load for the high-strength concrete specimens with column details is 23% greater than the strain corresponding to the peak compressive stress for that concrete.

Figure 3.35 shows plots comparing the load versus axial deformation envelopes for all of the specimens. The top two plots compare the specimens constructed with the same concrete, while the other three plots compare the normal and high-strength specimens designed with the same transverse confinement details. It is clear from these plots that the specimens constructed with the same concrete showed the same tensile performance and similar compressive performances up to approximately 75% of the peak load. After this loading level the specimens with the greater amount of transverse confinement had increased load carrying capacity and greater deformability. For the plots comparing the specimens with similar detailing, the specimens constructed with high-strength concrete had a stiffer compressive response and similar peak compressive strains as the normal-strength specimens. The rupture of the hoop reinforcement in Specimen H3 reduced its ability to deform in compression but up to that point the post-peak response was very good. Figure 3.36 shows all of the specimens at the completion of testing, allowing for a visual comparison of the failure of each.

3.5 Conclusions Based on Observed Behaviour

The following conclusions can be made based on the observed hysteretic responses of the axially loaded specimens.

1. The spacing and configuration of the transverse reinforcement dramatically changed the responses of the specimens for both concrete strengths. The post-peak compressive capacity of each of the specimens was greatly improved by reducing the spacing of the transverse reinforcement and supporting each longitudinal bar by the corner of a hoop.
2. The specimens detailed as ductile columns performed extremely well for both concrete strengths. The peak compressive strains and post-peak compressive capacities for these specimens increased with respect to the specimens with smaller amounts of transverse reinforcement. The post-peak response of the high-strength specimen was limited by the ductility of the high-strength transverse reinforcement. The high-strength concrete specimen with ductile detailing shows that high-strength concrete can perform as well as normal-strength concrete when adequate confinement is provided.
3. Spalling of the cover concrete was a significant event in the response of the specimens, with this occurring at a similar compressive strain for all specimens, just below 0.004, except for Specimen H1. The spalling of the cover concrete of Specimen H1 occurred at a compressive strain of 0.0024, which was probably instigated by the splitting cracks in the cover concrete reducing the lateral restraint of the longitudinal bars, resulting in the buckling of these bars.
4. Buckling of the longitudinal reinforcement was a significant event once the cover concrete had spalled. There was visible buckling of the longitudinal reinforcement in all of the specimens, with this event occurring at a smaller compressive strain as the spacing of the transverse reinforcement increased.
5. These tests on axially loaded specimens provide basic data for the development of more detailed behavioural models. In order to predict the reversed cyclic loading response, it is essential to account for the following:
   - confinement;
   - cover spalling;
   - bar buckling;
   - crack closing; and
   - strength of concrete

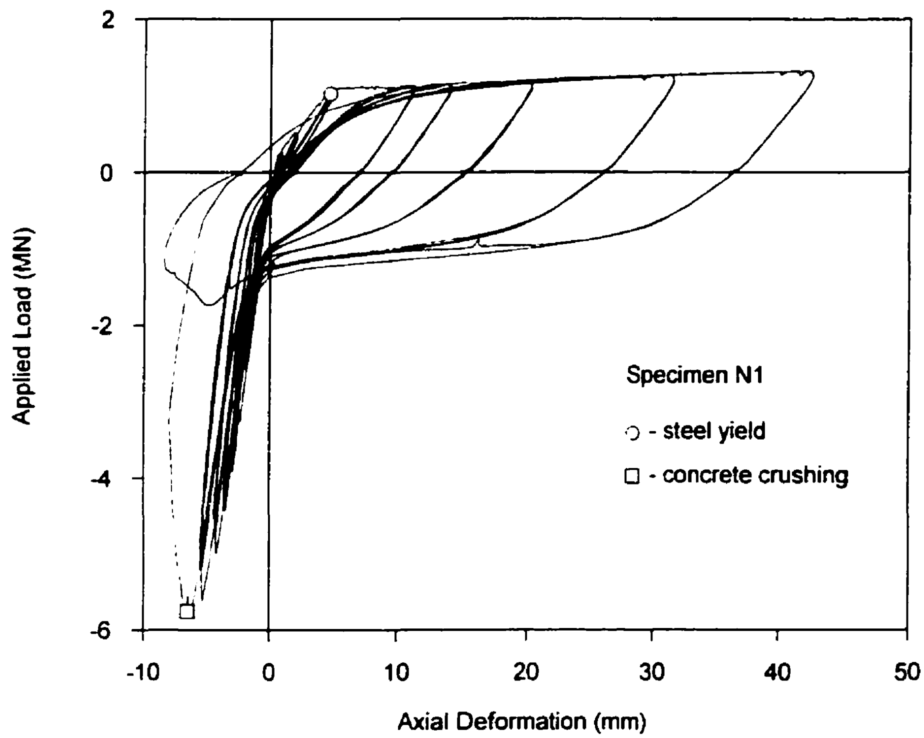

Figure 3.1 Load versus axial deformation response of Specimen N1

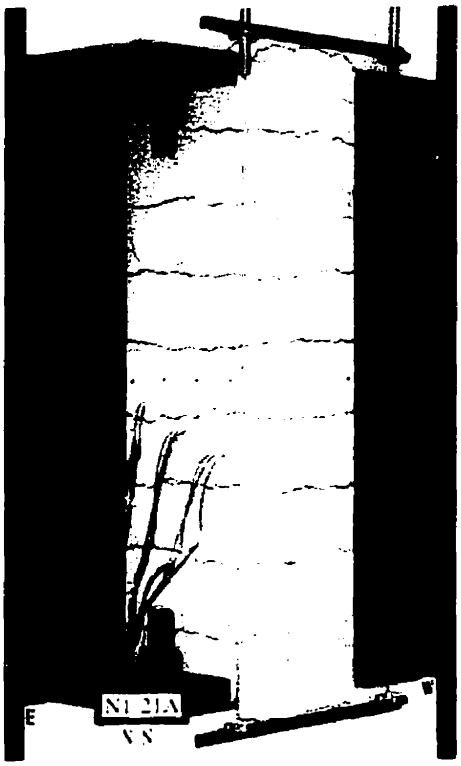

(a) deformation of $6.97\Delta_y$

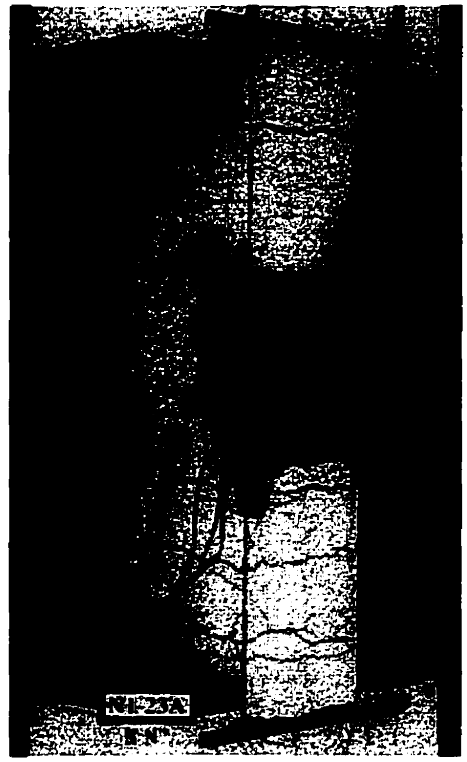

(b) cover spalling

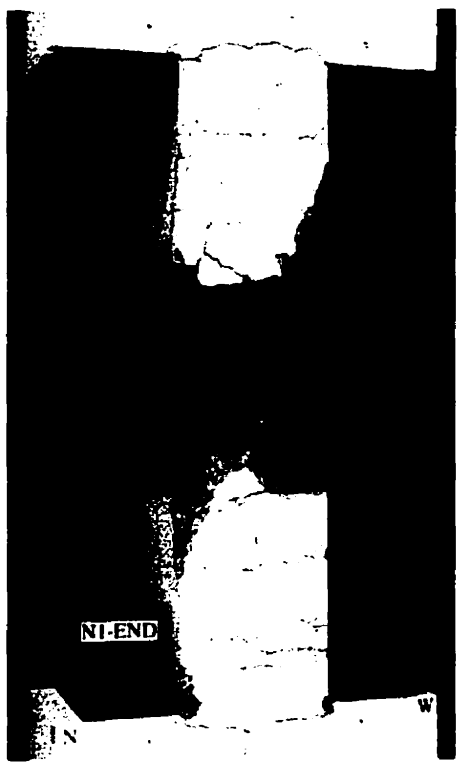

(c) completion of testing

Figure 3.2 Photographs of Specimen N1

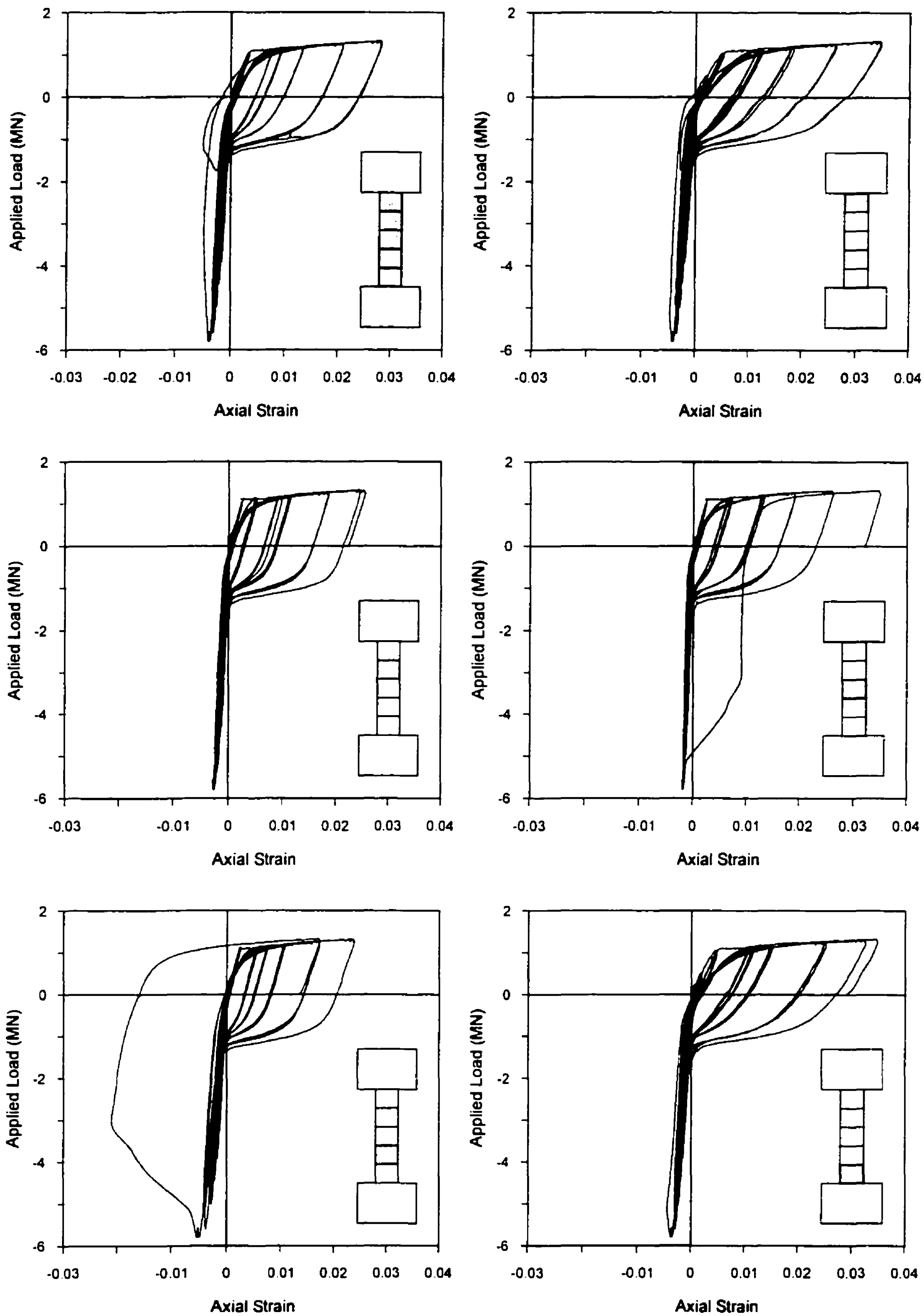

Figure 3.3 Axial strains in different segments of Specimen N1

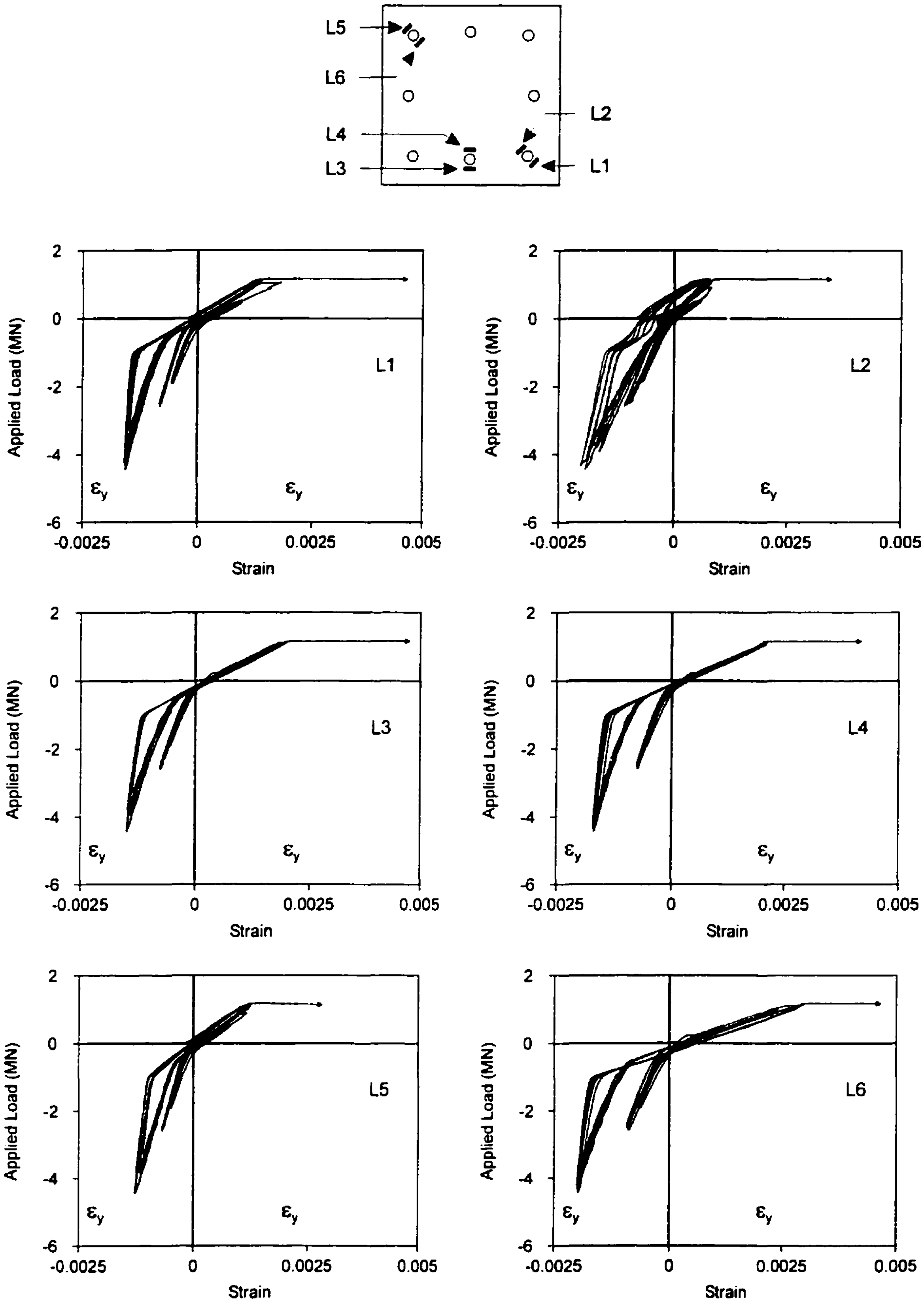

Figure 3.4 Measured strains in longitudinal reinforcement of Specimen N1

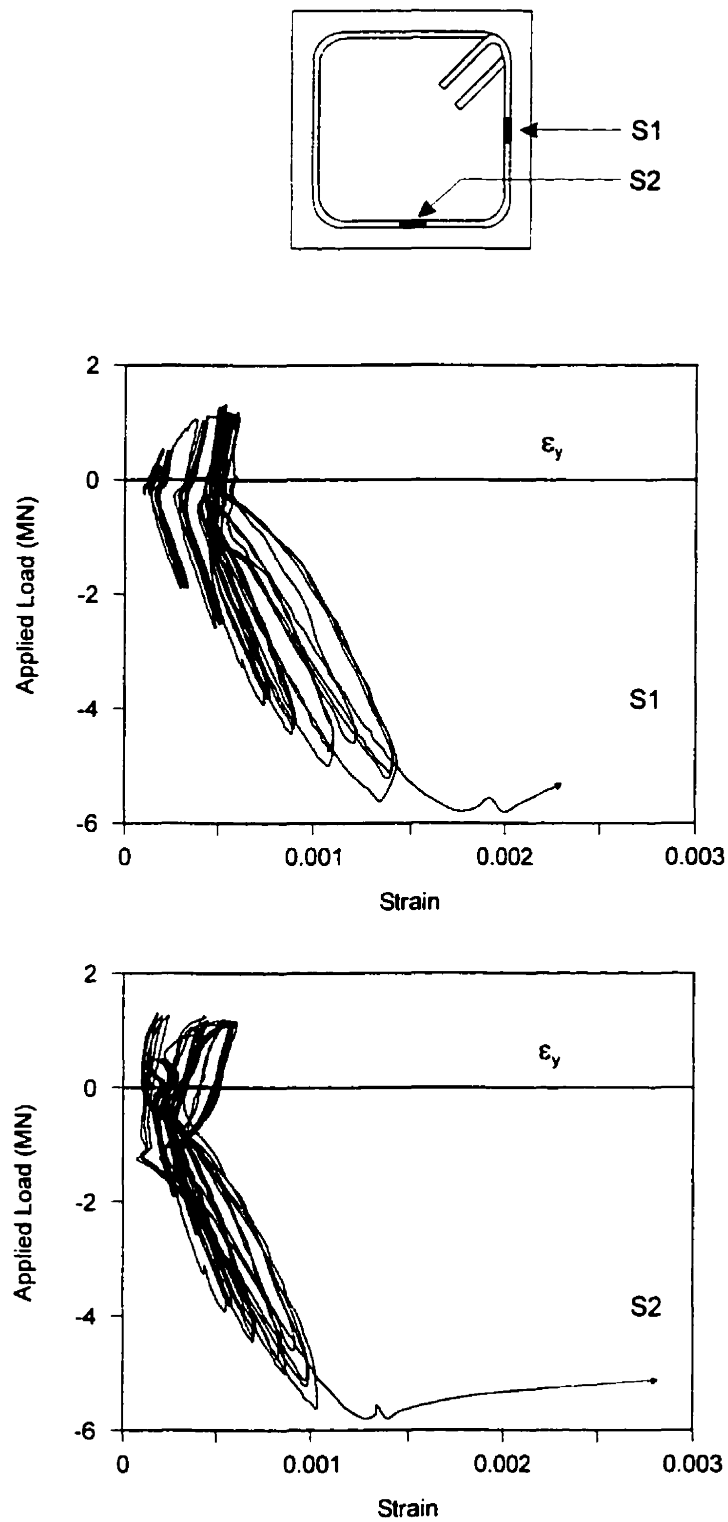

Figure 3.5 Measured strains in hoop reinforcement of Specimen N1

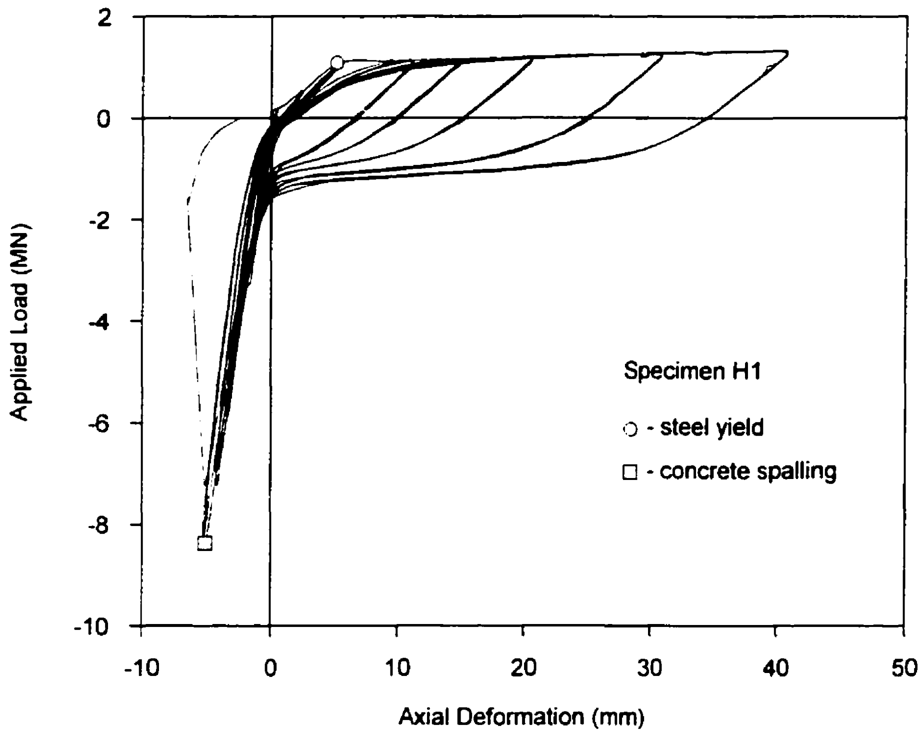

Figure 3.6 Load versus axial deformation response of Specimen H1

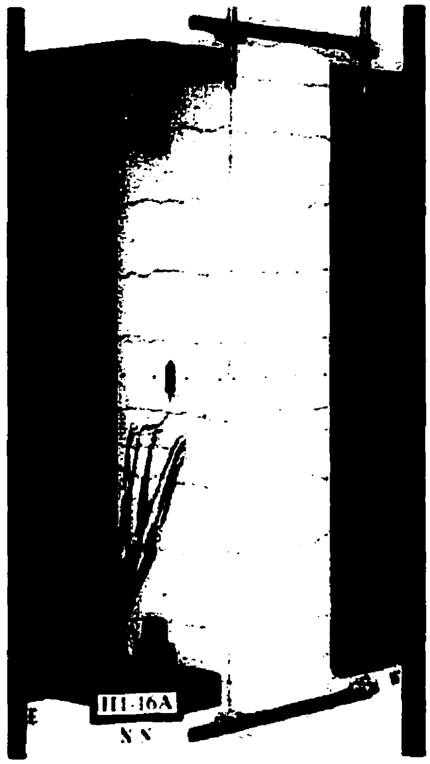

(a) deformation of 3.18Δ_y

(b) completion of testing

Figure 3.7 Photographs of Specimen H1

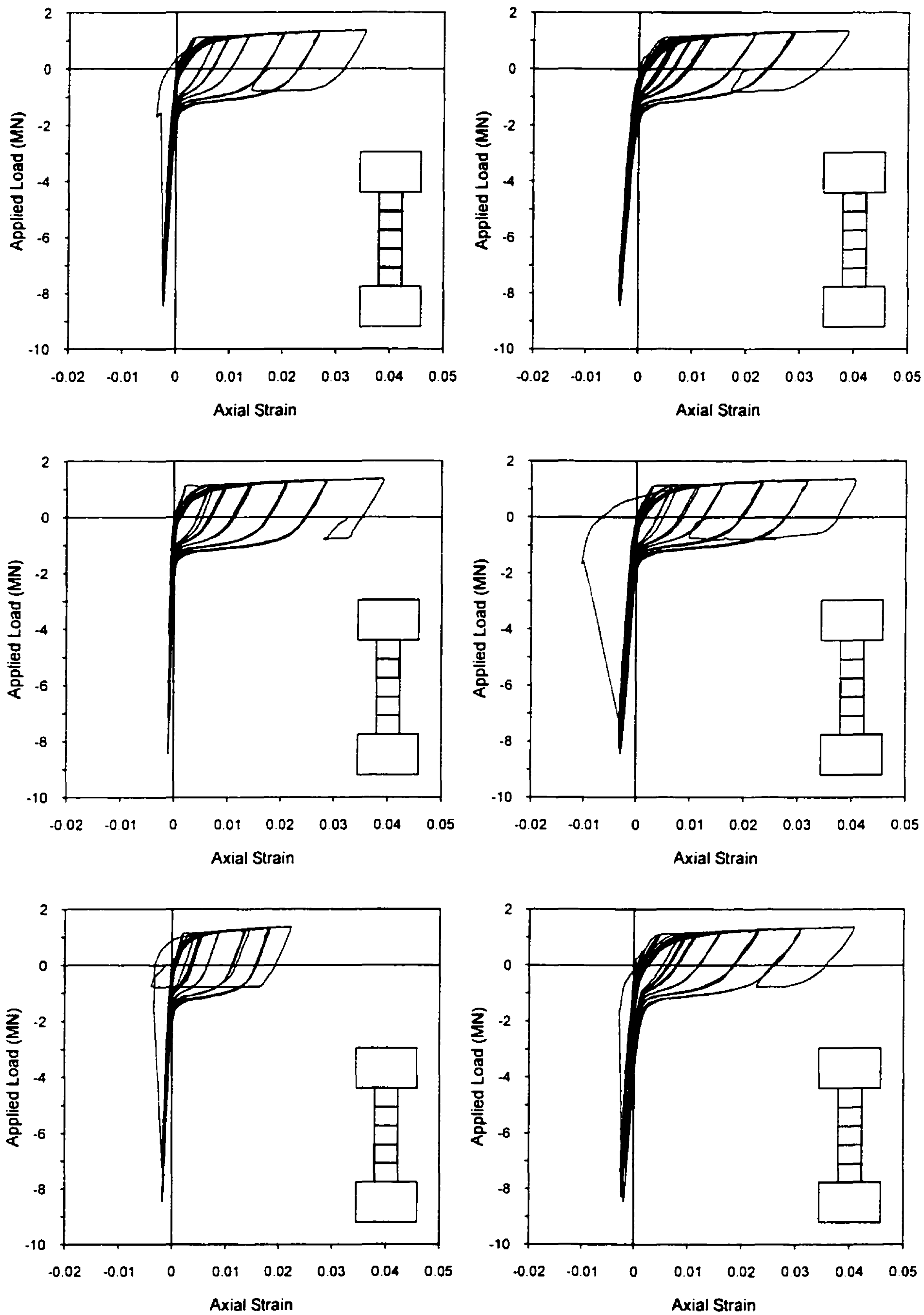

Figure 3.8 Axial strains in different segments of Specimen H1

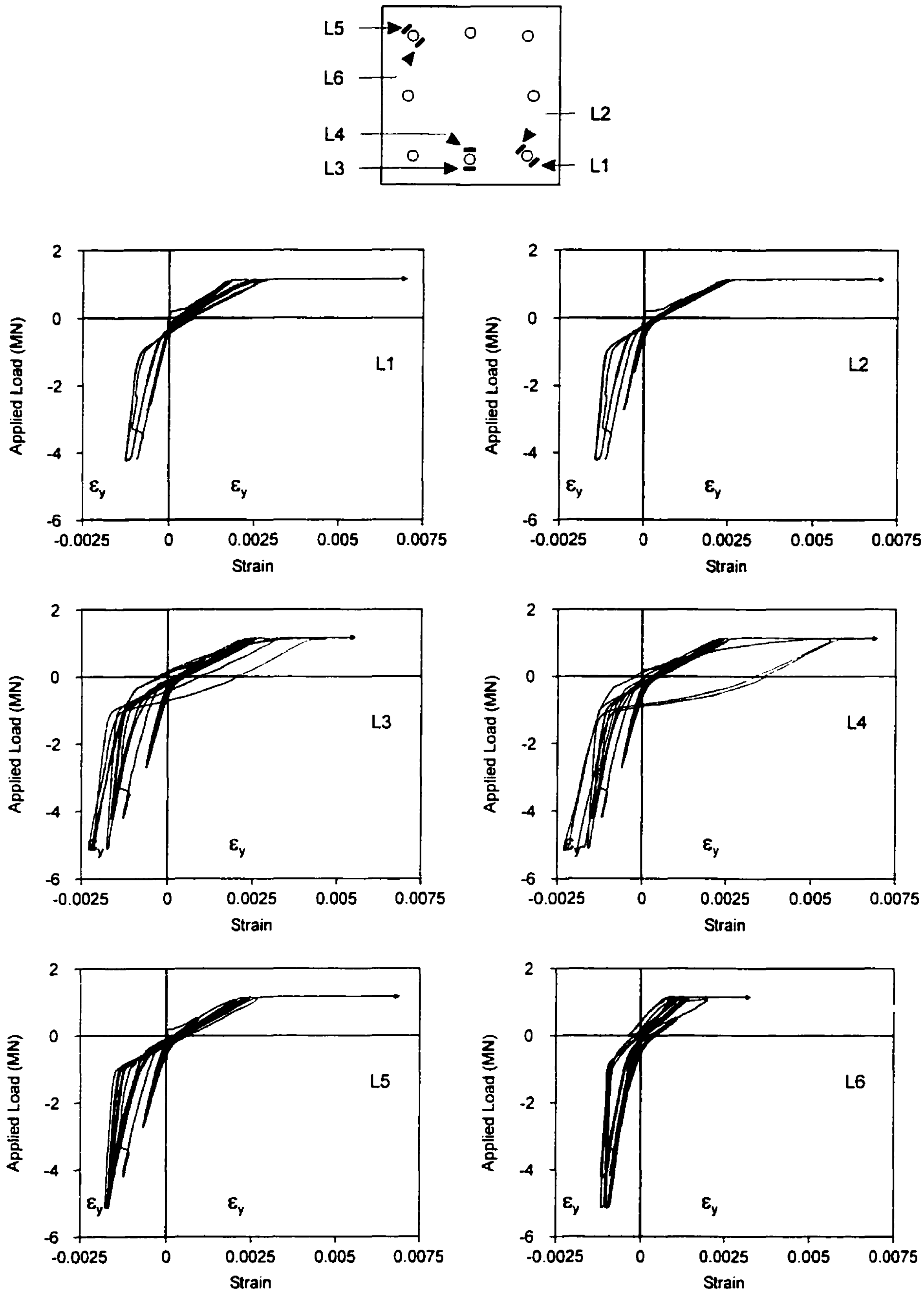

Figure 3.9 Measured strains in longitudinal reinforcement of Specimen H1

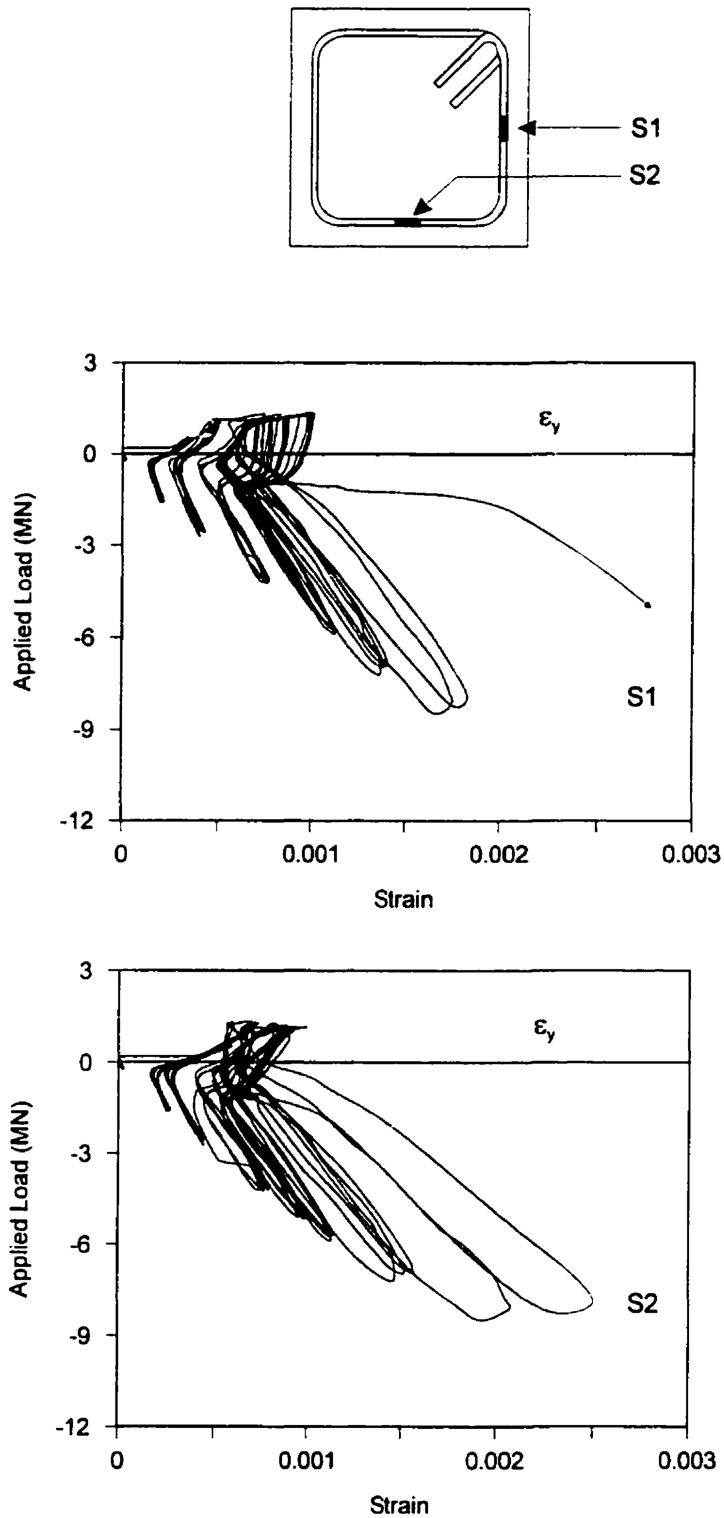

Figure 3.10 Measured strains in hoop reinforcement of Specimen H1

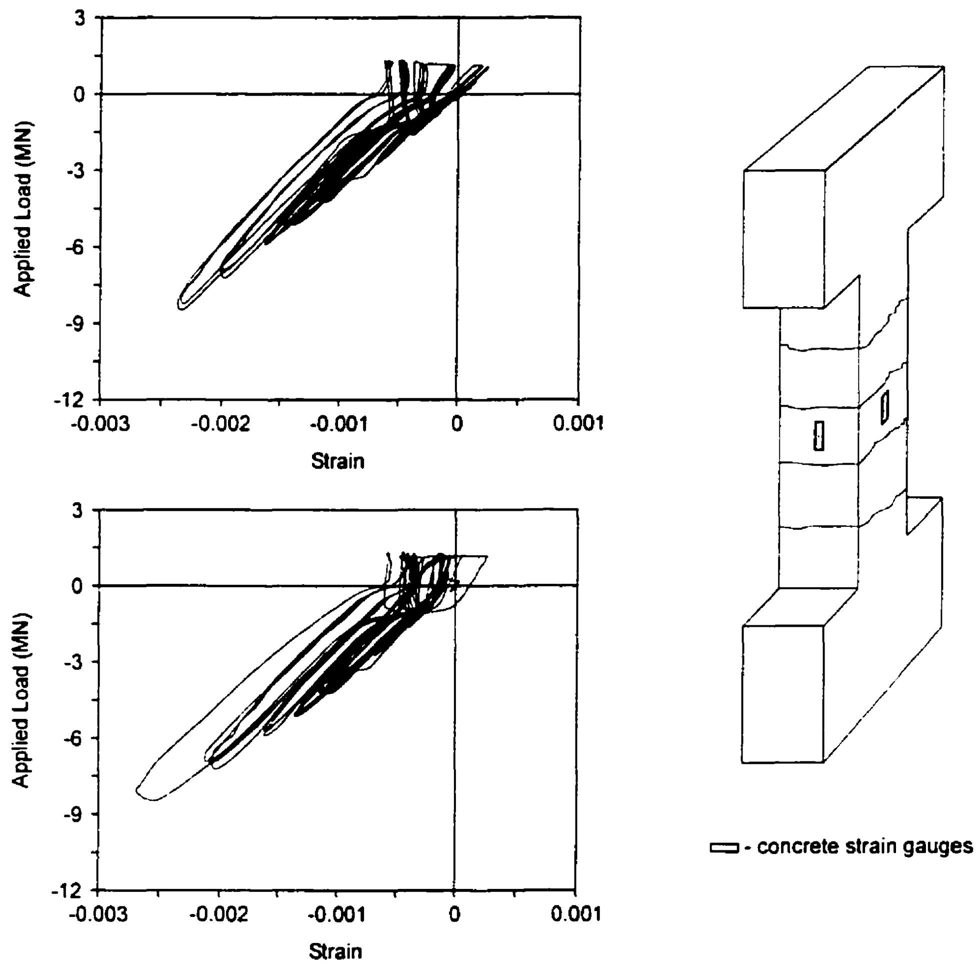

Figure 3.11 Measured axial concrete strains between cracks of Specimen H1

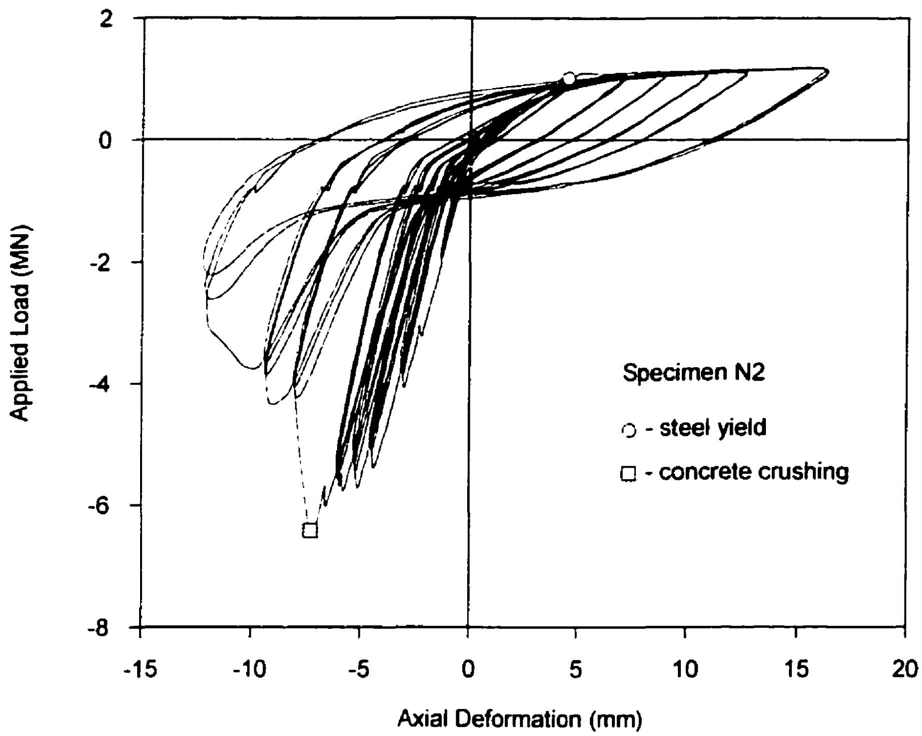

Figure 3.12 Load versus axial deformation response of Specimen N2

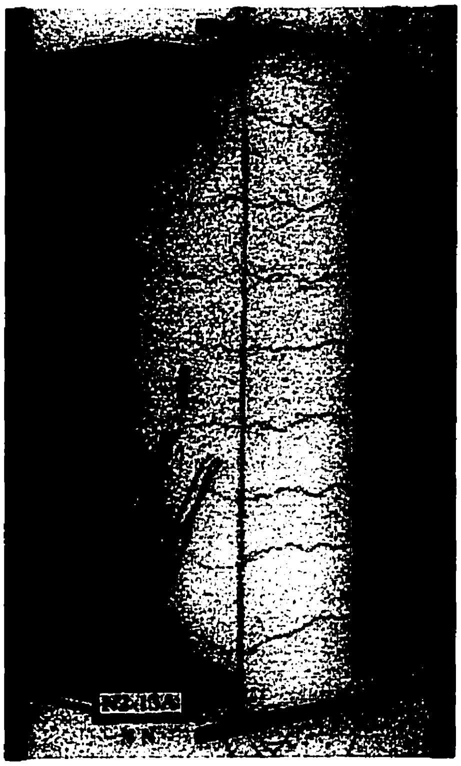

(a) deformation of $1.47\Delta_y$

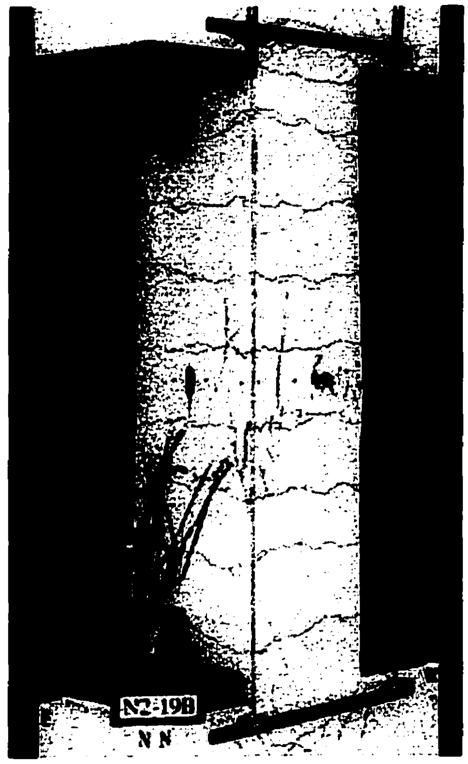

(b) concrete crushing

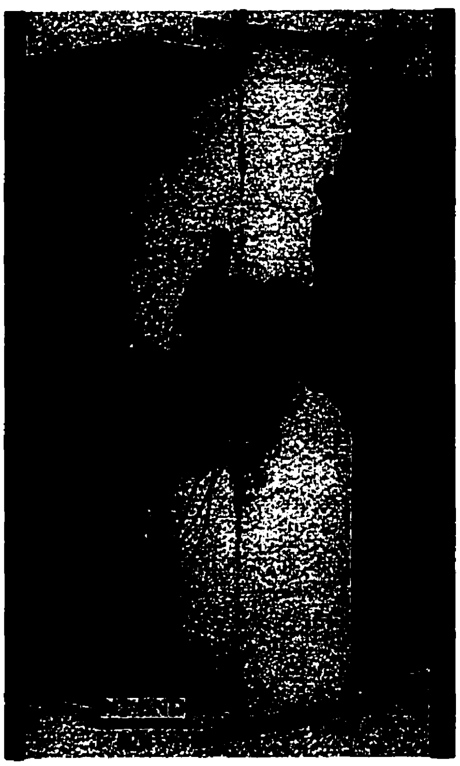

(c) completion of testing

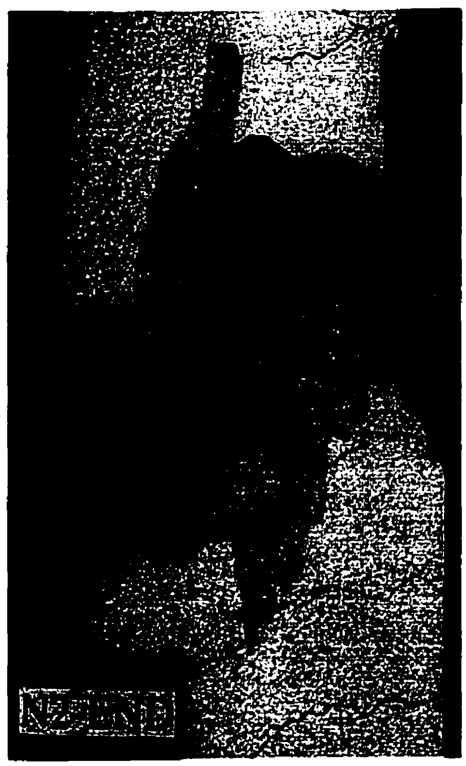

(d) close up at completion of testing

Figure 3.13 Photographs of Specimen N2

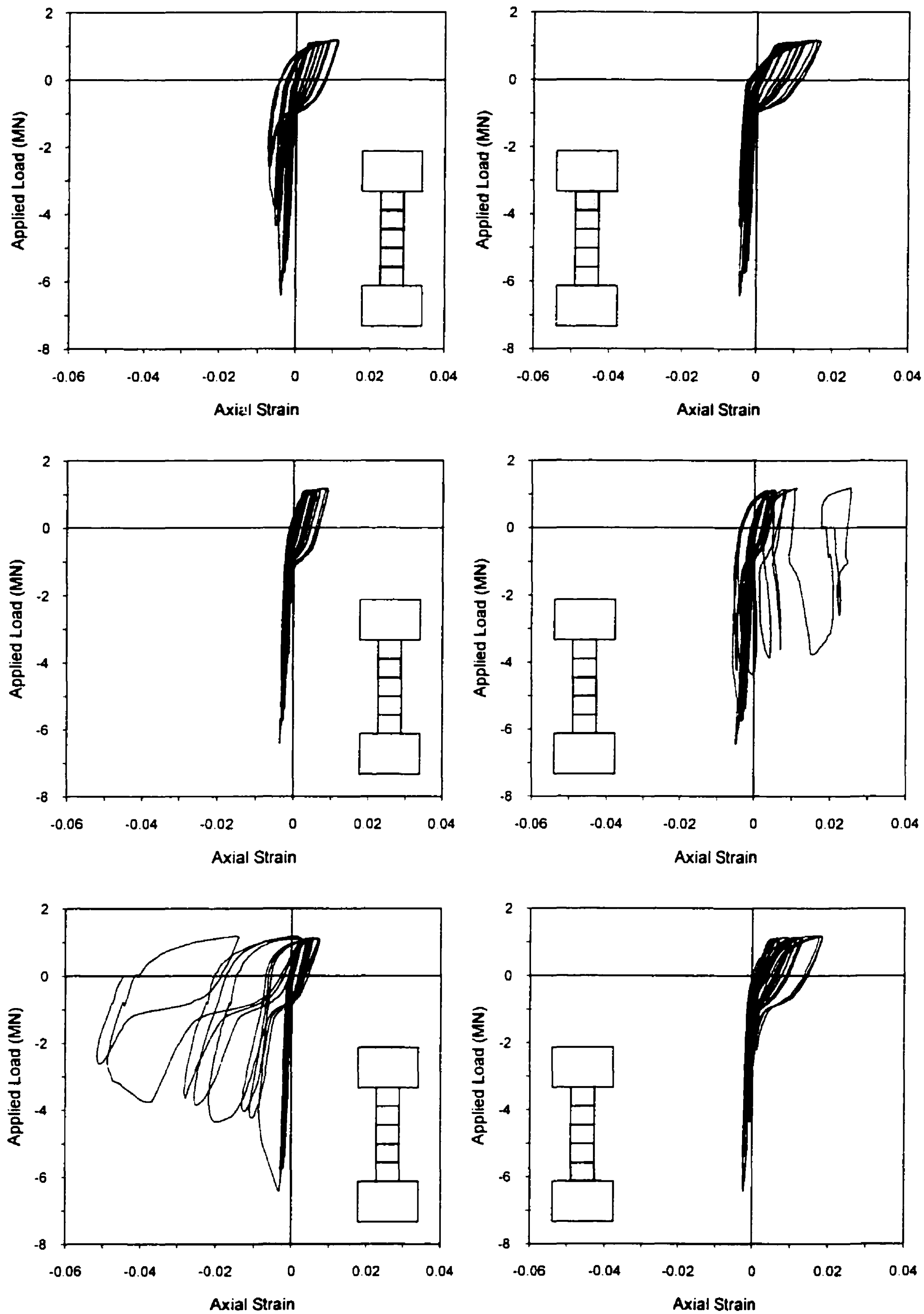

Figure 3.14 Axial strains in different segments of Specimen N2

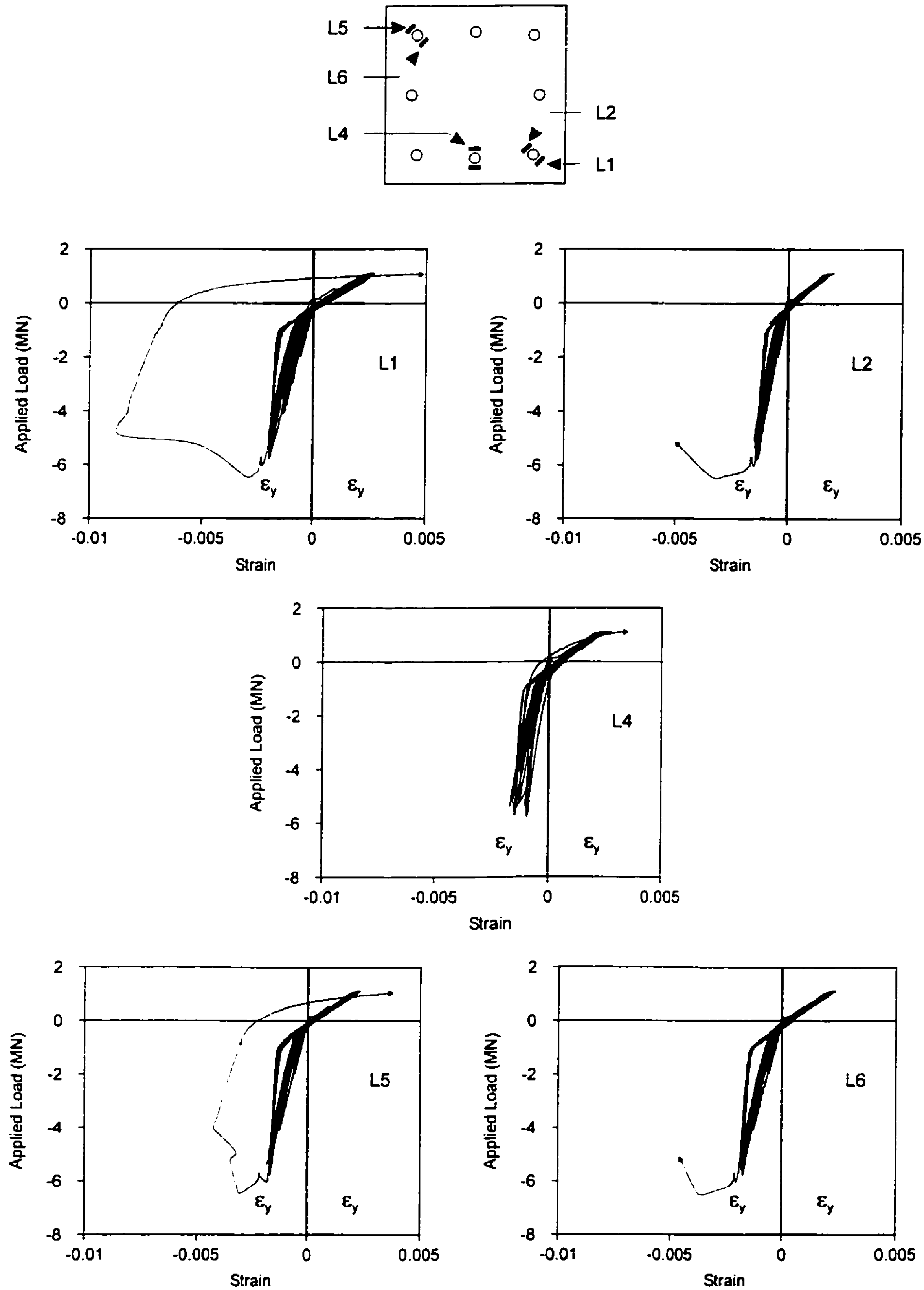

Figure 3.15 Measured strains in longitudinal reinforcement of Specimen N2

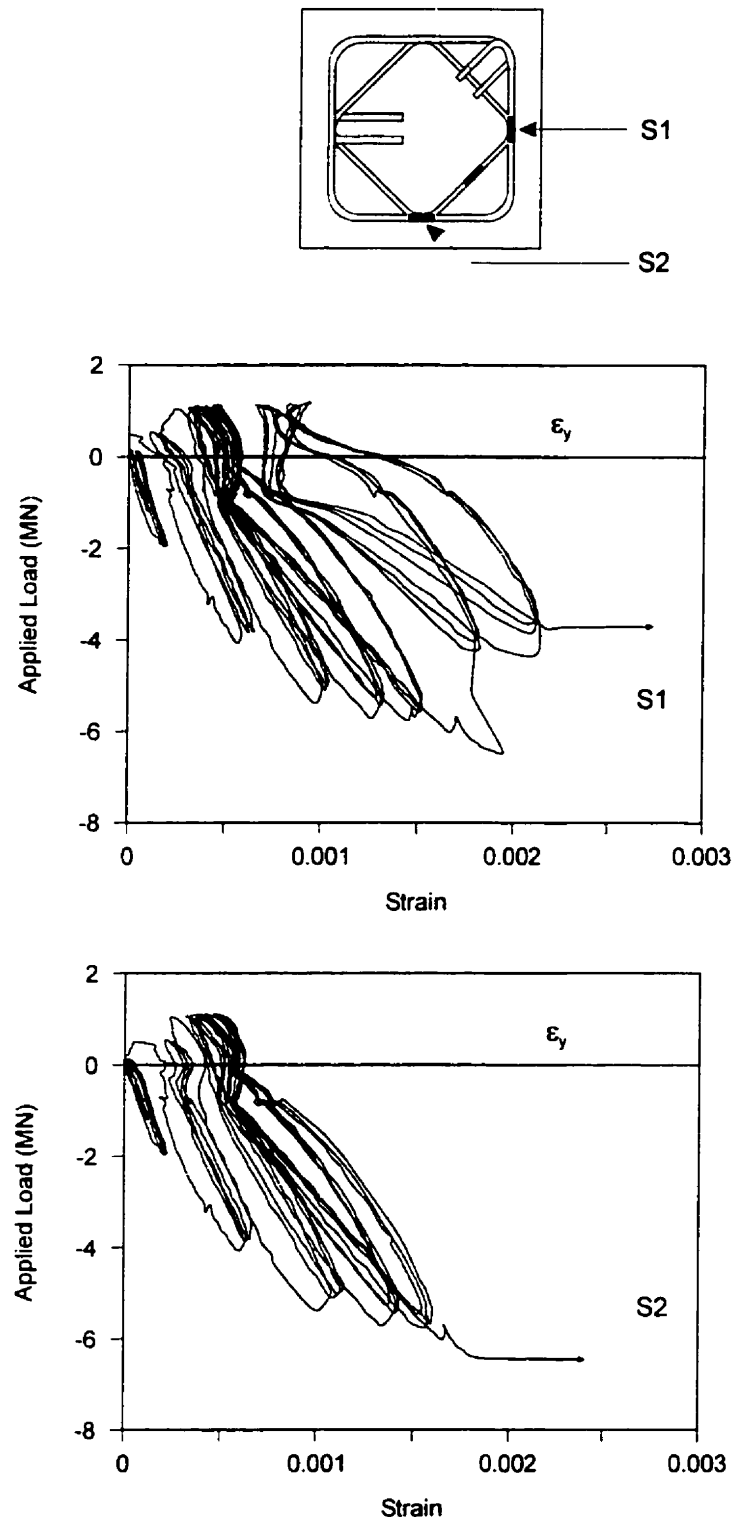

Figure 3.16 Measured strains in hoop reinforcement of Specimen N2

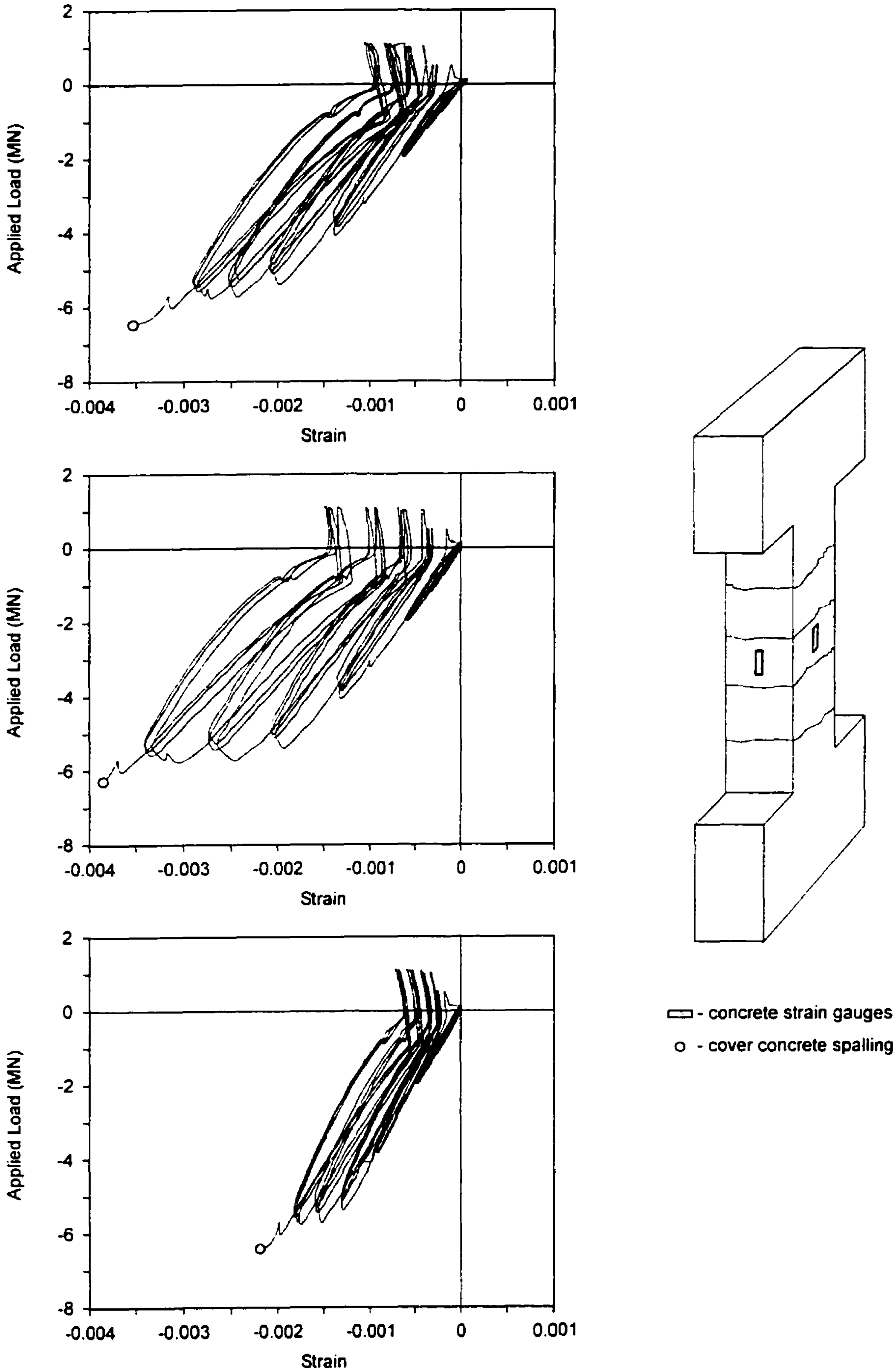

Figure 3.17 Measured axial concrete strains between cracks of Specimen N2

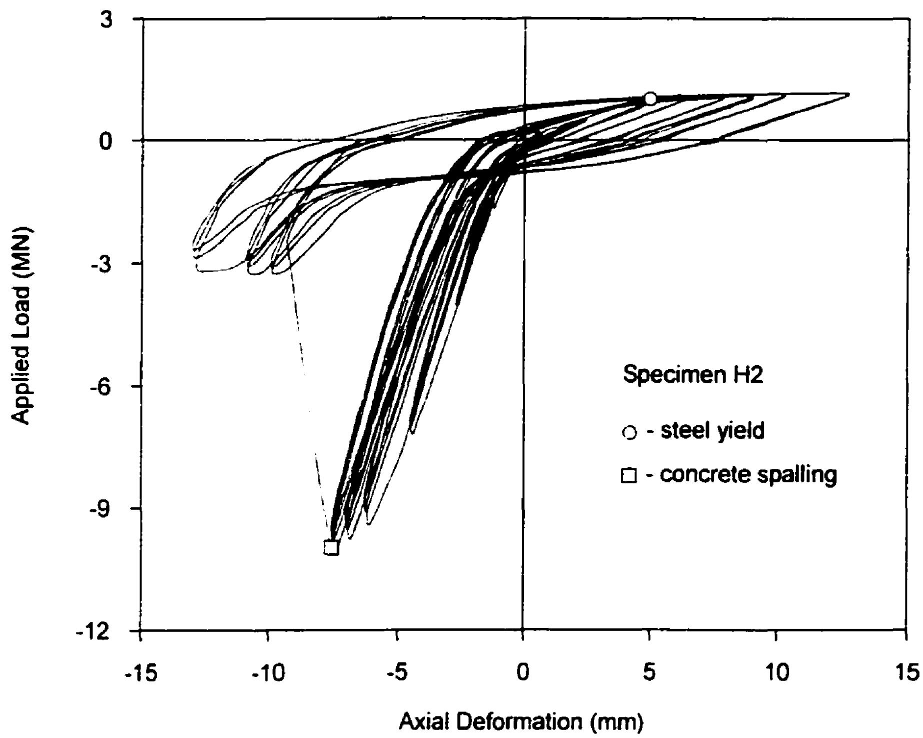

Figure 3.18 Load versus axial deformation response of Specimen H2

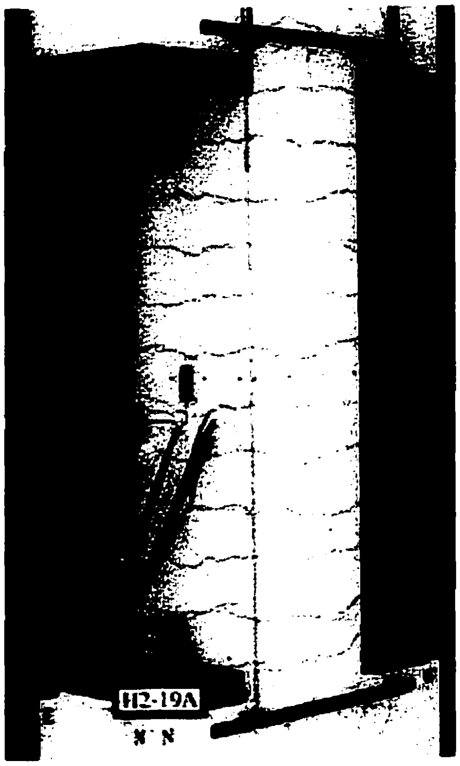

(a) deformation of 1.83Δ_y

(b) cover spalling

(c) completion of testing

Figure 3.19 Photographs of Specimen H2

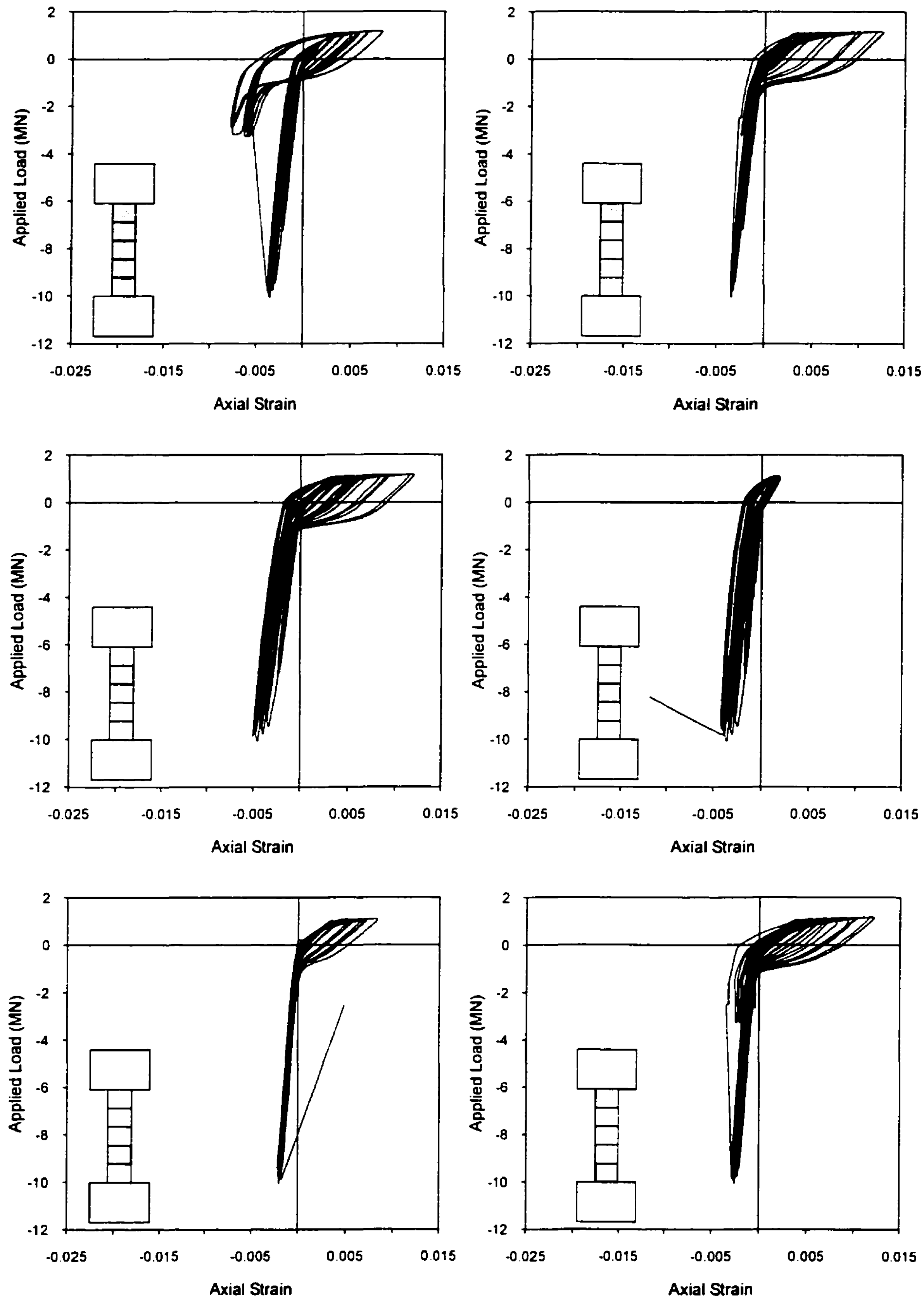

Figure 3.20 Axial strains in different segments of Specimen H2

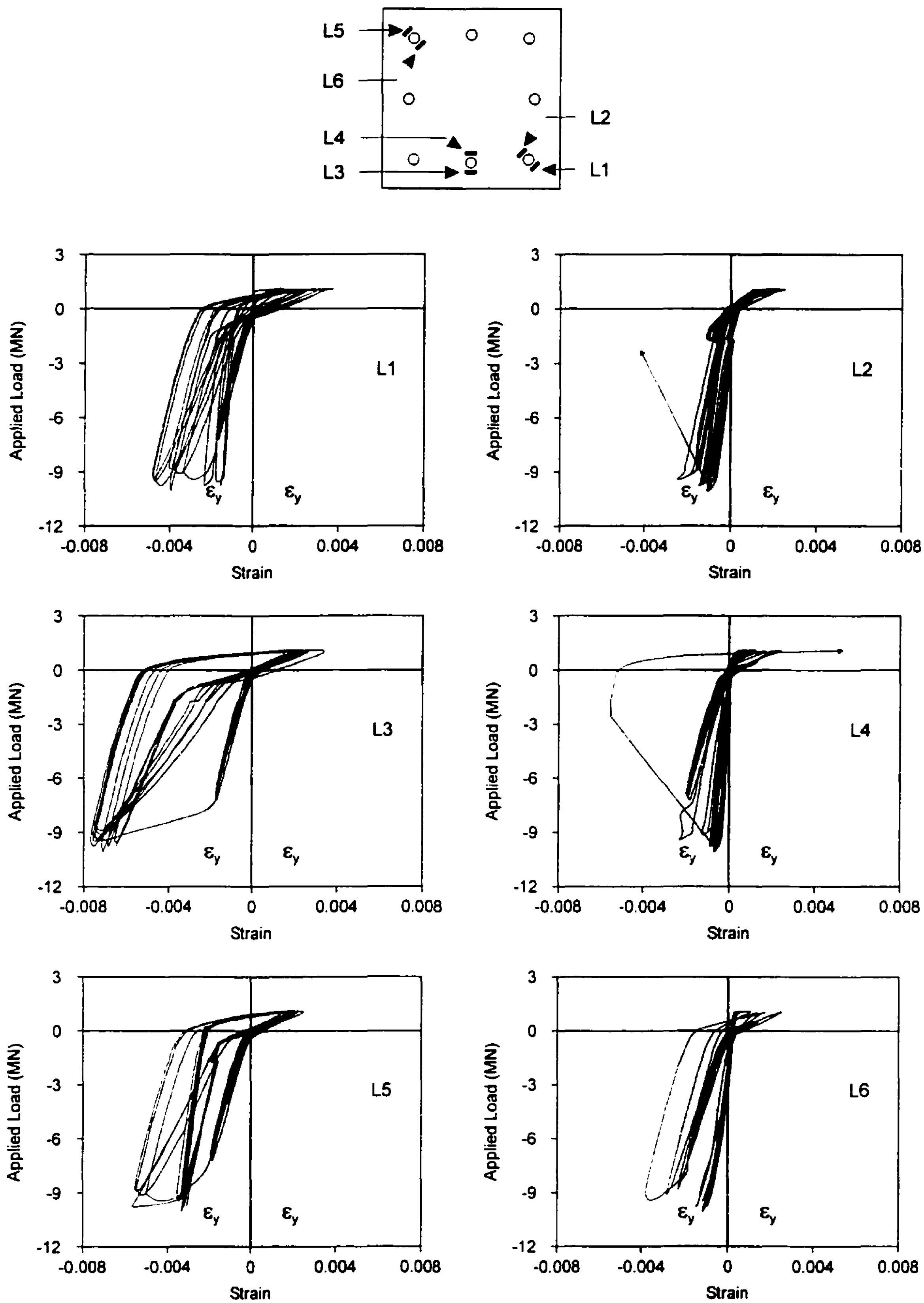

Figure 3.21 Measured strains in longitudinal reinforcement of Specimen H2

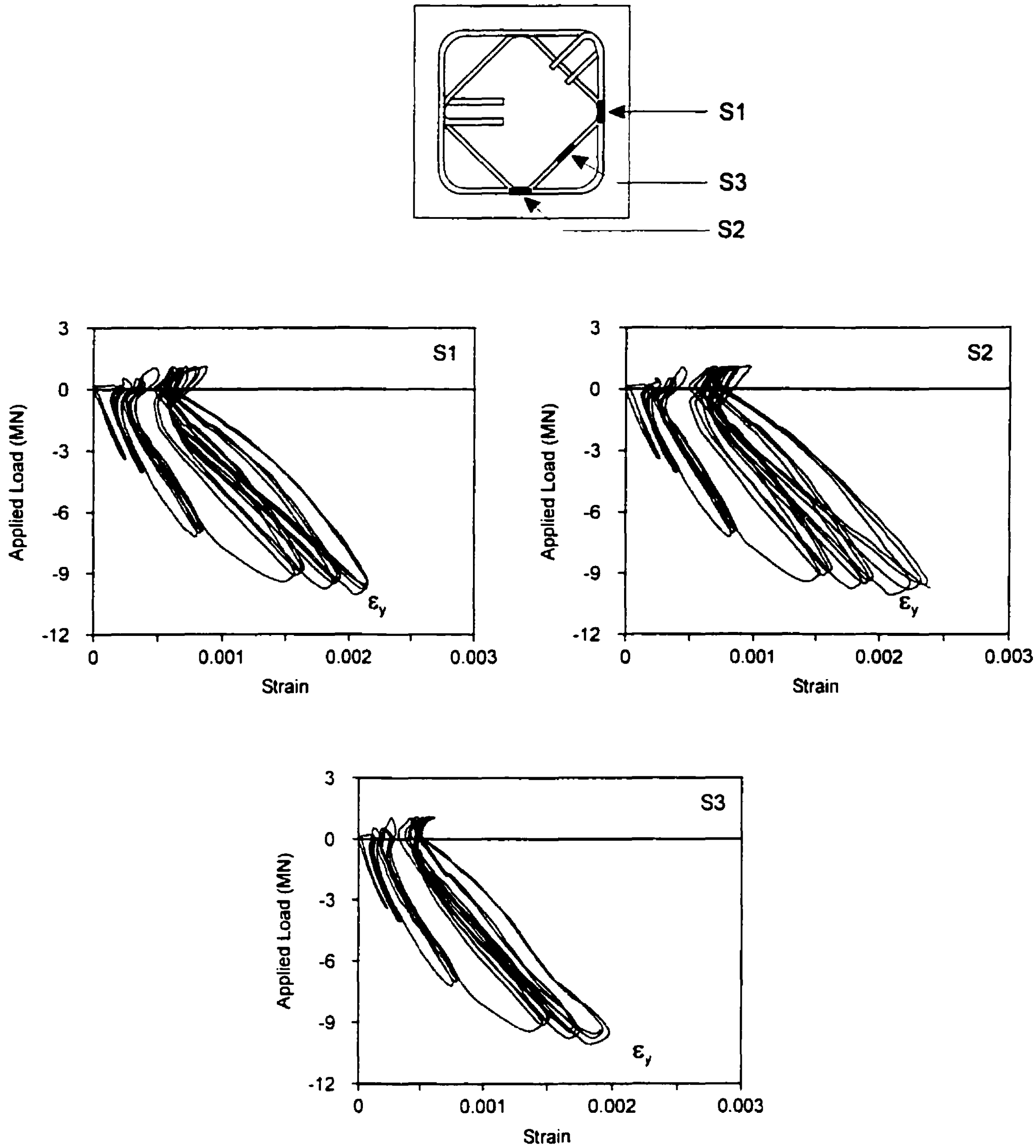

Figure 3.22 Measured strains in hoop reinforcement of Specimen H2

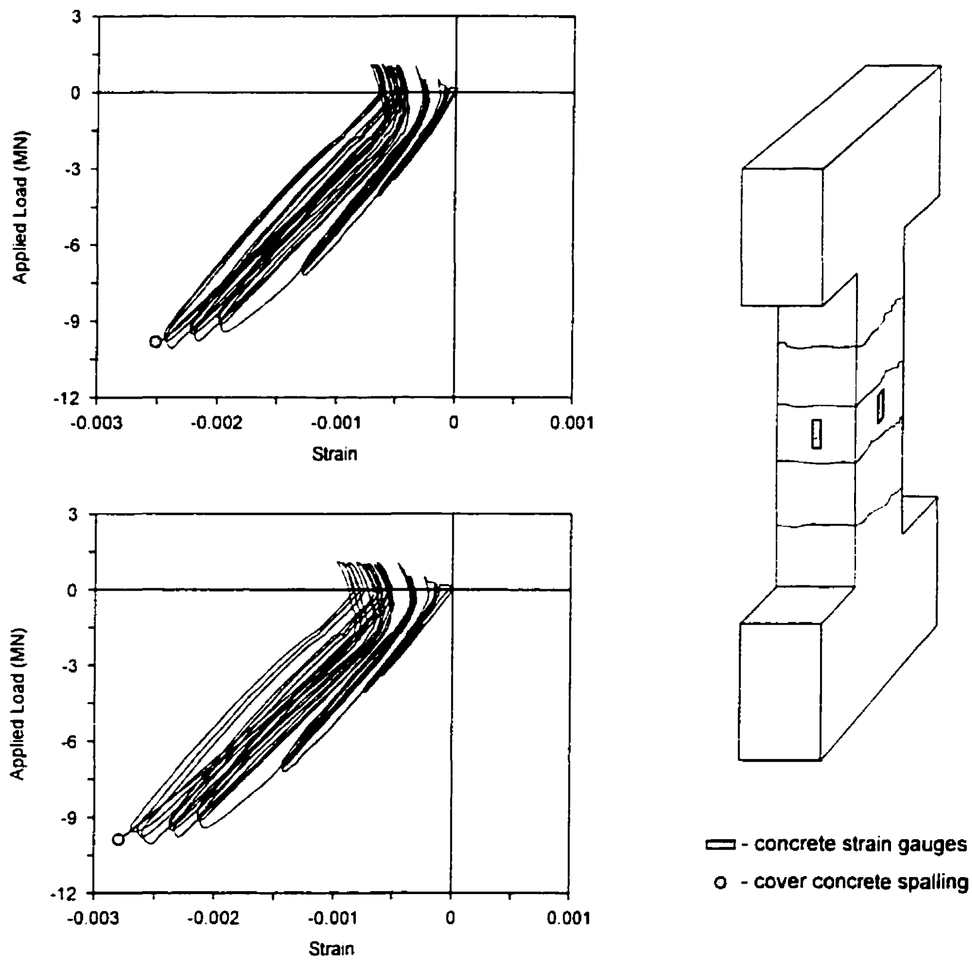

Figure 3.23 Measured axial concrete strains between cracks of Specimen H2

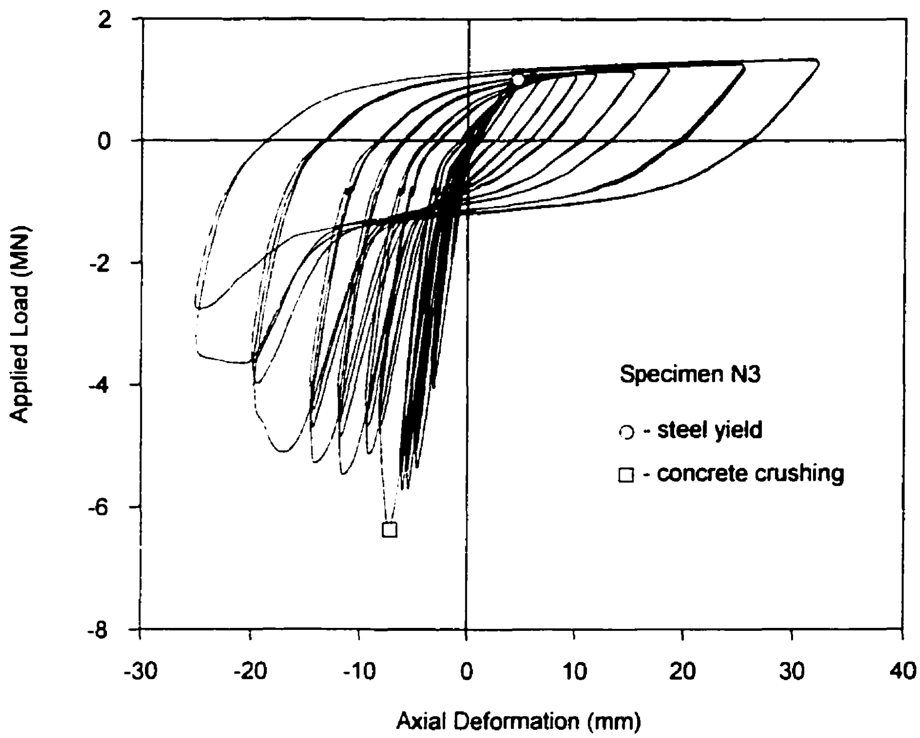

Figure 3.24 Load versus axial deformation response of Specimen N3

(a) deformation of $3.35\Delta_y$

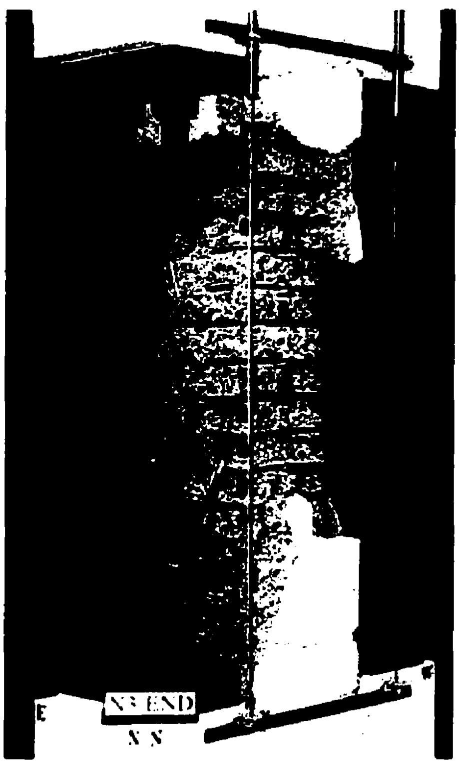

(b) completion of testing

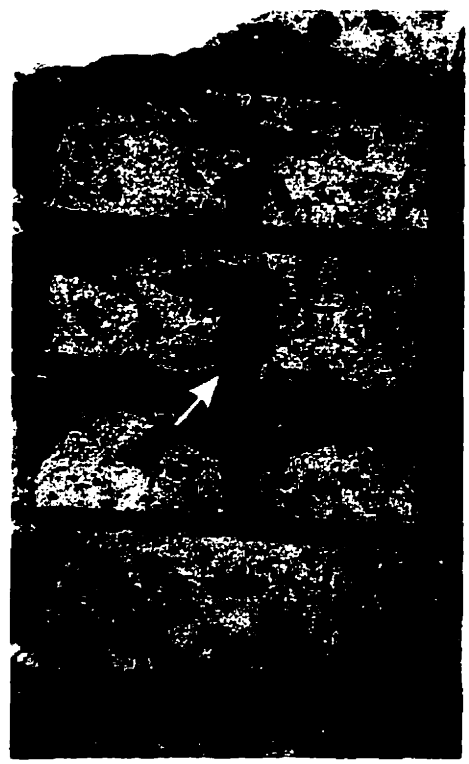

(c) ruptured longitudinal bar

Figure 3.25 Photographs of Specimen N3

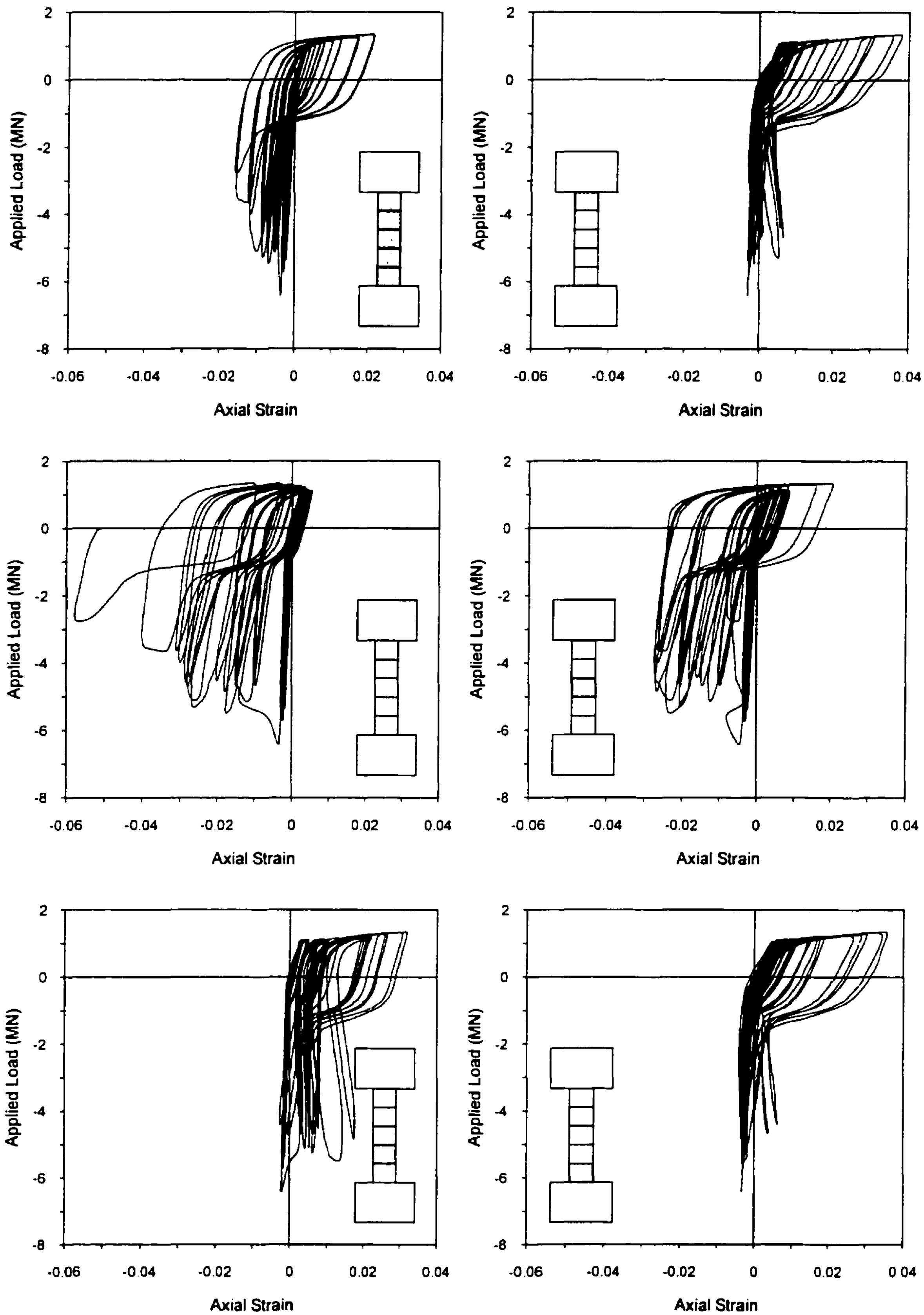

Figure 3.26 Axial strains in different segments of Specimen N3

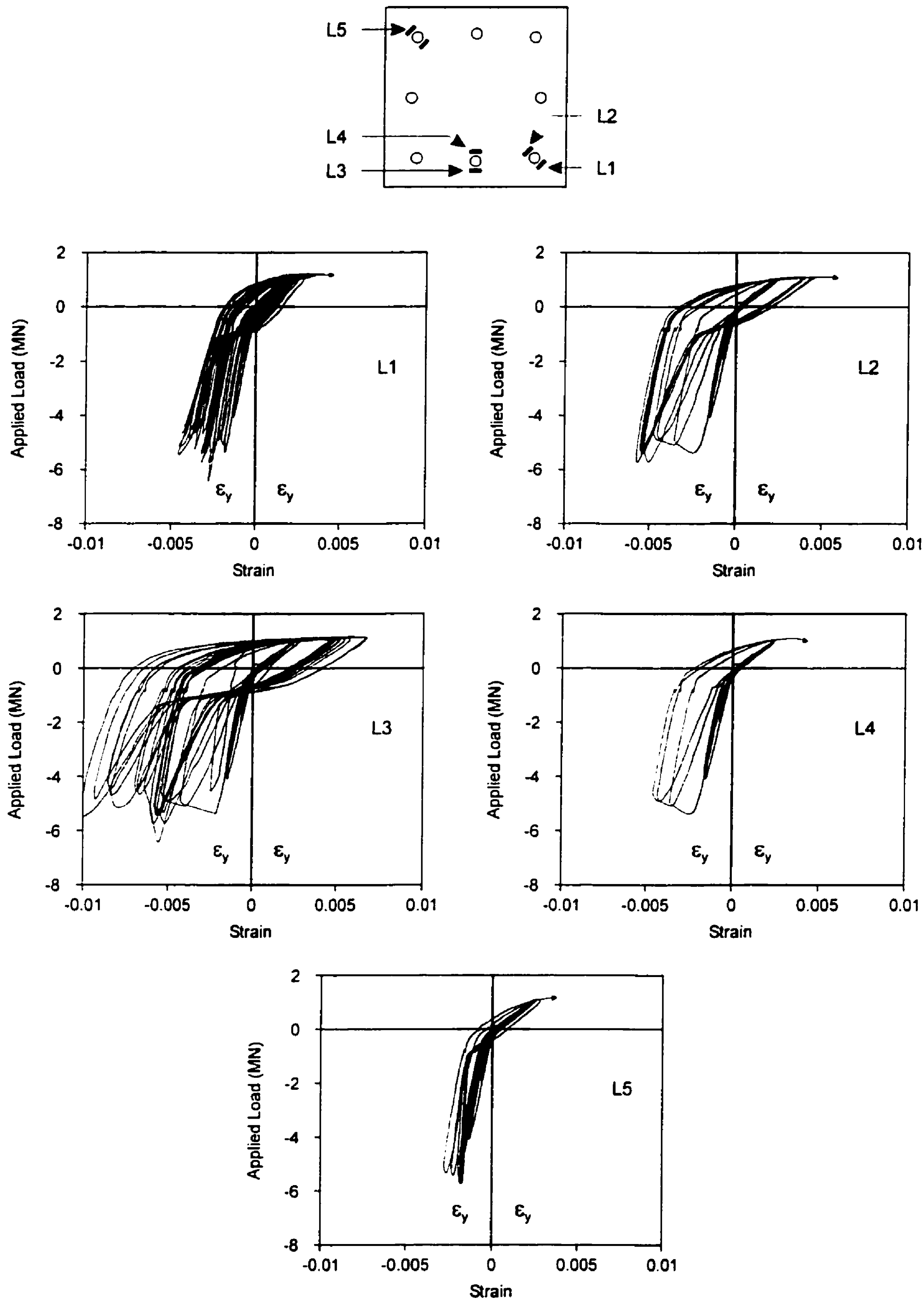

Figure 3.27 Measured strains in longitudinal reinforcement of Specimen N3

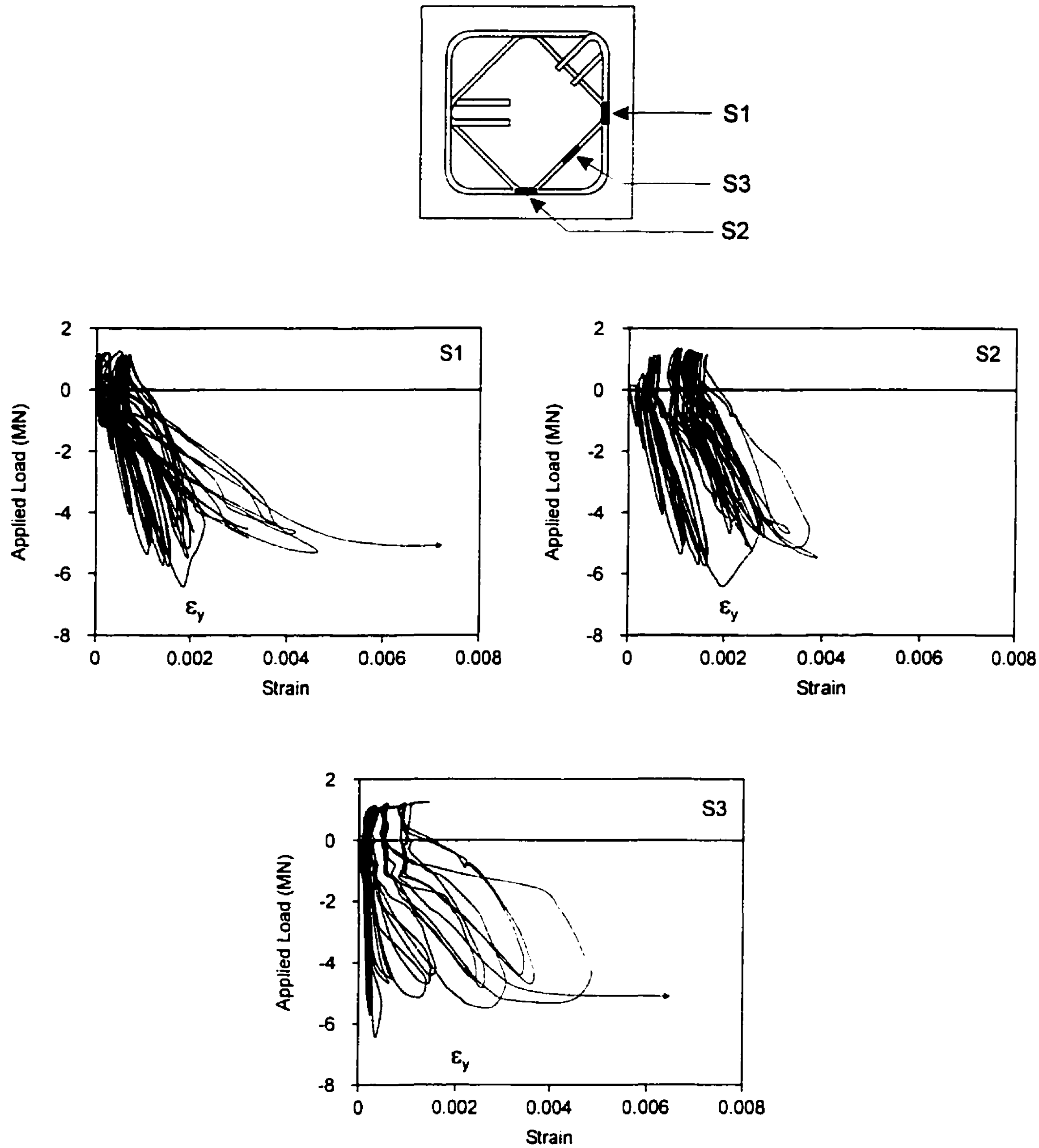

Figure 3.28 Measured strains in hoop reinforcement of Specimen N3

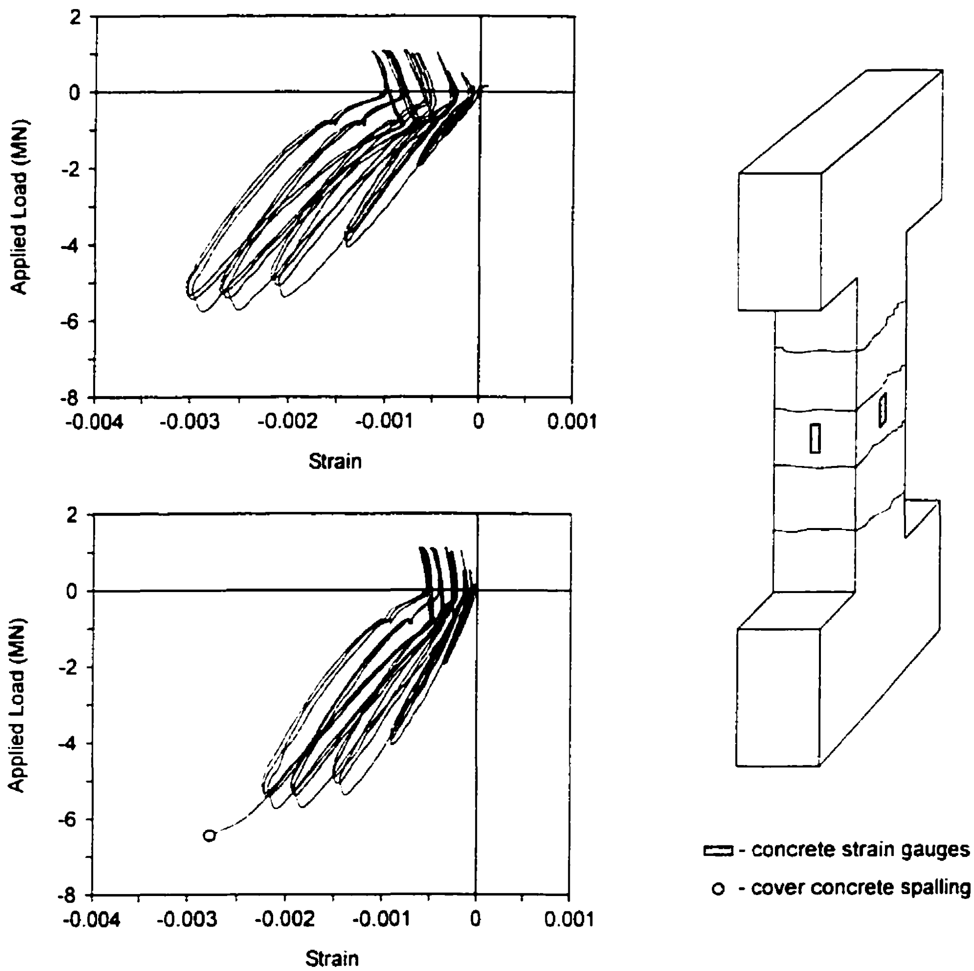

Figure 3.29 Measured axial concrete strains between cracks of Specimen N3

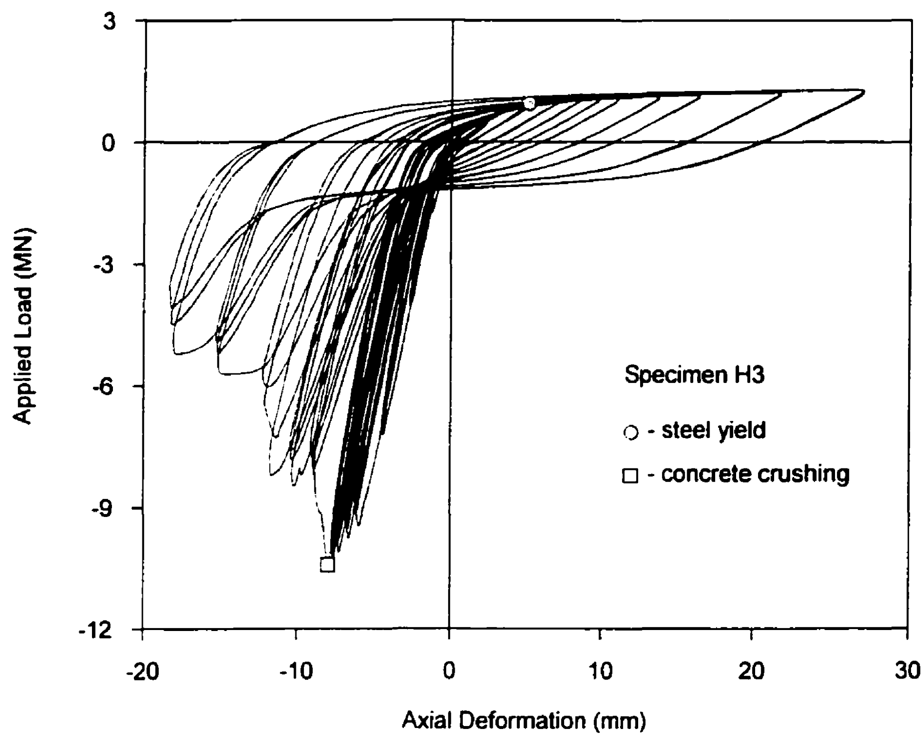

Figure 3.30 Load versus axial deformation response of Specimen H3

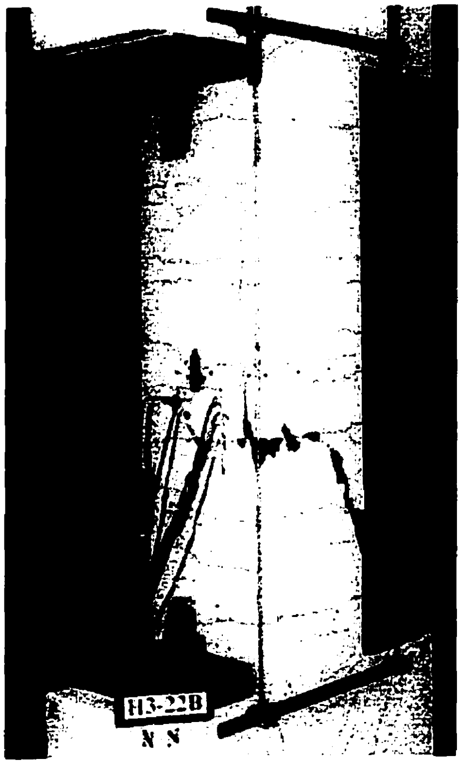

(a) concrete crushing

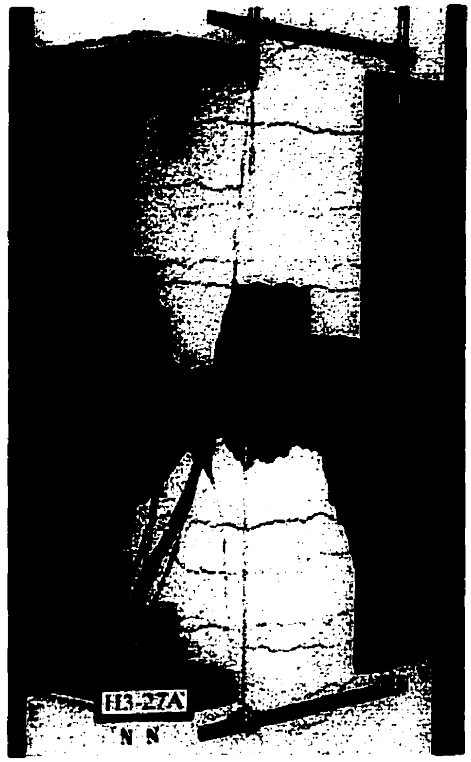

(b) deformation of $2.8\Delta_y$

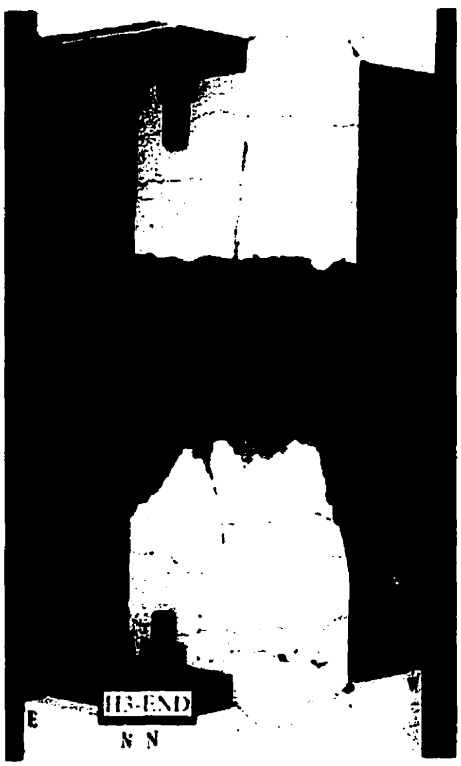

(c) completion of testing

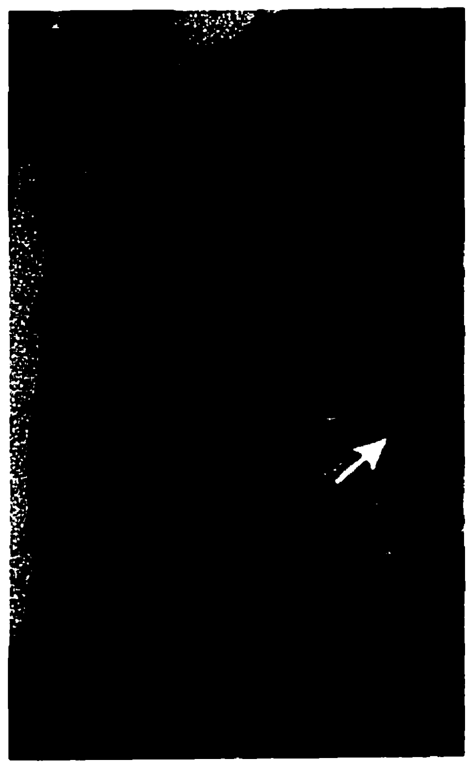

(d) ruptured hoop

Figure 3.31 Photographs of Specimen H3

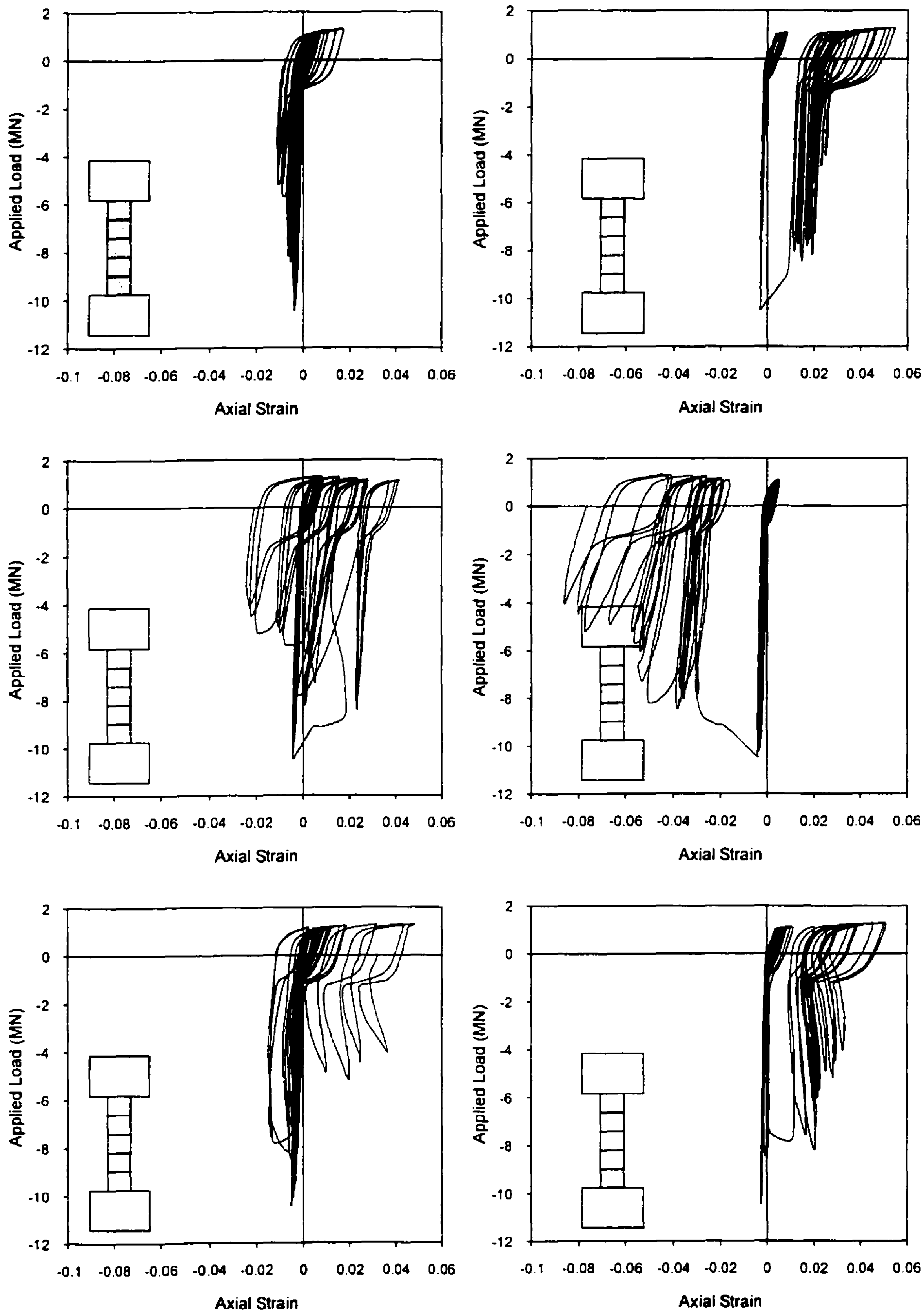

Figure 3.32 Axial strains in different segments of Specimen H3

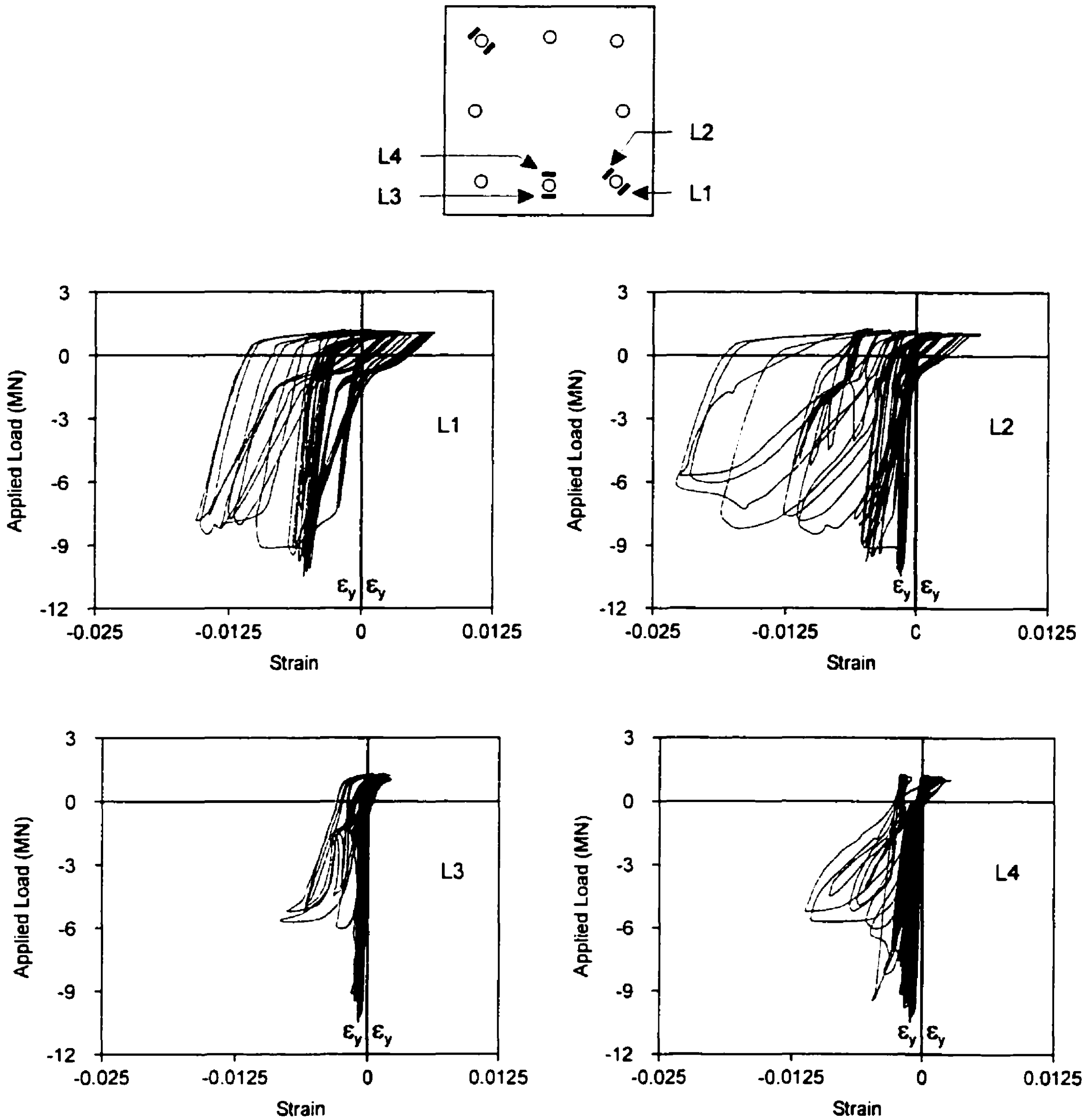

Figure 3.33 Measured strains in longitudinal reinforcement of Specimen H3

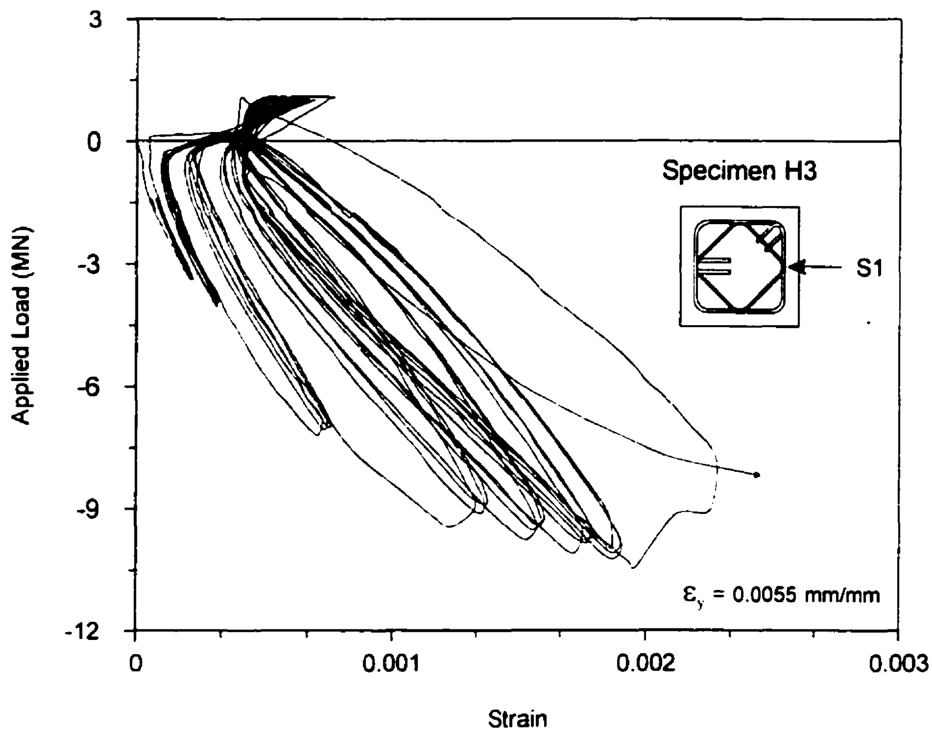

Figure 3.34 Measured strains in hoop reinforcement of Specimen H3

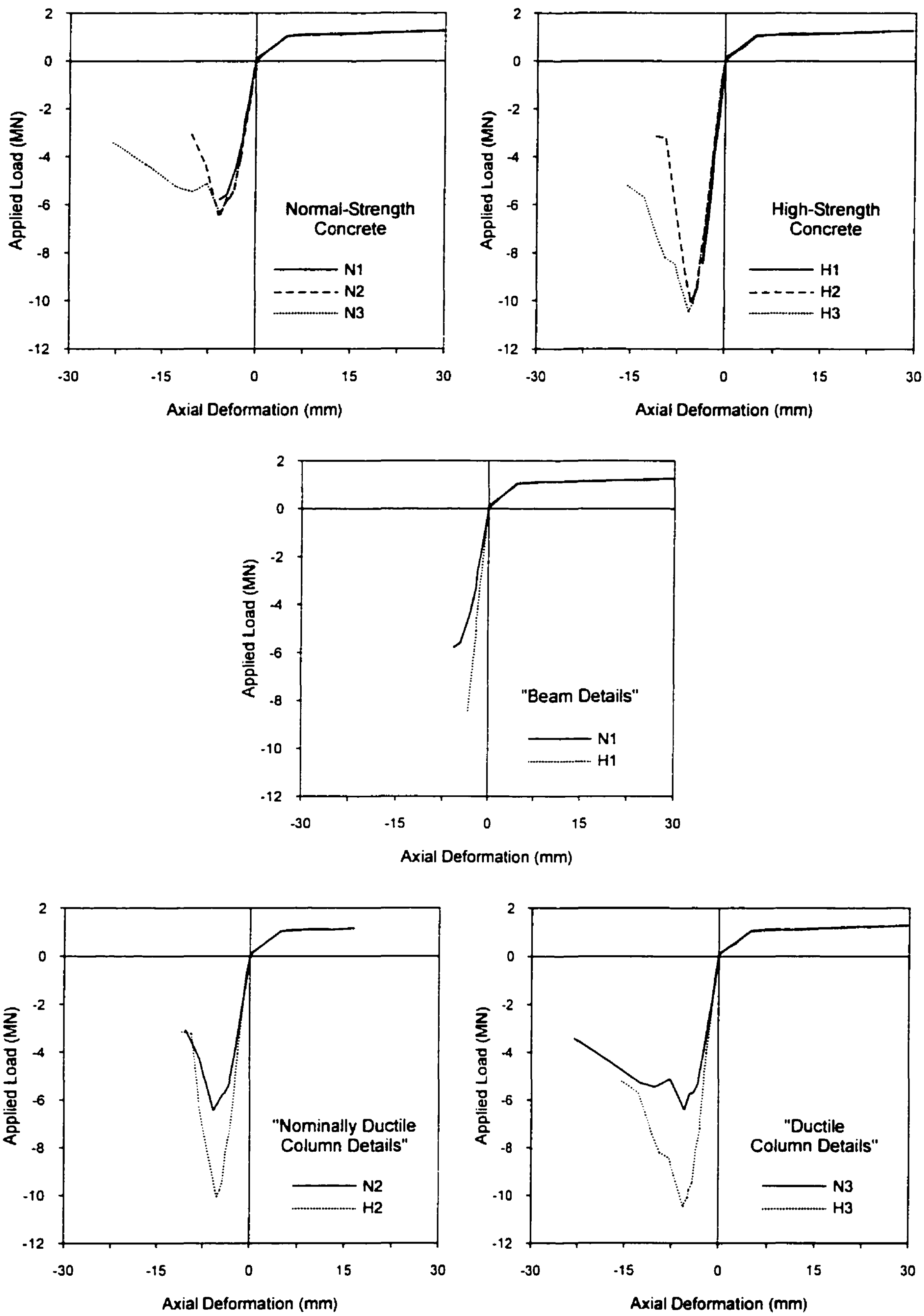

Figure 3.35 Seismic response envelopes of axially loaded specimens

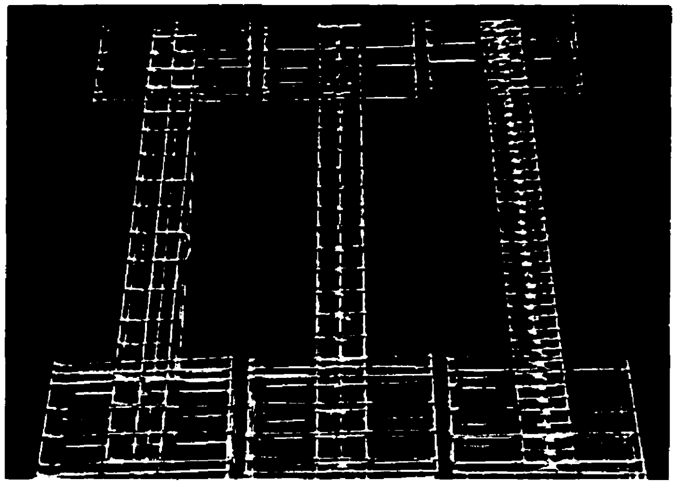

(a) reinforcing cages of high-strength specimens H1, H2 and H3

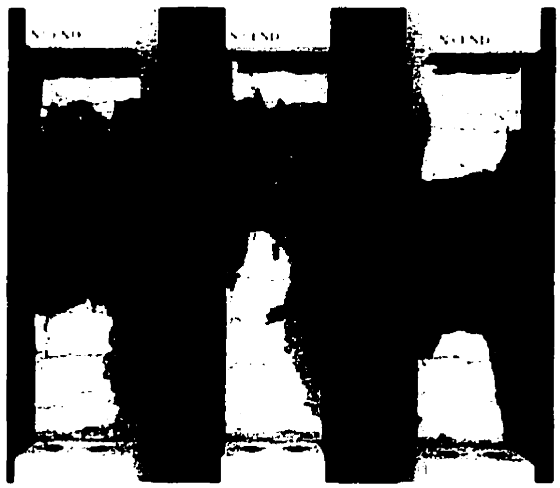

(b) normal-strength concrete specimens N1, N2 and N3

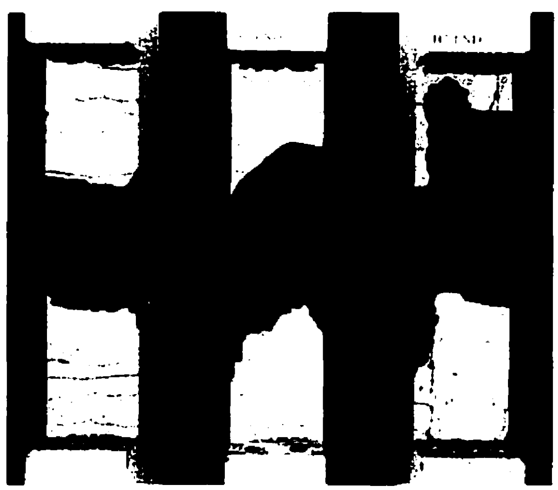

(c) high-strength concrete specimens H1, H2 and H3

Figure 3.36 Photographs of axially loaded specimens

Chapter 4

Predictions of Reversed Cyclic Loading Response of Axially Loaded Specimens

The predictions of the reversed cyclic loading responses of the six axially loaded specimens are presented in this chapter. These predictions were evaluated based on the contributions of the confined and unconfined concrete and the reinforcing steel. The influence of tension stiffening, the closing of tensile cracks and the axial loading history on the stress-strain response of concrete were included in the evaluation of the total concrete contribution. To evaluate the influence of tensile crack closing on the stress-strain response of concrete, a series of tests on both normal and high-strength concrete cylinders were performed. The results of these experiments are presented in Section 4.1. The influences of bar buckling and the loading history on the stress-strain response of the reinforcing bars were included in the evaluation of the steel contribution. A series of reversed cyclic loading tests was performed to determine the buckling behaviour of reinforcing steel with varying length-to-diameter ratios. These test results are presented in Section 4.2.

4.1 Influence of Crack Closing on the Stress-Strain Response of Concrete

Once tensile cracks in concrete have occurred, the perfect re-alignment of these cracked surfaces upon load reversal into compression is not achieved. Therefore, as a reinforced concrete specimen is loaded in compression after a tensile excursion sufficient to crack the concrete, a compressive stress develops within the concrete before the overall strain of the specimen reaches zero. The compressive stress, which has been developed within the concrete once zero strain is reached has been termed the crack closing stress, f_{cl}. Equation 4.1 was suggested by Légeron (1997) for the evaluation of this stress:

$$f_{cl} = \frac{f'_c}{10} \qquad (4.1)$$

A series of experiments were performed to evaluate the compressive response of normal and high-strength concrete with preformed cracks perpendicular to the applied load. A total of twelve 150 x 300 mm cylinders were cast, six from normal-strength concrete and six from high-strength concrete. For each concrete strength, three of these cylinders were tested to establish the typical stress-strain response of the concrete and the other specimens were used to evaluate the stress-strain response of the concrete with preformed cracks.

Four sets of strain targets were glued to each specimen. Three-point bending was used to split the cylinder specimens into two pieces resulting in a crack plane perpendicular to the axis of the cylinder. The two pieces were fitted together as closely as possible and the resulting tensile strain offset was measured using the strain targets. The average of the four measured tensile strains was taken as the tensile strain offset for the specimen. In reality the longitudinal reinforcing bars within the cross-section will act as a guide for the re-alignment of the cracked surfaces. Each specimen was then loaded in compression to determine its stress-strain response. At the start of each test the axial strain was set at zero, therefore the stress-strain response of the cracked cylinders from the test was corrected for the appropriate tensile offset. Figure 4.1 shows the compressive stress-strain response for each of the pre-cracked specimens. The peak compressive stress, the corresponding compressive strain and the crack closing stress were averaged for each test series and are given in Table 4.1.

Table 4.1 Experimental crack closing stress for normal and high-strength concrete

Specimen	f'_c	ε'_c	f_{cl}
uncracked	44.4 MPa	0.00230	-
cracked	44.5 MPa	0.00245	3.64 MPa
uncracked	72.8 MPa	0.00272	-
cracked	70.8 MPa	0.00269	4.53 MPa

Figure 4.1 indicates that just after the closing of the crack the stress-strain response of the pre-cracked cylinder coincides with that of the uncracked cylinder. From these tests it is suggested that the evaluation of the crack closing stress, f_{cl} be approximated using the following:

$$f_{cl} = \left(f'_c\right)^{1/3} \tag{4.2}$$

This effect of crack closing on the compressive stress-strain response of the concrete was modeled as a linear line starting at the strain of first contact, passing through f_{cl} at zero strain and rejoining the concrete stress-strain curve at the point of intersection with the envelope (see Fig. 4.1c). The modeled strain at first contact was calculated to best fit the experimental data, resulting in contact strains of -0.00036 and -0.00031 for the normal and high-strength concrete specimens, respectively.

4.2 Influence of Buckling on the Reversed Cyclic Loading Response of Reinforcing Bars

A series of tests on the tensile and compressive reversed cyclic loading response of individual reinforcing bars was conducted to investigate the effect of buckling on the stress-strain response of these bars. These tests involved different length-to-diameter ratios of the bars and also different loading histories. The free length of the bar between the hydraulic jaws of the MTS testing machine represents the spacing, s, between the transverse reinforcing bars in a column or a beam. The two loading histories selected simulated the induced straining of the longitudinal bars in reinforced concrete beams and columns subjected to reversed cyclic loading.

For these tests No. 25 reinforcing bars were used and all specimens for a particular loading history were cut from the same reinforcing bar. The properties of these reinforcing bars for monotonic loading in tension and compression are given in Table 4.2.

Table 4.2 Properties of reinforcing bars

	Loading	f_y	ε_y	ε_{sh}	E_{sh}
symmetric loading	tension	417 MPa	0.0021	0.0087	5355 MPa
	compression	425 MPa	0.0026	0.0101	5092 MPa
unsymmetric loading	tension	423 MPa	0.0024	0.0095	5314 MPa
	compression	439 MPa	0.0028	0.0124	4844 MPa

The length-to-diameter ratios, s/d, investigated were equal to 4, 6, 8, 12 and 16. The overall applied load and axial strain of each specimen were measured by the load cell and extensometer of the MTS testing machine. In order to capture the onset of buckling of the reinforcing bar two types of instrumentation were used. First, a linear voltage differential transducer was used to measure the lateral deflection at the mid-height of the bar and secondly, electronic strain gauges were glued at the mid-height of both sides of each specimen to capture the localized straining of the reinforcing bar. The strain gauges had gauge lengths of 2 mm and were glued between the ribs on the bar, 180 degrees apart.

The symmetrically loaded specimens were subjected to equivalent peak strains in the tensile and compressive cycles, while for the unsymmetrical series of tests, the peak tensile strain was four times greater than the peak compressive strain. This strain ratio for the unsymmetrical test series was used once the peak tensile strain had reached four times the yield strain. Prior to a tensile strain of $4\Delta_y$, the peak compressive strain for each cycle was held at the yield strain and the tensile strain was incremented by Δ_y, (i.e. for tensile strain = 3 Δ_y , compressive strain = Δ_y). The symmetrical and unsymmetrical loading histories simulate the induced straining of the longitudinal reinforcement of reinforced concrete columns and beams subjected to reversed cyclic loading, respectively.

The overall stress-strain responses of the reinforcing bars subjected to symmetrical loading are presented in Figs. 4.2 – 4.6 and the behaviour of the unsymmetrically loaded test specimens are given in Figs. 4.7 – 4.11. It is clear from these figures that as the length-to-diameter ratio, s/d, increases, the influence of buckling on the stress-strain response of the reinforcing bar becomes more pronounced. The buckling of the bar reduces the peak compressive stress reached during the cycle and this compressive stress decreases under continued compressive straining. Once buckling of the reinforcing bar has occurred the bar has a permanent lateral deformation, which is not removed during the tensile loading cycle as seen in Fig. 4.4b, for example. This phenomenon became more pronounced on each additional compressive cycle and also as the s/d ratio is increased. The commencement of buckling, of the reinforcing bar with a length-to diameter ratio of 12 was captured by the strain gauges as seen in Figs. 4.5c and d. The decrease in the compressive strain on one side of the bar and a simultaneous increase in the compressive strain of the other side indicated the direction of buckling. For this case the lateral deflection was in the direction of strain gauge SG1. This phenomenon was also captured by the strain gauges for the symmetrically loaded specimen with a s/d ratio of 16, see Fig. 4.6.

The envelopes of the reversed cyclic loading responses of these specimens are given in Figs. 4.12 and 4.13 for the symmetrically loaded and unsymmetrically loaded specimens, respectively. For both loading cases, the bars with s/d ratios of 4 and 6 reached compressive stresses in excess of the yield stress of the reinforcement and only showed signs of buckling after several loading cycles at multiples of Δ_y. The specimens with s/d equal to 8 were able to sustain the compressive yield stress for several post-yield cycles, after which the compressive capacity of these specimens started to decrease. The reinforcing bars with length-to-diameter ratios of 12 and 16 buckled once the compressive yield stress of the bar was reached and on subsequent cycles the compressive capacity of these specimens deteriorated.

The following modified version of the Ramberg-Osgood function suggested by Mattock (1979) for the stress-strain response of prestressing steel was used to describe the stress-strain response of the reinforcing bars after buckling:

$$f_s = E\varepsilon_s \left\{ A + \frac{1-A}{\left(1+(B\varepsilon_s)^C\right)^{1/C}} \right\} \tag{4.3}$$

Figure 4.14 shows this function with the parameters A and B illustrated on the graph. The parameter C defines the transition curve, with a larger value resulting in a more abrupt transition between the initial loading branch and the post-yielding branch. If the value of A is assumed to be zero, then the value of the y-intercept, (i.e. E/B) defines the peak compressive stress reached during a particular loading cycle as shown in Fig. 4.15. The experimentally determined variation in the parameter 1/B versus the peak compressive strain for all of the s/d ratios tested is given in Figs. 4.16 and 4.17 for the symmetrically and unsymmetrically loaded specimens, respectively. A decrease in the value of the parameter 1/B indicates a reduction in the peak compressive capacity of the reinforcing bar for that particular compressive loading cycle. For the specimens with s/d ratios of 12 and 16, the negative slope of the line indicates the rate of softening of the compressive capacity of the reinforcing bar due to buckling.

4.3 Predictions of Reversed Cyclic Loading Responses of Axially Loaded Specimens

The predictions of the reversed cyclic loading responses of the six axially loaded specimens are presented in Section 4.3.3. The analytical models for the concrete and reinforcing steel used for these predictions are given in the next two sections.

4.3.1 Analytical Model for Concrete

The selected model for the confined normal-strength concrete was that proposed by Mander et al (1988a). The complete stress-strain relationship of the confined concrete is given by Equation 1.4 and the peak confined compressive stress and corresponding strain were calculated using Equations 1.5 – 1.8. For the high-strength concrete specimens the peak confined compressive stress and the corresponding strain were calculated using Equations 1.11 and 1.12, respectively, as suggested by Li (1994). The complete stress-strain relationship for the confined high-strength concrete is defined by Equations 1.21 and 1.22 for the ascending and descending branches, respectively, as suggested by Cusson and Paultre (1995).

These confined concrete relationships were assumed to be valid only for the effectively confined core, A_e, which is defined by the following, suggested by Mander et al (1988a):

$$A_e = \left(b_c d_c - \sum_{i=1}^{n} \frac{(w_i^{'})^2}{6} \right) \left(1 - \frac{s^{'}}{2b_c} \right) \left(1 - \frac{s^{'}}{2d_c} \right) \tag{4.4}$$

Figure 1.5 shows the effectively confined core for a rectangular cross-section in plan and elevation illustrating the terms used in Equation 4.4.

The modulus of elasticity, E_c, of the concrete was evaluated as suggested by CSA Standard (1994), assuming normal density for the concrete (i.e. $\gamma_c = 2300$ kg/m^3) and is given by the following:

$$E_c = 3300\sqrt{f_{co}^{'}} + 6900 \tag{4.5}$$

The unconfined concrete was modeled using the expression suggested by Thorenfeldt et al (1987), which is a generalization of that suggested by Popovics (1973) and is given by:

$$f_c = \frac{f_{co}^{'} x r}{r - 1 + x^{rk}} \tag{4.6}$$

where

$f_{co}^{'}$, ε_{co}	= peak unconfined compressive stress and corresponding strain
x	= $\varepsilon_c / \varepsilon_{co}$
r	= $E_c / (E_c - E_{sec})$
E_{sec}	= $f_{co}^{'} / \varepsilon_{co}$
k	= decay factor, see Equation 4.7

The value of the decay factor, k, is taken equal to unity on the ascending branch up to the peak unconfined compressive stress, $f_{co}^{'}$ and is evaluated using the following equation for the descending branch, (Collins and Mitchell, 1997):

$$k = 0.67 + \frac{f'_{co}}{62} \geq 1.0 \tag{4.7}$$

The descending branch of the unconfined concrete is defined by Equation 4.6 until a limit strain, $a\varepsilon_{co}$, where a is 2 and 1.5, for normal and high-strength concrete, respectively. For strains larger than this limit strain, a linear line is drawn to the spalling strain, ε_{sp} , maintaining the rate of decay of the descending branch (see Fig. 4.18).

The following describes the modeling of the reversed cyclic loading response of the concrete. The compressive unloading branch is defined by Equation 1.42 as suggested by Martinez-Rueda and Elnashai (1997). The value of the plastic offset strain, ε_{pl} , is calculated using Equation 1.39 for an unloading strain, ε_{un} , less than the strain corresponding to $0.35f'_c$. For a larger unloading strain Equation 1.40 is used to calculate the plastic offset strain. Figure 4.19 shows the compressive unloading branch and important points used in these calculations.

The compressive reloading branch is defined by two linear lines which intersect the stress-strain relationship of the concrete at the returning point, (ε_{re}, f_{re}), see Fig. 4.20. The compressive reloading of the concrete begins at the tensile strain when the cracked surfaces first come in contact with each other. This linear line passes through the point defined as the closing stress, f_{cl} , which is the compressive stress reached when an overall strain of zero is achieved. This line is projected to the intersection with the softened reloading branch defined by the line connecting the plastic strain offset (ε_{pl} , 0) and the degraded stiffness point (ε_{un} , f_{new}). The reduced stress, f_{new}, corresponding to the previous maximum compressive strain is calculated using Equation 1.43. The values of f'_{cc2} and ε_{cc2} are given by the following:

$$f'_{cc2} = Rf'_{cc} \quad \text{and} \quad \varepsilon_{cc2} = R\varepsilon_{cc} \tag{4.8}$$

The axially loaded specimens were cycled three times at each increase in axial strain. For the predictions of these specimens the value of R was taken as 0.8 for the normal-strength concrete specimens and 0.9 for the high-strength concrete specimens, in order to account for softening of the concrete due to the multiple cycles at a particular peak compressive strain. The returning point (ε_{re}, f_{re}) at which the concrete stress-strain curve is rejoined is the intersection point between the linear projection of the reloading branch and the stress-strain response of the concrete. This method of calculating the returning point does not result in an unrealistic increase in the reloading stiffness between the degraded stiffness point and the return point.

The tensile response of the concrete is assumed to be linear up to the cracking of the concrete, f_{cr}, with a stiffness equivalent to the concrete tangent modulus, E_c. Once the concrete has cracked the average tensile stress in the concrete is calculated using the relationship suggested by Vecchio and Collins (1986) and modified by Collins and Mitchell (1987):

$$f_c = \frac{\alpha_1 \alpha_2 f_{cr}}{1 + \sqrt{500\varepsilon_c}} \tag{4.9}$$

where

α_1 = 1.0 for deformed bars, 0.7 for plain bars

α_2 = 1.0 for short term monotonic loading, 0.7 for repeated loading

f_{cr} = cracking stress of the concrete

ε_c = concrete strain

The tensile reloading branch is a linear line connecting the origin with the previous maximum tensile strain. The tensile response follows the tension stiffening base curve until tensile unloading. At that point the tensile unloading branch is assumed parallel to the reloading branch for that tensile cycle as shown in Fig. 4.21. The overall modeled reversed cyclic loading response of the concrete is given in Fig. 4.22.

4.3.2 Analytical Model for Reinforcing Steel

The reversed cyclic loading response of the reinforcing steel is defined in three parts. First, a linear line defines the elastic response of the steel with an initial stiffness of E_s and is valid until the tensile or compressive yielding of the reinforcement. At the first yielding of the reinforcement the yield plateau of the steel is defined as a horizontal line having a constant stress equal to f_y. After the first post-yield strain reversal the loading response of the steel is defined by a modified version of the Ramberg-Osgood function as given in Equation 4.3. The values of the parameters A, B and C were calculated based on experimental tests on the reinforcing steel. The unloading branch from a peak compressive or tensile stress has a slope equal to E_s. Figure 4.23 shows the overall modeled reversed cyclic response of the reinforcing steel.

For the inclusion of the buckling of the reinforcement the parameters A, B and C were modified to accurately describe the compressive stress-strain response of the buckled bar. The parameters were calculated based on the buckling tests described in Section 4.2 for the appropriate hoop spacing to bar diameter ratio, s/d, for the specimen. For a length-to-diameter ratio of 8 the parameters A, B and C were taken as -0.01995, 306.43 and 2, respectively. The effect of buckling of the reinforcement on the stress-strain response of the steel was included in the prediction once the spalling of the cover concrete had occurred.

4.3.3 Predictions of Axially Loaded Specimens

The details of the axially loaded specimens are given in Chapter 2. These specimens were 350 mm square and 1400 mm long, with eight No. 20 longitudinal bars. Table 4.3 gives the material properties used in the analysis for each of these specimens, including the area of the effectively confined core, A_e, from Equation 4.4.

The reversed cyclic loading response of the axially loaded specimens provides a means of validating the analytical modeling techniques for the concrete and steel responses. The predictions were made by choosing peak tensile and compressive strains for each cycle and incrementing the axial strains towards these target values. In the analysis the reversed cyclic loading stress-strain relationships described in this chapter were used in order to account for the following important characteristics:

(i) the different stress-strain characteristics of the confined and unconfined concrete;
(ii) the spalling of the cover concrete;
(iii) the influence of the details of the transverse reinforcement on the confinement of the core concrete;
(iv) the influence of crack closing;
(v) the effect of residual tension stresses between cracks;
(vi) the effect of concrete compressive strength on the stress-strain relationship;
(vii) the influence of the complete reversed cyclic stress-strain relationship of the reinforcing bar including the Bauschinger effect;
(viii) the effect of the hoop spacing to the longitudinal bar diameter ratio, s/d, on the non-linear response of the reinforcement; and
(ix) the influence of arrangement, spacing and yield stress of the transverse reinforcement on the confining effects of the concrete core.

The responses were predicted using a spreadsheet to account for all of the effects given above. This approach is suitable for these symmetrically reinforced axially loaded specimens since the member strains are uniform across the section. A computer program for predicting the reversed cyclic loading response of cross-sections subjected to both axial load and moment (i.e., linear varying strain distributions) is presented in Chapter 7.

Table 4.3 Material properties of the axially loaded specimens

Specimen	f'_c	Hoop Details	Hoop Spacing	f'_{cc}	A_e
N1	39.0 MPa	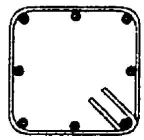	156 mm	45.8 MPa	38 832 mm^2
N2	39.0 MPa	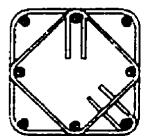	156 mm	50.4 MPa	31 857 mm^2
N3	39.0 MPa	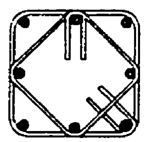	82 mm	65.9 MPa	45 710 mm^2
H1	76.5 MPa	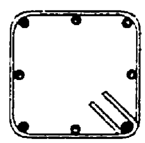	156 mm	82.5 MPa	38 832 mm^2
H2	76.5 MPa	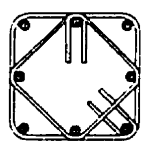	117 mm	92.3 MPa	38 847 mm^2
H3	76.5 MPa	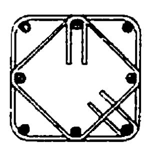	58 mm	123.2 MPa	50 739 mm^2

The predictions of the experimental responses of the axially loaded specimens constructed using normal-strength concrete are given in Figs. 4.24 – 4.29. For each of the specimens there are two figures illustrating the analytical prediction. The first compares the overall prediction with the experimental axial load versus axial strain. The second shows the predicted reversed cyclic stress-strain response of the unconfined and confined concrete and the reinforcing bars. The predictions for the specimens constructed with normal-strength concrete agree very well with the experimental results. The tensile and compressive stiffness of each of the specimens was very accurately predicted for all of the specimens. The post-peak behaviour of Specimens N2 and N3 was also predicted very well, including the evaluation of the concrete plastic strain offset, ε_{pl}. There was, however an underestimation of ε_{pl} for the final compressive loading loop for both specimens with "column details".

The predicted and experimental responses of the specimens constructed with high-strength concrete are given in Figs. 4.30 – 4.35. The experimental results were predicted very well for all of these specimens. The stiffness of each of the specimens in tension and compression was predicted accurately. The experimental post-peak response of Specimen H2 was not captured by the instrumentation due to the abrupt spalling of the cover concrete, therefore the analytical prediction continues further than the measured strain. The response of the specimen with "ductile column details" was predicted very well. The slight overestimation of the compressive capacity in the last two cycles can be attributed to the rupture of some of the transverse reinforcement, resulting in a loss of confinement of the concrete core, thus reducing the compressive capacity of the concrete core.

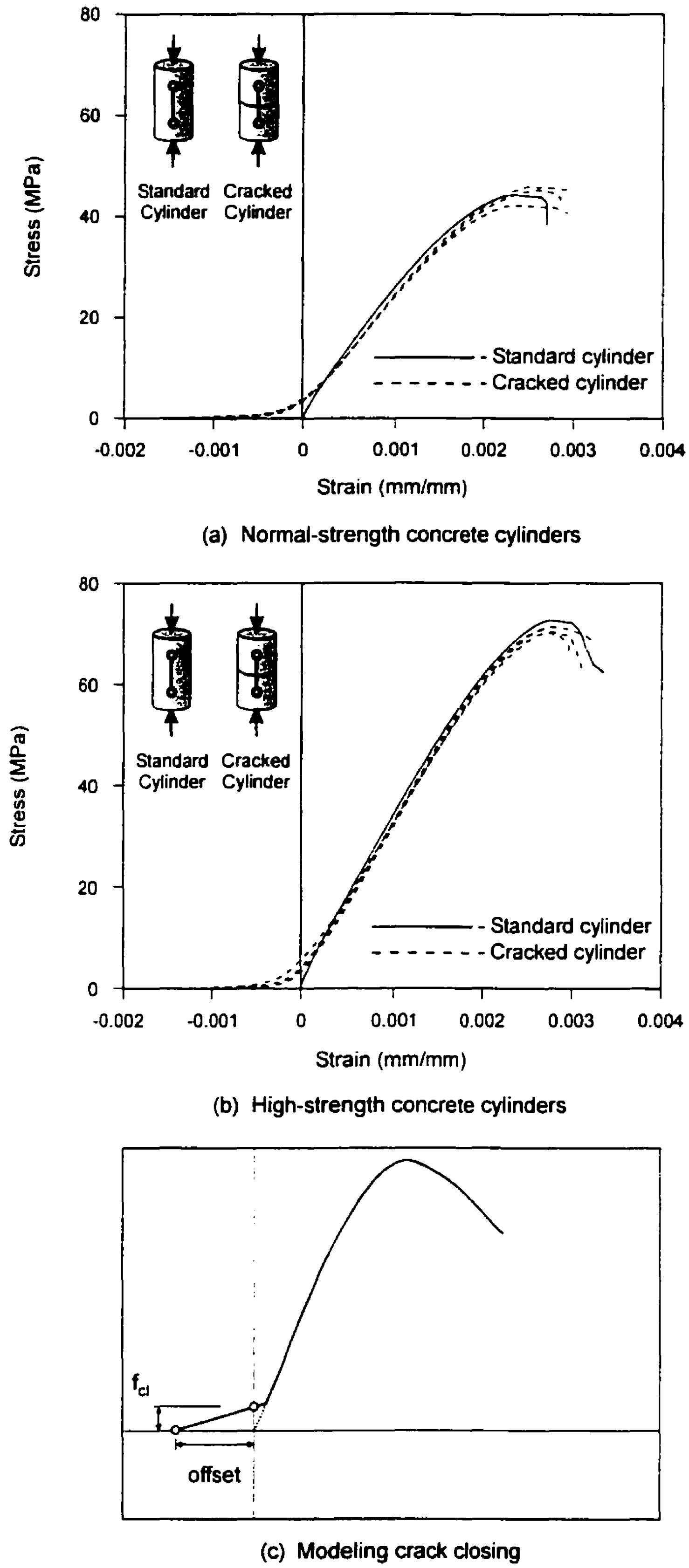

Figure 4.1 Compressive response of concrete cylinders with horizontal cracks

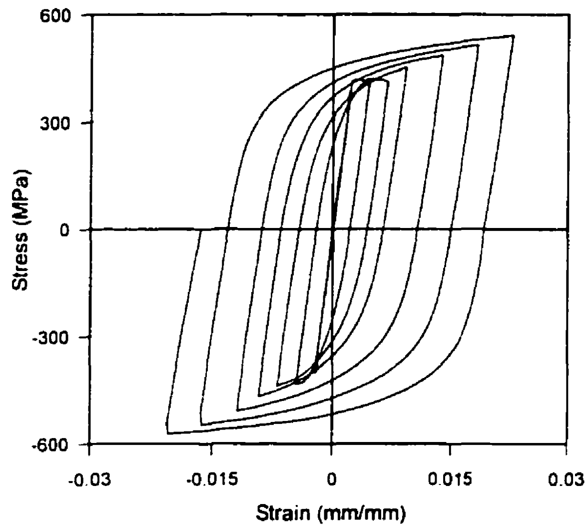

(a) Axial stress vs strain

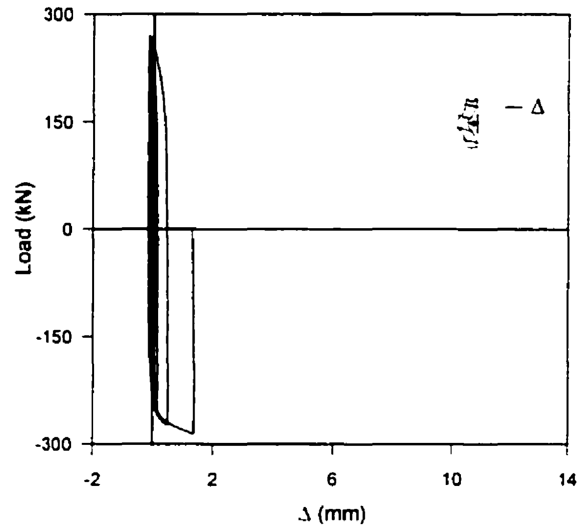

(b) Applied load vs lateral deflection

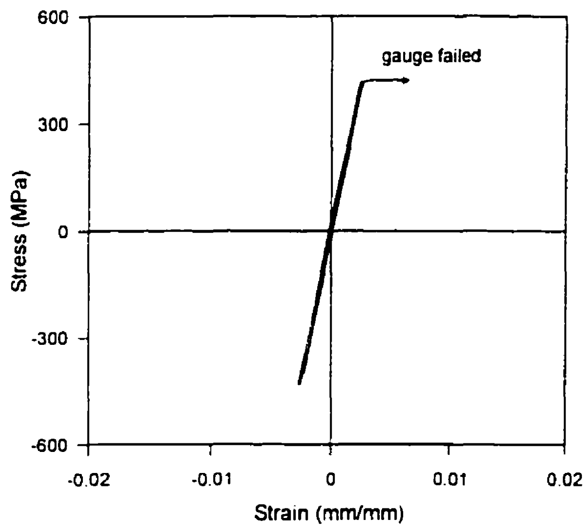

(c) Axial stress vs strain gauge SG1

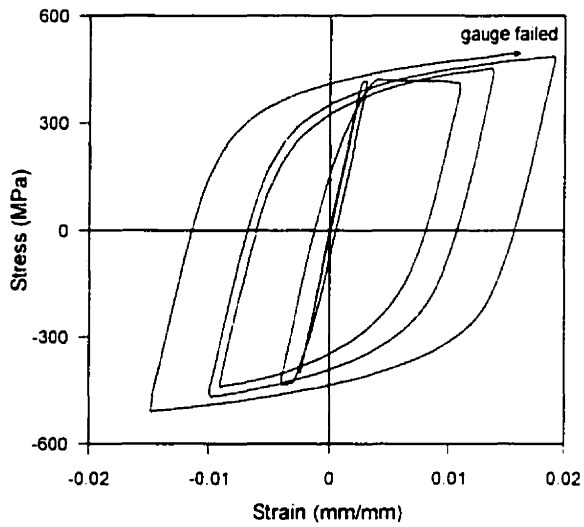

(d) Axial stress vs strain gauge SG2

Figure 4.2 Symmetrically loaded reinforcing bar with s/d = 4

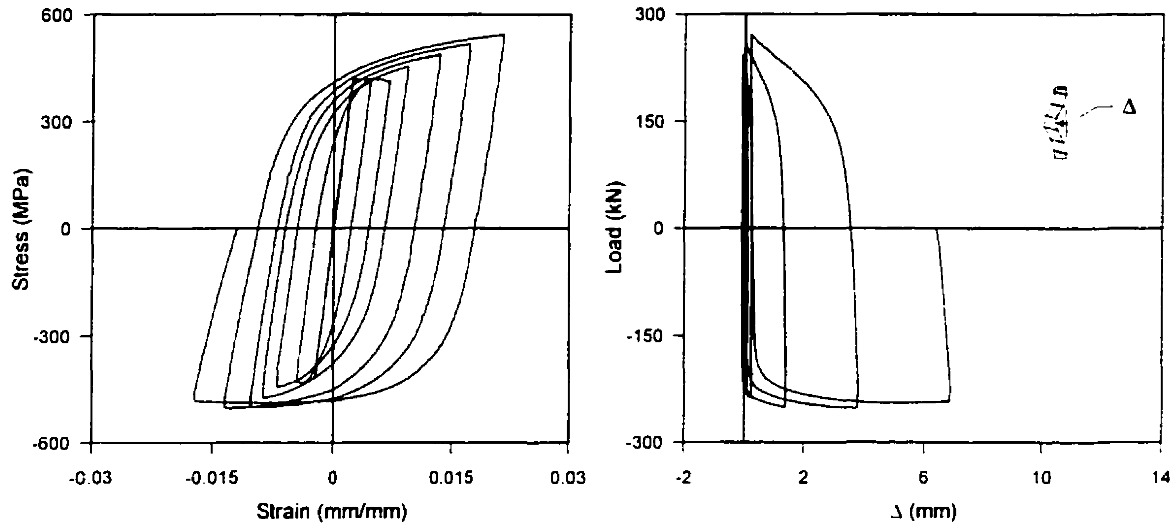

(a) Axial stress vs strain

(b) Applied load vs lateral deflection

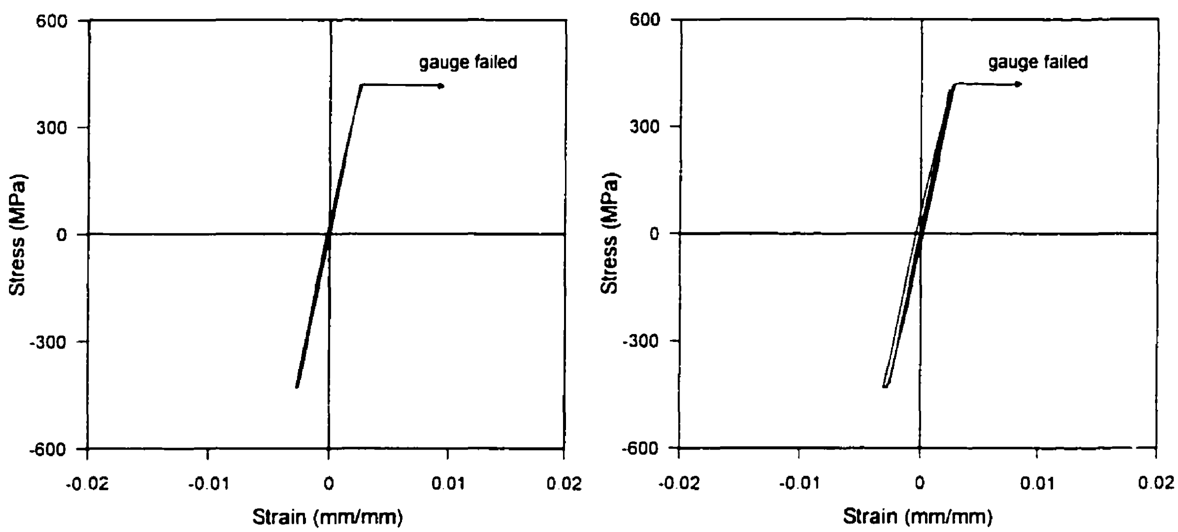

(c) Axial stress vs strain gauge SG1

(d) Axial stress vs strain gauge SG2

Figure 4.3 Symmetrically loaded reinforcing bar with s/d = 6

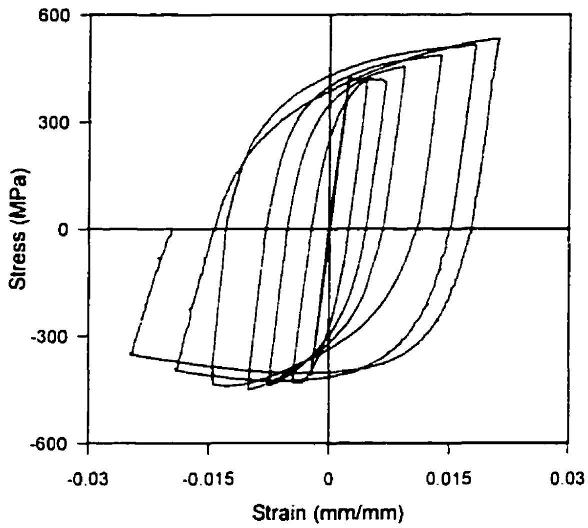

(a) Axial stress vs strain

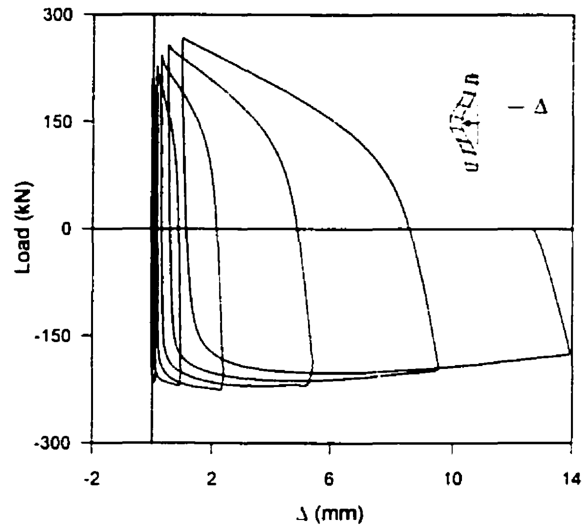

(b) Applied load vs lateral deflection

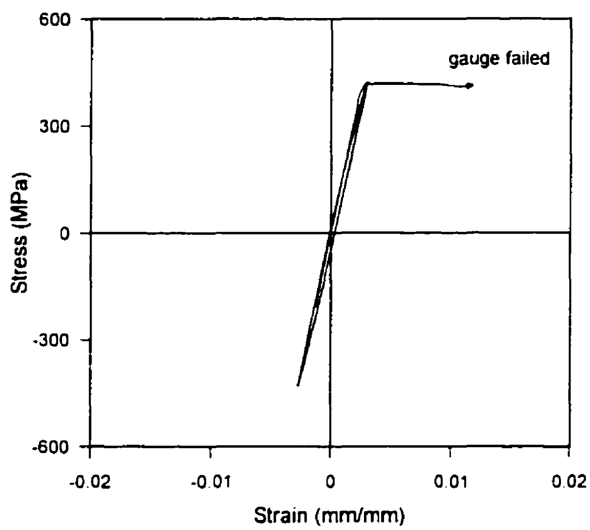

(c) Axial stress vs strain gauge SG1

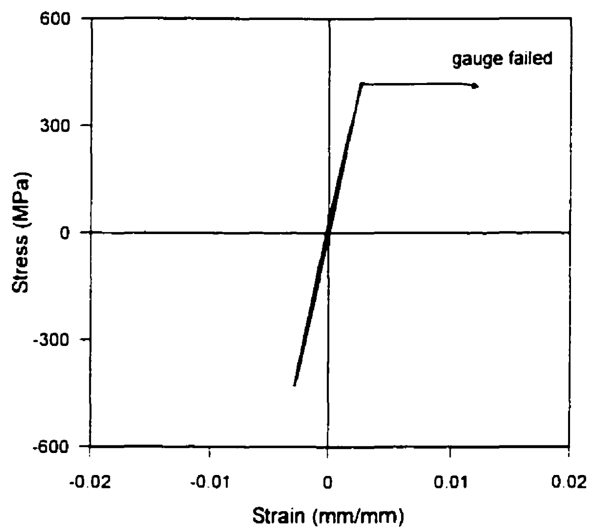

(d) Axial stress vs strain gauge SG2

Figure 4.4 Symmetrically loaded reinforcing bar with s/d = 8

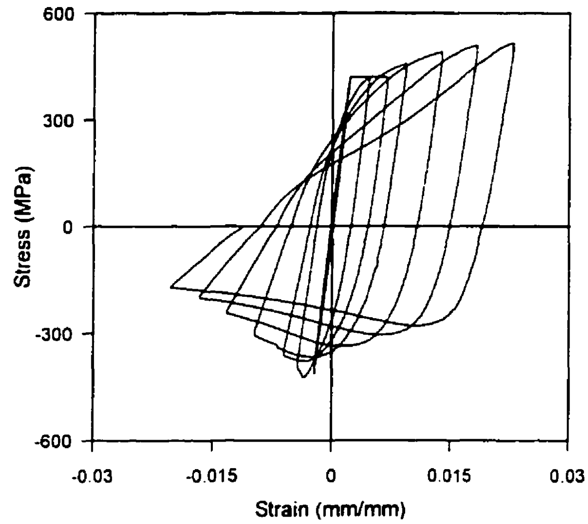

(a) Axial stress vs strain

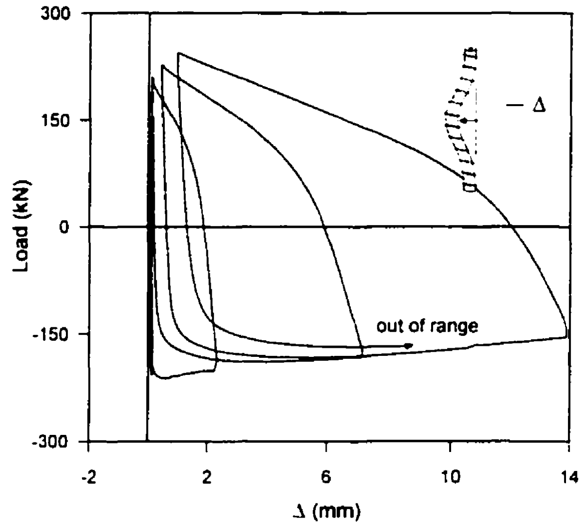

(b) Applied load vs lateral deflection

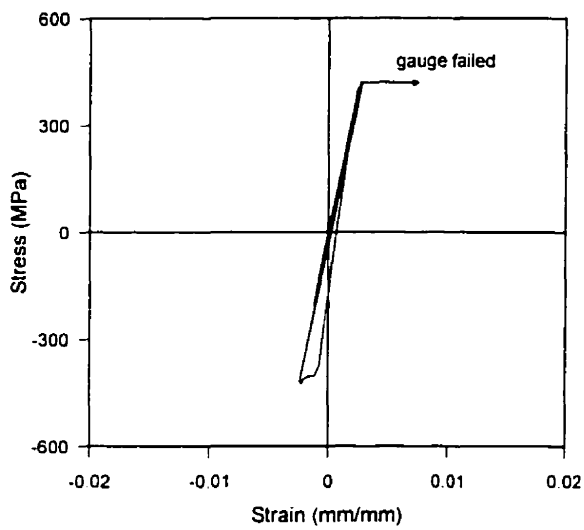

(c) Axial stress vs strain gauge SG1

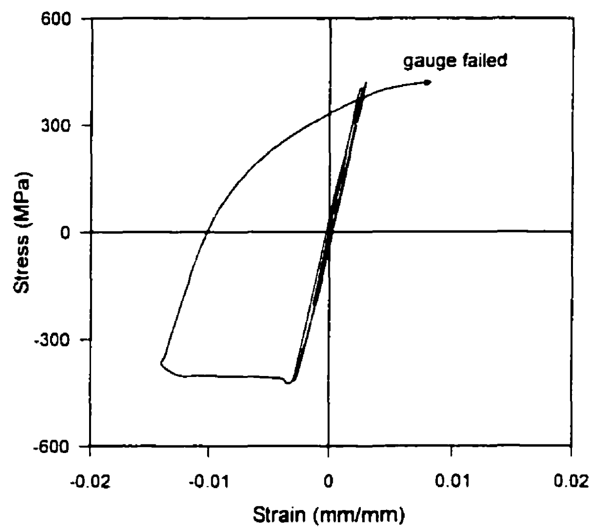

(d) Axial stress vs strain gauge SG2

Figure 4.5 Symmetrically loaded reinforcing bar with s/d = 12

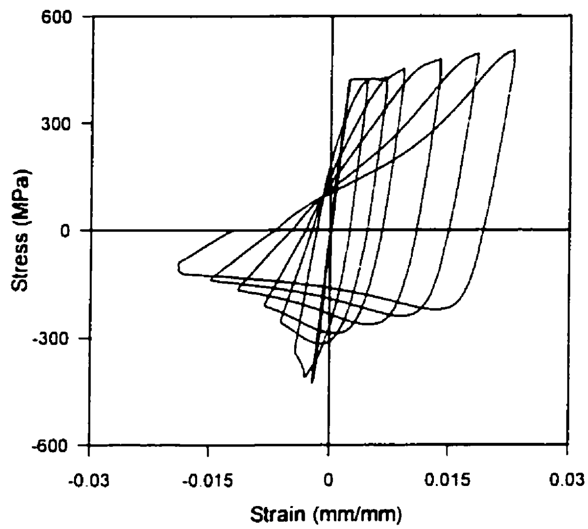

(a) Axial stress vs strain

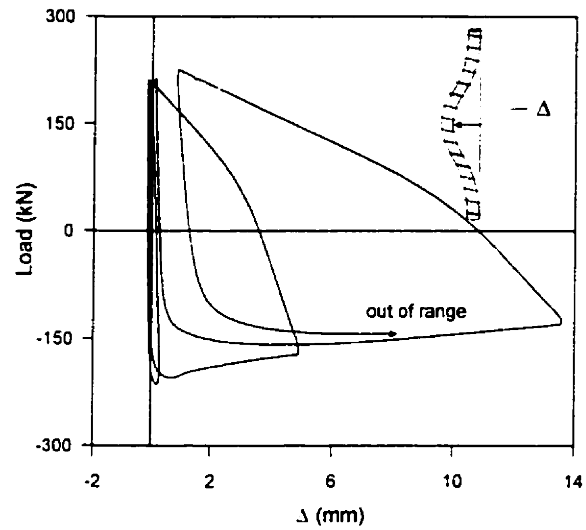

(b) Applied load vs lateral deflection

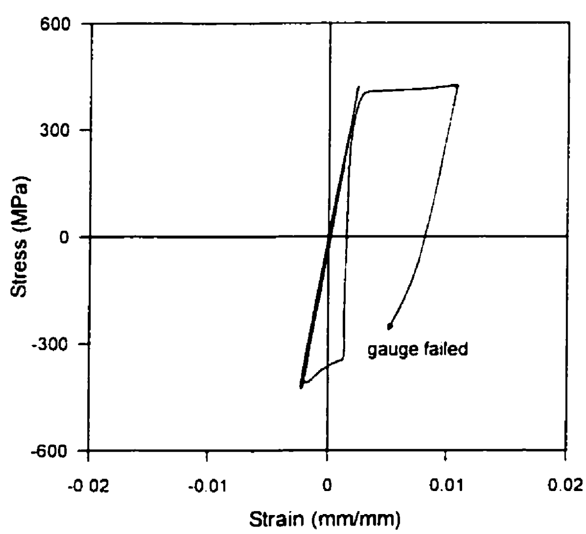

(c) Axial stress vs strain gauge SG1

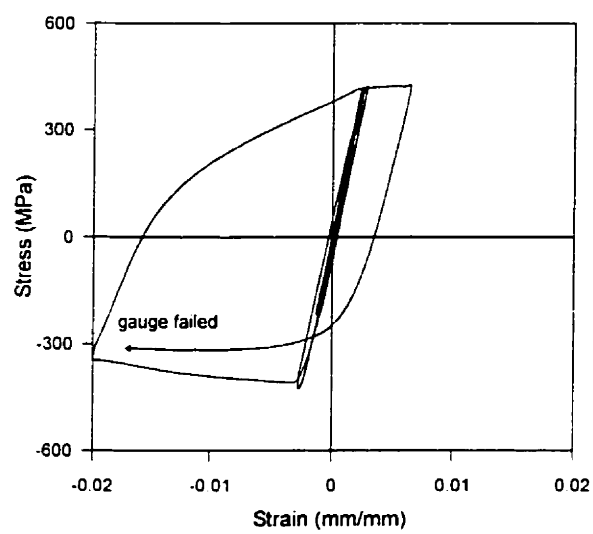

(d) Axial stress vs strain gauge SG2

Figure 4.6 Symmetrically loaded reinforcing bar with s/d = 16

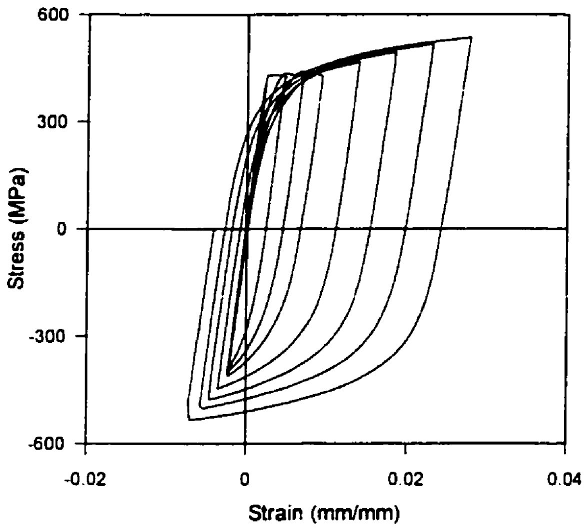

(a) Axial stress vs strain

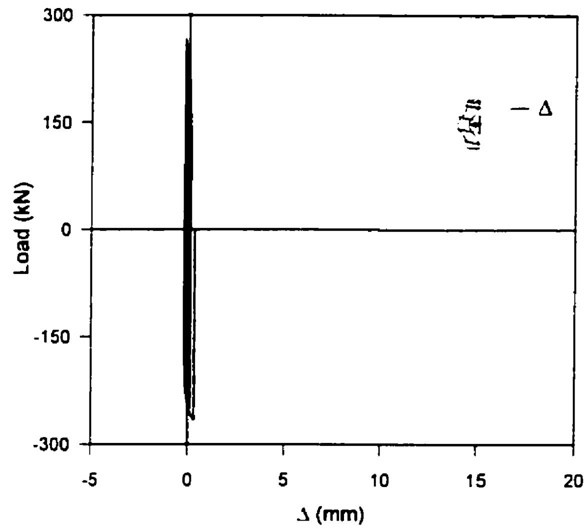

(b) Applied load vs lateral deflection

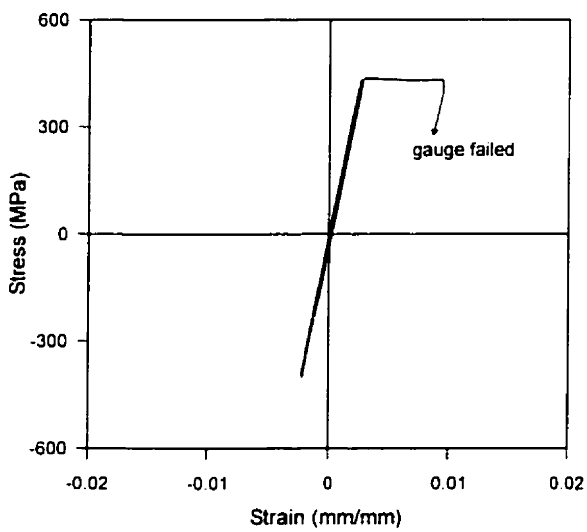

(c) Axial stress vs strain gauge SG1

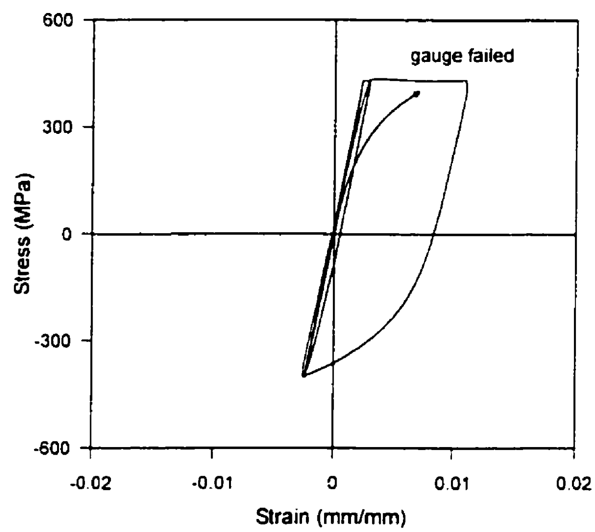

(d) Axial stress vs strain gauge SG2

Figure 4.7 Unsymmetrically loaded reinforcing bar with s/d = 4

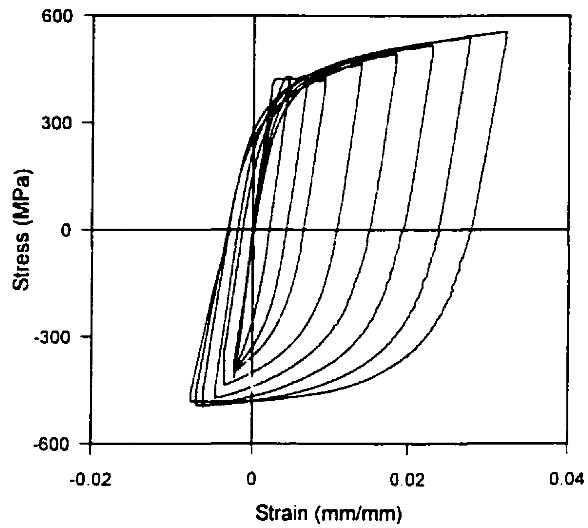

(a) Axial stress vs strain

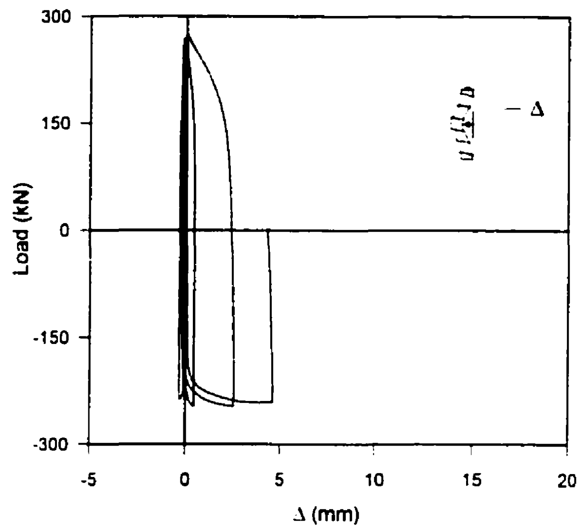

(b) Applied load vs lateral deflection

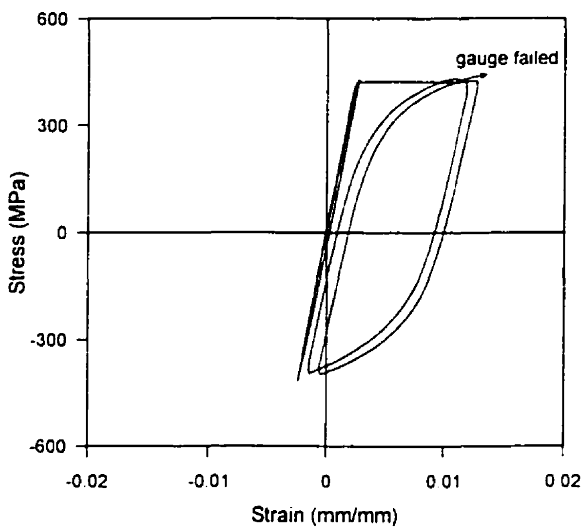

(c) Axial stress vs strain gauge SG1

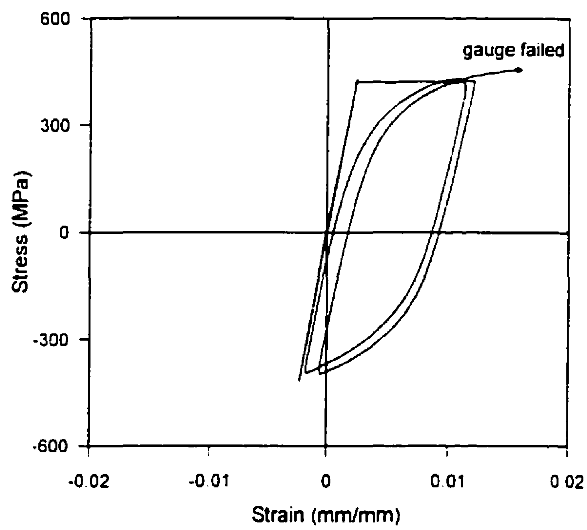

(d) Axial stress vs strain gauge SG2

Figure 4.8 Unsymmetrically loaded reinforcing bar with s/d = 6

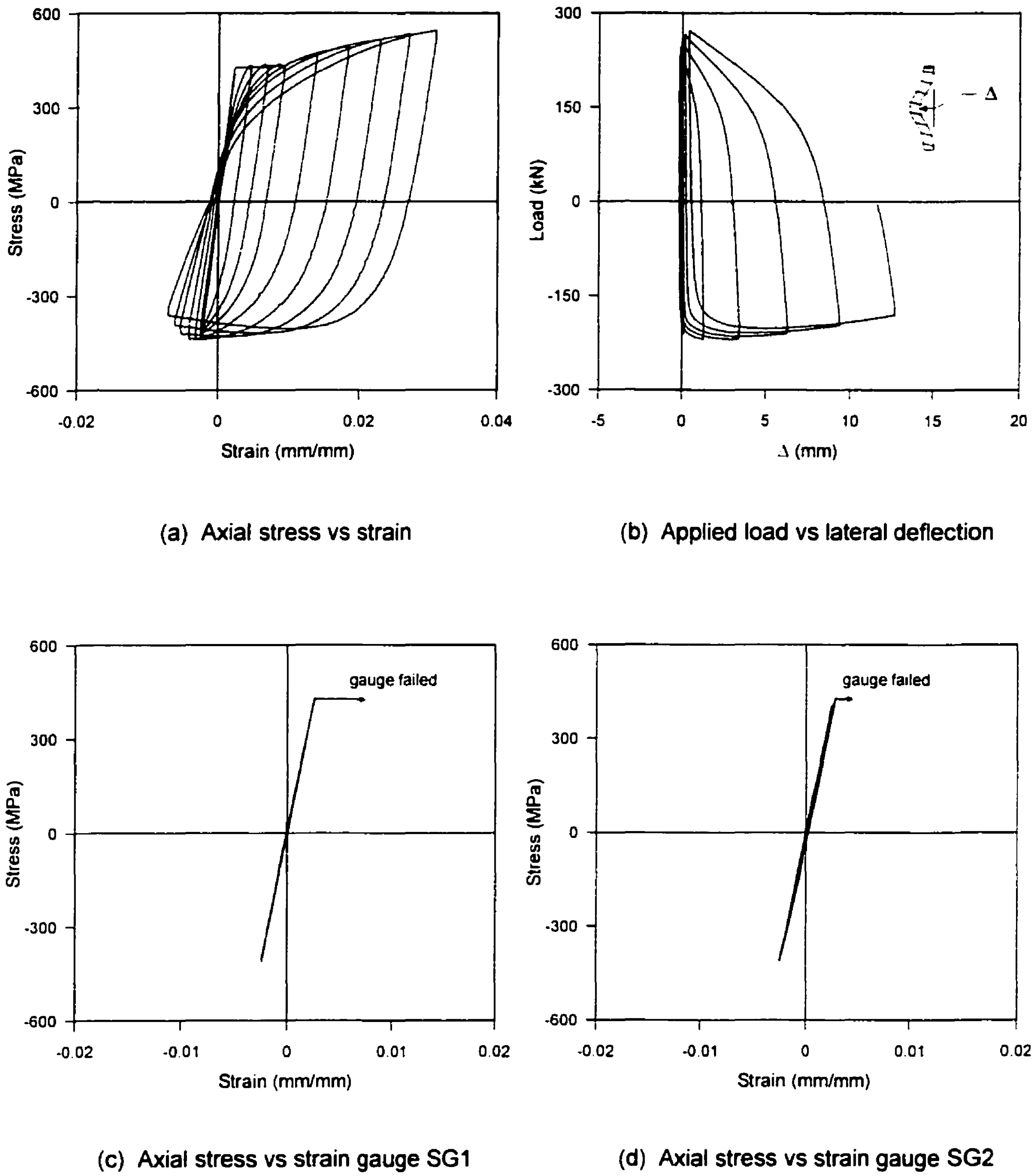

Figure 4.9 Unsymmetrically loaded reinforcing bar with s/d = 8

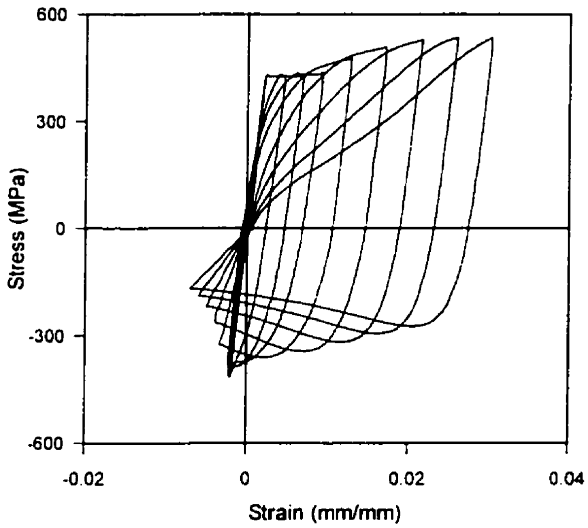

(a) Axial stress vs strain

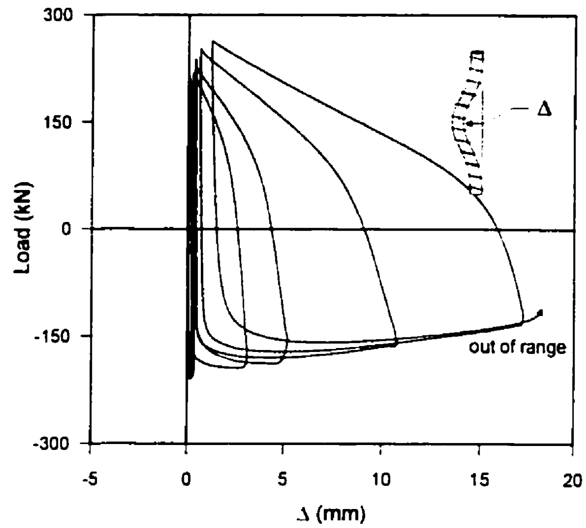

(b) Applied load vs lateral deflection

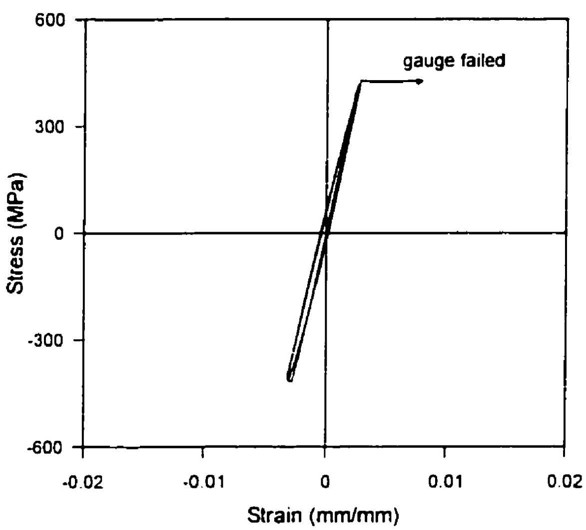

(c) Axial stress vs strain gauge SG1

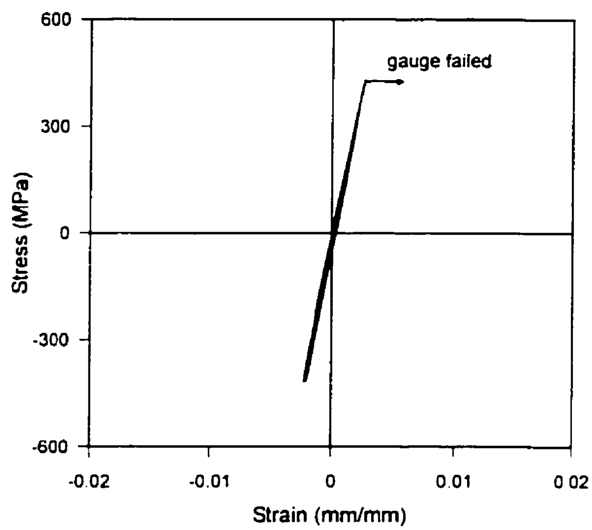

(d) Axial stress vs strain gauge SG2

Figure 4.10 Unsymmetrically loaded reinforcing bar with s/d = 12

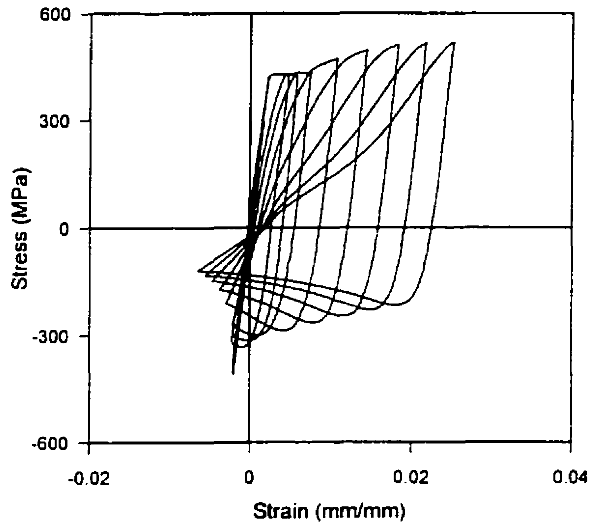

(a) Axial stress vs strain

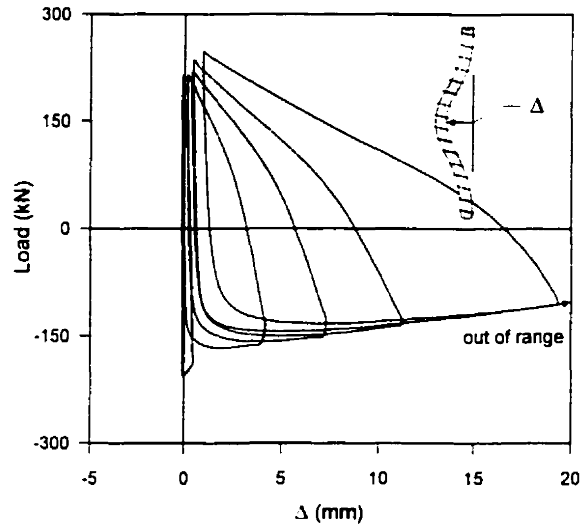

(b) Applied load vs lateral deflection

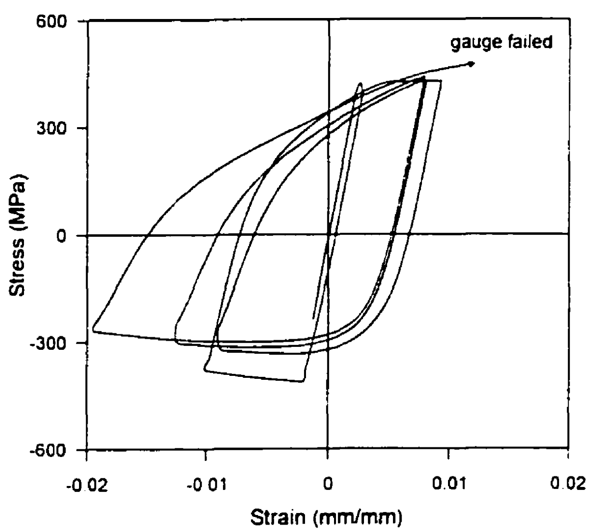

(c) Axial stress vs strain gauge SG1

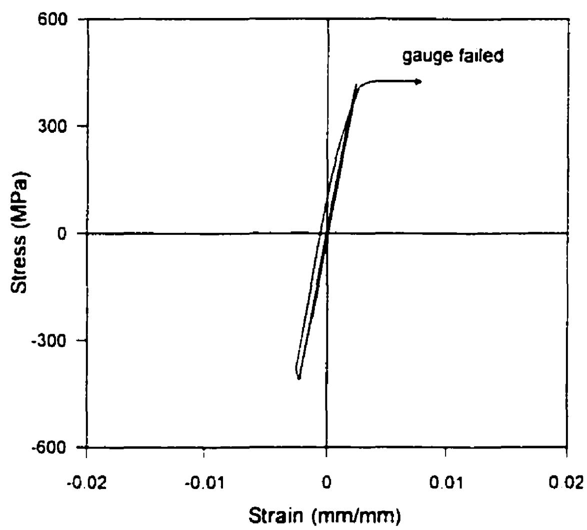

(d) Axial stress vs strain gauge SG2

Figure 4.11 Unsymmetrically loaded reinforcing bar with s/d = 16

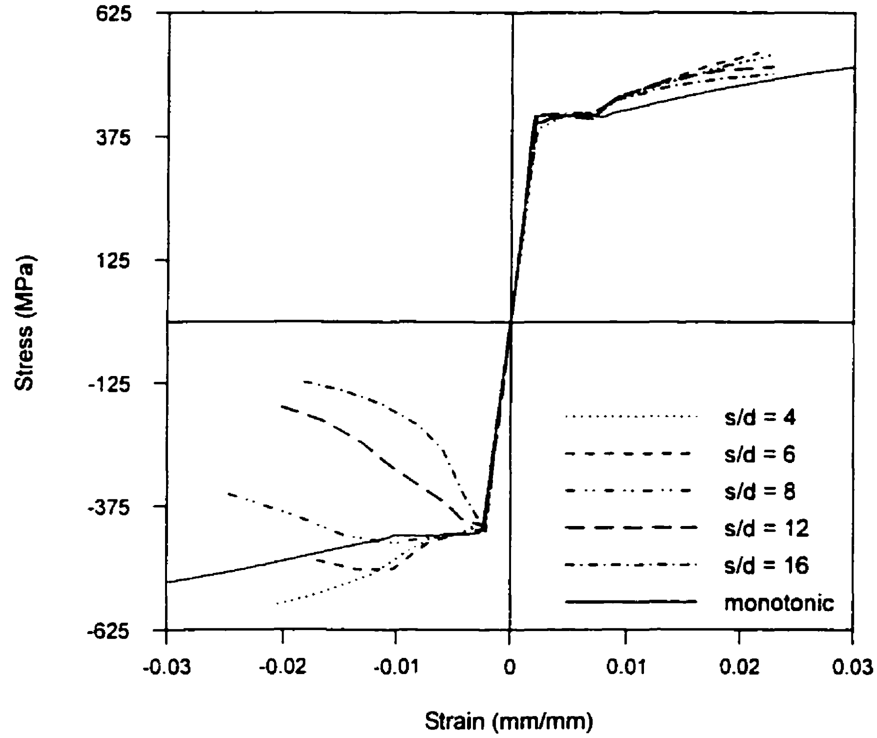

Figure 4.12 Stress versus strain envelopes for symmetrically loaded reinforcing bars

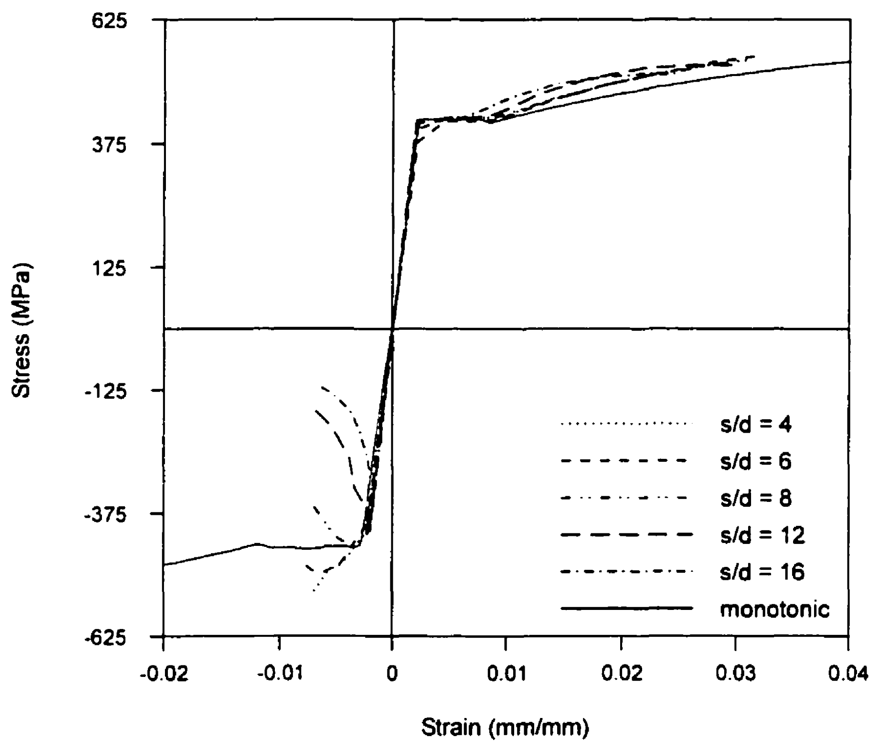

Figure 4.13 Stress versus strain envelopes for unsymmetrically loaded reinforcing bars

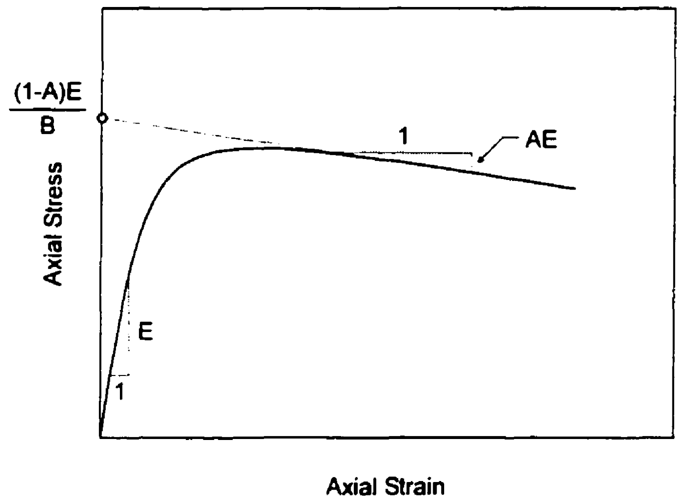

Figure 4.14 Parameters of modified Ramberg-Osgood function (Mattock, 1979)

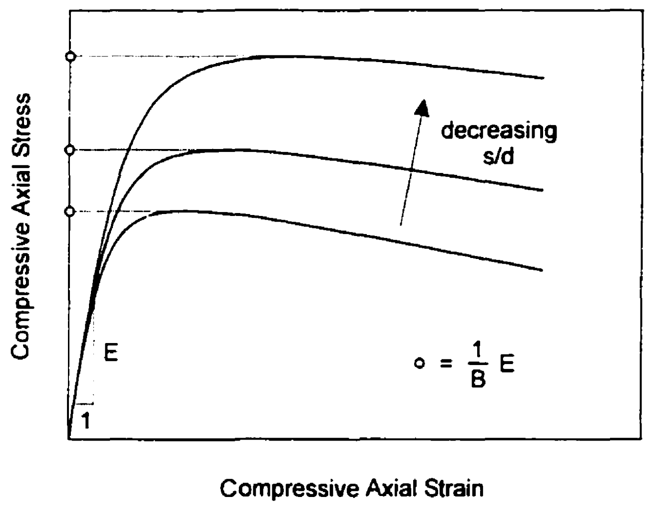

Figure 4.15 Evaluation of parameter 1/B at a selected ductility level

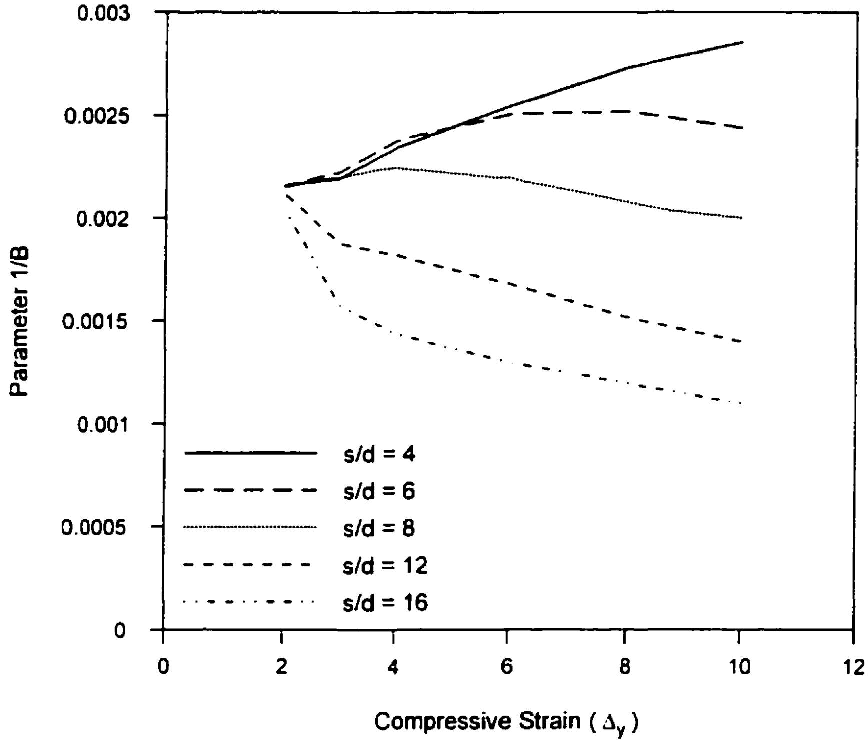

Figure 4.16 Parameter 1/B versus compressive strain for symmetrically loaded reinforcing bars

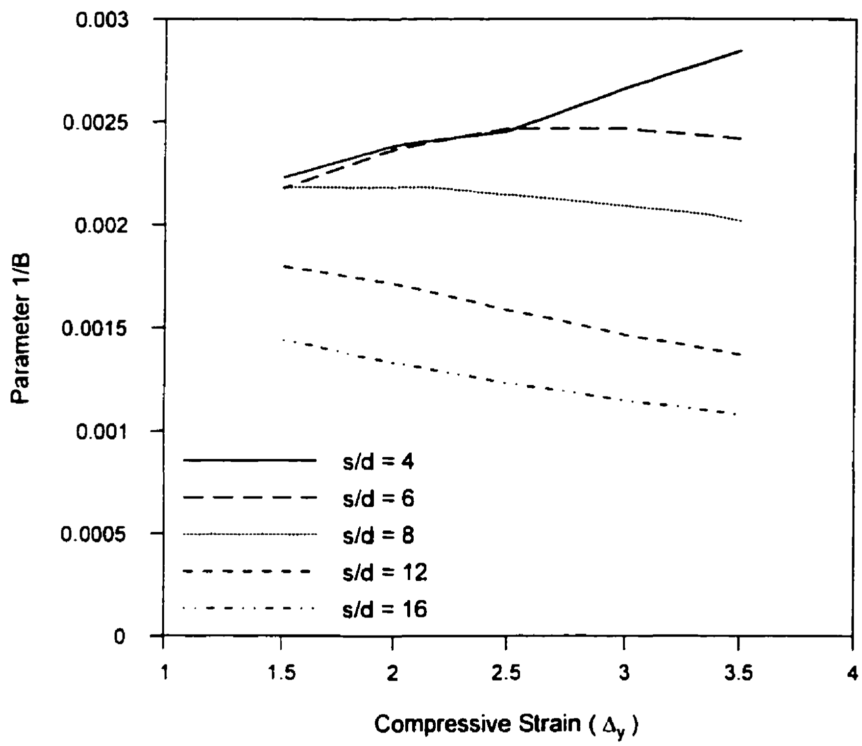

Figure 4.17 Parameter 1/B versus compressive strain for unsymmetrically loaded reinforcing bars

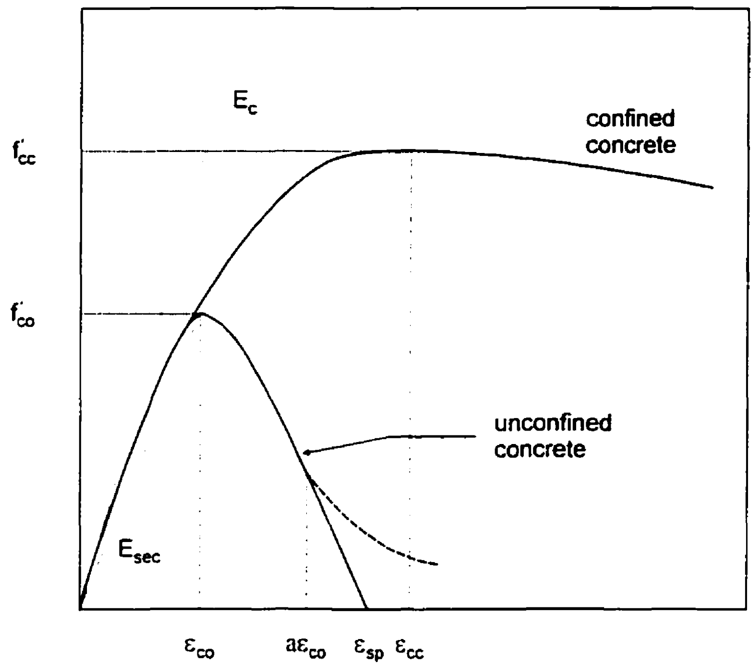

Figure 4.18 Stress-strain relationship for unconfined and confined concrete

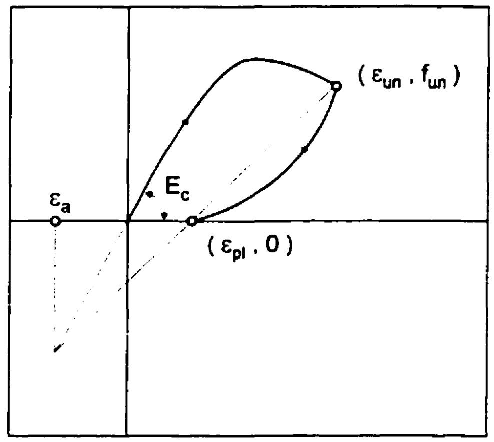

Figure 4.19 Concrete plastic offset strain, ε_{pl} and compressive unloading curve

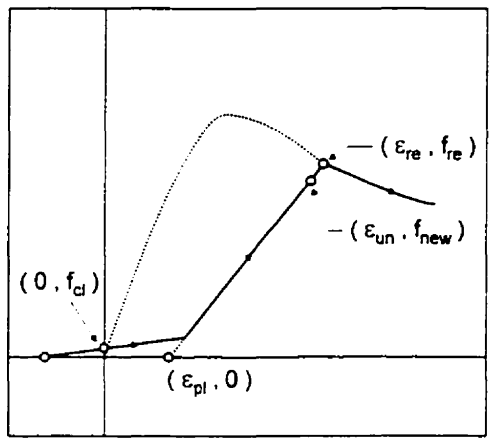

Figure 4.20 Key points on compressive reloading branch of concrete

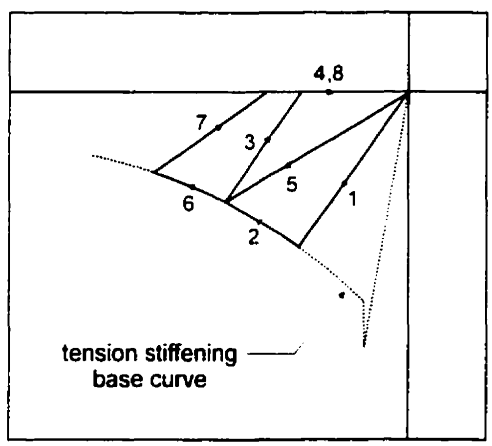

Figure 4.21 Tensile unloading and reloading branches

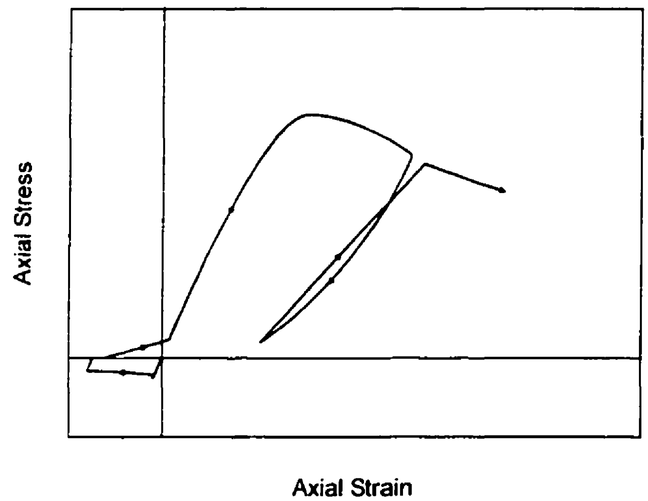

Figure 4.22 Modelled reversed cyclic loading response of concrete

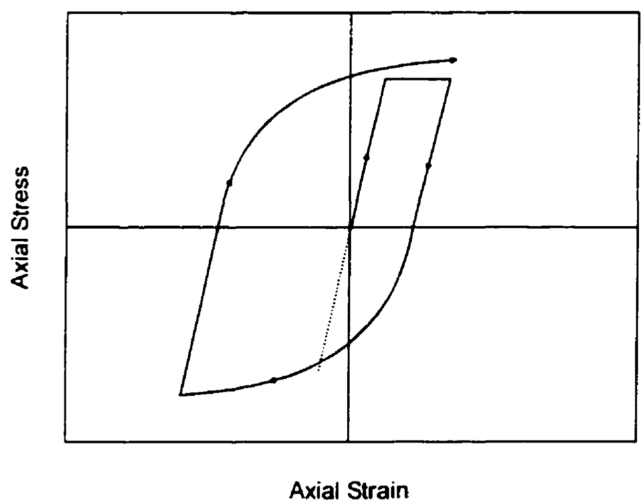

Figure 4.23 Modelled reversed cyclic loading response of reinforcing steel

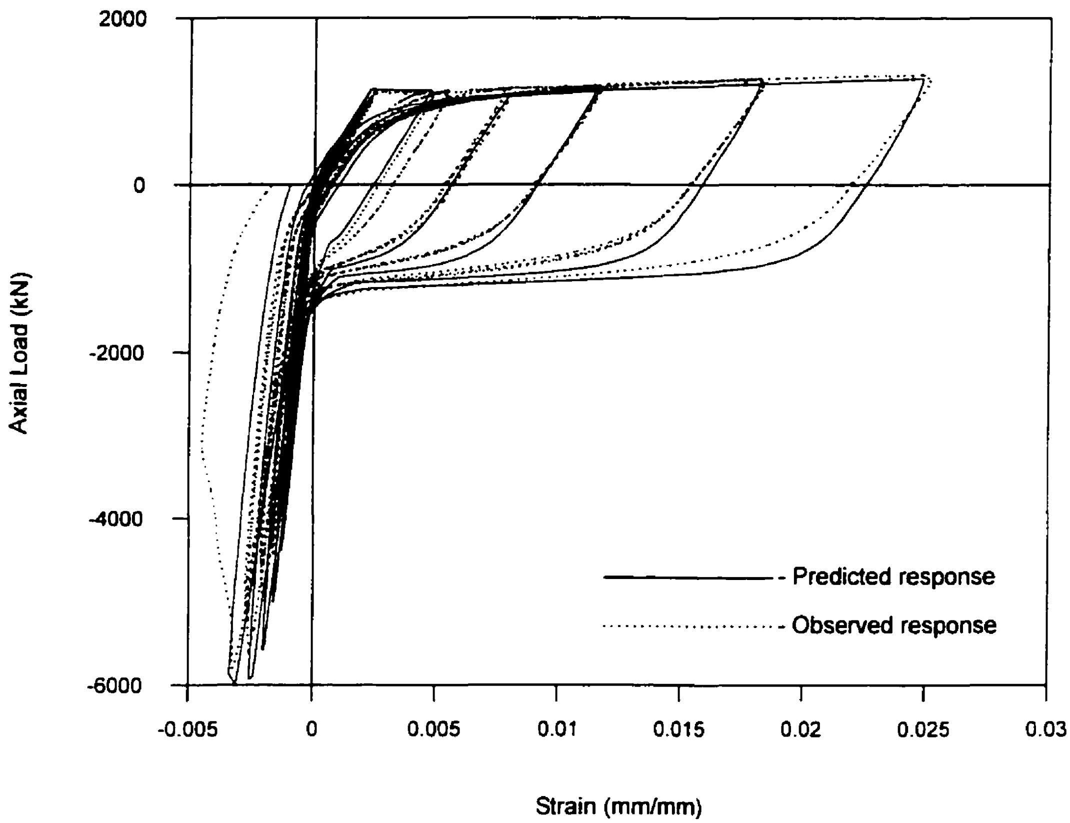

Figure 4.24 Observed and predicted response of Specimen N1

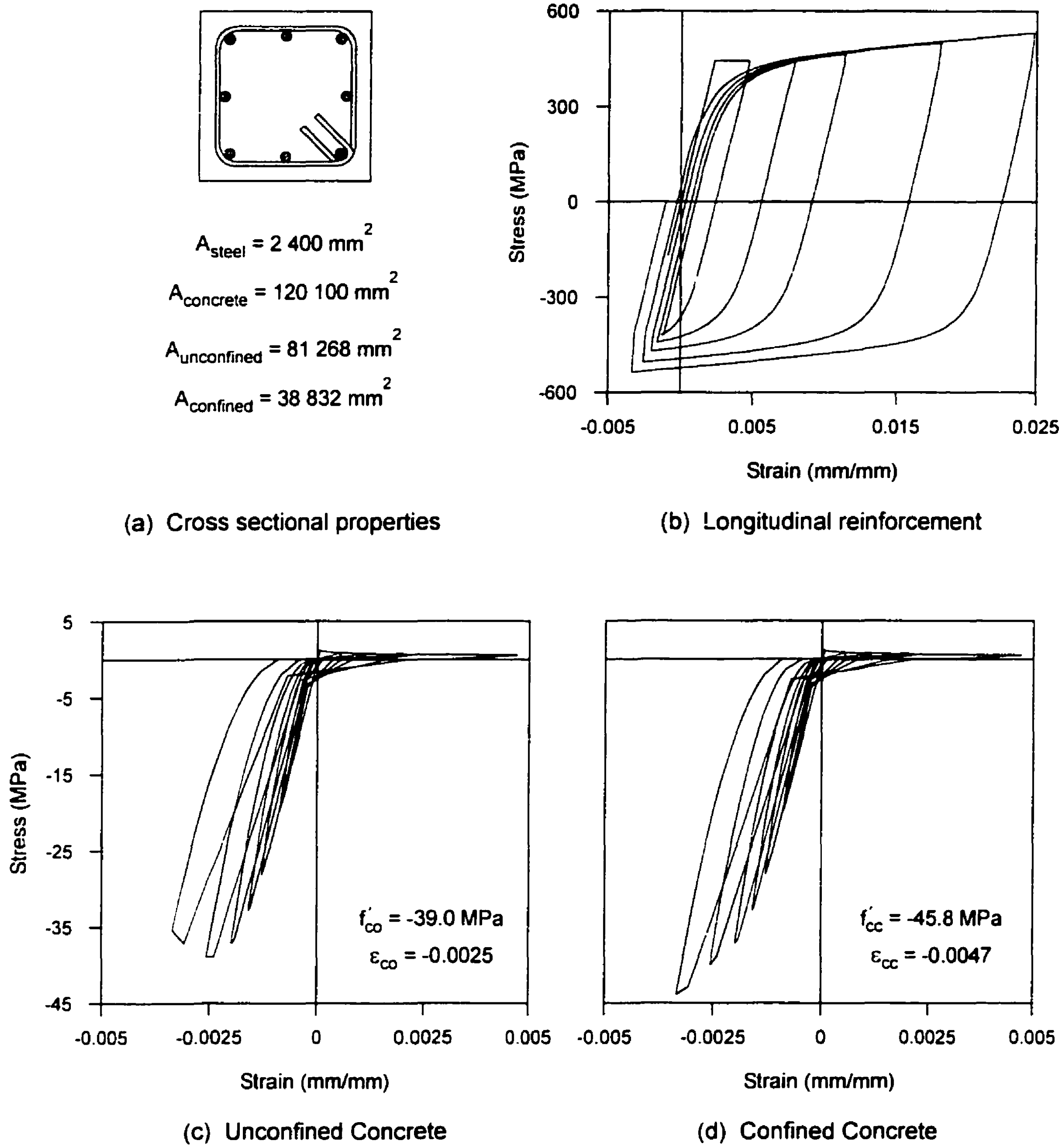

Figure 4.25 Predicted material responses for Specimen N1

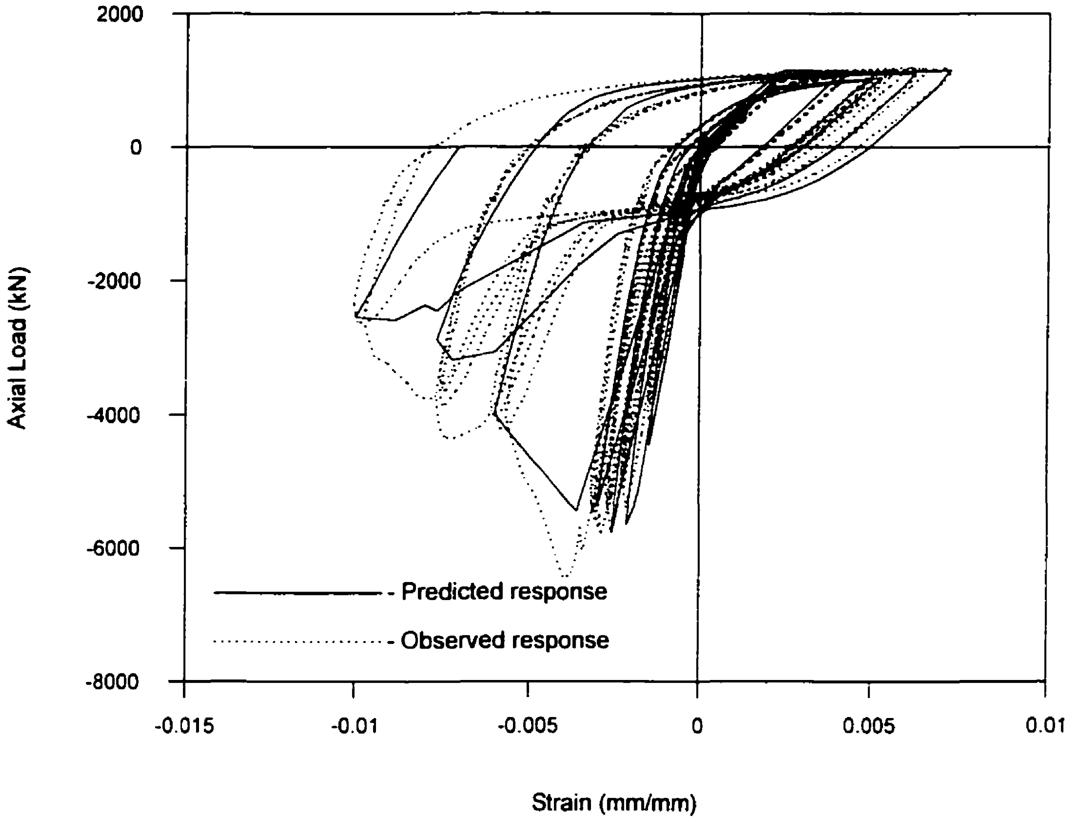

Figure 4.26 Observed and predicted response of Specimen N2

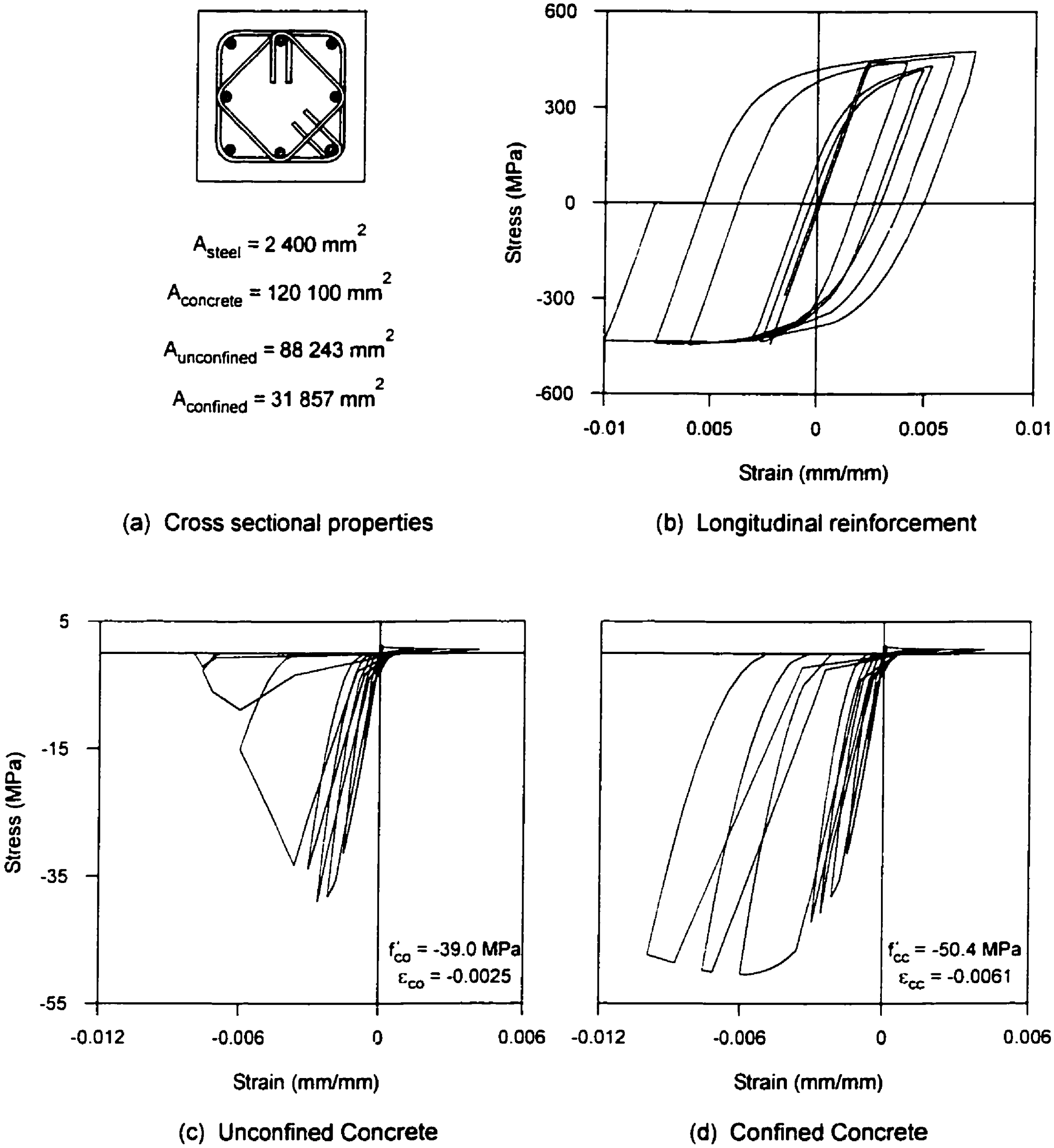

Figure 4.27 Predicted material responses for Specimen N2

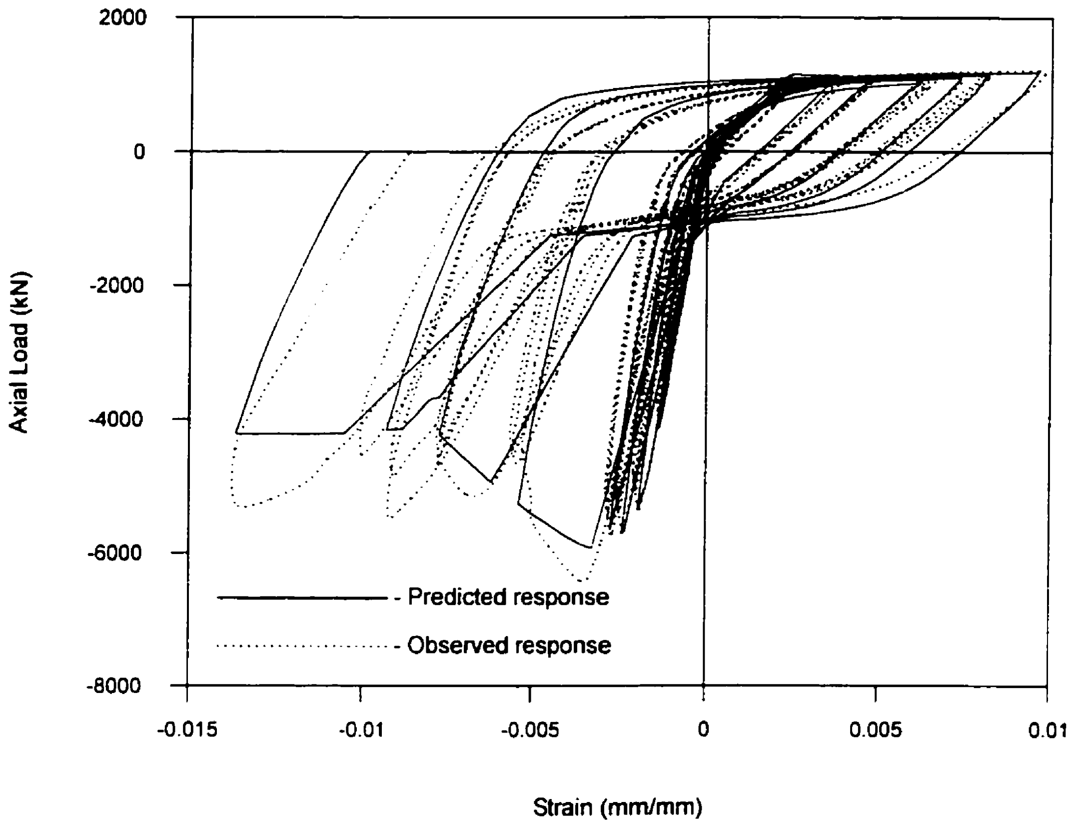

Figure 4.28 Observed and predicted response of Specimen N3

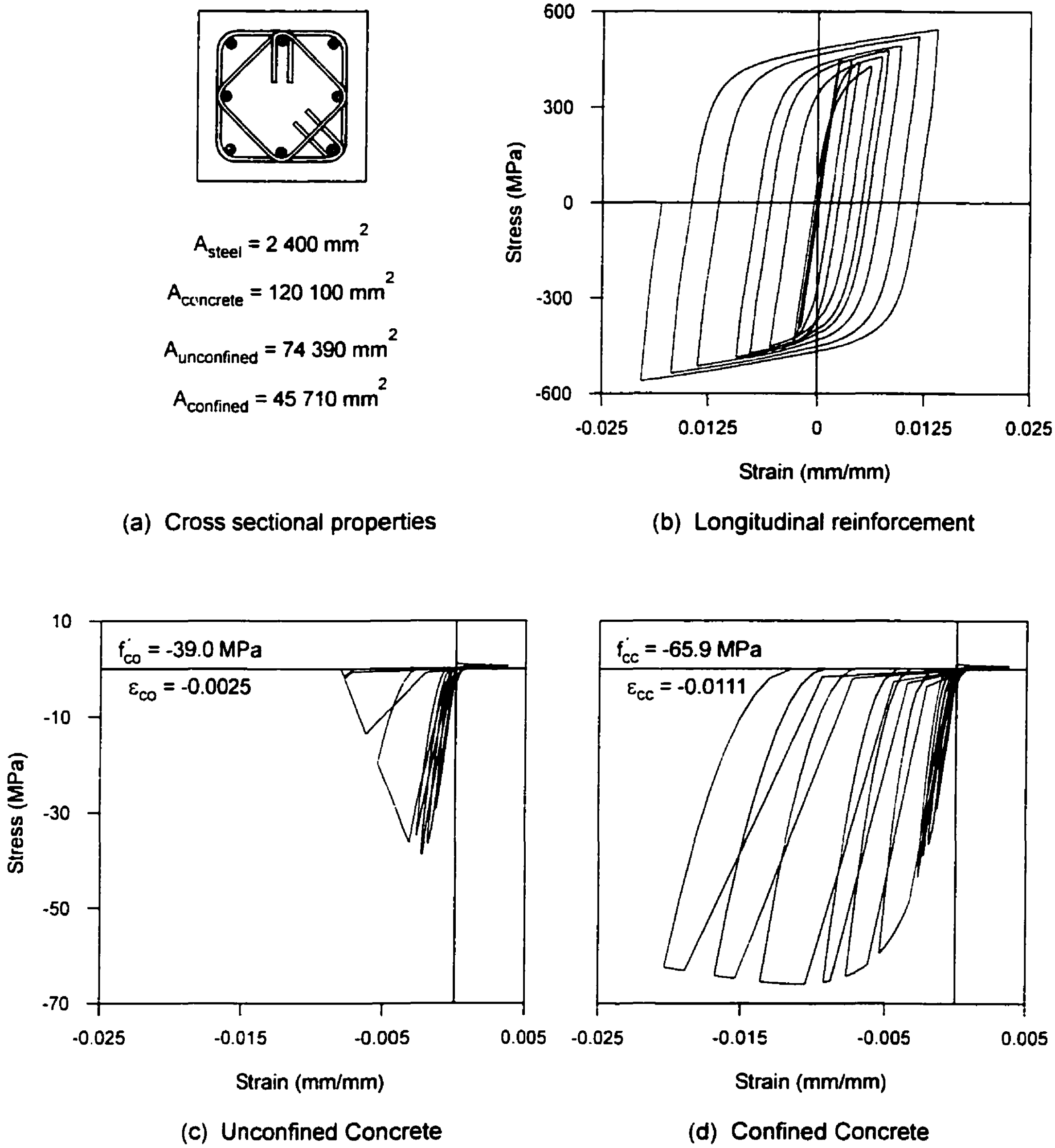

Figure 4.29 Predicted material responses for Specimen N3

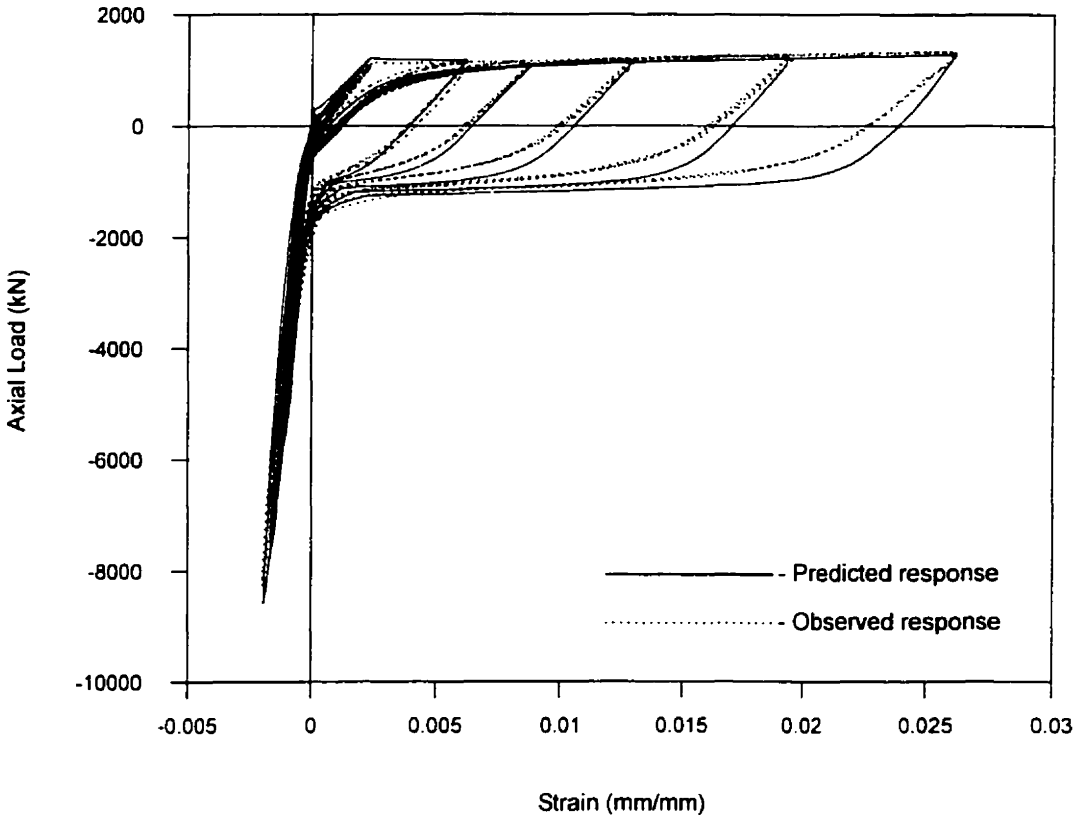

Figure 4.30 Observed and predicted response of Specimen H1

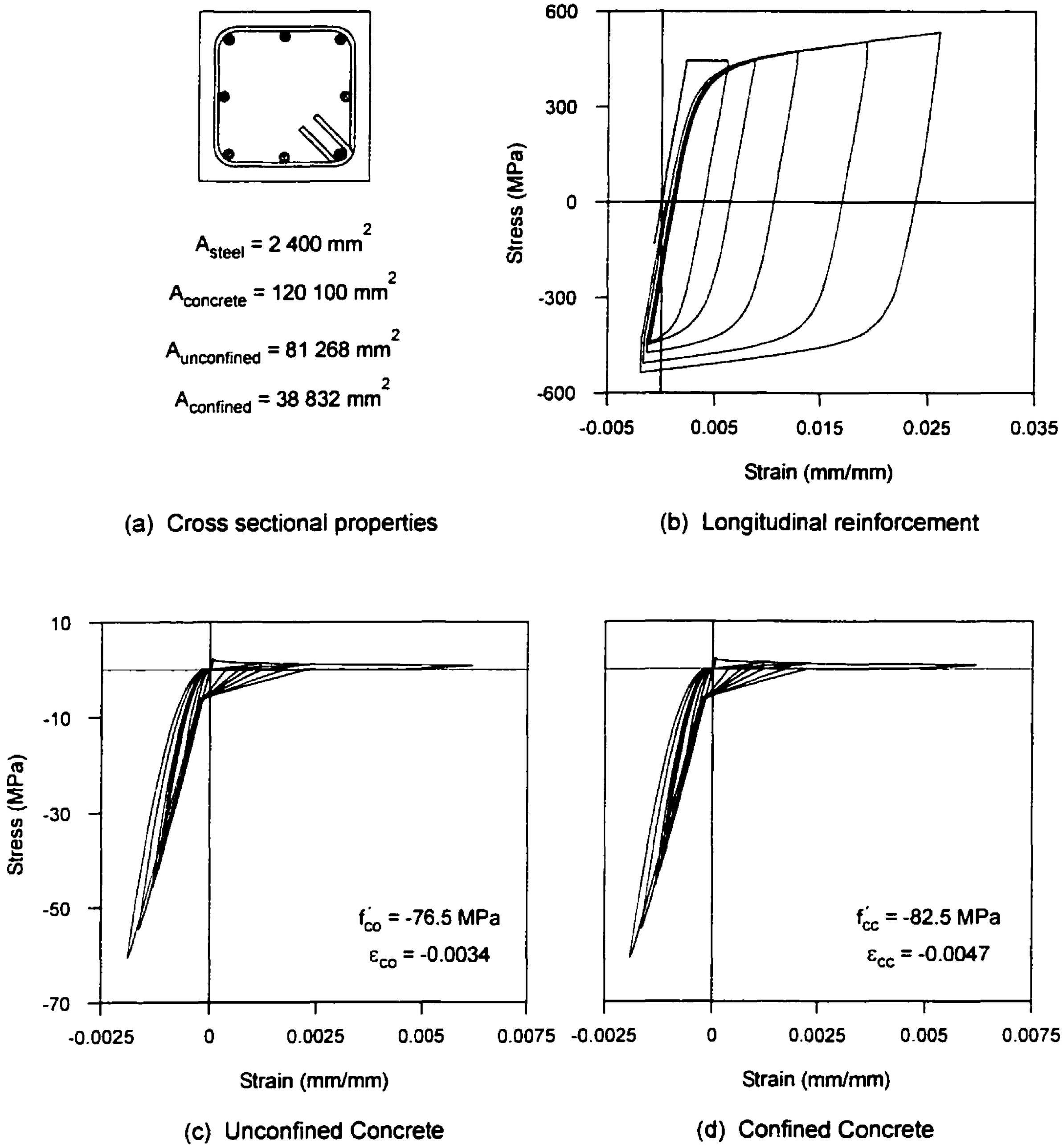

(a) Cross sectional properties

(b) Longitudinal reinforcement

(c) Unconfined Concrete

(d) Confined Concrete

Figure 4.31 Predicted material responses for Specimen H1

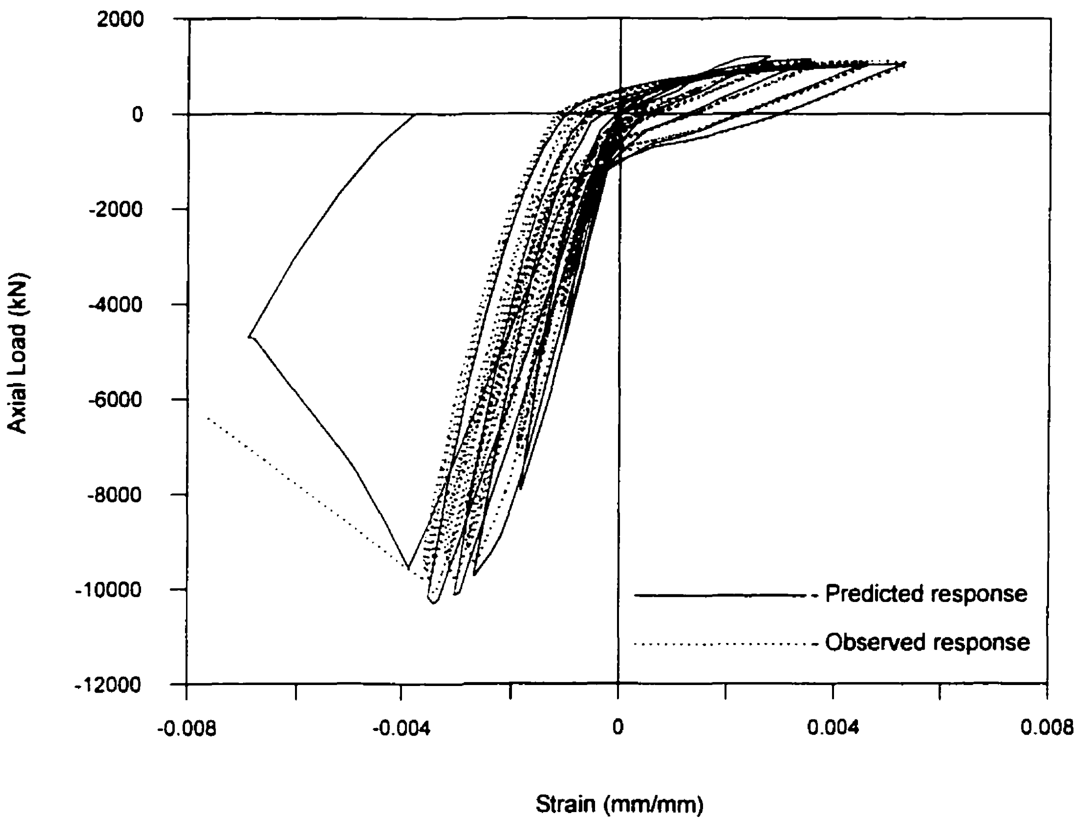

Figure 4.32 Observed and predicted response of Specimen H2

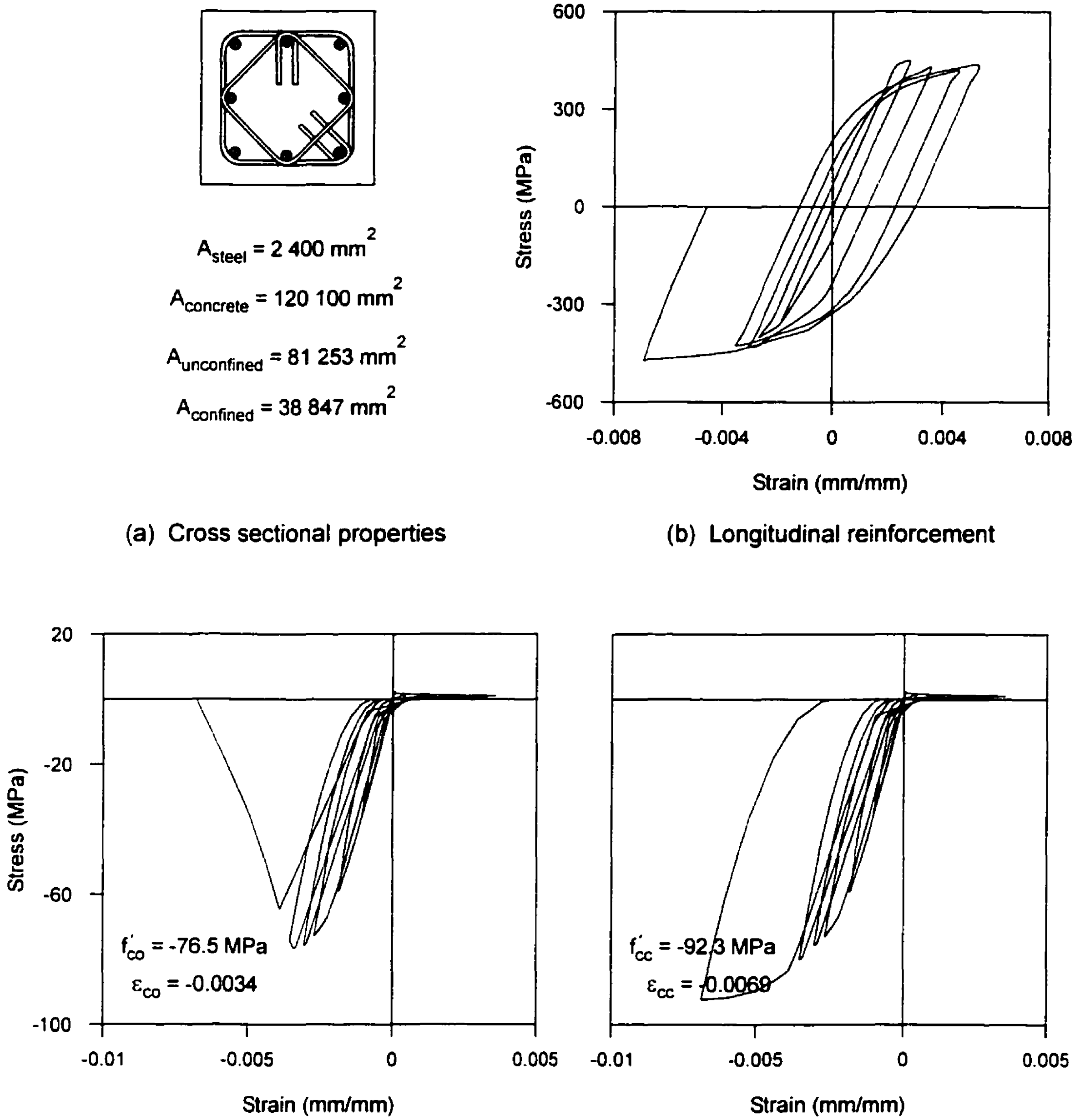

(a) Cross sectional properties

(b) Longitudinal reinforcement

(c) Unconfined Concrete

(d) Confined Concrete

Figure 4.33 Predicted material responses for Specimen H2

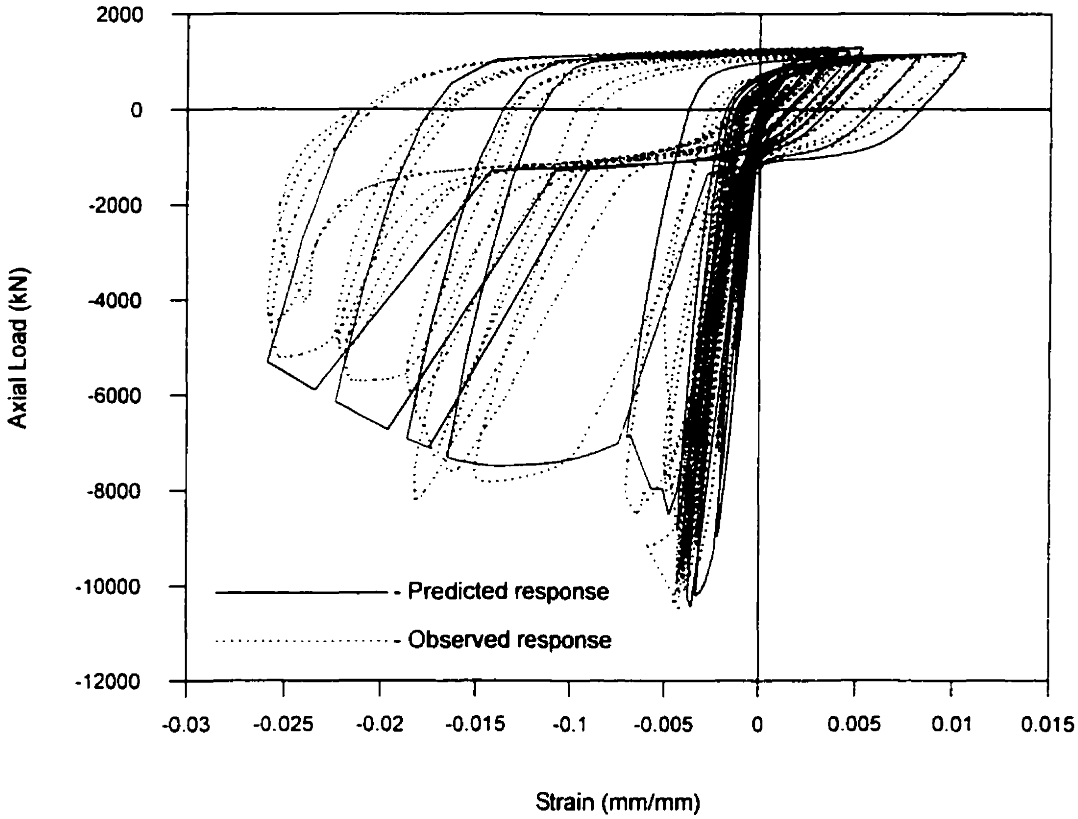

Figure 4.34 Observed and predicted response of Specimen H3

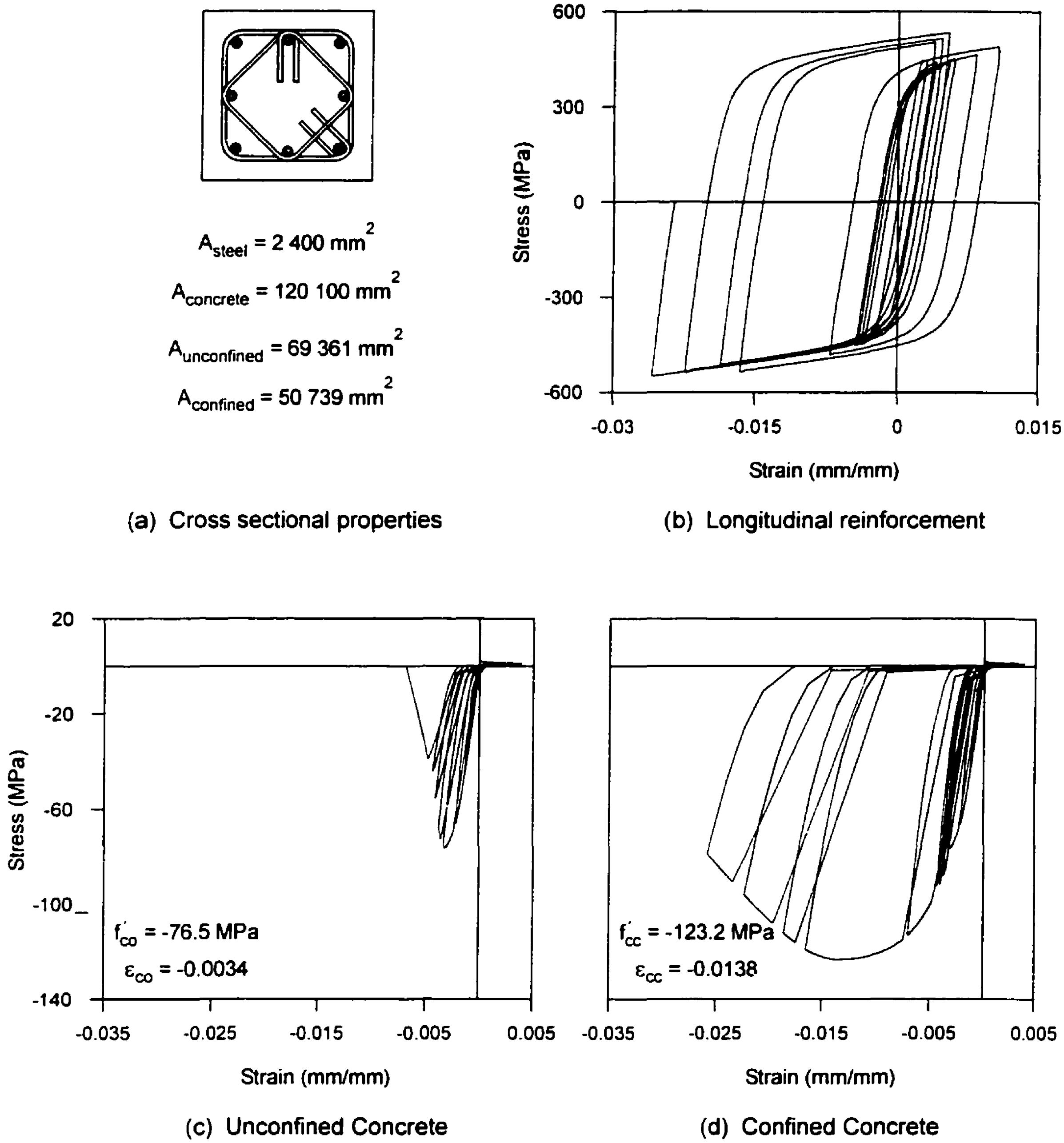

Figure 4.35 Predicted material responses for Specimen H3

Chapter 5

Description of Coupling Beam Specimens

This experimental programme was conducted to investigate the effect of high-strength concrete on the reversed cyclic response of conventionally reinforced concrete coupling beams. Specimens were designed using normal (30 MPa) and high-strength (70 MPa) concretes. For each concrete strength, two specimens were constructed; one detailed as a ductile reinforced coupling beam (R = 3.5), the second as a nominally ductile beam (R = 2.0). These specimens were designed in accordance with Clause 21, Special Provisions for Seismic Design, of CAN/CSA A23.3-M94 (CSA, 1994). The seismic behaviour of these specimens is presented in Chapter 6.

5.1 Coupling Beam Details

Figure 5.1 shows the dimensions and reinforcement details of a typical specimen. The 500 mm deep by 300 mm thick coupling beams were connected to wall segments at each end. The beams had 3-No. 25 reinforcing bars, top and bottom, with 2-No. 10 skin reinforcing bars at mid-height. The clear concrete cover for the beam was taken as 30 mm, which results in an effective depth, d, of 448 mm. The longitudinal reinforcing bars were embedded into the walls a length of 1100 mm, ($>1.5\ l_d$), to ensure adequate development of the bars at the beam-wall interface. The clear span of the beam was chosen to be 1800 mm, resulting in a span-to-depth ratio of 4.0. These dimensions were selected to investigate the performance of conventionally reinforced coupling beams with the minimum permitted span-to-depth ratio (Clause 21.3.1). The resulting moment-to-shear ratio at the face of the walls was 0.9 m.

The design of the transverse reinforcement of the beams is presented in the following sections.

5.1.1 Nominally Ductile Coupling Beams

These specimens were designed to satisfy the nominal ductility requirements of Clause 21.9 of the CSA Standard, CSA A23.3-94. The shear reinforcement was designed such that the nominal moment capacity of the member could be developed. Although no specific guidance is given in the code for calculating the factored shear capacity of nominally ductile beams, the angle of principal compression was assumed to be 45° and the concrete contribution was taken as 50% of the value determined from Equation 11-6 of the CSA Standard. This level of concrete contribution was selected since a reduced ductility level is expected in the plastic hinge region of a nominally ductile coupling beam, than for a ductile coupling beam. The resulting spacings of the hoops were 131 mm and 142 mm for the normal, (NR2) and high-strength, (MR2) concrete beams, respectively. These spacings were chosen, even though they exceeded the d/4 limit (111 mm) of Clause 21.9.2.1.2, in order to evaluate the shear behaviour of the beams without having an excess of shear reinforcement. It is noted that these spacings were kept smaller than the maximum spacing required to control the buckling of the longitudinal bars (i.e., less than $8d_b$). For each of these beam specimens the first hoop was located 50 mm from the face of each wall.

5.1.2 Ductile Coupling Beams

The force modification factor, R, for these beams is dependent on the degree of coupling of the system. The degree of coupling is dependent on the axial tension and compression forces within the walls resulting from shear forces developed in the coupling beams. The shear design of the ductile coupling beam was based on the provisions of Clause 21.7.3.1 for shear reinforcement in ductile frame members. The beam design shear force corresponds to the shear required to develop the probable moment resistance of the beam. The entire shear force is carried by the transverse reinforcement since the concrete contribution is assumed to be zero. The resulting hoop spacing was 90 mm and 85 mm for the normal, (NR4) and high-strength, (MR4) concrete specimens, respectively. These closely spaced hoops were required over a length equal to 2d from the face of each wall and hence were required over the entire length of the coupling beams. The first hoop was located at a distance of one-half of the hoop spacing from the face of the wall, (see Fig. 5.2).

5.1.3 Wall Details

The 300 mm thick, 1500 mm long and 1500 mm high walls, shown in Fig. 5.1, were identical for all four specimens. A region of concentrated reinforcement, consisting of 4-No. 25 vertical reinforcing bars, was provided at the inside edge of each wall. This concentrated reinforcement was tied with No. 10 hoops at a spacing of 250 mm in accordance with Clause 7.6.5.2, since this portion of the wall was assumed to be outside of the plastic hinge region.

Outside of the concentrated reinforcement region, two curtains of No. 10 reinforcing bars at a spacing of 200 mm were supplied in both the horizontal and vertical directions. Two additional No. 25 reinforcing bars were placed at the outside face of each wall to aid in construction.

5.2 Material Properties

5.2.1 Concrete

Two batches of ready-mix concrete with a minimum specified compressive strength of 30 MPa and 70MPa were used for the normal and high-strength concrete specimens, respectively. The two specimens of the same compressive strength were cast from the same batch to ensure consistency between the specimens. The mix design for each of these batches of concrete is given in Table 5.1.

Table 5.1 Concrete mix proportions

Component	30 MPa	70 MPa
cement, (kg/m^3)	355	480
fine aggregate, (kg/m^3)	790	850
coarse aggregate, (kg/m^3)	1040	1015
water, (L/m^3)	178	135
water-cement ratio	0.50	0.25
water reducing agent, (L/m^3)	1.11	1.63
superplasticizer, (L/m^3)	-	13.0
air entraining agent, (L/m^3)	0.18	-
retarding agent, (L/m^3)	-	0.78
slump, (mm)	100	250
air content	8.2 %	2.6 %
density, (kg/m^3)	2364	2494

All four of these specimens remained in the formwork and were moist cured for a total of five days after casting. Before each test, a set of three 150 x 300 mm cylinders, was tested to determine the average compressive strength of the concrete, f_c', and another set was tested to measure the average splitting tensile stress, f_{sp}. The average modulus of rupture, f_r, was determined by conducting a third point flexural test over a span of 300 mm on a set of three 100 x 100 x 400 mm beams. The shrinkage strain of the concrete over time was also measured for each of the concrete batches. Table 5.2 summarizes the measured concrete properties. The stress-strain relationship and the shrinkage strain over time, for each batch of concrete, are shown in Fig. 5.3 and Fig. 5.4, respectively.

Table 5.2 Concrete properties

Concrete	f'_c, MPa (std. dev.)	ε'_c (std. dev.)	f_{sp}, MPa (std. dev.)	f_r, MPa (std. dev.)
30 MPa	41.0 (0.73)	0.0022 (0.00009)	3.06 (0.125)	3.77 (0.026)
70 MPa	79.8 (0.57)	0.0030 (0.00003)	5.55 (0.322)	6.31 (0.269)

5.2.2 Reinforcing Steel

The properties of the reinforcing steel are given in Table 5.3. For a member designed for a force modification factor, R, greater than 2, the reinforcing steel must conform to CSA Standard G30.18 and be of weldable grade. For consistency, all of the specimens were constructed using the same weldable grade steel. Tension tests were performed on three random coupons for each bar size and an extensometer with gauge lengths of 50 and 150 mm, for the No. 10 and No. 25 bars respectively, was used to determine the steel strains. Figure 5.5 shows typical stress-strain relationships for the reinforcement.

Table 5.3 Reinforcing steel properties

Bar Description	f_y, MPa (std. dev.)	ε_y (std. dev.)	ε_{sh} (std. dev.)	f_{ult}, MPa (std. dev.)	ε_{rupt} (std. dev.)
No. 10 W	428 (11.3)	0.0023 (0.00016)	0.0165 (0.00211)	587 (6.5)	0.183 (0.0241)
No. 25 W	433 (1.9)	0.0023 (0.00013)	0.0148 (0.00026)	592 (0.3)	0.188 (0.0061)

5.3 Test Setup

The test setup and loading procedure for these coupling beam tests was the same as used by Harries (1995). Figure 5.6a indicates the location of the test specimen in the coupled wall structure. Analysis of a coupled wall system indicates that the critical coupling beam is located one third the way up the wall. A single coupling beam and a portion of the wall directly above and below this beam are represented by each test specimen. Under lateral loading of the coupled wall structure it is assumed that the centroidal axes of the walls remain parallel at all levels, see Fig. 5.6b. The manner in which the test setup simulates the applied shear, V, and relative deflection, δ, is shown in Fig. 5.6c.

Figure 5.7 shows a photograph of the setup for the coupling beam tests. The reinforced concrete walls were post-tensioned to the two steel reaction beams in order to simulate the compressive load on the walls due to the self weight of the structure. The high-strength threaded rods were strapped to the outside of the wall at 250 mm spacing and post-tensioned to 225 kN, resulting in a uniform compressive stress of 3 MPa in each wall.

The beam supporting the fixed wall was post-tensioned to the reaction floor in the laboratory using high-strength threaded rods with a total tie down force of 1.5 times the expected maximum applied load. The tie down closest to the coupling beam was post-tensioned to 1.25 times the maximum applied load, while the other was tensioned to 0.25 times the maximum applied load.

The loading beam was moved in a reversed cyclic manner using hydraulic rams located above and below the reaction floor. The line of action of these loading rams was located at the centre-line of the coupling beam. Adjustment of the leveling ram during the testing process ensured that the centroidal axes of the walls remained parallel.

Each wall was restrained from out-of-plane movement. The fixed wall was rigidly connected to a support frame post-tensioned to the reaction floor. A similar frame, with heavy duty rollers attached, prevented the out-of-plane movement of the loaded wall. During the testing of all of the specimens, no significant out of plane movement was observed.

5.4 Instrumentation

Figure 5.8 illustrates the location of the instrumentation used for the coupling beam test specimens. Four linear voltage differential transducers (LVDT's), two attached to each wall, measured the vertical displacements of the walls, allowing the calculation of the relative displacement between the walls and were also used to ensure that the centroidal axes remained parallel during testing. Four load cells measured the applied load at the centre of the coupling beam and an additional load cell measured the corrective load to keep the walls parallel.

An array of LVDT's measured the horizontal movements of the top and bottom of both ends of the beam, allowing the curvatures of a number of sections to be determined. Two LVDT rosettes, (0° - 45° - 90°) were located approximately half of the shear depth, d, from the face of each wall. These provided the evaluation of the principal shear, tensile and compressive strains of the beam at the critical cross section.

Electrical resistance strain gauges, at the quarter points, were glued to the central longitudinal reinforcing bar on the top and bottom faces of the beam. Additional strain gauges were attached to the hoop reinforcement at the mid-height of both vertical legs. Every second hoop, within a distance of d, from the face of the wall, was instrumented. These gauges provided detailed strain measurements at critical positions along the length of the coupling beam.

5.5 Loading Histories

The loading history for the coupling beam specimens is shown, schematically in Fig. 5.9. For all test specimens an upward load and deflection of the loaded wall was taken as positive.

The tests were conducted in "load control" until the general yielding of the section was realized and in "deflection control", thereafter. At each load or deflection level the specimens were cycled three times, with each cycle including a tensile and compressive peak. Load control involved cycling the test specimen at pre-determined load levels until general yielding was reached. After this point the specimens were cycled at multiples of the general yield deflection. Table 5.4 gives the load or deflection peaks and the value of general yield displacement, Δ_y, used during testing. The actual values of the yield deflection and load, for each of the test specimens, were determined after post-processing of the collected data. The location of general yielding, which represents flexural yielding, was determined using a bilinear approximation of the response envelope of the specimen; with the elastic portion being defined by the secant stiffness at first yield of the longitudinal reinforcement, (Paulay and Priestley, 1992).

Table 5.4 Summary of loading histories of coupling beam specimens

Specimen	NR2	NR4	MR2	MR4
Load Control	±50 kN ±150 kN	±50 kN ±150 kN	±50 kN ±150 kN	±50 kN ±150 kN
Δ_y	±16 mm	±15 mm	±14 mm	±13 mm
Deflection Control	$\pm 2\ \Delta_y$ $\pm 3\ \Delta_y$	$\pm 2\ \Delta_y$ $\pm 3\ \Delta_y$ $\pm 4\ \Delta_y$	$\pm 2\ \Delta_y$ $\pm 3\ \Delta_y$ $\pm 4\ \Delta_y$	$\pm 2\ \Delta_y$ $\pm 3\ \Delta_y$ $\pm 4\ \Delta_y$ $\pm 5\ \Delta_y$

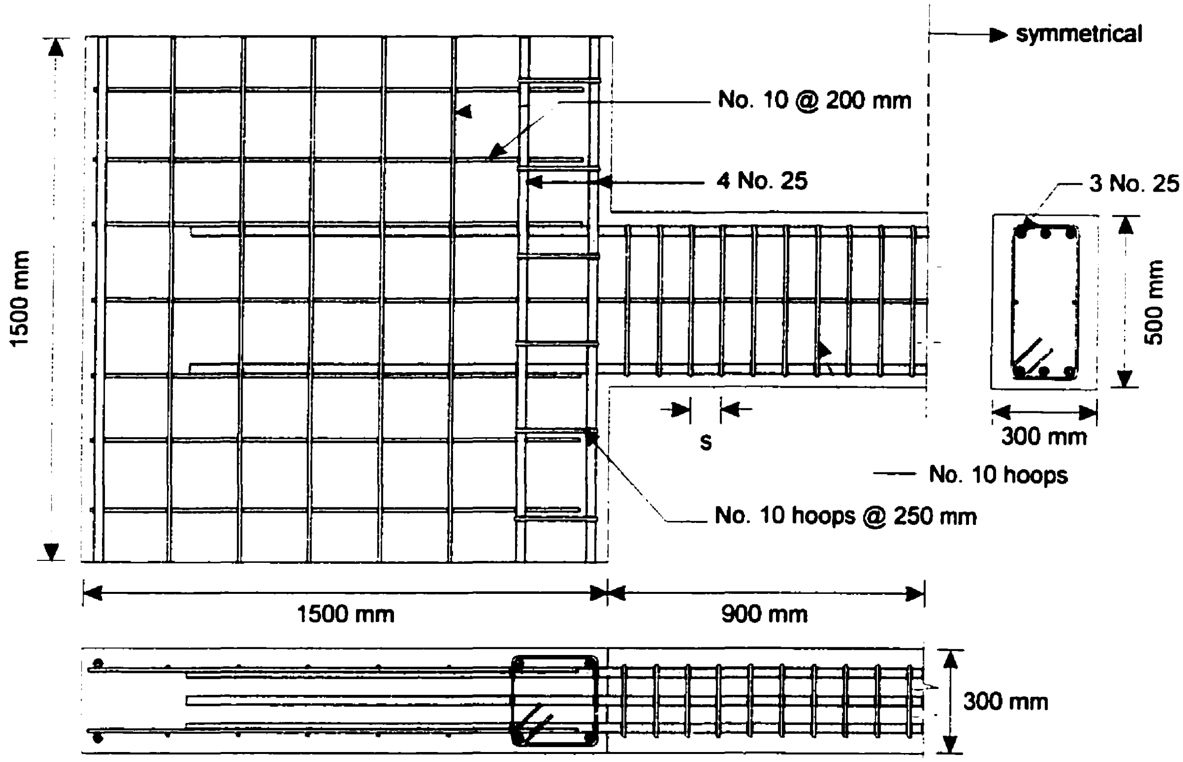

Figure 5.1 Coupling beam and wall reinforcing details

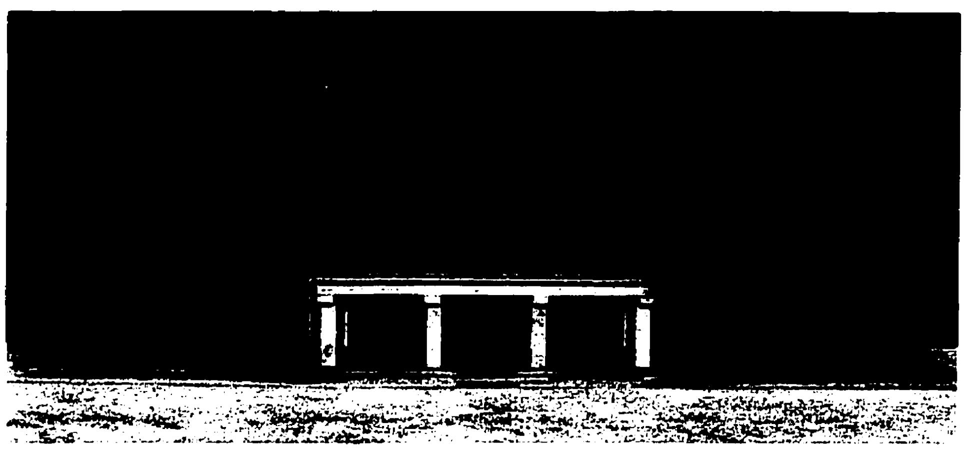

Figure 5.2 Reinforcing cage for Specimen NR4

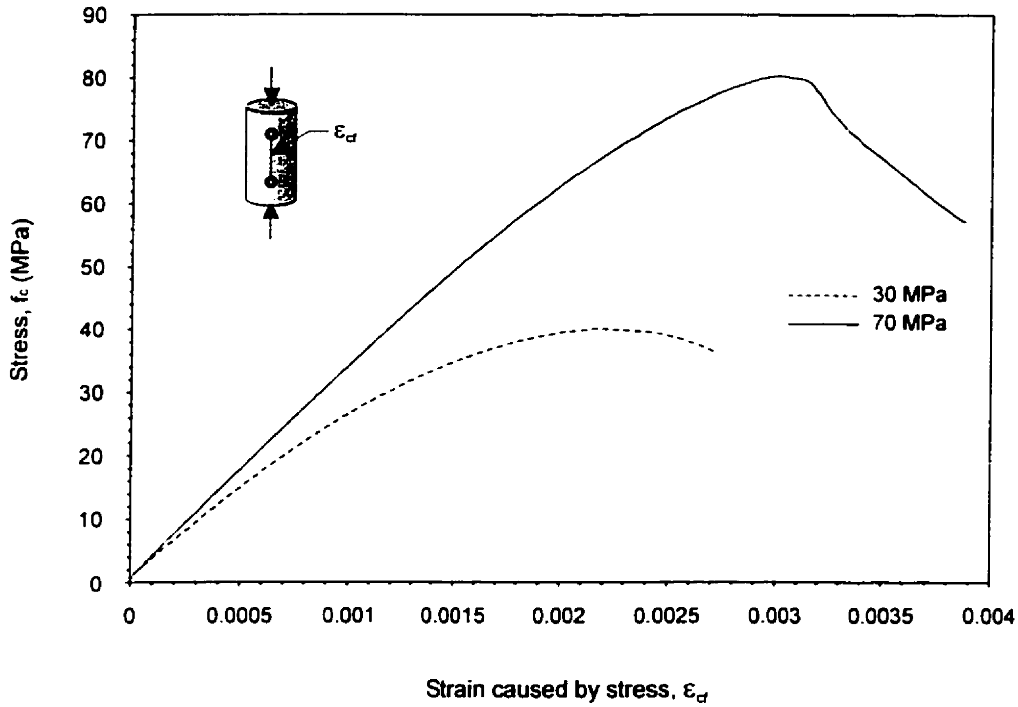

Figure 5.3 Typical compressive stress-strain responses for concrete

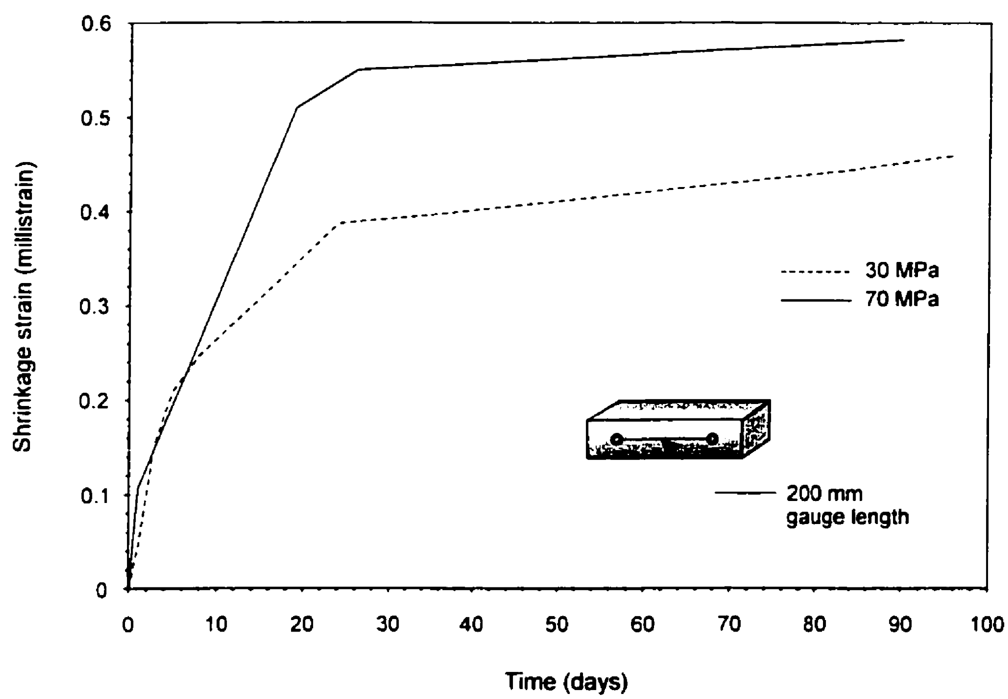

Figure 5.4 Average shrinkage strains measured in concrete prisms

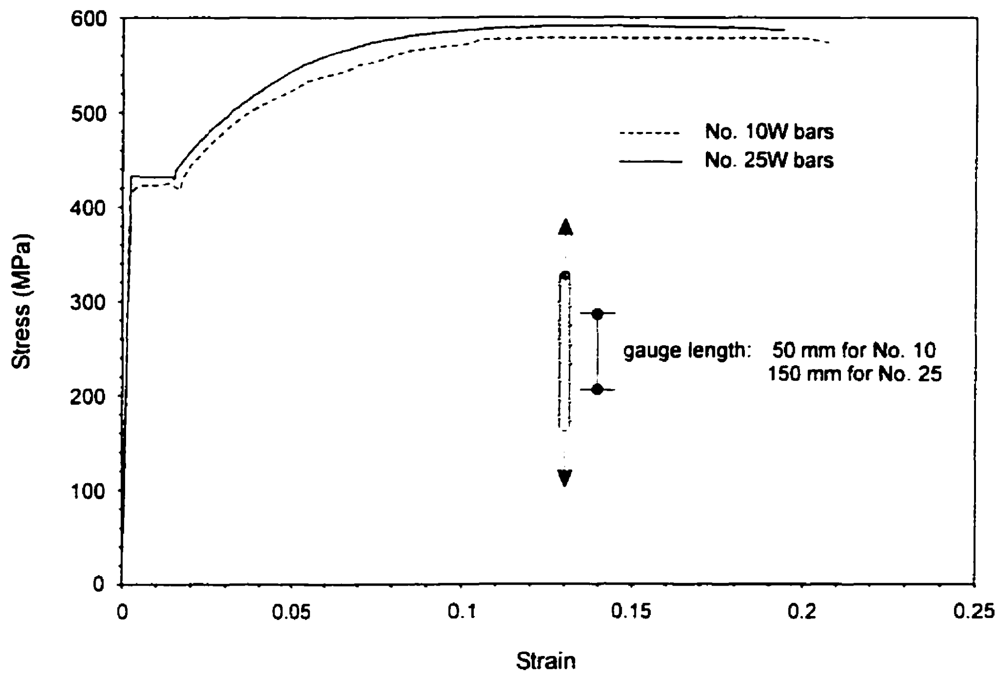

Figure 5.5 Typical stress-strain responses for reinforcing steel

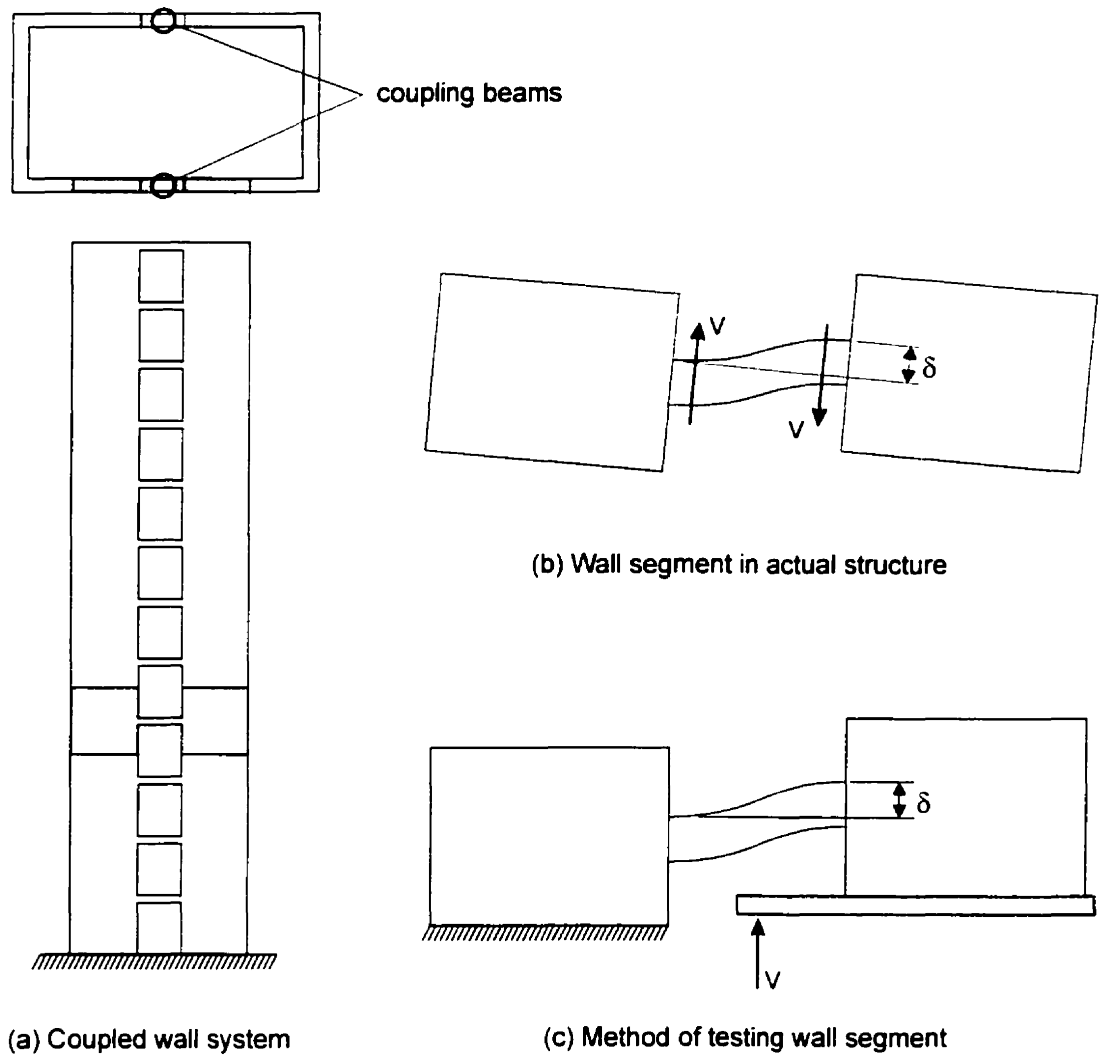

Figure 5.6 Method of simulating actual coupled wall behaviour

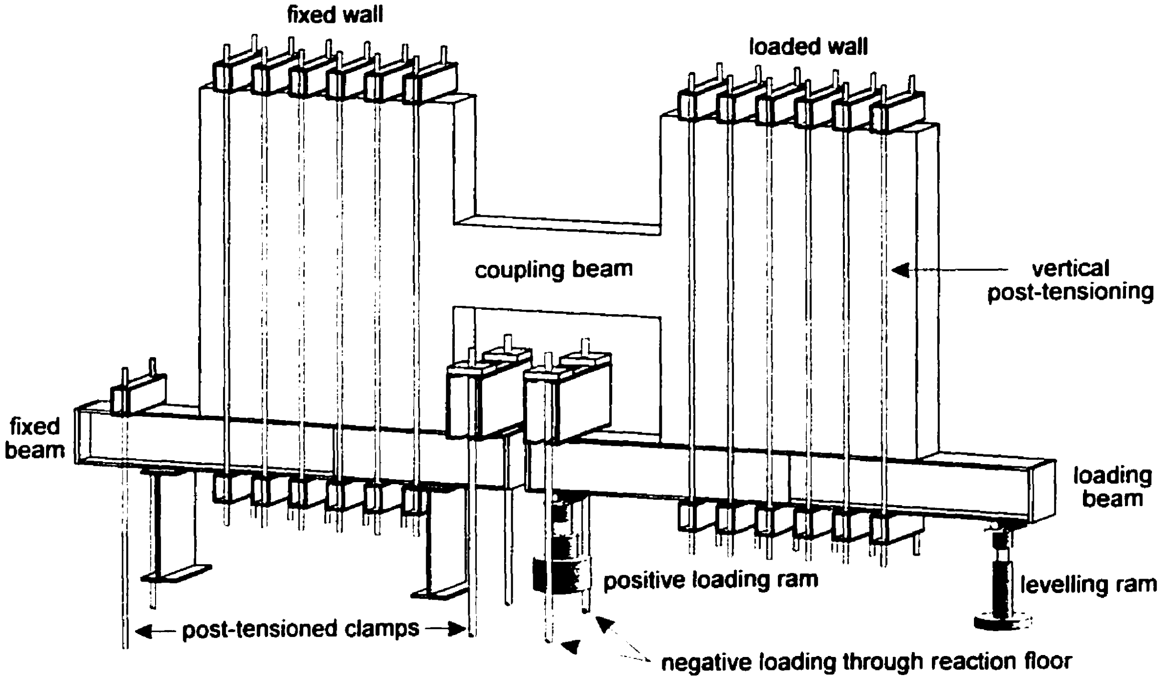

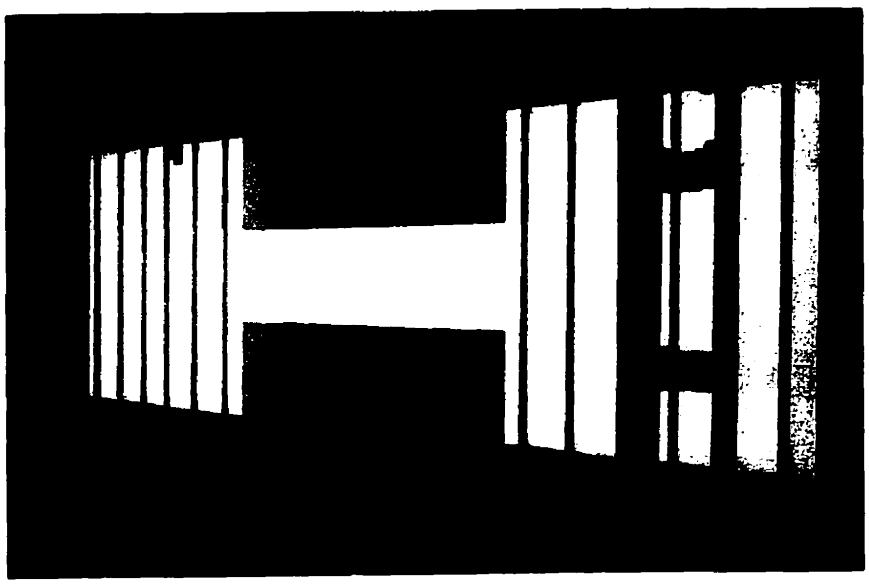

Figure 5.7 Schematic and photograph of test setup for coupling beam specimens

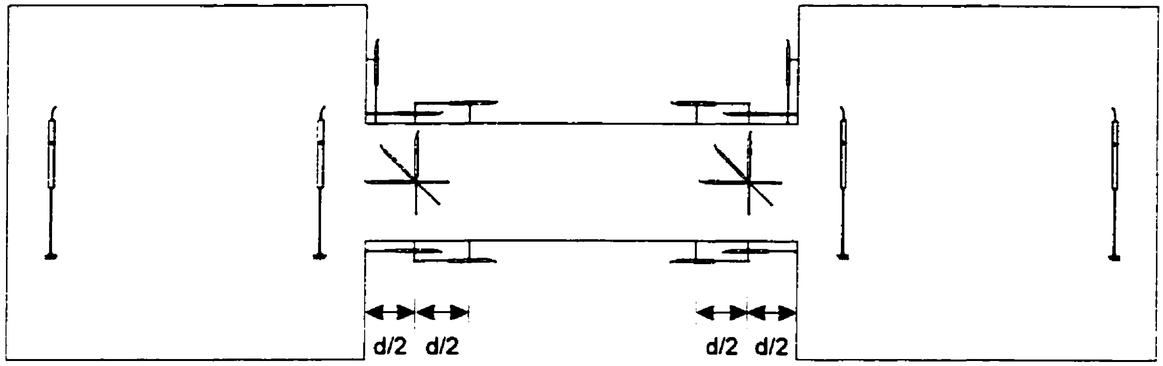

(a) Locations of LVDT's

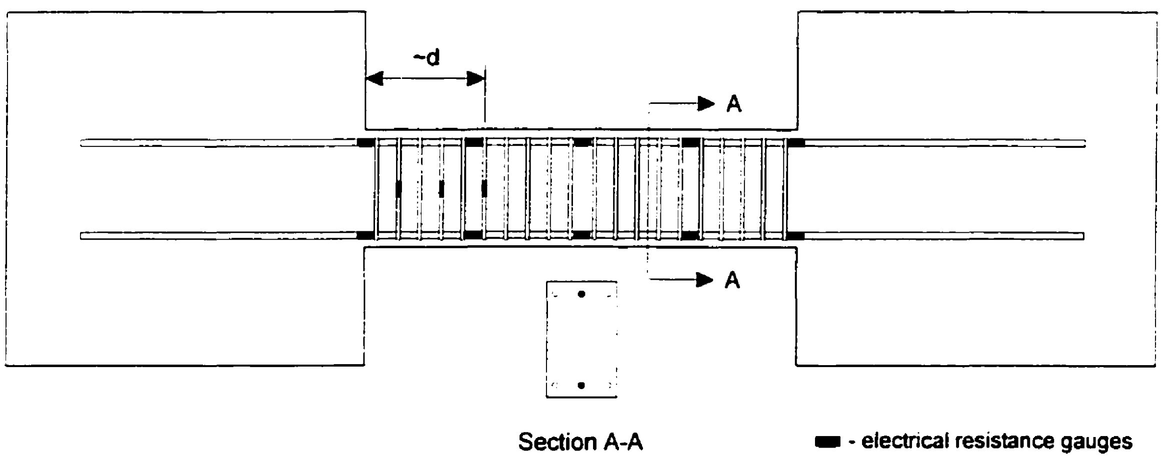

(b) Locations of electrical resistance strain gauges

Figure 5.8 Instrumentation of coupling beam specimens

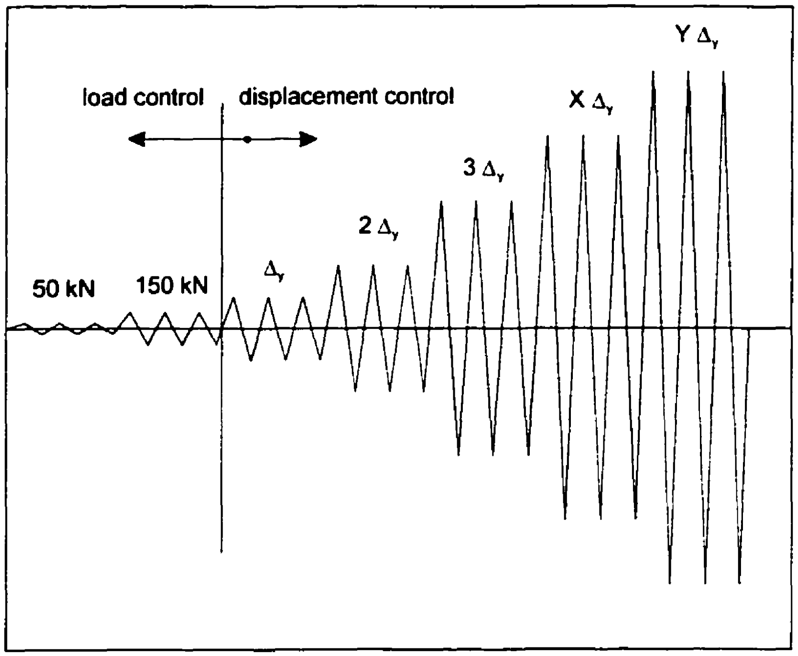

Figure 5.9 Schematic representation of loading histories for coupling beam specimens

Chapter 6

Behaviour of Coupling Beam Specimens

This chapter presents a detailed description of the observed experimental behaviour of the concrete coupling beams and compares the reversed cyclic responses of each of these specimens.

For the load-deflection plots; the load corresponds to the shear applied to the coupling beam and the deflection represents the relative vertical movement between the fixed and loaded walls. During testing, differential rotations between the walls were measured enabling and the overall vertical deflection to be corrected for these rotations. These corrections were small and had very little effect on the overall displacements of the specimens.

Summaries of the peak loads and deflections for key load stages are given in Tables 6.1 through 6.4. These summaries include the first load stage for each increment of load or deflection. All of the peak loads and defections for each of the specimens are given in Appendix B. The load stage designations A and B represent positive (upwards) and negative (downwards) loads and deflections, respectively.

6.1 Observed Behaviour of Concrete Coupling Beams

6.1.1 Specimen NR2

This specimen was constructed using normal-strength concrete and was designed as a nominally ductile beam. The shear design utilized 50% of the shear contribution of the concrete, which resulted in a hoop spacing of 131 mm. Figure 6.1 gives the applied load versus relative displacement of this specimen. The load stage peak loads and deflections are presented in Table 6.1.

This specimen cracked during the first loading cycle. These cracks were vertical and were located on the top and bottom of the beam, within 50 mm of the interface between the beam and the wall, which coincided with the location of the first hoop closest to the wall. Minor elongation of these hairline cracks occurred during the second and third cycles at this load level. Further cracking occurred as this specimen was loaded towards an applied shear of 150 kN,

Table 6.1 Key load stages for Specimen NR2

Load Stage	Positive (A) Cycle		Negative (B) Cycle		Notes
	Applied Shear (kN)	Relative Deflection (mm)	Applied Shear (kN)	Relative Deflection (mm)	
1	49.1	0.90	-45.6	-0.63	first cracking
4	141.2	5.68	-139.7	-4.29	$\cong 0.5\ M_y$
7	294.2	16.34	-312.2	-15.81	$+1.13\Delta_y$, $-1.10\Delta_y$
10	324.1	31.04	-326.0	-31.95	$+2.16\Delta_y$, $-2.22\Delta_y$
13	317.7	47.13	-336.1	-48.15	$+3.27\Delta_y$, $-3.34\Delta_y$

which corresponds to approximately half of the yield moment, $0.5M_y$, which was predicted as 130 kNm. Diagonal tensile stresses due to shear caused these cracks to form at approximately a 45° angle as they propagated towards the mid-depth of the beam. These cracks formed at an average spacing of 125 mm, which is very close to the spacing of the transverse hoops. The cracks within the beam were about 0.1 mm in width and the interface cracks reached a width of 0.2 mm at the peak load levels of the sixth cycle.

Vertical cracks within the walls formed as this specimen was loaded towards general yielding. These cracks indicated the propagation of yield along the length of the longitudinal beam reinforcement. Several flexure-shear cracks formed along the length of the beam. At the end of the third cycle at this deflection level the crack widths at the mid-height of the beam reached a maximum of 0.5 mm, while the largest cracks at the wall interface were 0.8 mm in width. The load and deflection corresponding to general yielding of this specimen was determined by using a bi-linear approximation of the load-deflection response, as shown in Fig. 6.1. The general yield deflection was 14.4 mm, which is the average of the positive and negative general yield deflections

The three cycles at twice the yield deflection resulted in some crack extensions but no new cracks formed within the beam, but there was some further cracking within the walls. The width of the cracks at the interface continued to increase, reaching a maximum of 3 mm. There was evidence of crushing of the concrete at the beam-wall interface and at the intersection of the principal shear cracks at the mid-height of the beam.

During the first loop at $3.3\Delta_y$ there were a few new cracks and existing cracks increased in widths to 4 mm and 1.25 mm at the interface and mid-height of the beam, respectively. During the negative loading portion of this cycle, a portion of the cover concrete located at the bottom of the beam spalled. At this point in the test the beam had increased in length by 13 mm. During the following two cycles there was evidence of shear sliding along the inclined shear cracks. This shear deformation is evident in the pinching of the hysteretic loops in the load-deflection diagram. At the completion of the test there was severe spalling of the beam cover concrete exposing the longitudinal and transverse reinforcement with the yielding of this reinforcement clearly evident. Figure 6.2 shows the specimen at the completion of testing.

Figure 6.3 presents the moment-curvature responses of the beam in two regions along the beam. The moment plotted corresponds to the calculated moment at the centre of the region considered. It is clear that the major flexural deformations were limited to the region closest to the beam-wall interface. The positive curvatures, which peaked after the first cycle at $2.2\Delta_y$, began to decrease within the interface region, R1. This was due to the increased influence of shear deformations on the response of the beam. This is evident from the increase in the shear strain, γ, at the critical section located a distance of d/2 from the interface as shown in Fig. 6.4. Only the shear cracks in the positive direction passed through the strain rosette, resulting in a lack of symmetry in the shear strains shown in Fig. 6.4.

Figure 6.5 shows the strains in the longitudinal reinforcement at various positions along their length. The strain gauge location in bold type has been plotted and the shaded region indicates elastic response of the steel. It is clear that the strain levels in the longitudinal reinforcement decrease as the location moves towards the mid-span of the beam. The transverse hoop reinforcement experienced yielding after general yielding in flexure occurred. The maximum strain in the hoops was 3.96×10^{-3}, or 1.72 times the yield strain (see Fig. 6.6).

6.1.2 Specimen NR4

This specimen was constructed using normal-strength concrete and was designed as a ductile coupling beam. The transverse reinforcement was designed to resist the shear corresponding to flexural hinging with the concrete contribution taken as zero. This resulted in a hoop spacing of 90 mm. The applied load versus relative displacement of this specimen is given in Fig. 6.7. The peak loads and deflections corresponding to key load steps are presented in Table 6.2.

First cracking of this specimen occurred during the first loading cycle. These hairline cracks extended only slightly during the next two cycles at this load level. Flexural-shear cracks

Table 6.2 Key load stages for Specimen NR4

Load Stage	Positive (A) Cycle		Negative (B) Cycle		Notes
	Applied Shear (kN)	Relative Deflection (mm)	Applied Shear (kN)	Relative Deflection (mm)	
1	49.3	0.78	-72.1	-0.99	cracking
4	136.38	5.12	-164.2	-5.04	$\cong 0.5\ M_y$
7	283.6	15.11	-320.0	-14.58	$+1.20\Delta_y$, $-1.16\Delta_y$
10	321.1	28.97	-331.1	-30.60	$+2.30\Delta_y$, $-2.43\Delta_y$
13	320.2	44.13	-344.3	-45.14	$+3.50\Delta_y$, $-3.58\Delta_y$
16	293.4	59.07	-209.8	-60.32	$+4.69\Delta_y$, $-4.79\Delta_y$

started to develop as this specimen was loaded to half of the yield moment. These cracks were spaced at approximately two stirrup spacings, or 180 mm, apart and reached an average width of 0.15 mm at the level of the longitudinal steel.

While loading towards general yielding of the coupling beam, several wall cracks developed indicating the development of the longitudinal reinforcement embedded in the wall. Several flexural-shear cracks developed within the beam up to 800 mm from the face of either wall. There was minor crack propagation but no new crack development during the other two cycles at this deflection. The cracks at the beam-wall interfaces and within the beam reached widths of 1.0 mm and 0.4 mm, respectively. The general yield deflection for Specimen NR4 was determined to be 12.6 mm.

During the three loading cycles at $2.3\Delta_y$ there was no new cracking within the beam, with the existing cracks reaching widths of 0.8 mm and 3.0 mm within the beam and at the interface, respectively. Some new cracks developed within the central portion of the walls, indicating the progression of yielding within the longitudinal reinforcement. There was evidence of minor flaking of the concrete at the interface between the beam and the wall during these loading cycles.

As this specimen was cycled at $3.5\Delta_y$, there was some minor elongation of the existing cracks but no new cracks formed. The crack widths continued to increase dramatically. The interface cracks grew to a width of 5.0 mm. Only the cracks located within approximately 250 mm from the interface continued to increase in width, reaching 3.0 mm. During the negative portion of the final cycle at this deflection level, the bottom cover concrete spalled exposing the transverse and the longitudinal reinforcement. The longitudinal reinforcement showed signs of excessive yielding and was beginning to buckle. The hoops showed no signs of yielding, however the bottom leg was starting to bend due to the initiation of buckling of the longitudinal reinforcement.

During the first cycle towards a peak displacement of $4.7\Delta_y$, there was further spalling of the cover concrete. The beam started to slide along the wall at the interface and this became the dominant deformation contribution. The capacity of the coupling beam greatly diminished as the resistance was produced by dowel action of the longitudinal reinforcement. This type of failure resulted from the elongation of the coupling beam caused by the excessive yielding of the longitudinal reinforcement. Figure 6.8 shows Specimen NR4 at the completion of testing.

Figure 6.9 shows the moment-curvature response of two regions within the coupling beam. It is clear that flexural deformation was limited to region R1, while region R2 remained virtually elastic. This coupling beam was dominated by flexural deformations up to the third loop at $3.5\Delta_y$. During the second loop at $3.5\Delta_y$ pinching of the moment-curvature response indicates the increased influence of shear deformations on the seismic response of this specimen. Figure 6.10 shows the shear strain conditions for a section of the coupling beam located 250 mm from the beam-wall interface. The vertical strain, ε_v, and the principal tensile strain, ε_1, started to increase more dramatically during the cycles at $3.5\Delta_y$ which shows the increased influence of shear deformations on the overall response of the coupling beam.

The longitudinal reinforcement located at the beam-wall interface underwent extreme straining as can be see in Fig. 6.11. The load versus strain response of the transverse reinforcement is shown in Fig. 6.12. This hoop is located at approximately the critical section, d/2 from the beam-wall interface.

6.1.3 Specimen MR2

This specimen was constructed using high-strength concrete and was designed as a nominally ductile beam resulting in a hoop reinforcement spacing of 142 mm. The shear reinforcement was designed using the assumption that the concrete contribution was 50% of the typical code amount. Figure 6.13 gives the applied load versus relative displacement of this specimen. The load stage peak loads and deflections are presented in Table 6.3.

The estimated cracking moment, M_{cr}, was 52.4 kNm, which is equivalent to an applied shear of 58.2 kN. The first loading stage was elastic for this specimen, however during the

Table 6.3 Key load stages for Specimen MR2

Load Stage	Positive (A) Cycle Applied Shear (kN)	Positive (A) Cycle Relative Deflection (mm)	Negative (B) Cycle Applied Shear (kN)	Negative (B) Cycle Relative Deflection (mm)	Notes
1	49.7	0.75	-51.37	-0.41	elastic
4	144.74	5.97	-150.5	-3.59	$\cong 0.5\ M_y$
7	273.5	14.90	-301.6	-12.87	$+1.15\Delta_y$, $-0.99\Delta_y$
10	330.3	25.88	-343.3	-28.15	$+1.99\Delta_y$, $-2.17\Delta_y$
13	320.6	40.96	-354.0	-42.10	$+3.15\Delta_y$, $-3.24\Delta_y$
16	277.5	55.37	-334.2	-56.02	$+4.25\Delta_y$, $-4.31\Delta_y$

second positive cycle a hairline crack developed at the top-right reentrant corner due to the presence of a shrinkage crack at that location. As this specimen was loaded to approximately $0.5M_y$ several flexural-shear cracks developed at a spacing of about 100 mm. These beam cracks had an average width of 0.2 mm and were located up to 450 mm from the inside face of each wall.

Further cracking within the beam occurred while the specimen was loaded towards general yielding. These cracks extended over the entire length of the beam reaching widths of 0.4 mm at some locations. The vertical interface cracks reached maximum widths of 0.5 mm at the peak loads. Several vertical cracks formed within each of the walls during these loading cycles, resulting from the development the tensile forces within the longitudinal steel . After post-reduction of the data, the general yield deflection, Δ_y, was taken as 13.0 mm.

During the three loading cycles at $2.0\Delta_y$, there was further crack development within both of the walls of this test specimen, but not along the length of the beam. The existing cracks within the beam extended in length and increased in width. These crack widths varied greatly and reached a maximum of 1.75 mm at a distance 200 mm from the inside wall face, which is approximately the location of the critical section for shear. The cracks at the reentrant corners reached a peak value of 1.75 mm during the loading cycles at this deflection level.

Further crack propagation occurred during the three cycles at $3.2\Delta_y$. The cracks at the beam-wall interface increased in width to 2.5 mm by the end of these cycles. The flexural-shear cracks increased dramatically reaching widths of 4.0 mm at the mid-height of the beam. This was evidence of the increasing contribution of shear deformation to the overall response of the test specimen. The pinching of the hysteretic loops of the load-deflection response at this load level also show the increased influence of shear deformation, see Fig. 6.13. The concrete cover on the bottom of the beam spalled as this specimen was loaded towards the negative peak deflection of $4.3\Delta_y$. This exposed the transverse reinforcement and yielding of this steel was evident. The loss of capacity of this test specimen was due to sliding along the inclined shear cracks developed in the beam and Fig. 6.14 shows this specimen at the completion of testing.

The moment-curvature response of Specimen MR2 is given in Fig. 6.15. The region located closest to the wall accounted for most of the flexural deformations. The second and third loops at $2.0\Delta_y$ saw a decrease in the peak curvatures reached compared with the first loop at this deflection. This was due to the increasing effect of shear deformations on the seismic response of the system. This is also noticeable in the shear strain versus load plot given in Fig. 6.16. The increase in the vertical strain during the positive and negative loading cycles illustrates that the rosette located at the critical section spanned both of the primary shear cracks.

Figure 6.17 shows the strain distribution in the longitudinal reinforcement along its length. The strain gauges located at the beam-wall interface underwent excessive straining. The strain level within the longitudinal reinforcement decreases towards the middle of the beam. The strain in the instrumented hoop reinforcement is given in Fig. 6.18. The development of inclined cracks close to the gauge location on hoop S1 resulted in a large increase in the hoop strain.

6.1.4 Specimen MR4

This specimen was constructed using high-strength concrete and was designed as a ductile coupling beam. The hoop spacing of the beam transverse reinforcement was 85 mm. The applied load verses relative displacement of this specimen is given in Fig. 6.19. The load stage peak loads and deflections are presented in Table 6.4.

The first three loading cycles, ±50 kN, resulted in no cracking of the test specimen. The first cracking of the specimen occurred as it was loaded towards a positive load equivalent to $0.5M_y$. These hairline cracks formed at an average spacing of 100 mm and were located up to 400 mm from the inside face of each wall. Symmetrical cracks formed during the negative portion of this loading loop.

As the specimen was loaded towards general yielding there was further cracking within the beam and some cracks were initiated within the walls. The interface cracks reached a width

Table 6.4 Key load stages for Specimen MR4

Load Stage	Positive (A) Cycle		Negative (B) Cycle		Notes
	Applied Shear (kN)	Relative Deflection (mm)	Applied Shear (kN)	Relative Deflection (mm)	
1	45.3	0.56	-51.9	-0.60	elastic
4	145.5	5.43	-154.5	-4.27	$\cong 0.5\ M_y$
7	280.4	13.84	-290.8	-12.05	$+1.13\Delta_y$, $-0.99\Delta_y$
10	329.1	24.88	-336.5	-26.39	$+2.04\Delta_y$, $-2.16\Delta_y$
13	338.3	37.89	-350.9	-38.68	$+3.10\Delta_y$, $-3.17\Delta_y$
16	340.1	50.78	-356.4	-52.37	$+4.16\Delta_y$, $-4.29\Delta_y$
19	348.4	63.72	-347.1	-65.47	$+5.22\Delta_y$, $-5.37\Delta_y$

of 0.5 mm and the average beam flexural-shear crack was 0.25 mm in width. The second and third loops at general yield resulted in minimal extensions of the cracks. After post-reduction of the data the general yield deflection, Δ_y, was taken as 12.2 mm, as shown in Fig. 6.19.

During the first loop at 2.0 Δ_y, there was some further cracking in the beam and the walls. There was only minor elongation of existing cracks during the second and third cycles at this deflection. The cracks at the beam-wall interface reached thickness up to 3.0 mm, while the cracks within the beam varied from hairline at the mid-span of the beam, to 1.5 mm at the ends of the beam.

During the three cycles at $3.1\Delta_y$ there was widening and extension of the existing cracks but no new cracking occurred within the beam. The cracks located close to ends of the beam continued to increase in width, with the interface cracks reaching approximately 5.0 mm in width. Further vertical cracking within the walls occurred during these cycles, indicating the progression of yielding within the longitudinal reinforcement. This type of behaviour was also observed during the three cycles at $4.1\Delta_y$. At the completion of the third loop at this ductility level the beam had increased in overall length by 17.0 mm.

There was some minimal cover spalling at the beam-wall interface during the first loop at $5.2\Delta_y$. The bottom cover of the beam located close to the wall completely spalled during the second cycle at this deflection level, exposing the transverse and longitudinal reinforcement. There was evidence of extreme yielding of the exposed longitudinal and transverse steel. At these large displacement levels this specimen lost capacity due to shear sliding along the beam-wall interface. At this stage shear resistance of the coupling beam was a result of dowel action of the longitudinal steel. Figure 6.20 shows this specimen at the end of testing.

Figure 6.21 shows the moment-curvature response of this specimen. The peak curvatures reached in region R1 during the cycles at $2.0\Delta_y$ were consistent for all three cycles. This demonstrates that the flexural deformation component to the overall response remains constant. Region R2 displays an essentially elastic response until the this specimen was cycled at a deflection equivalent to $4.2\Delta_y$. The shear strain conditions of this specimen at the critical section of the beam are given in Fig. 6.22. The vertical strain within the beam started to increase dramatically as this specimen was cycled at $4.2\Delta_y$. Figures 6.23 and 6.24 show the strain versus load response of the longitudinal and transverse steel, respectively. The excessive yielding of the longitudinal steel at the interface is clearly evident. The increases in the vertical stains within the beam are clearly evident from the extensive straining of the hoop reinforcement.

6.2 Comparison of Reversed Cyclic Responses of Concrete Coupling Beams

6.2.1 Hysteretic Responses

Figure 6.25 shows the reversed cyclic responses of each of the coupling beam specimens and the seismic response envelopes for each of the specimens is given in Fig. 6.26. All of the specimens performed similarly up to a ductility level of about $3\Delta_y$, with the high-strength concrete specimens reaching a slightly higher maximum applied load. After this point pinching of the hysteresis loops began to occur in all of the specimens, due to the influence of shear deformations. These phenomena are more noticeable in the nominally ductile beams, which were more susceptible to shear distress, due to the smaller amount of transverse reinforcement within the beams. Both of the nominally ductile beams failed due to a loss of shear capacity within the beam.

A plastic hinge formed at the beam-wall interface of both of the ductile coupling beams. The longitudinal reinforcement underwent extensive yielding in this region resulting in an increase in the length of the beam. This elongation resulted in large cracks forming at the interface, thus virtually eliminating the compressive capacity of the concrete until the residual tensile strain in the longitudinal reinforcement was removed. The longitudinal reinforcement would carry the compressive load until gap closure, possibly causing the longitudinal reinforcement to buckle, even with the short unsupported length. This could have prompted the spalling of the cover concrete. The spalling of the cover concrete was a very significant behavioural event, resulting in a sudden loss of capacity. Furthermore, the gap formed at the interface diminishes the shear capacity of the concrete along this crack, therefore the shear resistance of the cross section was dependent on dowel action of the longitudinal reinforcement.

The high-strength concrete specimens performed very well, achieving larger ductilities than their companion normal-strength concrete beams. Furthermore, there were no signs of an abrupt, brittle failure mode in the high-strength concrete beams. Cover spalling in the high-strength concrete beams occurred at larger displacement ductilities than that observed in the normal-strength concrete beams.

Figure 6.27 shows the vertical strain at the critical section located d/2 from the beam-wall interface for each of the specimens tested. These plots show the vertical strain up to and including the second loop at $3\Delta_y$. The lack of symmetry in the plots for the normal-strength specimens was due to the crack pattern in the region. One of the principal shear cracks did not pass through the gauge length of the vertical LVDT. The influence of the additional transverse reinforcement for the specimens designed as ductile beams, can be seen in these strain diagrams. At equivalent ductility levels the vertical strains recorded in the nominally ductile beams are greater than the strains in the companion ductile coupling beams. Also, the specimens constructed using high-strength concrete seemed to undergo smaller vertical straining compared to their normal-strength concrete counterparts.

6.2.2 Energy Dissipation

Figure 6.28 shows the cumulative energy dissipated versus displacement for each specimen. From this plot it is clear that the high-strength concrete specimens dissipated more energy than their companion normal-strength concrete specimens. Up to a deflection of approximately 25 mm (~ $2\Delta_y$) the energy dissipated by each specimen is similar. Beyond this point the nominally ductile beams exhibited pinching in their hysteretic responses, which is indicative of reduced energy dissipation. Figure 6.29 shows the cumulative energy dissipated versus ductility level for each specimen. This plot eliminates the differences in the yield deflections of each of the specimens. From this plot it is clear that each specimen dissipated approximately equivalent energy up to $3\Delta_y$, with the high-strength concrete ductile coupling beam performing the best overall.

6.2.3 Stiffness and Damping

The stiffness value, α, is determined by calculating the slope of the line connecting the positive and negative peaks, as shown in Fig. 6.30a. The peak to peak stiffness versus ductility level for each of the specimens is given in Fig. 6.31.

As expected, the high-strength concrete specimens exhibited a greater initial stiffness than their normal-strength concrete companion specimens. Also the ductile coupling beams were slightly stiffer than the compatible nominally ductile beams, initially. As the tests progressed the stiffness displayed by each of the specimens reduced to similar values at the end of testing.

In order to compare the energy dissipation response of each of the specimens, an equivalent elastic damping coefficient, β, was determined as shown in Fig. 6.30b.

$$\beta = \frac{A_1}{2\pi A_2} \tag{6.1}$$

where

A_1 = the area within the hysteresis loop of one half cycle

A_2 = the area of the triangle defined by an equivalent elastic stiffness to the peak load and corresponding deflection of the half cycle

A greater ability to dissipate energy is given by a larger elastic damping coefficient. For comparison the largest elastic damping coefficient would be for an elastic-plastic response. Thus $\beta = 2/2\pi$ or $1/\pi$, which is equal to 31.8%.

The equivalent elastic damping coefficient vs ductility is given in Fig. 6.32. The band width of each of the graphs depicts the change in the coefficient during the three cycles at a particular ductility. The specimens have been plotted on two graphs, one for the ductile coupling beams and the other for the nominally ductile beams. Each of the specimens performed equally up to a ductility level of $2\Delta_y$. After this point the ductile coupling beams displayed a better ability to dissipate energy. The beams constructed using high-strength concrete and normal-strength concrete showed an approximately equal ability to dissipate energy.

6.3 Conclusions Based on Observed Behaviour

The following conclusions can be made based on the observed hysteretic responses of the concrete coupling beams.

1. The specimens constructed with high-strength concrete performed as well or better than the normal-strength concrete companion beams for both the nominally ductile and ductile detailed beams.
2. The reversed cyclic loading responses of the nominally ductile beams, R = 2, was not significantly affected by shear distress until a ductility level greater than 3. Therefore the inclusion of 50% of the concrete contribution, given by Eq. 11-6 of the CSA Standard, to the shear capacity of the nominally ductile beams was appropriate.
3. Due to the large side cover on the coupling beam the spalling of the cover concrete was a major event, resulting in a loss of load and stiffness of the coupling beam.
4. The large longitudinal elongation of the beams resulted in eventual interface shear failure. The restraint from the floor slabs may significantly reduce this elongation and hence this mode of failure would likely be significantly delayed.

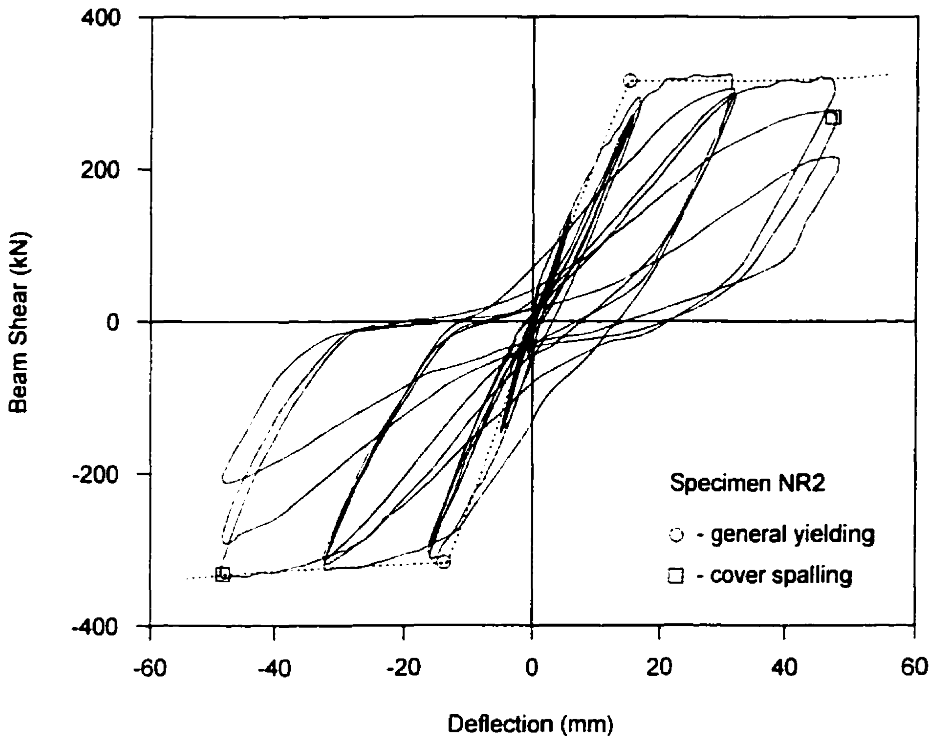

Figure 6.1 Hysteretic response of Specimen NR2

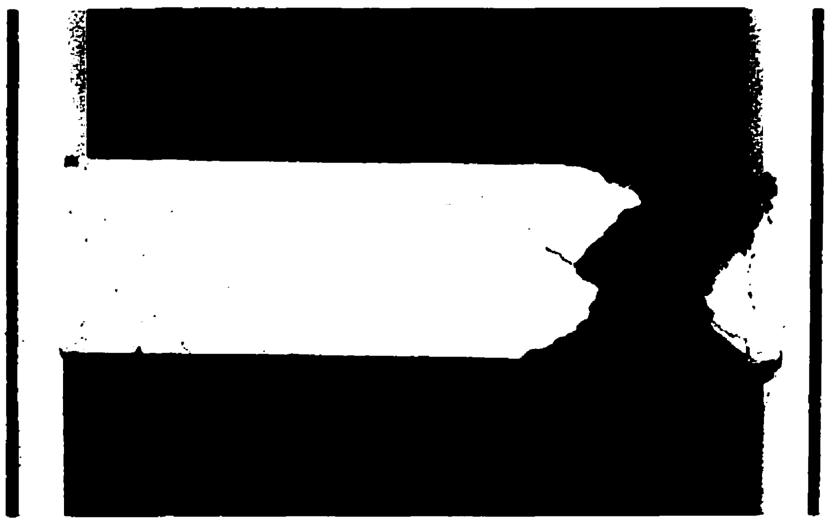

(a) Overall view of test specimen

(b) Close up of spalled region

Figure 6.2 Specimen NR2 at completion of testing

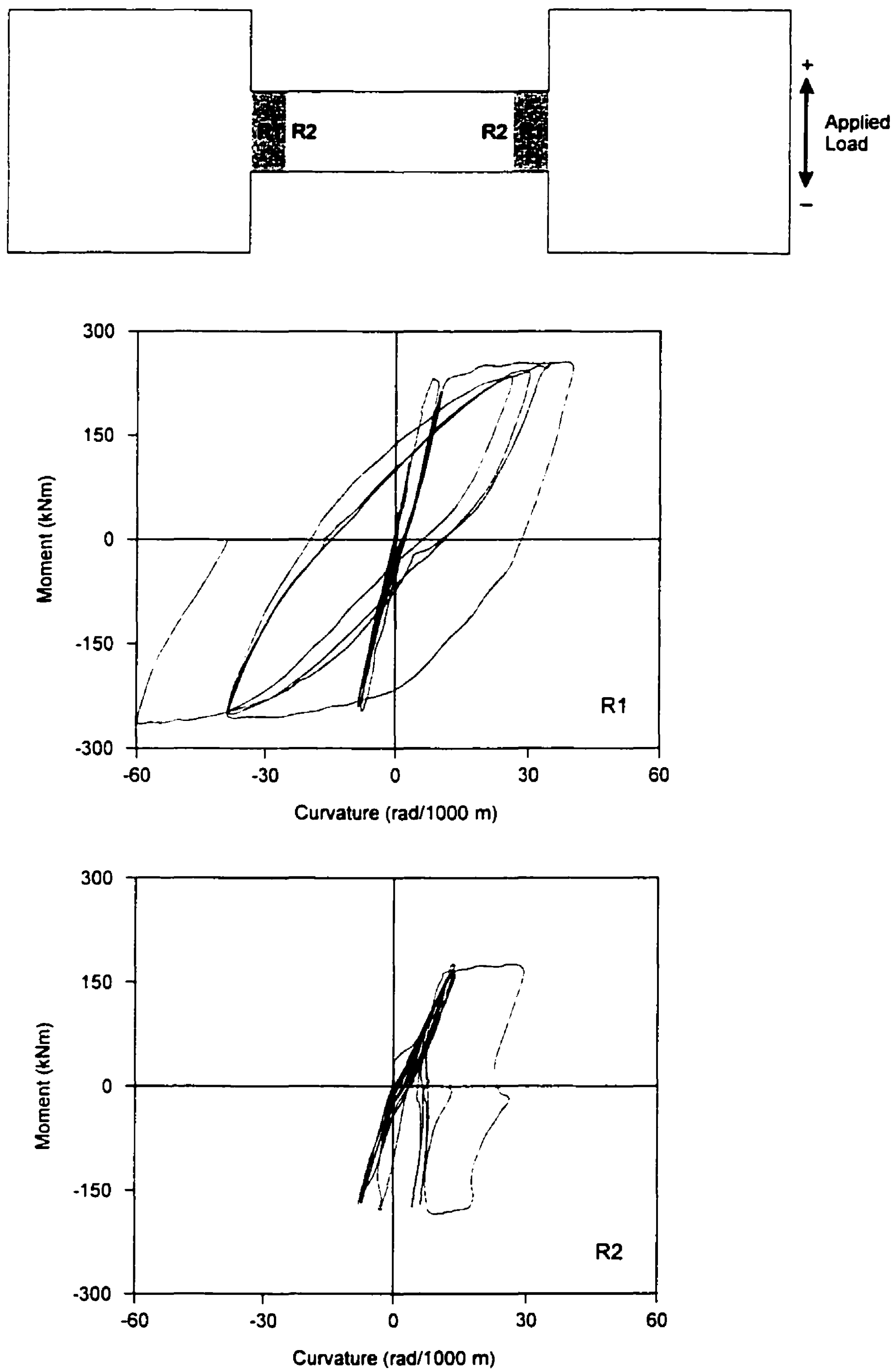

Figure 6.3 Moment-curvature response of Specimen NR2

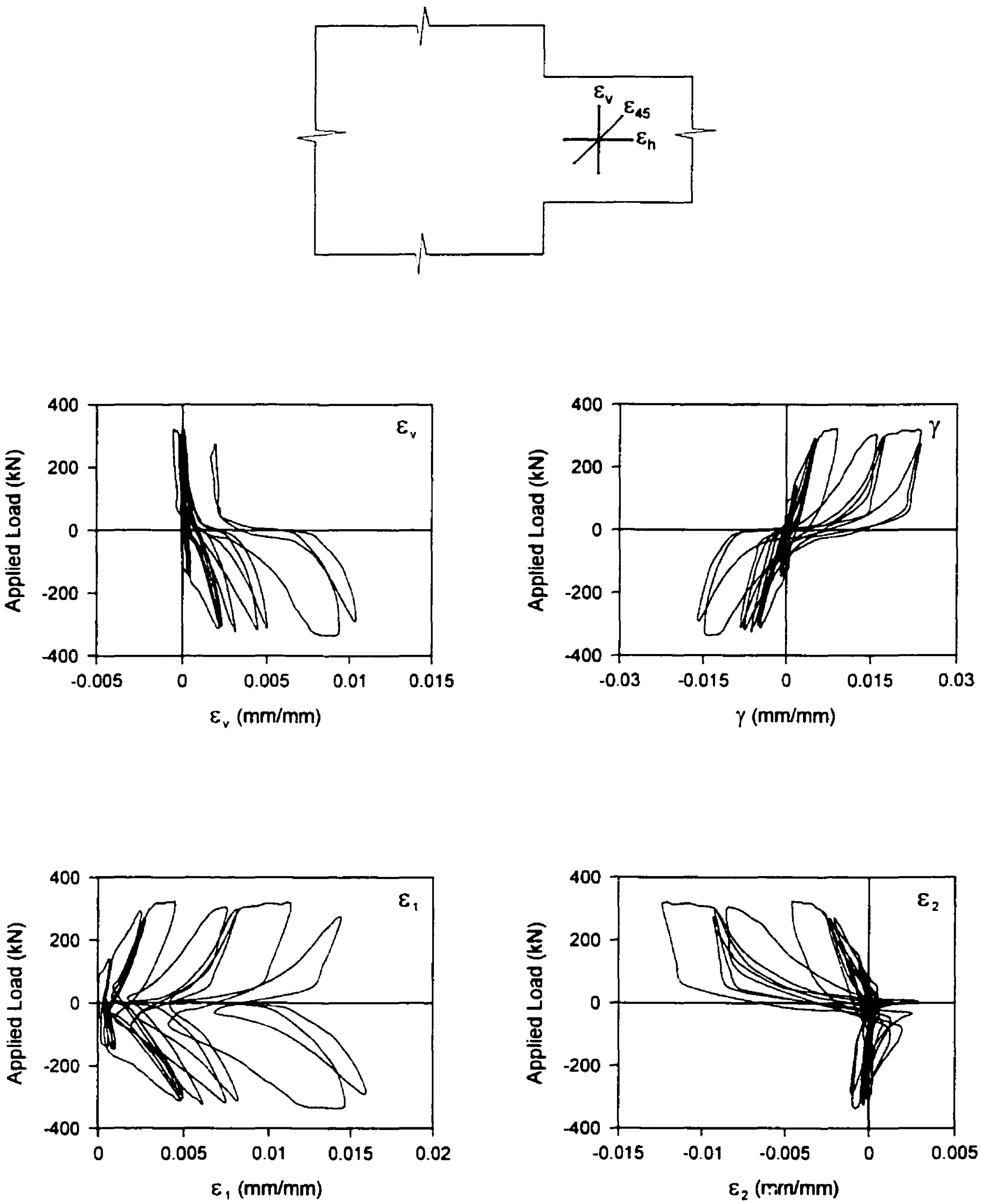

Figure 6.4 Strain conditions of Specimen NR2

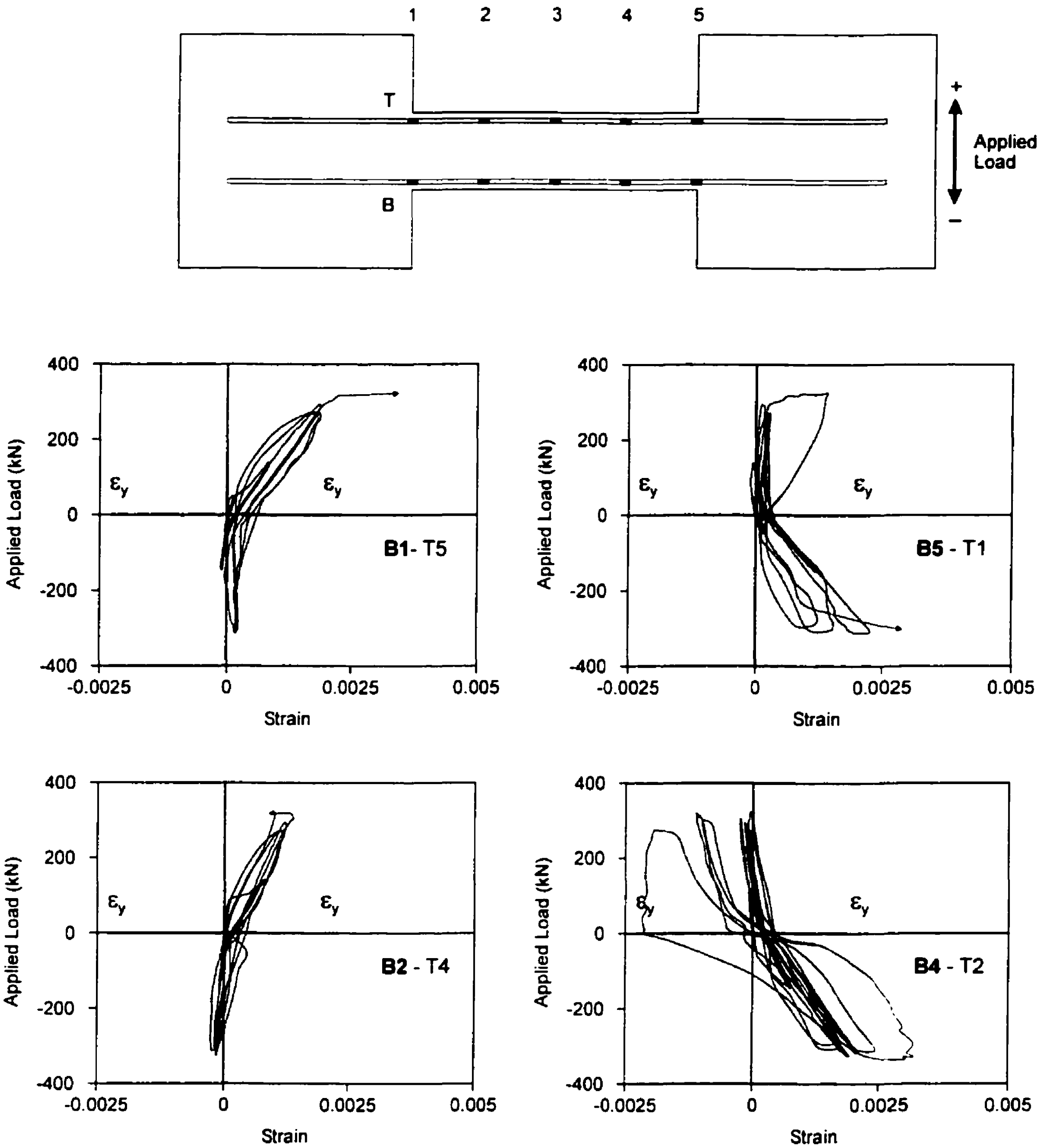

Figure 6.5 Measured strains in longitudinal reinforcement of Specimen NR2

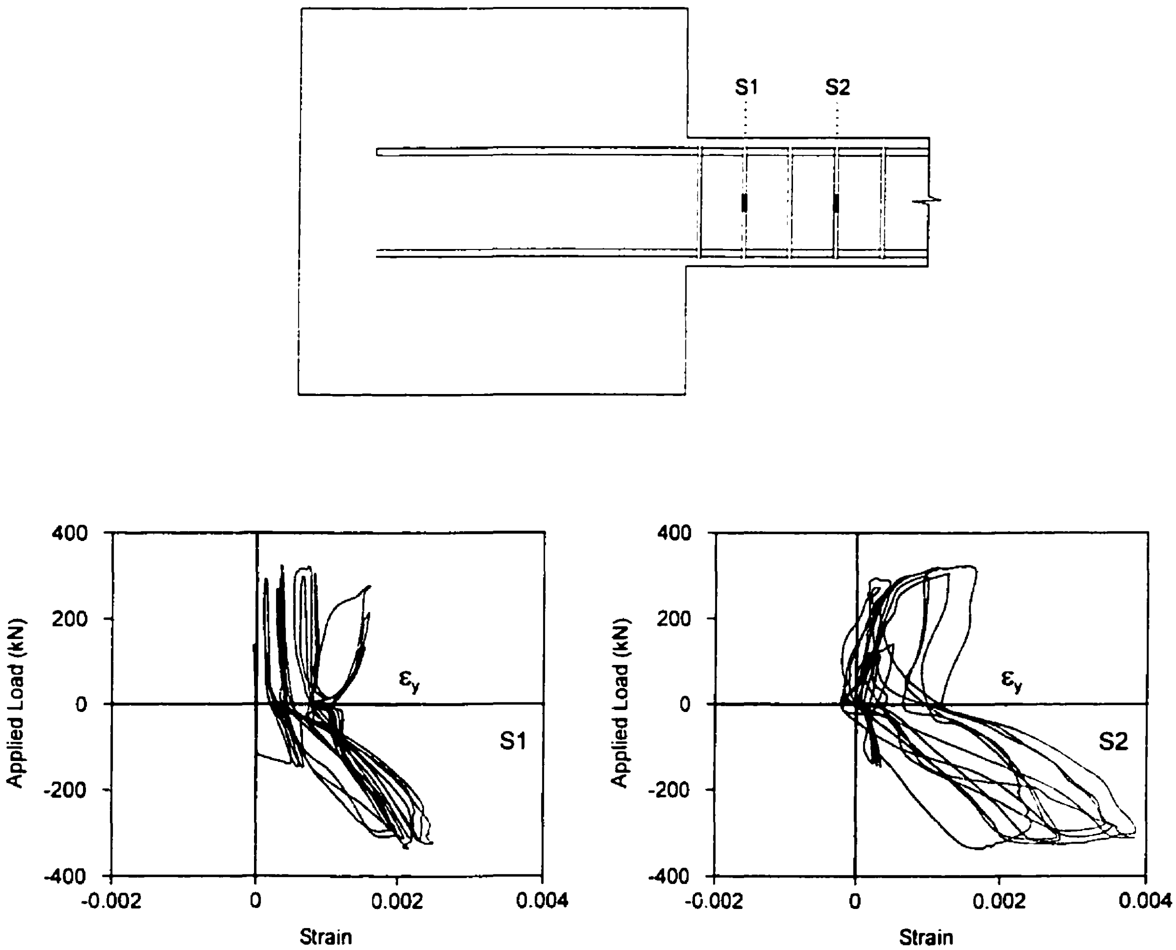

Figure 6.6 Measured strains in hoop reinforcement of Specimen NR2

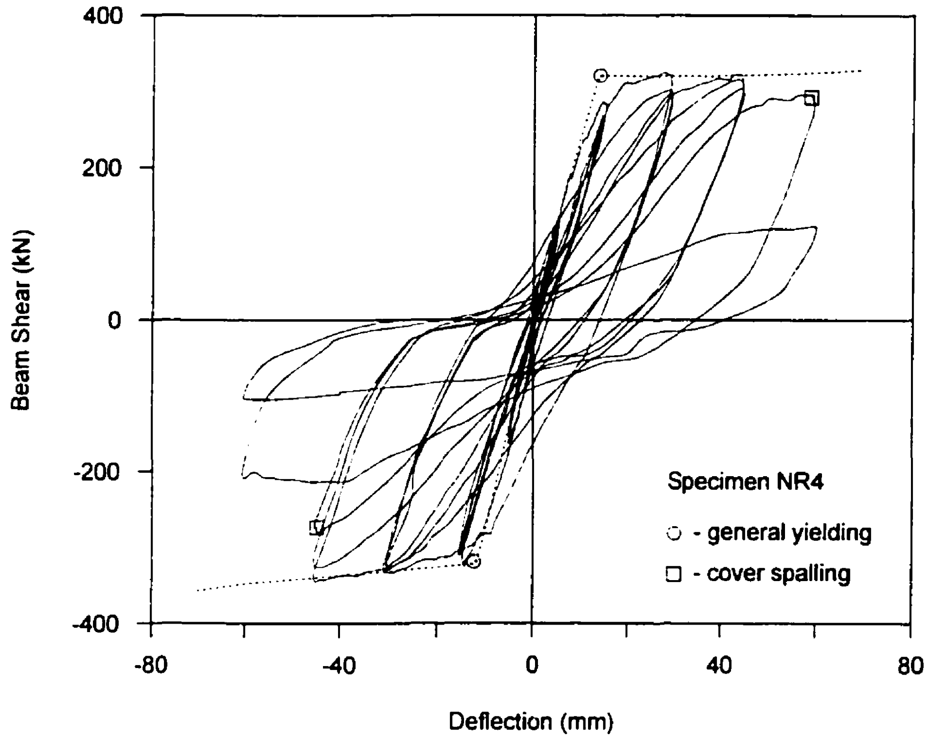

Figure 6.7 Hysteretic response of Specimen NR4

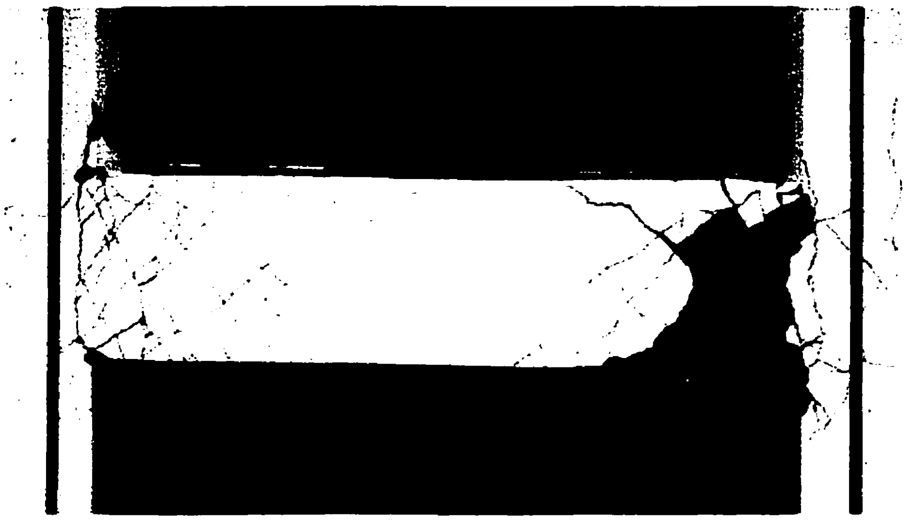

(a) Overall view of test specimen

(b) Close up of spalled region

Figure 6.8 Specimen NR4 at completion of testing

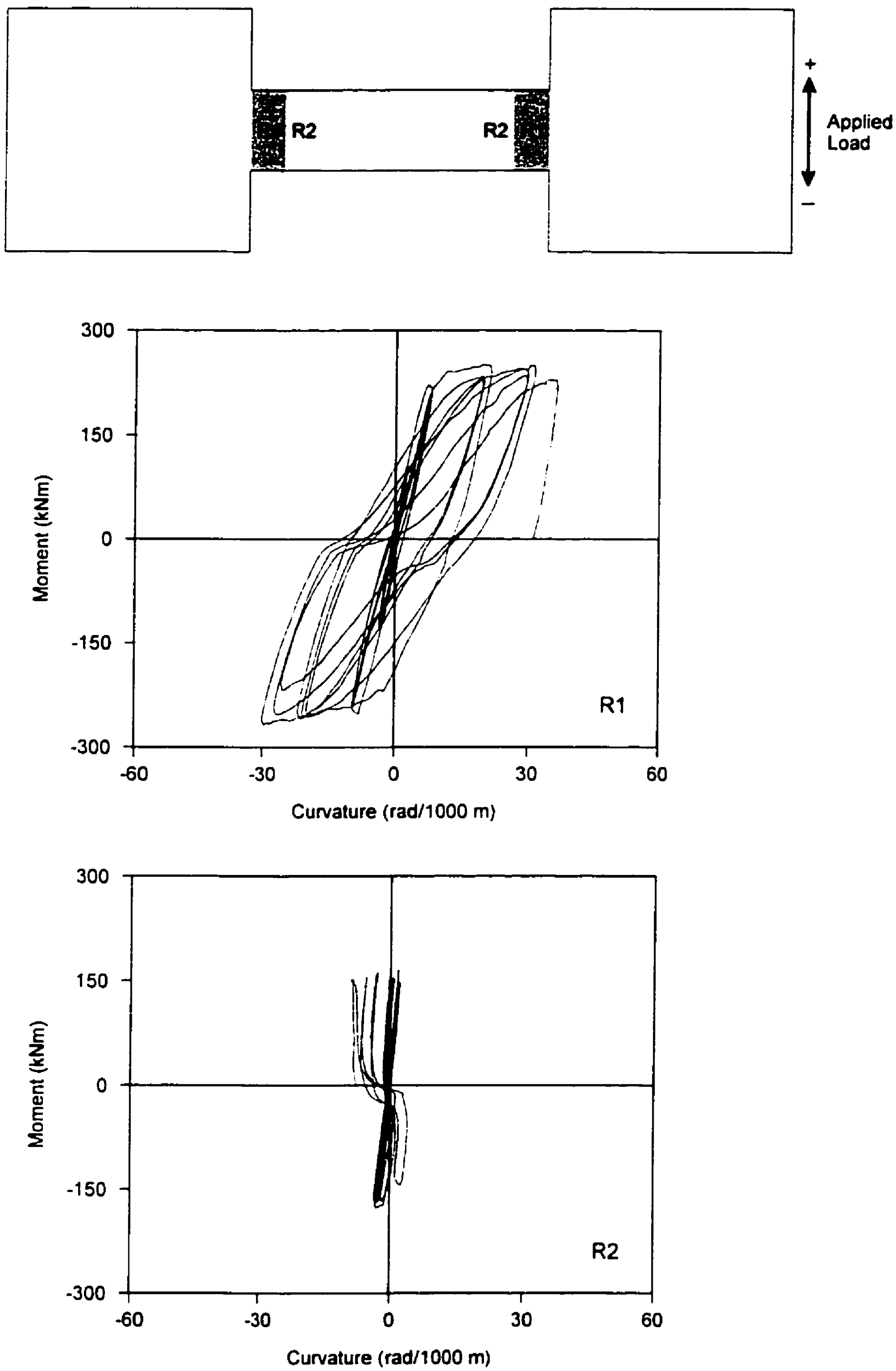

Figure 6.9 Moment-curvature response of Specimen NR4

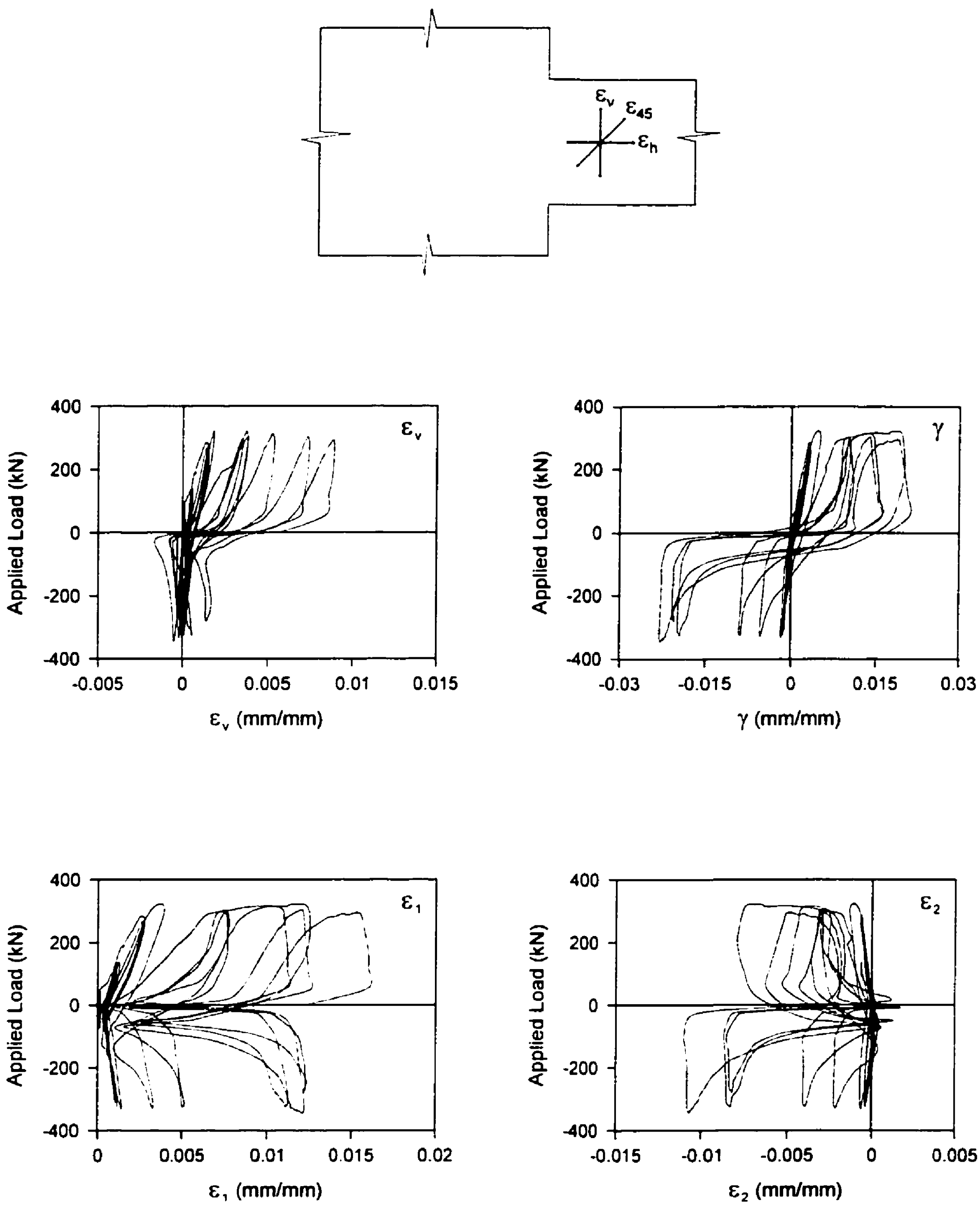

Figure 6.10 Strain conditions of Specimen NR4

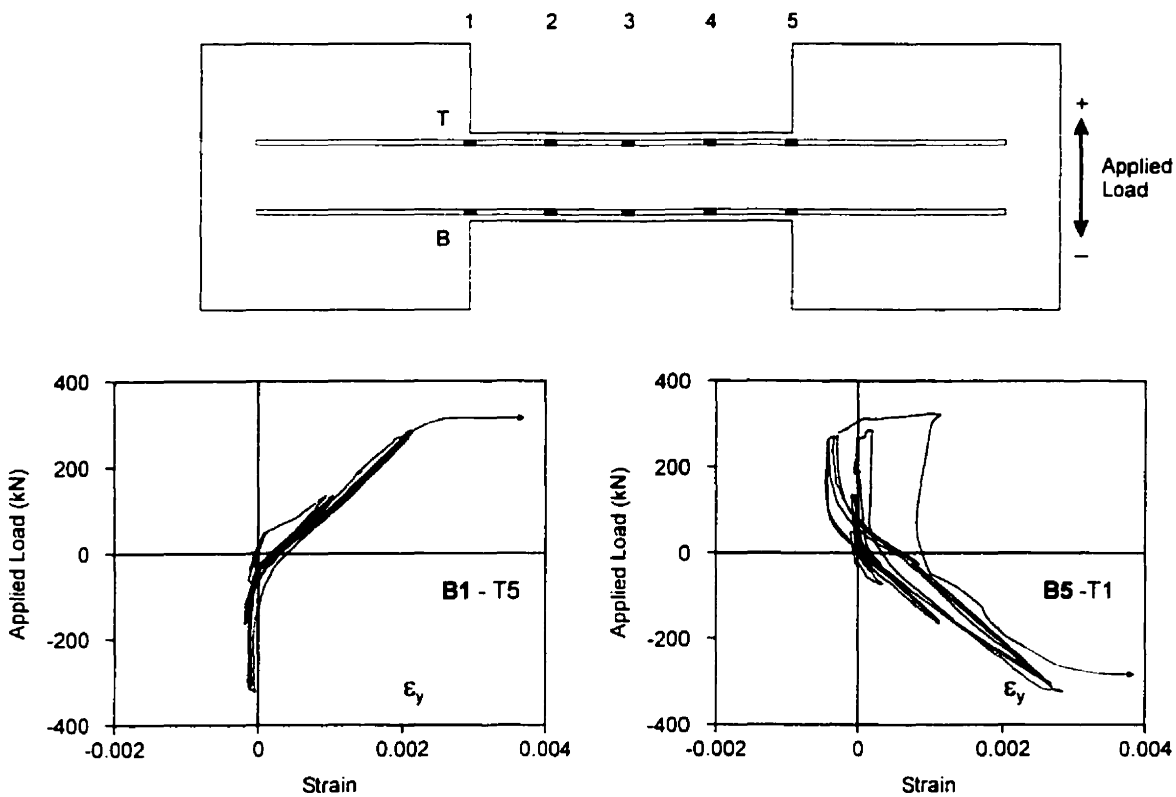

Figure 6.11 Measured strains in longitudinal reinforcement of Specimen NR4

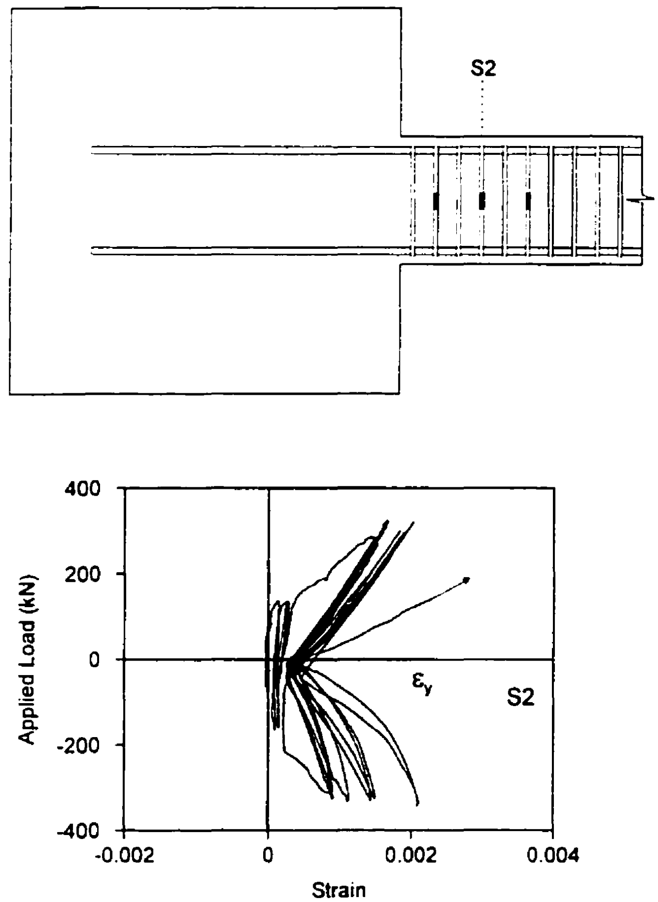

Figure 6.12 Measured strains in hoop reinforcement of Specimen NR4

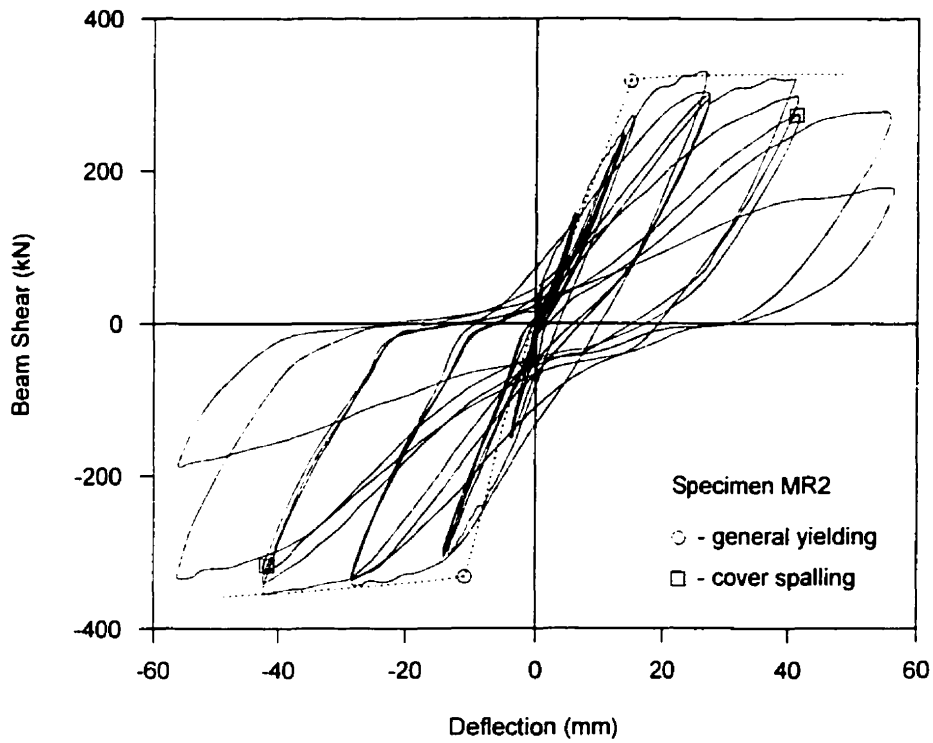

Figure 6.13 Hysteretic response of Specimen MR2

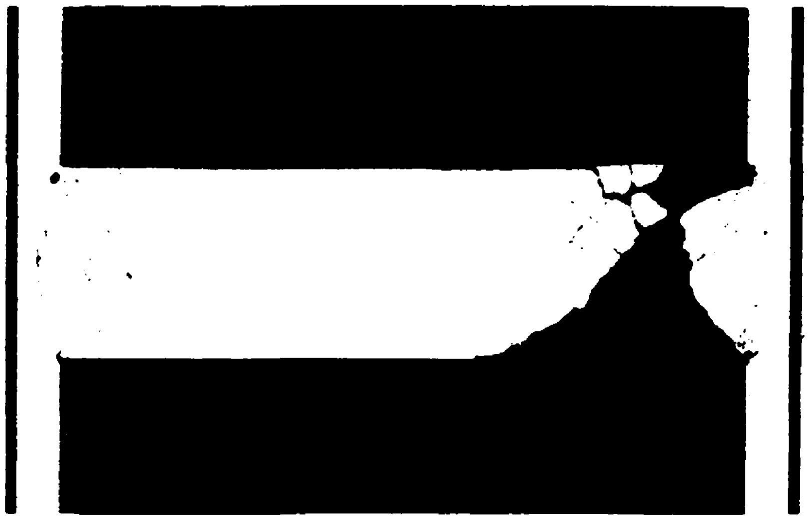

(a) Overall view of test specimen

(b) Close up of spalled region

Figure 6.14 Specimen MR2 at completion of testing

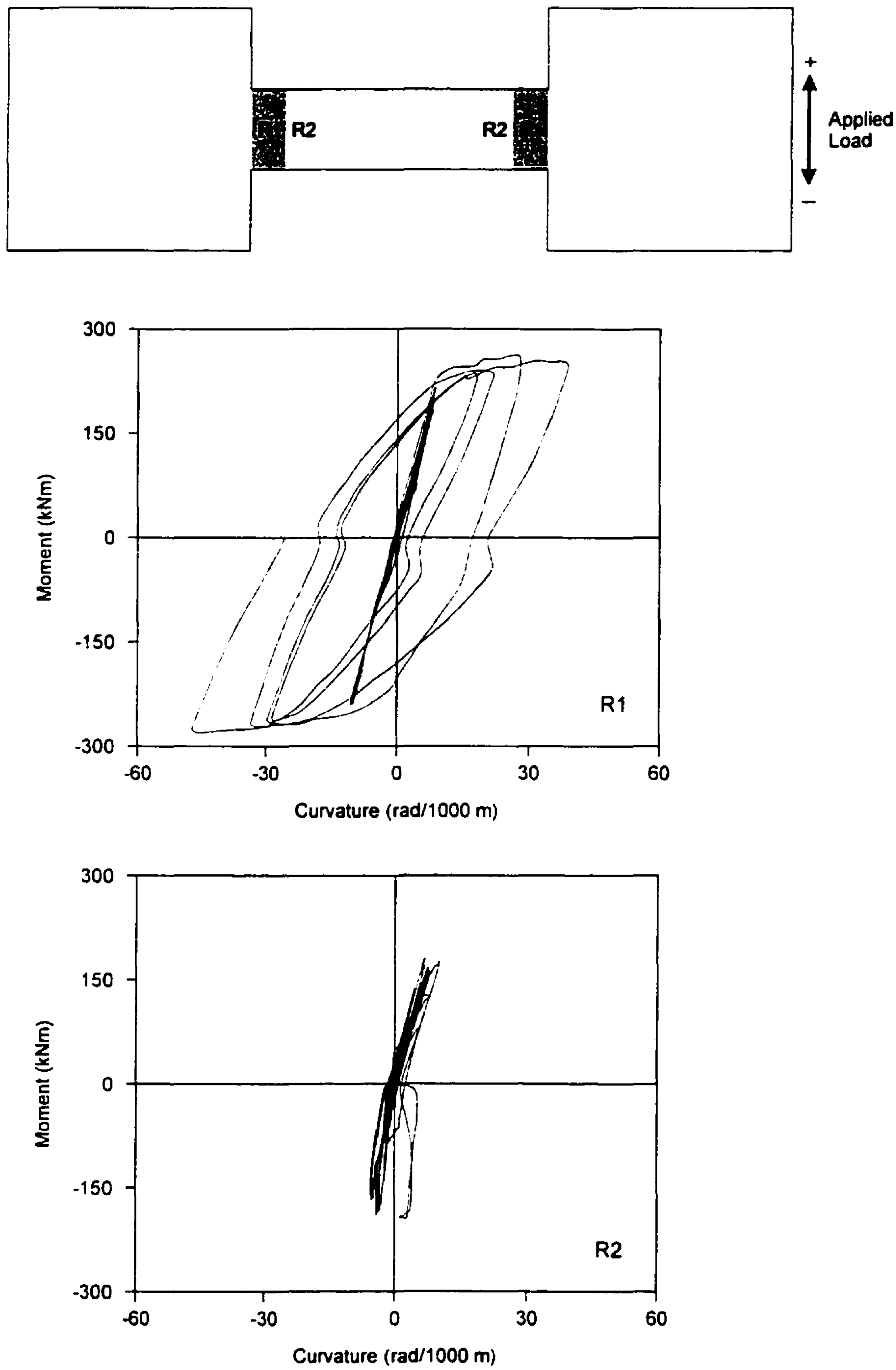

Figure 6.15 Moment-curvature response of Specimen MR2

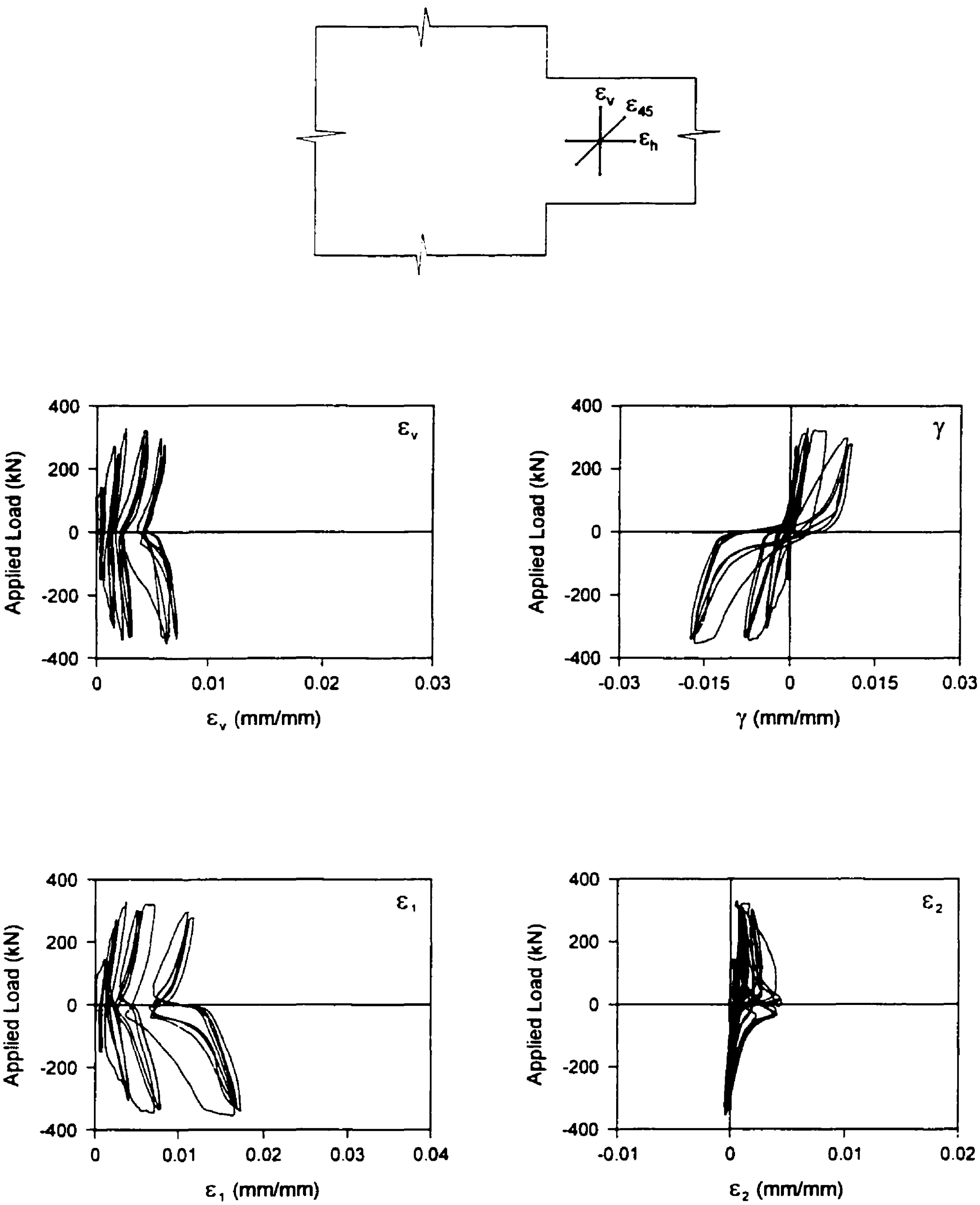

Figure 6.16 Strain conditions of Specimen MR2

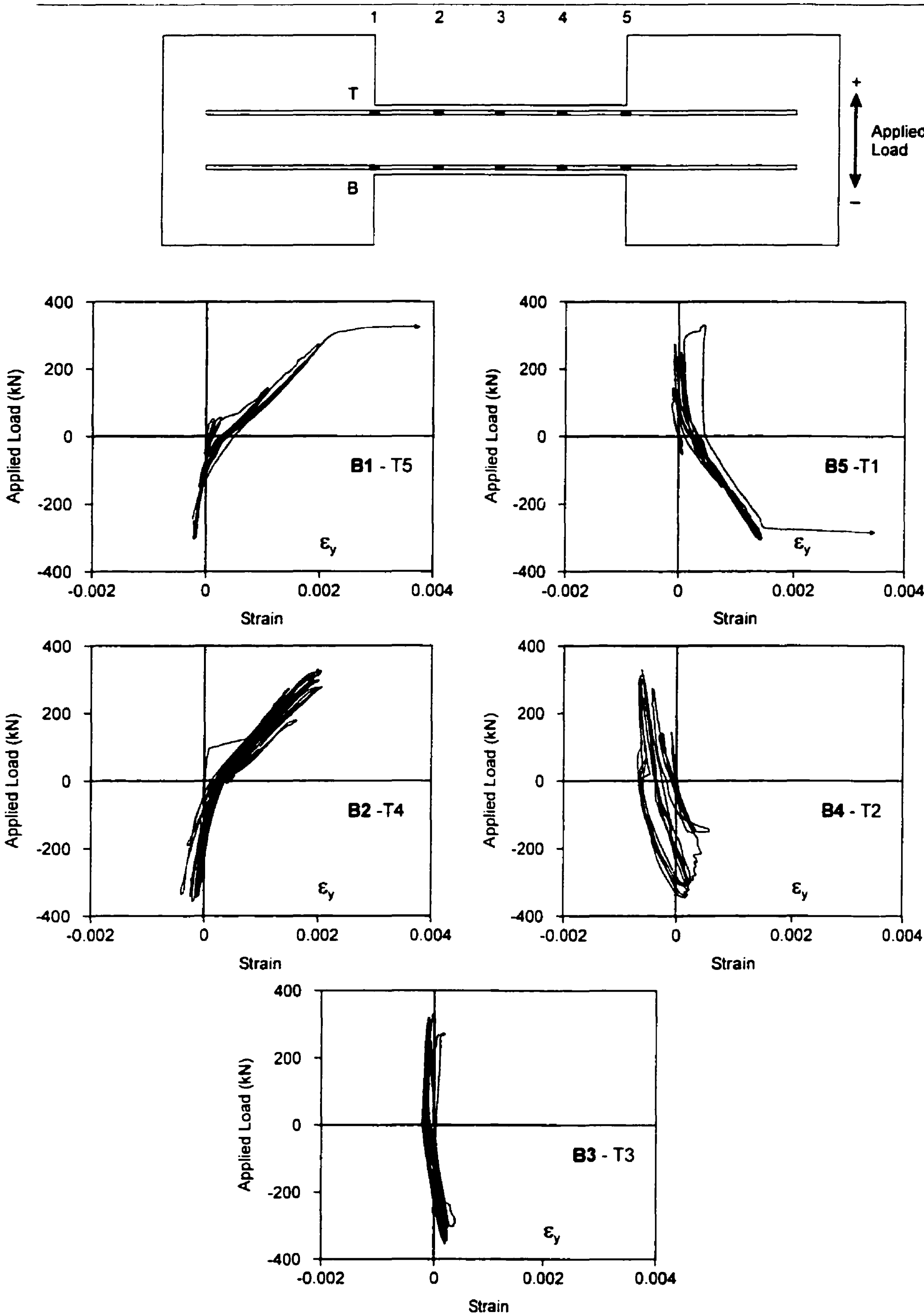

Figure 6.17 Measured strains in longitudinal reinforcement of Specimen MR2

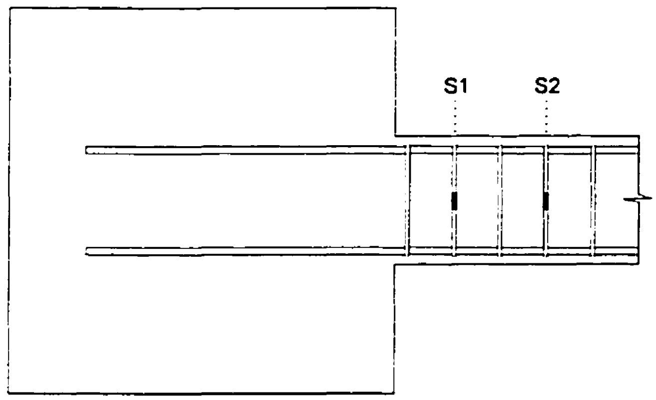

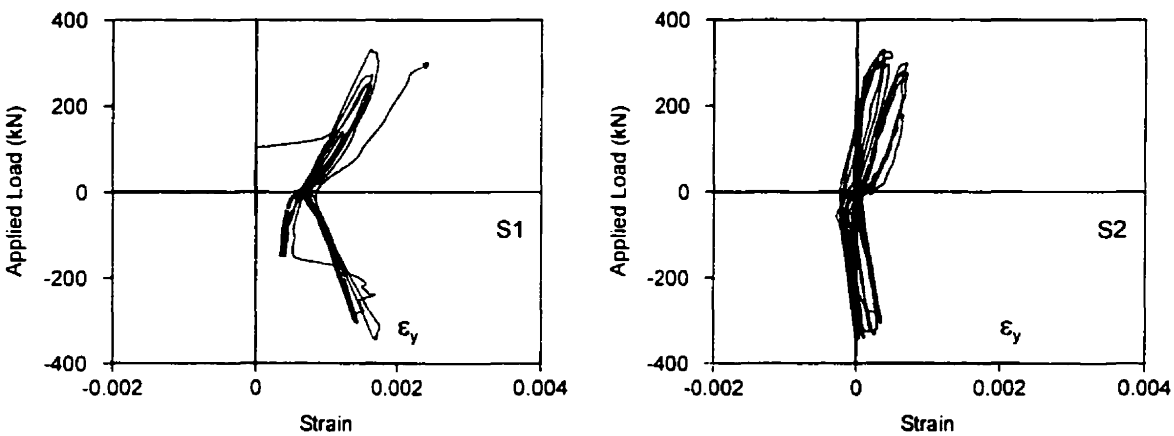

Figure 6.18 Measured strains in hoop reinforcement of Specimen MR2

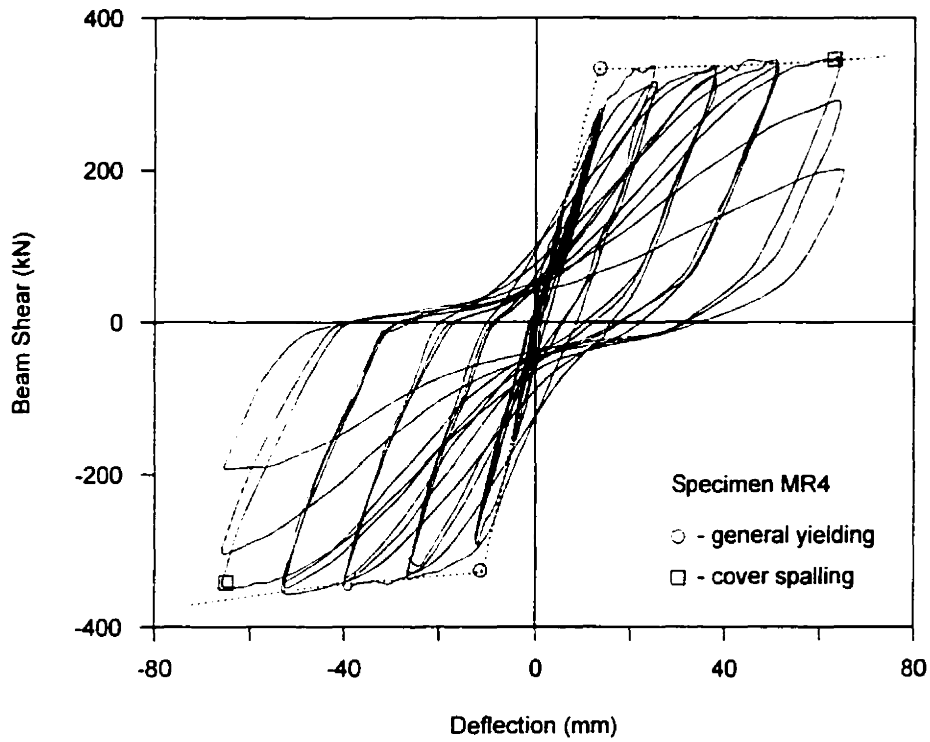

Figure 6.19 Hysteretic response of Specimen MR4

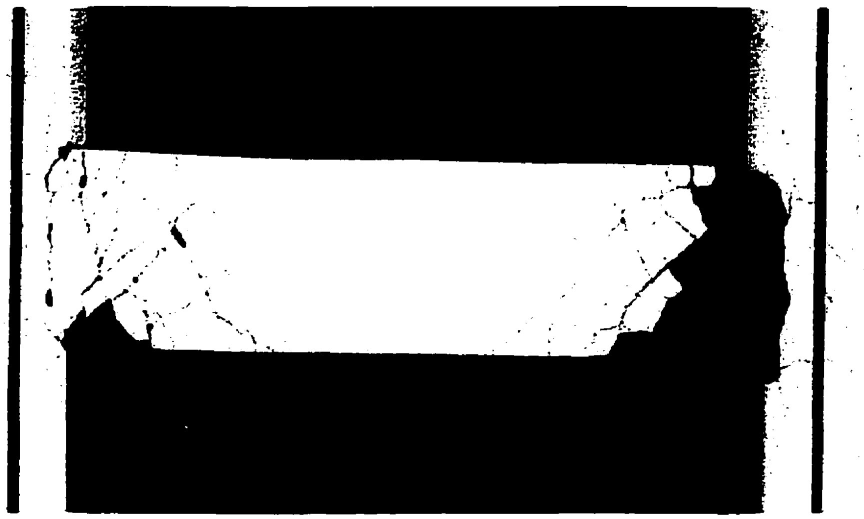

(a) Overall view of test specimen

(b) Close up of spalled region

Figure 6.20 Specimen MR4 at completion of testing

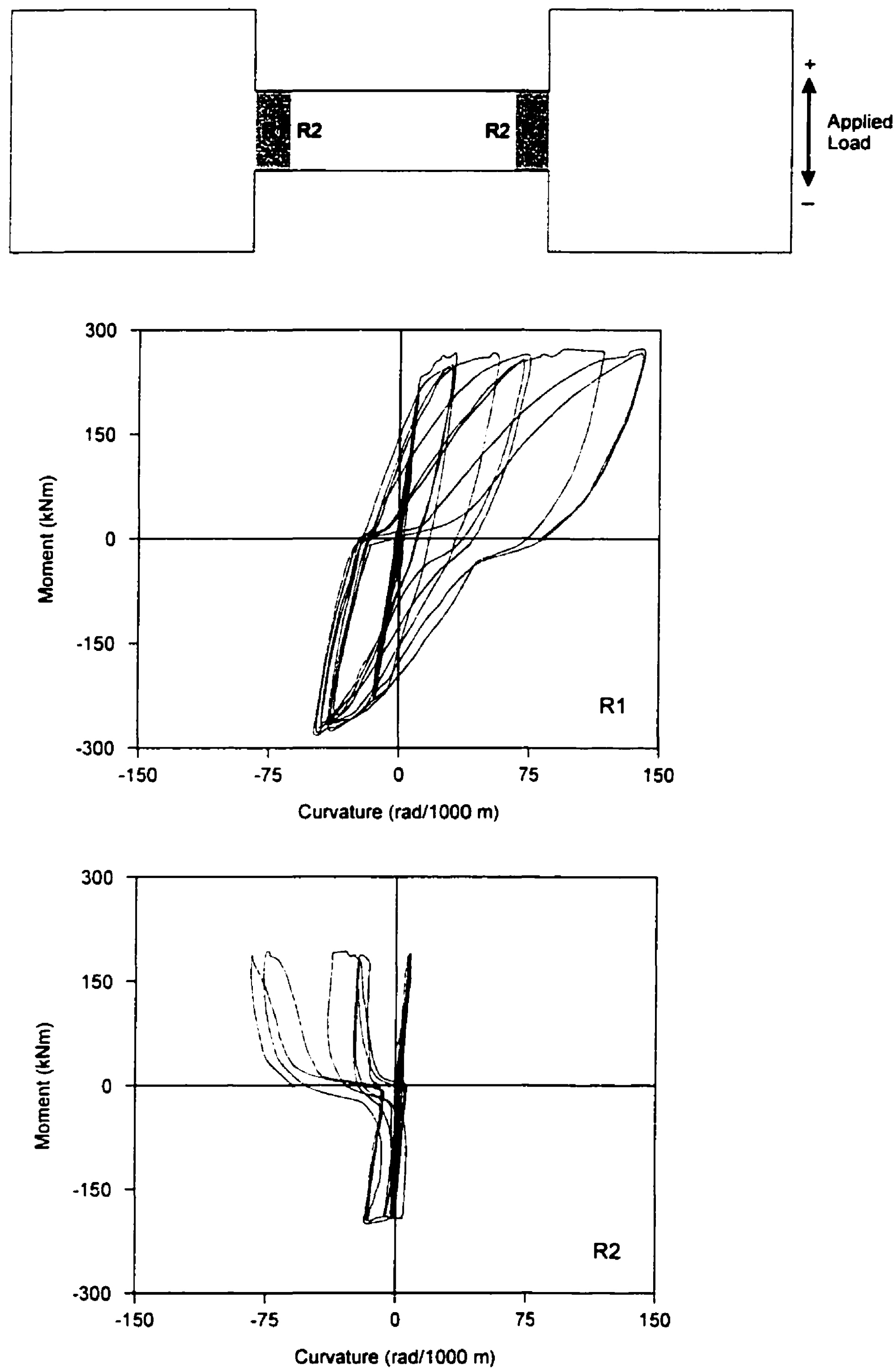

Figure 6.21 Moment-curvature response of Specimen MR4

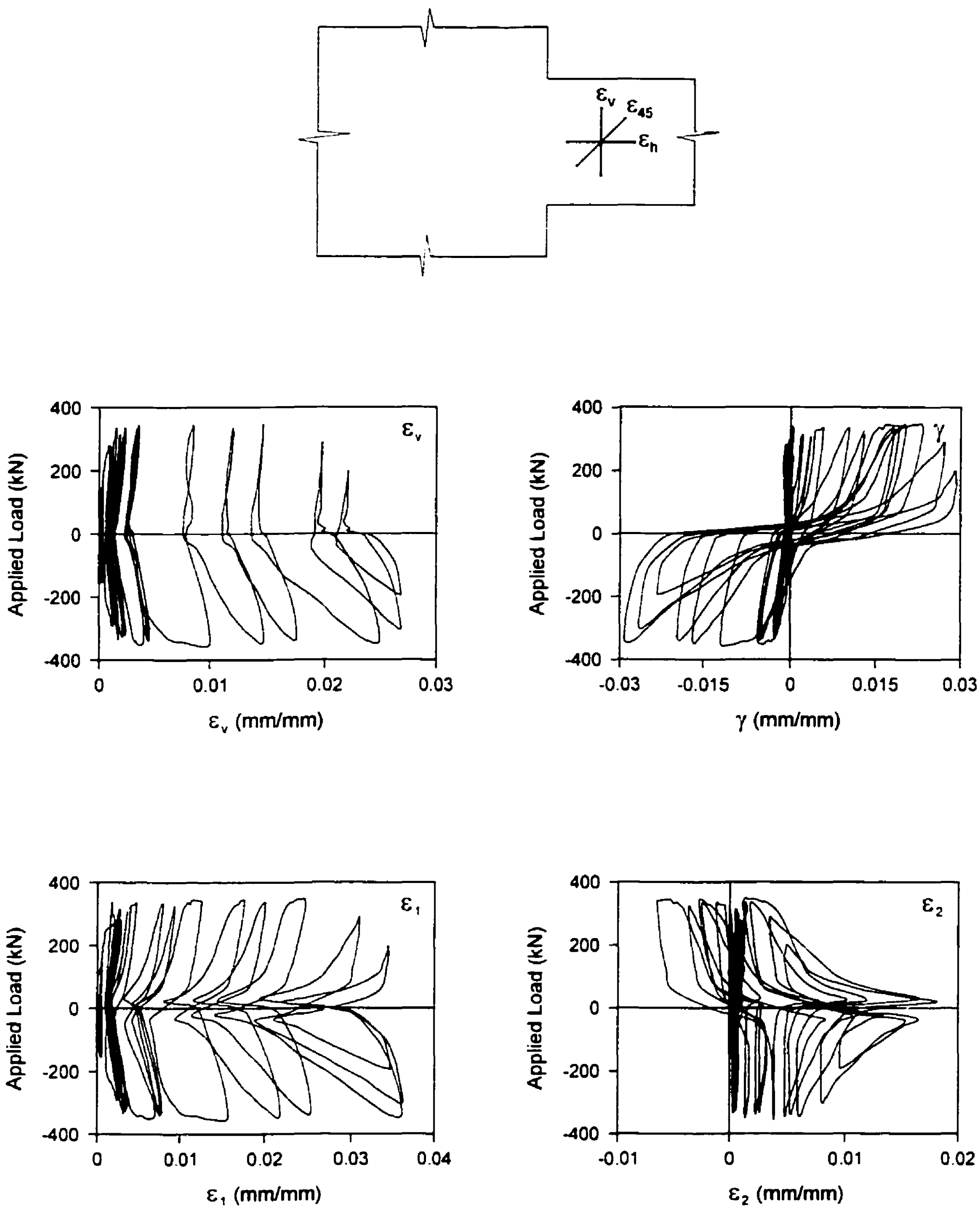

Figure 6.22 Strain conditions of Specimen MR4

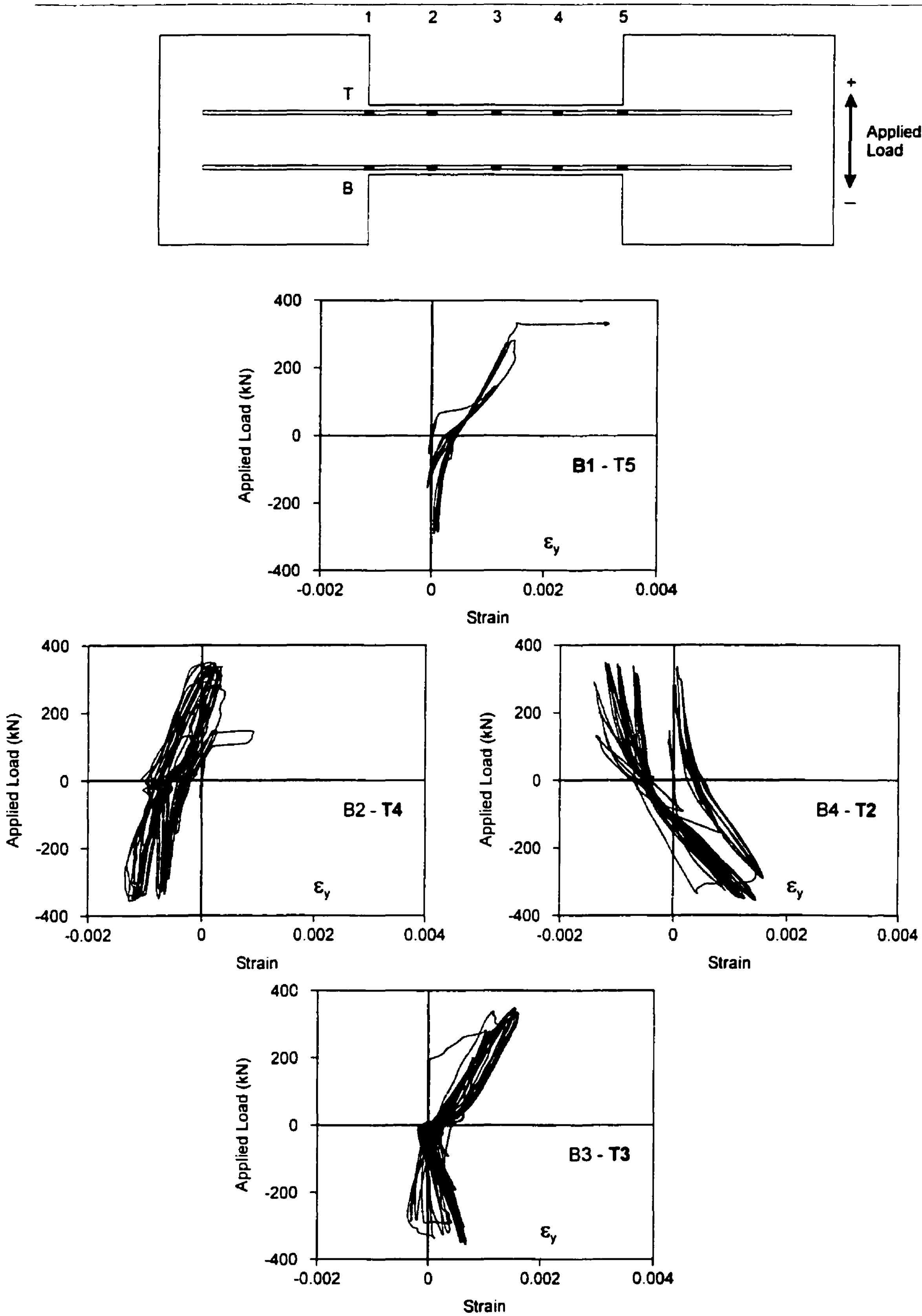

Figure 6.23 Measured strains in longitudinal reinforcement of Specimen MR4

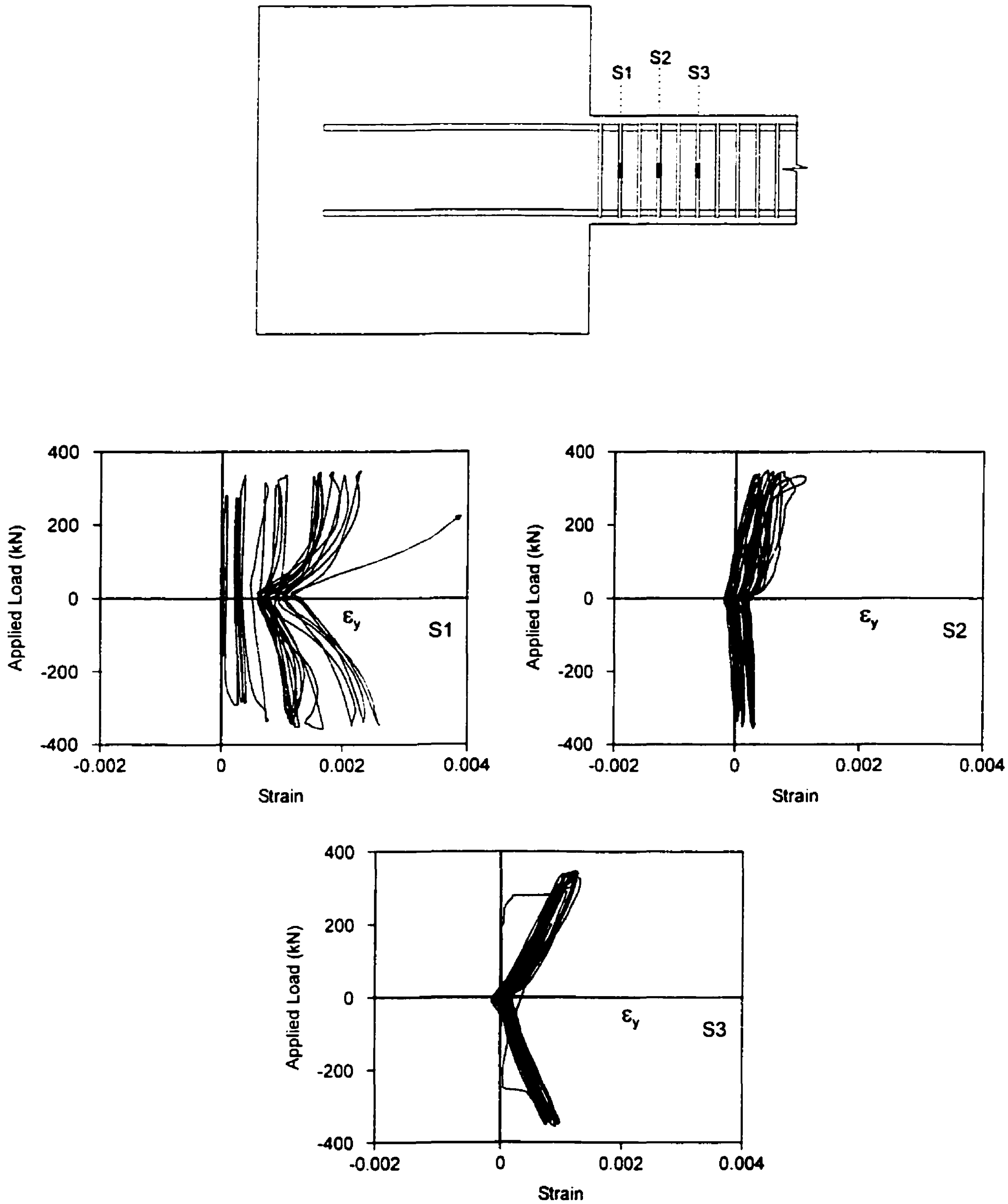

Figure 6.24 Measured strains in hoop reinforcement of Specimen MR4

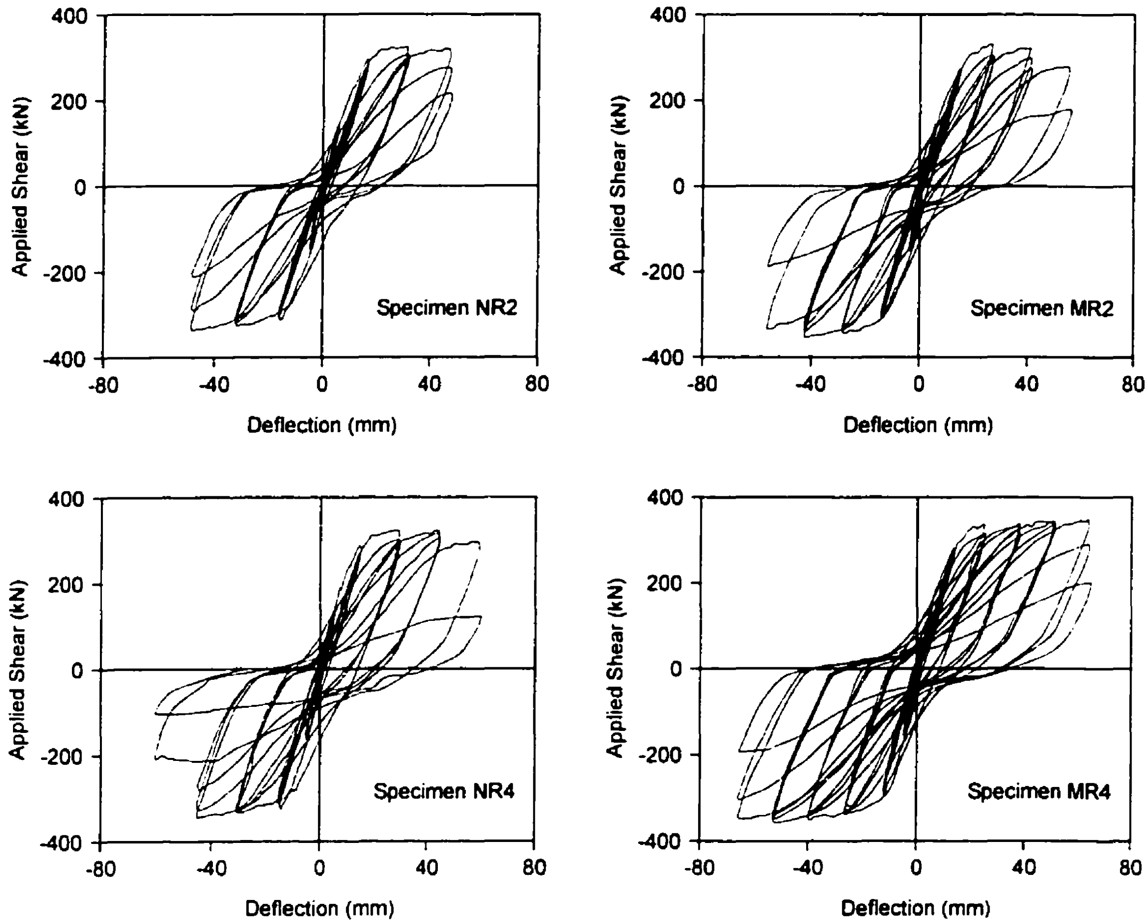

Figure 6.25 Hysteretic responses of beam specimens

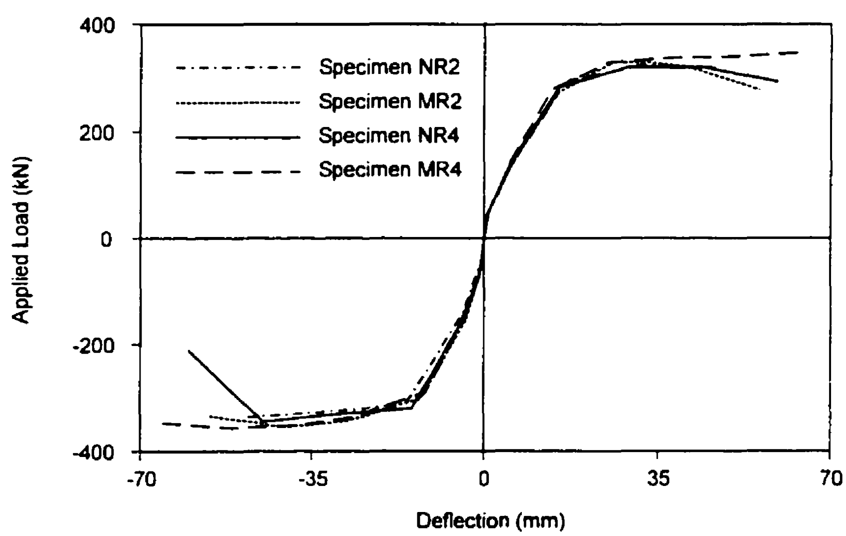

Figure 6.26 Seismic response envelopes for reinforced concrete coupling beams

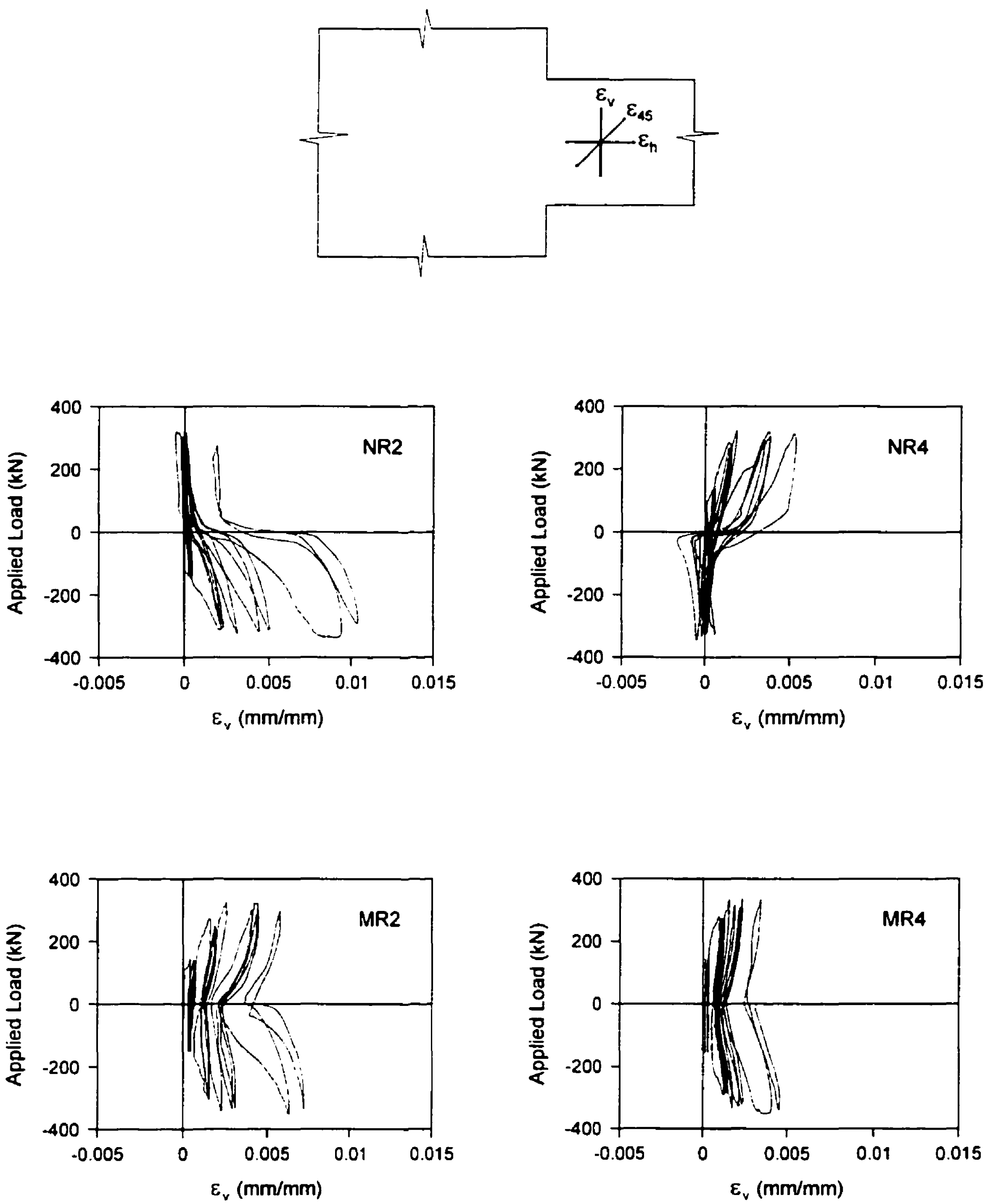

Figure 6.27 Vertical strain, ε_v, of beam specimens

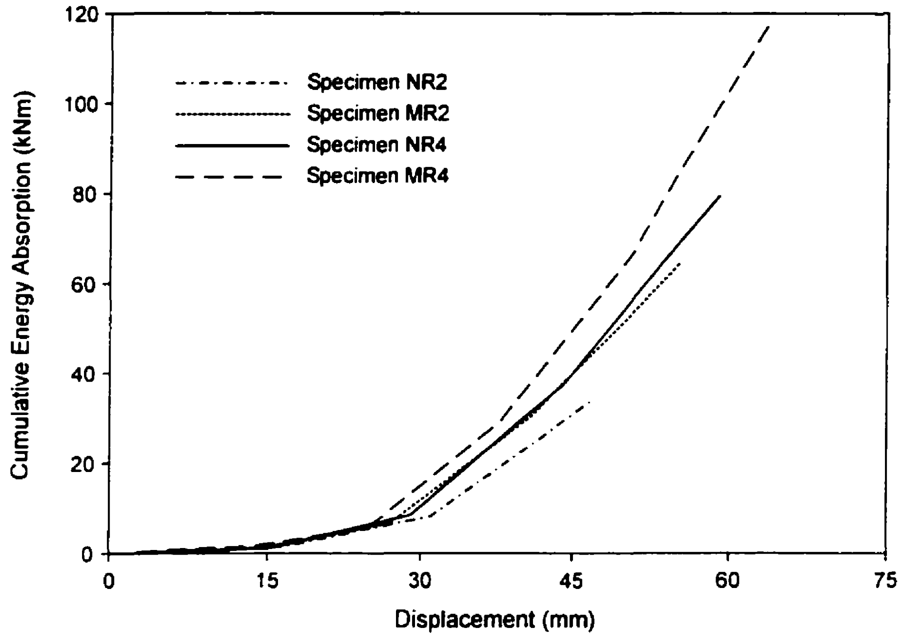

Figure 6.28 Cumulative hysteretic energy absorption versus displacement

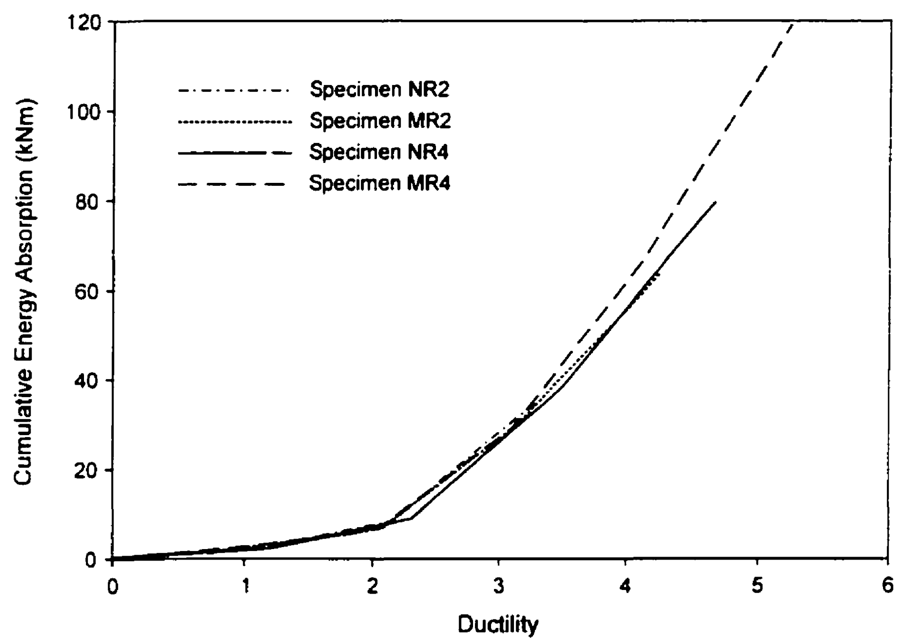

Figure 6.29 Cumulative hysteretic energy absorption versus ductility level

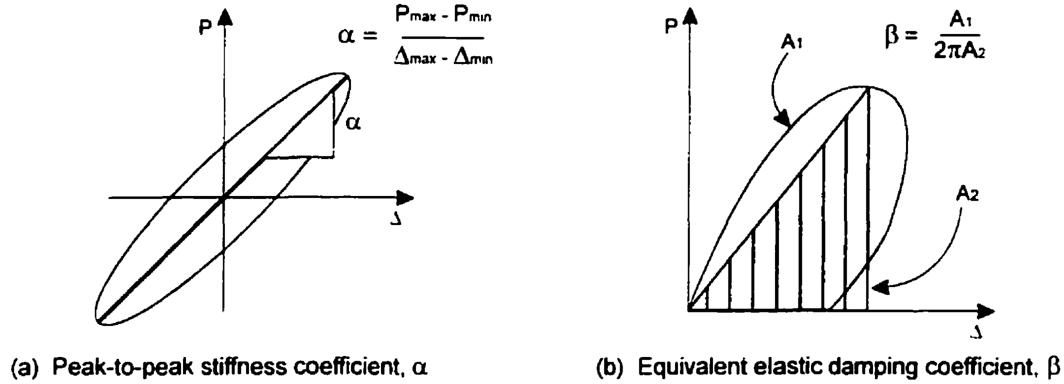

Figure 6.30 Definition of coefficients α and β

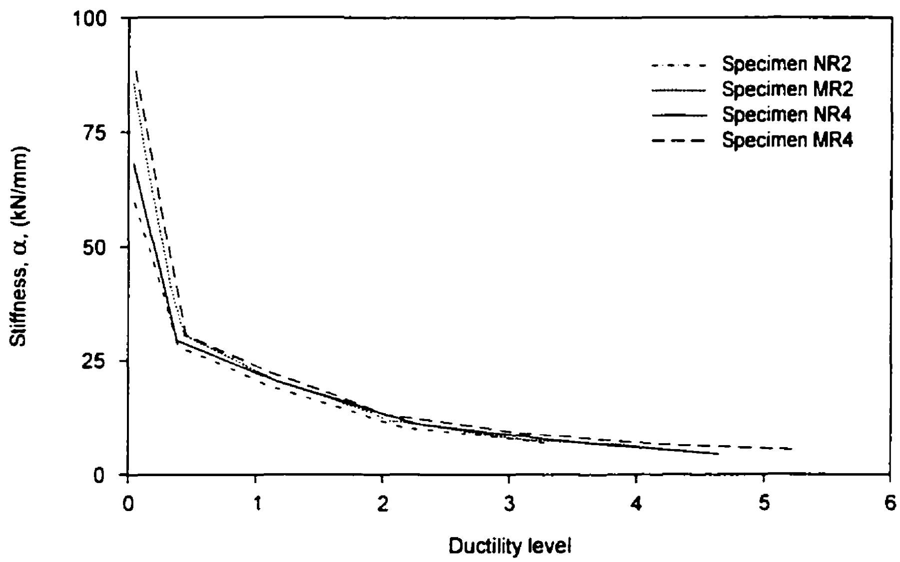

Figure 6.31 Peak-to-peak stiffnesses of beam specimens

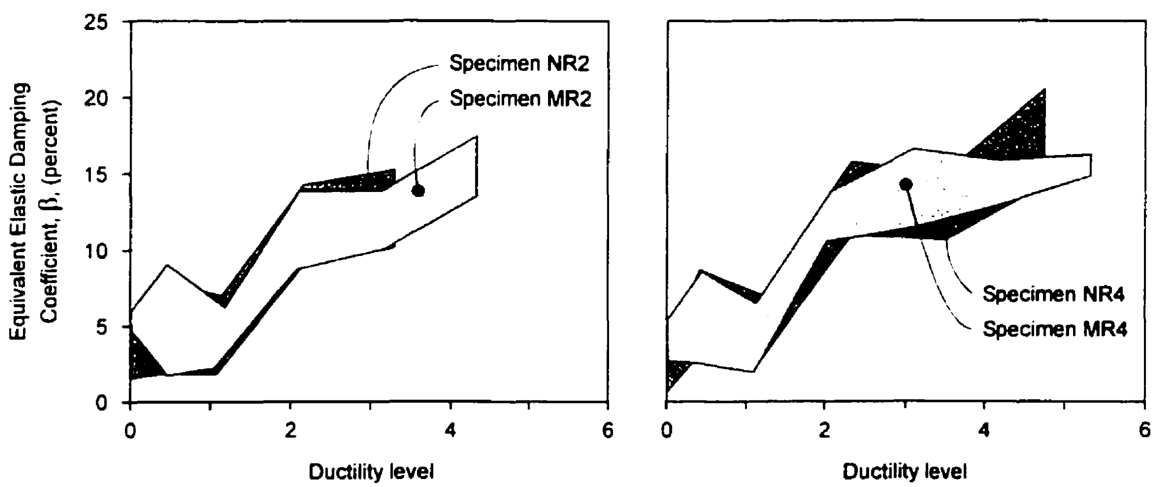

Figure 6.32 Equivalent elastic damping coefficients for beam specimens

Chapter 7

Predictions of Reversed Cyclic Loading Response of Beams and Walls

This chapter presents the computer program developed to predict the hysteretic moment-curvature response of flexural members constructed with reinforced concrete. This FORTRAN program performs a plane sections analysis of the reinforced concrete section, assuming that strains vary linearly over the depth of the cross-section. Assuming that the curvature, ϕ , and the strain at the mid-depth of the cross section, ε_{cen} , are known, the entire strain profile is defined, thus allowing the calculation of the axial load, N, and corresponding moment, M, (see Fig. 7.1). This is accomplished by evaluating the stresses in the concrete and steel, determining the stress resultants to find the resultant axial load, and the resultant moment of the stress resultants. The program evaluates the moment and axial load at small increments of both positive and negative curvature to selected peak curvatures, allowing the complete reversed cyclic moment-curvature response to be evaluated. A sample data file explaining the data input file and the program source code are given in Appendix C.

The following sections describe the input required for the program and the calculations performed to evaluate the reversed cyclic moment-curvature response for a given cross-section. The behavioural models used to determine the reversed cyclic response of the concrete and steel are described in Chapter 4.

For this program, tension is assumed to be positive, thus a constant compressive axial load would be input as a negative quantity. The units used in the input and output files of this program are as follows: distance is described in millimetres (mm), stress is in megaPascals (MPa) and strains are given in millistrain.

7.1 Data Input

7.1.1 Material Properties

It is assumed that the section to be evaluated is constructed using reinforced concrete, thus requiring the definition of the material properties of the concrete and the reinforcing steel. Material resistance factors for the concrete and steel can be included in the analysis of the section, however if the nominal capacity of the member is desired then these factors would be taken equal to unity.

Up to a total of six types of concrete can be specified for the cross-section. This allows for the definition of the unconfined concrete and 5 different types of confined concrete. If the level of confinement varies over the cross-section, the different levels of confinement can be included in the analysis by choosing different confinement parameters.

The stress-strain response of the unconfined concrete is defined by five parameters; the peak compressive stress, f'_{co} ; the corresponding strain, ε_{co} ; the tensile cracking stress, f_{cr} ; the assumed spalling strain, ε_{sp} ; and the product of the tension stiffening factors, α_1 and α_2 . The product of the tension stiffening factors, $\alpha_1\alpha_2$, for seismic loading is taken as 0.7 for deformed bars and 0.49 for plain reinforcing bars (Collins and Mitchell, 1987).

The six parameters defining the confined concrete include the peak confined compressive stress, f'_{cc} , and the corresponding strain, ε_{cc} . In addition, for concrete in tension the tensile cracking stress and the tension stiffening factors are assumed to be the same as those for the unconfined concrete. The final two parameters, k_1 and k_2 , define the descending branch of the stress-strain response of confined high-strength concrete as suggested by Cusson and Paultre (1995). If the unconfined concrete is not constructed with high-strength concrete, these two parameters do not enter into the evaluation of the response of the system and therefore a value of zero can be input into the program.

A total of five different types of reinforcing steel can be defined in the program, with each being defined by a total of nine parameters, which allows for the definition of the stress-strain response of the steel after yielding, including the Bauschinger effect and buckling of the longitudinal reinforcement. The parameters required are the yield modulus divided by 1000, (E / 1000), the yield stress, f_y , and the ultimate stress, f_{ult}. The other parameters are used to define the Ramberg-Osgood function as modified by Mattock (1979). Two sets of values for the coefficients A, B, and C are used, (see Section 1.1.7). The first set defines the stress-strain response of the longitudinal reinforcement before buckling and the second defines the post-buckling behaviour of the reinforcement. The coefficients defining the post-buckling response are used for the evaluation of the stress in the longitudinal reinforcement in compression only. The values of A and B define the bilinear representation of the stress-strain curve, as shown in Fig. 7.2. The value of C defines the transition curve connecting these lines, with a larger value of C resulting in a more abrupt transition.

7.1.2 Cross-Sectional Geometry

The geometry of the cross-section is defined with respect to a reference axis, which is usually located at the bottom of the cross-section. A total of 30 layers of concrete can be used to describe the cross-section of the specimen. These layers are defined by 5 properties, which are a shape index, the distance from the reference axis to the bottom of the layer, the width and height of the layer and the concrete type. If two types of concrete are located at the same elevation the respective areas are calculated and input into the program as two separate layers. Figure 7.3 indicates the values of the shape index for various shapes and indicates the definitions of the other dimensional parameters for a concrete layer. If longitudinal reinforcement is present within the concrete layer, the displaced area of concrete must be taken into account by reducing the width of the layer accordingly.

The longitudinal steel reinforcement is defined by its vertical position in the cross-section with respect to the reference axis, the area of the steel at that location and the steel type. A total of 10 layers of steel can be defined for the cross-section.

7.1.3 Problem Definition

In order to define the problem the program requires the constant applied axial load, the shear-to-moment ratio and the peak curvatures. The convergence of the solution is dependent on the selected constant applied axial load, with a compressive load being input as a negative value.

The effect of shear on the cyclic response of the cross-section is included in the analysis by applying an equivalent axial tension to the system, see Fig.7.4. Assuming the compressive stresses resisting shear are acting at an inclined angle of 45°, the equivalent axial tension required to equilibrate the horizontal component of the compressive stresses is equal to the shear force, (i.e., V / tan 45°), at the selected analysis location along the length of the specimen. Since at a given location, the shear-to-moment ratio is known, the shear force can be determined based on the evaluated moment. This technique allows the effect of shear on the moment capacity of the cross-section to be included in the analysis. However, the pinching of the cyclic response, which is a result of significant shear distress, is not included in this analysis.

The final parameters to be defined are the peak curvatures to which the cross-section will be cycled. Each peak curvature defines the maximum curvature of each half cycle and a total of 20 peak curvatures can be input into the program. Since the analysis is dependent on loading history, these peaks are listed in sequential order of evaluation, starting with the first desired peak curvature.

7.2 Problem Solution

The first step in the solution is to select a curvature at which to perform the calculations evaluating the axial load and moment capacity of the cross-section. This increment is a fraction of the peak curvature that was selected from the input data. By incrementally increasing or decreasing the curvature, the cyclic moment-curvature response of the cross-section can be evaluated.

At the selected curvature the strain at the mid-depth of the cross section is required to completely describe the strain profile. For the first set of calculations the value of the mid-depth strain is taken as zero, with this value being adjusted until convergence of the solution for the given curvature. At the next selected curvature the mid-depth strain is initially taken equal to the correct mid-depth strain at the previous curvature, with this being adjusted until convergence of the solution.

Once the strain profile has been established, the stresses in the concrete and steel are determined, with the axial load being evaluated by integrating the stresses over the cross-section. For the concrete layers, the stresses at the top, mid-height and bottom of each layer are determined. The resulting axial force for each layer is evaluated by using the volume integral formulae given in Fig. 7.5. The axial load in each steel layer is determined by calculating the stress in the steel at that location and multiplying by the corresponding area of steel. By adding up the axial loads from each of the concrete and steel layers the total axial force, N, on the cross-section can be determined.

The corresponding moment about the centroid of the cross-section is found by initially evaluating the turning moment about the reference axis. The stresses calculated in the concrete and steel layers are multiplied by the corresponding distances to the reference axis, with the resulting values being integrated over the cross-sectional area using the same technique as stated for the axial load. Knowing the moment about the reference axis, the axial load and the location of the moment axis, the turning effect about the moment axis, M, can be determined.

The calculated value of the axial load, N, is then compared with the required constant axial load, N5, plus the equivalent axial tension accounting for the effect of shear, ΔN. This axial tension is calculated by multiplying the shear-to-moment ratio by the calculated moment, M, which corresponds to the evaluated axial load. If the difference between N and (N5+ΔN) is within acceptable limits, the calculated results are accepted for that curvature. If the result is within acceptable tolerances, the strains in each of the material layers are compared to the maximum strains experienced in previous cycles. These maximum strains and corresponding stresses are used to define the loading and unloading curves of the concrete and steel in subsequent cycles. The program would then increment the curvature and perform these calculations again until the peak curvature is reached at which point the sign of the increment of curvature is changed and the unloading branch is evaluated. This procedure is continued until the moment-curvature response of the cross-section has been calculated for all selected peak curvatures.

If the difference between N and (N5+ΔN) is not acceptable, a new estimate of the strain at the mid-height of the cross-section is selected and the calculations of the axial load and moment are performed again as previously stated. If a previous estimate of the centroidal stain is available linear interpolation or extrapolation is used to evaluate the new estimate. The centroidal strain is incremented by a small amount if no other estimate is available. This method usually produces acceptable solutions efficiently. However sometimes this technique results in a closed loop of unacceptable solutions. In this case a "brute-force" method using very small increments of strain is used to determine the acceptable solution for a given curvature.

7.3 Predictions of Experimental Results

This program was used to predict the experimental moment-curvature responses of a normal-strength concrete flexural wall that was tested by Tupper (1999) and the four concrete coupling beams that were presented in Chapters 5 and 6.

7.3.1 Flexural Wall

The flexural wall tested by Tupper had a cross section which was 1000 mm by 152 mm and a length of 3.95 m. The main flexural reinforcement consisted of eight No. 20 bars confined by 6 mm ties concentrated at each end of the wall as shown in Fig 7.6. These confining ties were spaced at 76 mm in the plastic hinge region at the base of the wall and were spaced at 152 mm elsewhere. Transverse reinforcement was supplied on both faces of the wall at a spacing of 215 mm over the full height of the test specimen. The peak compressive strength of the concrete was 38.7 MPa and the main flexural reinforcement had a yield stress of 450 MPa. This specimen was tested with a constant compressive axial load of 600 kN and a point load was applied in a reversed cyclic manner at a distance 3.75 m from the base of the wall, (see Fig. 7.6).

The critical section located at the base of the wall was selected for the analysis of this flexural wall. The resulting shear-to-moment ratio for this location was 0.267 m^{-1}. The 6 mm ties confining the main flexural reinforcement provided confinement of the concrete in that location, resulting in a peak confined concrete stress of 45.9 MPa. There were thirteen peak curvatures selected for the analysis, with the maximum positive and negative curvatures being 30 and –16.6 rad/1000m respectively. The predicted and experimental moment-curvature responses are given in Fig. 7.7. It can be seen that the predicted response is very close to the experimental results, with good estimation of the initial stiffness and the peak moments before and after the yielding of the longitudinal reinforcement. There was also good correlation between both the loading and unloading branches of the responses for all of the selected curvatures.

7.3.2 Coupling Beams

The details of the coupling beams are given in Chapter 5. These beams were 300 mm wide, 500 mm high and 1.8 m long, with three No. 25 longitudinal bars at the top and bottom faces of the cross-section. Table 7.1 gives of the material properties used in the analysis for each of these specimens, including the area of the effectively confined core, A_e.

Table 7.1 Material properties of the coupling beam specimens

Specimen	f'_c	Hoop Spacing	f'_{cc}	A_e
NR2	41 MPa	131 mm	49.4 MPa	37 565 mm^2
NR4	41 MPa	90 mm	55.3 MPa	46 451 mm^2
MR2	79.8 MPa	142 mm	87.4 MPa	35 303 mm^2
MR4	79.8 MPa	85 mm	96.2 MPa	47 583 mm^2

The position along the length of the beam selected for the analysis was located at a distance of 100 mm from the face of the wall, which corresponds to Region R1 in the moment vs curvature plots given in Chapter 6. At this location the shear-to-moment ratio is $1.25m^{-1}$, since these beams were subjected to double curvature over their length. This location was approximately at the mid-span of the LVDTs used to calculate the curvatures at the ends of the beams, thus providing compatibility between the analytical and experimental results.

The results of the analyses for the normal-strength concrete specimens are given in Fig. 7.8 and Fig. 7.9, for the nominally ductile and ductile coupling beams, respectively. The predicted responses agree very well with the experimental data. The initial stiffnesses and peak moments were accurately predicted for both the nominally ductile and ductile coupling beam specimens.

The predicted and experimental moment-curvature responses of the nominally ductile and ductile high-strength concrete coupling beams are given in Fig. 7.10 and Fig. 7.11, respectively. The predicted cyclic responses of these high-strength concrete beams were very close to the experimental results. The prediction of the loading and unloading branches was accurate for both of these specimens.

It is noted that the pinching effects due to shear were not that significant, even for the case of the nominally ductile specimens that had been designed for shear accounting for some contribution of the concrete in tension.

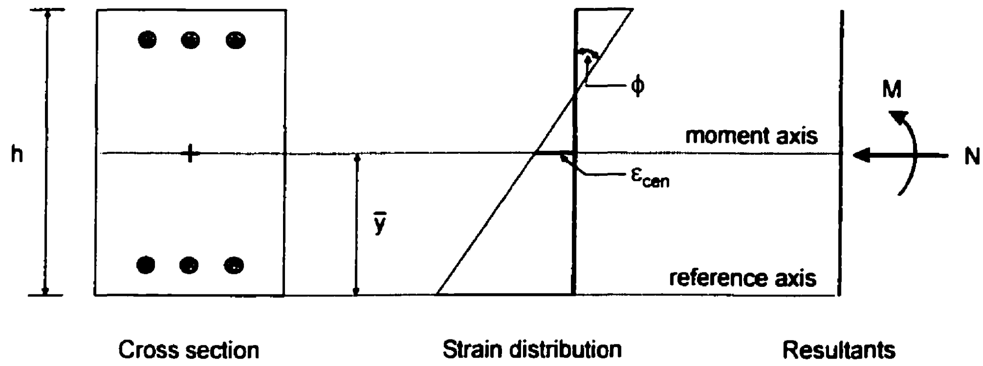

Figure 7.1 Plane sections analysis of a reinforced concrete cross-section

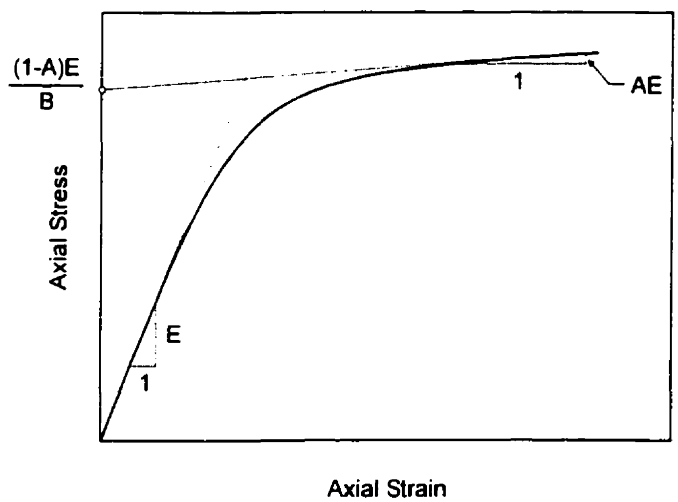

Figure 7.2 Parameters of modified Ramberg-Osgood function (Mattock, 1979)

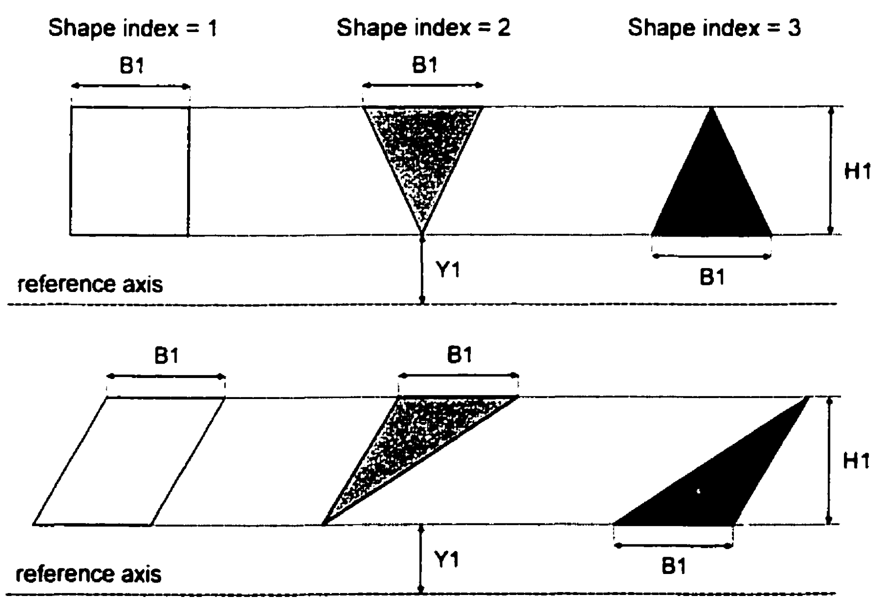

Figure 7.3 Concrete layer shape definitions

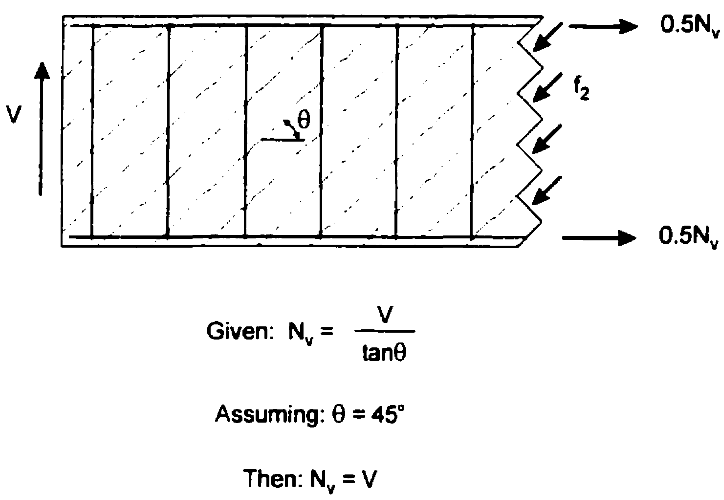

Figure 7.4 Evaluation of equivalent axial tension corresponding to shear force

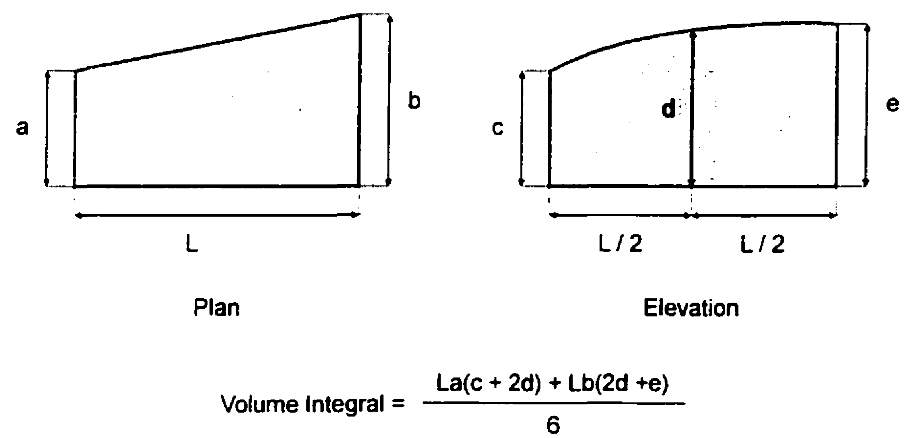

Figure 7.5 Volume integral for the calculation of the force component of a concrete layer

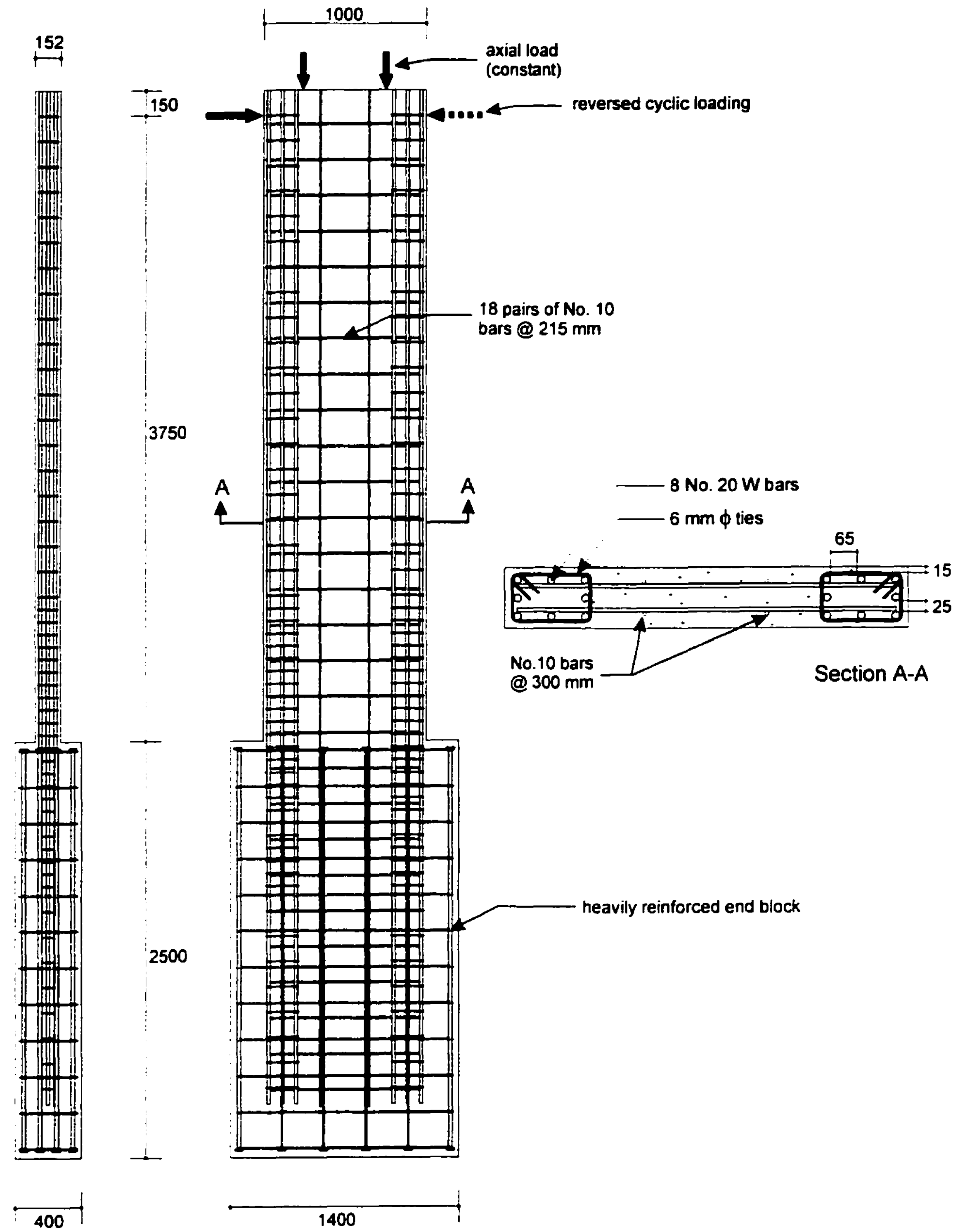

Figure 7.6 Details of reinforcement for Specimen W3 (Tupper, 1999)

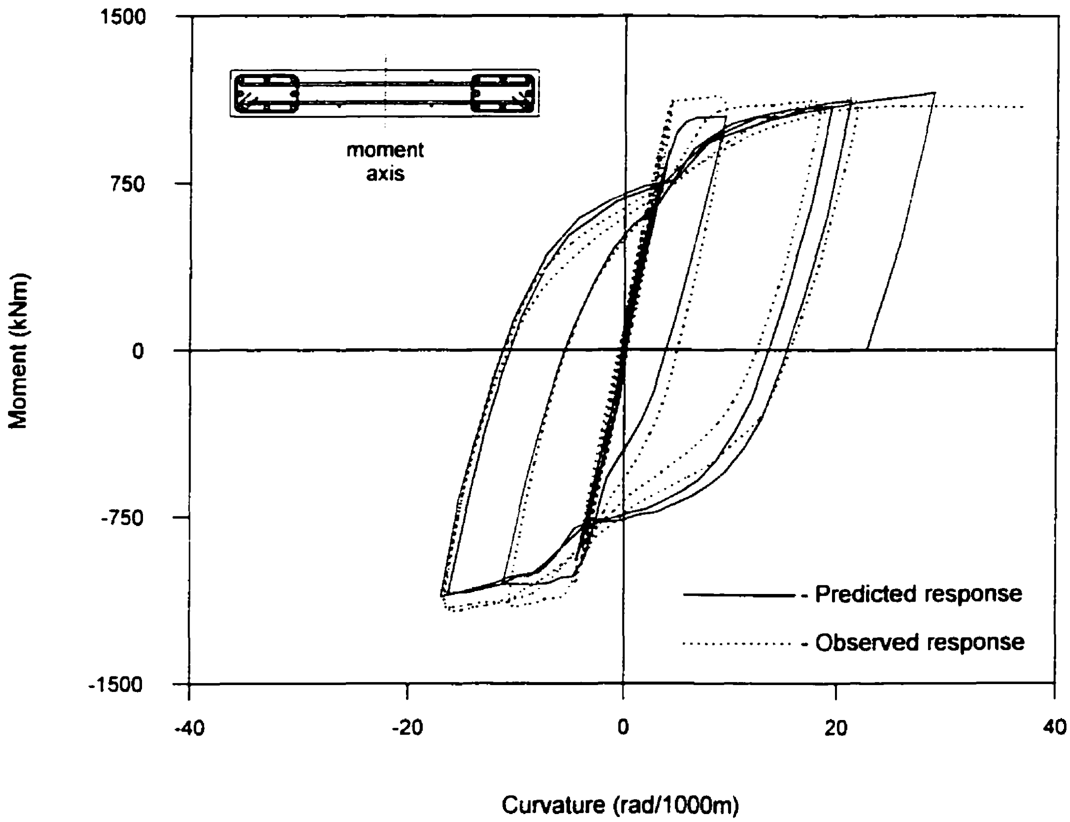

Figure 7.7 Observed and predicted moment-curvature response of Specimen W3 tested by Tupper (1999)

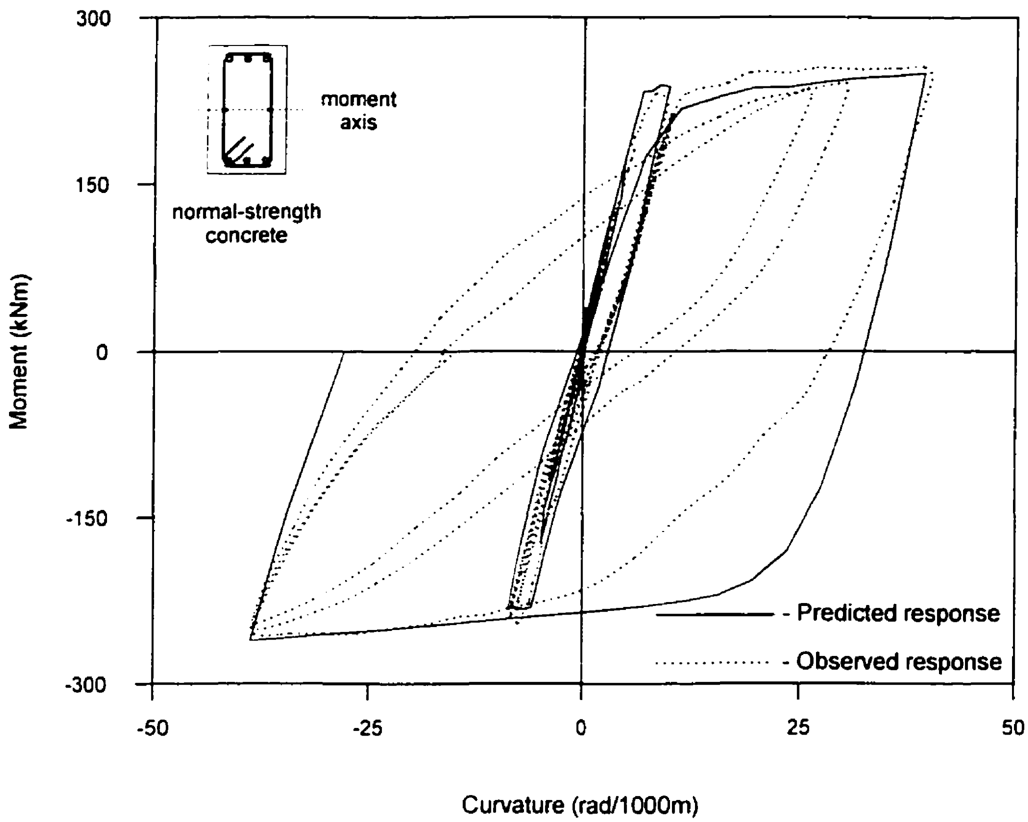

Figure 7.8 Observed and predicted moment-curvature response of Specimen NR2

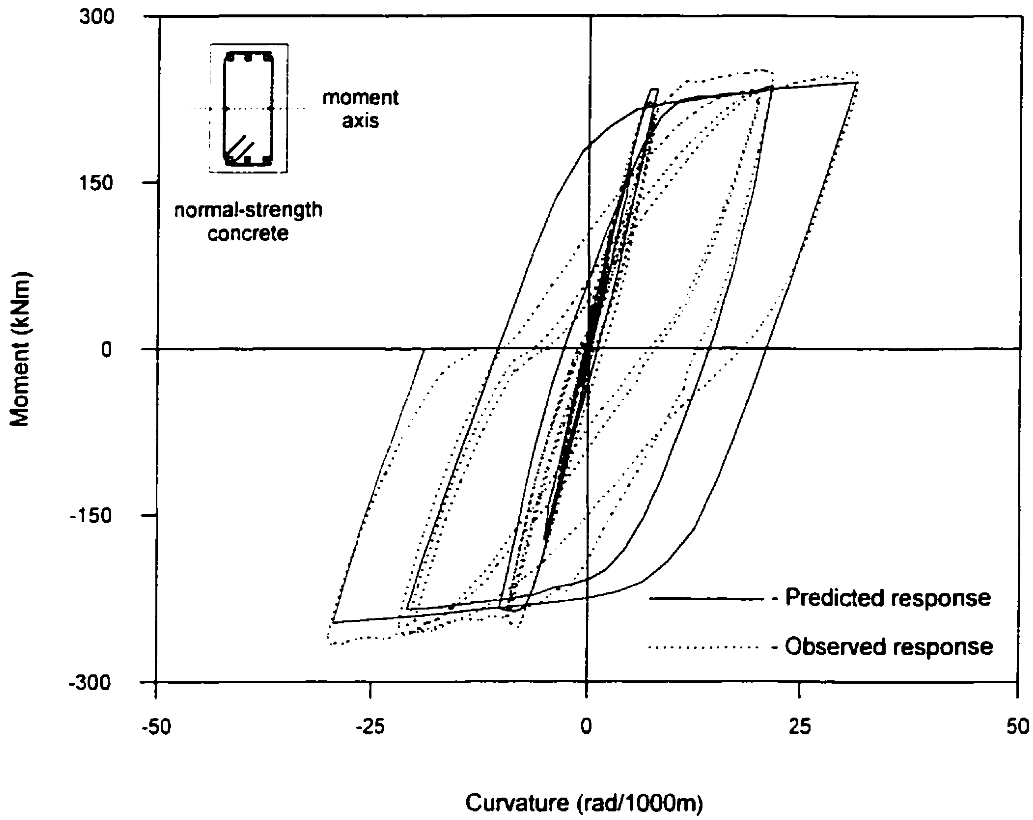

Figure 7.9 Observed and predicted moment-curvature response of Specimen NR4

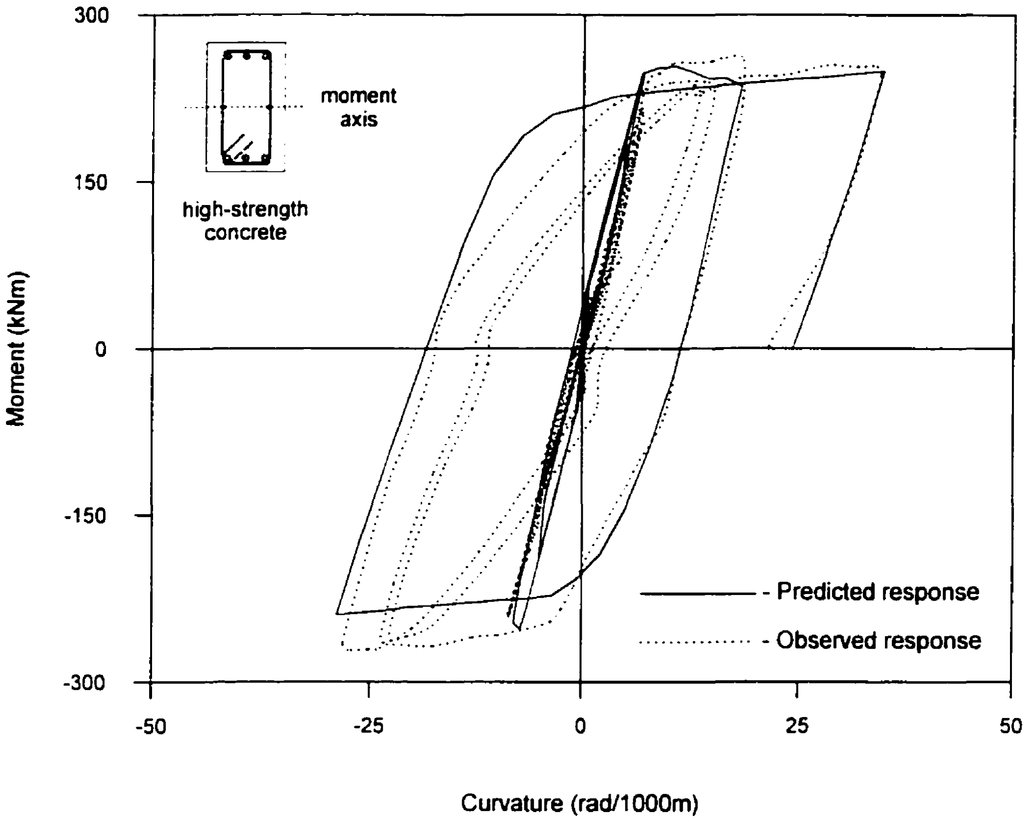

Figure 7.10 Observed and predicted moment-curvature response of Specimen MR2

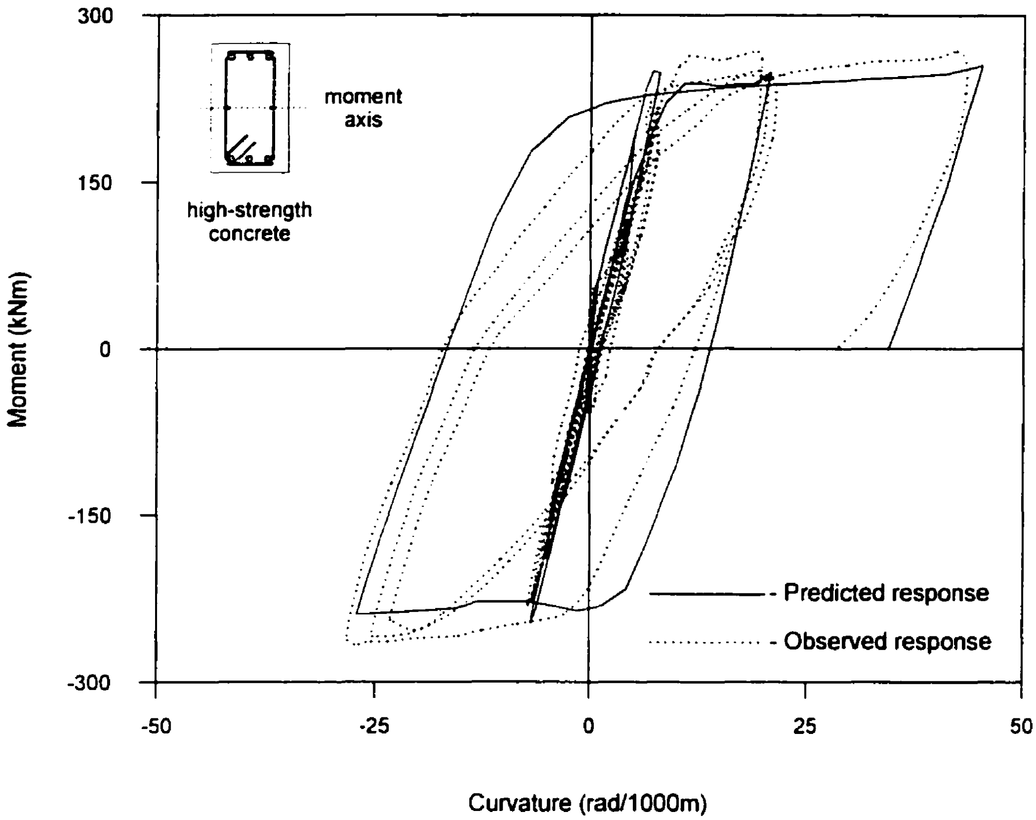

Figure 7.11 Observed and predicted moment-curvature response of Specimen MR4

Chapter 8

Conclusions

The conclusions based on the experimental and analytical programmes are summarized below.

8.1 Experimental Programme

8.1.1 Axially Loaded Specimens

Six specimens were constructed using normal and high-strength concrete and contained varying amounts of transverse reinforcement consistent with both beam and column detailing requirements for different ductility levels. These tests examined the influence of several parameters, including the effect of confinement, bar buckling and concrete strength. From this series of tests the following conclusions can be made:

(i) The spacing and configuration of the transverse reinforcement dramatically changed the response of the specimens for both concrete strengths. The post-peak compressive capacity of each of the specimens was greatly improved by reducing the spacing of the transverse reinforcement and supporting each longitudinal bar by the corner of a hoop.

(ii) The specimens detailed as ductile columns performed extremely well for both concrete strengths. The peak compressive strains and post-peak compressive capacities for these specimens increased with respect to the specimens with smaller amounts of transverse reinforcement. The post-peak response of the high-strength specimen was limited by the ductility of the high-strength transverse reinforcement that was used.

(iii) Buckling of the longitudinal reinforcement was a significant event once the cover concrete had spalled. There was visible buckling of the longitudinal reinforcement of all of the specimens, with this event occurring at smaller compressive strains as the spacing of the transverse reinforcement increased.

(iv) Spalling of the cover concrete was a significant event in the response of the specimens, with this occurring at similar compressive strains for all specimens, except for Specimen H1.

8.1.2 Tests on Materials

The effect of buckling of the longitudinal reinforcement was critical for the compressive response of each of the axially loaded specimens, and hence a series of tests on the tensile and compressive cyclic response of individual bars was conducted. From these tests it was determined that as the length-to-diameter ratio increased, the influence of buckling on the stress-strain response of the reinforcing bar became more pronounced. Also, the buckling of the bar reduced the peak compressive stress reached during a loading cycle and this peak compressive stress decreased under repeated compressive straining. These tests enabled the modeling of the post-buckling stress-strain response of the reinforcing bars.

From the tests on axially loaded specimens it was also noted that the closing of cracks had an influence on the compressive response of the concrete. Therefore, a series of simple tests were performed to evaluate this phenomenon. These tests resulted in the development of a relationship for the evaluation of the closing stress and a behavioural model of this influence on the compressive stress-strain response of concrete.

8.1.3 Concrete Coupling Beams

Reversed cyclic loading tests were carried out on conventionally reinforced nominally ductile and ductile coupling beams constructed with normal and high-strength concrete. These tests investigated the effect of the design and detailing of the transverse reinforcement, as well as the strength of the concrete. The following conclusions can be made based on this series of tests:

(i) The specimens constructed with high-strength concrete performed as well or better than the normal-strength concrete companion beams for both the nominally ductile and ductile detailed beams.

(ii) The reversed cyclic loading responses of the nominally ductile beams were not significantly affected by shear distress until a ductility level greater than 3. Therefore the inclusion of 50 percent of the concrete contribution to the shear capacity of the nominally ductile beams in the design of the transverse reinforcement was appropriate.

(iii) The large longitudinal elongation of the beams resulted in eventual sliding shear failures at the beam-wall interfaces. The restraint provided by the floor slabs surrounding the walls and beam may significantly reduce this elongation and hence this mode of failure would become less significant.

(iv) Due to the large side cover on the coupling beam the spalling of the cover concrete was a major event, resulting in a decrease in load and stiffness of the coupling beam.

8.2 Analytical Programme

Analytical models for the prediction of the reversed cyclic loading response of concrete and steel were presented. The model for the reversed cyclic stress-strain response of concrete included the influence of the transverse reinforcement on the confinement of the core, the effect of the compressive strength, the closing of cracks on compressive response, the residual tensile stresses between cracks and the strain history of the concrete. The model of the reinforcing steel, included the influence of the complete reversed cyclic stress-strain relationship of the steel including the Bauschinger effect and the effect of buckling of the longitudinal reinforcement. These models were used to predict the reversed cyclic responses of the axially loaded specimens. The complete reversed cyclic loading response of each of the specimens was very accurately predicted, even the highly non-linear post-peak behaviour of the specimens with "column details".

The tension-compression material models were used to develop a plane sections computer program, with the capability of evaluating the reversed cyclic moment-curvature response of cross-sections subjected to both axial load and moment. The effect of shear on the cyclic response of the cross-section was included in the analysis by applying an equivalent axial tension to the section. This program was used to predict the responses of the four coupling beams presented and a flexural wall tested by Tupper (1999). The experimental moment-curvature responses of all of these specimens were accurately predicted using this program.

8.3 Future Research

Suggestions for future research are given below:

(i) An experimental programme on the reversed cyclic response of walls with nominal ductility would provide much needed guidance on the design and detailing requirements appropriate for these elements.

(ii) The behavioural models of the bars and cracked concrete could be implemented in a more extensive computer program capable of predicting the reversed cyclic loading response of reinforced concrete subjected to moment, shear and axial load.

(iii) The influence of axial restraint from the presence of reinforced concrete slabs on the reversed cyclic loading response of coupling beams could drastically change the response and failure mechanisms of the coupling beams. Analytical and experimental studies on the reversed cyclic loading behaviour of coupling beams with varying degrees of axial restraint are needed to better understand this phenomenon.

Statement of Originality

The original contributions described in this thesis include:

(i) Six full-scale axially loaded specimens were tested to assess their performance under reversed cyclic tension and compression. These specimens were constructed using normal and high-strength concrete with varying amounts of transverse reinforcement consistent with both beam and column detailing requirements for different ductility levels.

(ii) Four full-scale concrete coupling beams were tested to evaluate their responses under reversed cyclic loading. These specimens were detailed as nominally ductile and ductile beams and constructed using both normal and high-strength concrete.

(iii) A series of ten tests on the reversed cyclic tension and compression response of individual reinforcing bars was conducted. These tests involved different length-to-diameter ratios of the bars to study the influence of buckling of the bars between ties. The tests also considered two loading histories, which were selected to simulate the induced straining of the longitudinal bars in reinforced concrete beams and columns subjected to reversed cyclic loading.

(iv) A series of tests were performed to evaluate the effect of the closing of cracks on the compressive stress-strain response of concrete. These tests were performed on both normal and high-strength concrete specimens to evaluate the influence of concrete strength.

(v) Analytical models for the reversed cyclic response of concrete and steel were presented and used to predict the reversed cyclic tension-compression responses of the axially loaded specimens, (i.e., uniform strains across the section).

(vi) These tension-compression models were used to develop a plane sections analysis program, which was capable of evaluating the reversed cyclic moment-curvature response of concrete members subjected to both axial load and moment, (i.e., linear varying strain distributions).

References

ACI Committee 318, (1989). *ACI 318-89, Building Code Requirements for Reinforced Concrete*, American Concrete Institute, Detroit, Michigan.

ACI Committee 318, (1995). *ACI 318-95, Building Code Requirements for Reinforced Concrete*, American Concrete Institute, Detroit, Michigan.

ACI Committee 363, (1992). *ACI 363R-92, State-of-the-Art Report of High Strength Concrete*, American Concrete Institute, Detroit, Michigan.

ACI-ASCE Committee 352, (1985). *Recommendations for Design of Beam-Column Joints in MonolithicReinforced Concrete Structures*, ACI Journal, V. 82, No. 3, May-June, pp. 266-283.

ACI-ASCE Committee 352, (1995). *ACI 352R-95, Recommendations for Design of Beam-Column Joints in Monolithic Reinforced Concrete Structures*, American Concrete Institute, Detroit, Michigan.

Associate Committee on the National Building Code, (1990). *National Building Code of Canada 1990 and Supplement to the National Building Code of Canada 1990*, National Research Council of Canada, Ottawa, Ontario.

Associate Committee on the National Building Code, (1995). *National Building Code of Canada 1995 and Supplement to the National Building Code of Canada 1995*, National Research Council of Canada, Ottawa, Ontario.

Azizinamini, A., Kuska, S.S.B., Brungardt, P., Hatfield, E., (1994). *Seismic Behaviour of Square High-Strength Concrete Columns*, ACI Structural Journal, V.91, No.3, May-June, pp. 336-345.

Bayrak, O., Sheikh, S.A., (1996). *Confinement Steel Requirements for High-Strength Concrete Columns*, Eleventh World Conference on Earthquake Engineering, Acapulco, Mexico, Paper No. 463.

Bayrak, O., Sheikh, S.A., (1998). *Confinement Reinforcement Design Considerations for Ductile HSC Columns*, ASCE Journal of Structural Engineering, V. 124, No. 9, September, pp. 999-1010.

Bertero, V.V., Popov, E.P., (1977). *Seismic Behavior of Ductile Moment-Resisting Reinforced Concrete Frames-Reinforced Concrete Structures in Seismic Zones*, ACI Publication SP-53, American Concrete Institute, Detroit, Michigan, pp. 247-291.

Bresler, B., Gilbert, P.H., (1961). *Tie Requirements for Reinforced Concrete Columns*, ACI Journal, V. 58, No. 5, November, pp. 555-569.

Bristowe, S., Cook, W.D., Mitchell, D., (1997). *Influence of High-Strength Concrete on the Seismic Response of Coupling Beams*, Proceedings 1997 CSCE Annual Conference, Sherbrooke, Quebec, May 27-30, V. 4, pp. 319-328.

Bristowe, S., Cook, W.D., Mitchell, D., (1999). *Reversed Cyclic Axial Loading Tests on Reinforced Concrete Members*, Proceedings Eighth Canadian Conference on Earthquake Engineering, Vancouver, B.C., June 13-16.

Canadian Standards Association, (CSA), (1984). *CSA Standard A23.3-M84 - Design of Concrete Structures*, Canadian Standards Association, Rexdale, Ontario.

Canadian Standards Association (CSA), (1994). *CSA Standard A23.3-94, Design of Concrete Structures*, Canadian Standards Association, Rexdale, Ont.

Castele, D.J., (1988). *Effect of Column Strength on the Seismic Response of Concrete Frames*, M.Eng. Thesis, Department of Civil Engineering and Applied Mechanics, McGill University, Montreal, Quebec, 96 pp.

Collins, M.P., Mitchell, D., (1987). *Prestressed Concrete Basics*, Canadian Prestressed Concrete Institute, Ottawa, Ontario, 614 pp.

Collins, M.P., Mitchell, D., (1997). *Prestressed Concrete Structures*, Response Publications, Toronto/Montreal, 766 pp.

Collins, M.P., Mitchell, D., MacGregor, J.G., (1993). *Structural Design Considerations for High-Strength Concrete*, Concrete International: Design & Construction, V.15, No.5, May, pp.27-34.

Cusson, D., Paultre, P., (1992). *Behaviour of High Strength Concrete Columns Confined by Rectangular Ties Under Concentric Loading*, Report SMS-92/02, Department of Civil Engineering, University of Sherbrooke, 36 pp.

Cusson, D., Paultre, P., (1995). *Stress-Strain Model for Confined High-Strength Concrete*, ASCE Journal of Structural Engineering, V. 121, No. 3, March, pp. 468-477.

DiFranco, M.A., (1993). *Effect of Spandrel Beam on the Seismic Response of Concrete Frames*, M.Eng. Thesis, Department of Civil Engineering and Applied Mechanics, McGill University, Montreal, Quebec, 131 pp.

Ehsani, M.R., Alameddine, F., (1991). *Design Recommendations for Type 2 High-Strength Reinforced Concrete Connections*, ACI Structural Journal, V. 88, No. 3, May-June, pp. 277-291.

Ehsani, M.R., Moussa, A.E., Vallenilla, C.R., (1987). *Comparison of Inelastic Behavior of Reinforced Ordinary- and High-Strength Concrete Frames*, ACI Structural Journal, V. 84, No. 2, March-April, pp. 161-169.

Ehsani, M.R., Wight, J.K., (1985). *Exterior Reinforced Concrete Beam-to-Column Connections Subjected to Earthquake-Type Loading*, ACI Journal, V. 82, No. 4, July-August, pp. 188-195.

Fafitis, A., Shah, S.P., (1985). *Predictions of Ultimate Behavior of Confined Columns Subjected to Large Deformations*, ACI Journal, V. 84, No. 4, July-August, pp. 423-433.

Harries, K.A., (1995), *Seismic Design and Retrofit of Coupled Walls Using Structural Steel*, Ph.D. Thesis, Department of Civil Engineering and Applied Mechanics, McGill University, May, 229 pp.

Karsan, D., Jirsa, J.O., (1969). *Behaviour of Concrete Under Compressive Loadings*, ASCE Journal of the Structural Division, V. 95, No. ST12, December, pp. 2543-2563.

Kent, D.C., Park, R., (1971). *Flexural Members with Confined Concrete*, ASCE Journal of the Structural Division, V. 97, No. ST7, July, pp. 1969-1990.

Kent, D.C., Park, R., (1973). *Cyclic Load Behaviour of Reinforcing Steel*, Strain (Journal of the British Society of Strain Measurement), V. 9, No. 3, July, pp. 98-103.

Légeron, F., (1997). *Comportement Sismique des Structures en Béton Ordinaire et en Béton à Haute Performance Armé*, Ph.D. Thesis, Département de génie civil, Université de Sherbrooke, et Matériaux et structures, École Nationale des Ponts et Chaussées, Août, 235 pp.

Légeron, F., Paultre, P., (1996a). *Seismic Behaviour of High-Strength Concrete Columns*, Proceedings of the Fourth International Symposium on the Utilization of High-Strength/High-Performance Concrete, Paris, France, May 29-31, V. 3, pp. 883-891.

Légeron, F., Paultre, P., (1996b). *Comportement en flexion composée de poteaux en béton à hautes performances*, Bulletin des Laboratoires des Ponts et Chaussées, Réf. 4004, Mars-Avril, pp. 37-50.

Li, B., (1994). *Strength and Ductility of Reinforced Concrete Members and Frames Constructed Using High-Strength Concrete*, Ph.D.Thesis, Department of Civil Engineering, University of Canterbury, May, 373 pp.

Ma, S.M., Bertero, V.V., Popov, E.P., (1976). *Experimental and Analytical Studies on the Hysteretic Behavior of Reinforced Concrete Rectangular and T-Beams*, EERC Report No. 76-2, Earthquake Engineering Research Center, University of California, Berkeley, May, 241 pp.

Mander, J. B., Priestley, M. J. N., Park R., (1988a). *Theoretical Stress-Strain Model for Confined Concrete*, ASCE Journal of Structural Engineering, V. 114, No. 8, August, pp.1804-1826.

Mander, J. B., Priestley, M. J. N., Park R., (1988b). *Observed Stress-Strain Model for Confined Concrete*, ASCE Journal of Structural Engineering, V. 114, No. 8, August, pp.1827-1849.

Marquis, G.M., (1997). *Effect of High-Strength Concrete on the Seismic Response of Concrete Frames*, M.Eng. Thesis, Department of Civil Engineering and Applied Mechanics, McGill University, July, 117 pp.

Martinez-Rueda, J.E., Elnashai, A.S., (1997). *Confined Concrete Model Under Cyclic Load*, Materials and Structures, V. 30, April, pp. 139-147.

Mattock, A.H., (1979). *Flexural Strength of Prestressed Concrete Sections by Programmable Calculator*, PCI Journal, V. 24, No. 1, January-February, pp. 32-54.

Mau, S.T., (1990). *Effect of Tie Spacing on Inelastic Buckling of Reinforcing Bars*, ACI Structural Journal, V. 87, No. 6, November-December, pp. 671-677.

Mau, S.T., El-Mabsout, M., (1989). *Inelastic Buckling of Reinforcing Bars*, ASCE Journal of Engineering Mechanics, V. 115, No. 1, January, pp. 1-17.

Menegotto, M., Pinto, P.E., (1973). *Method of Analysis of Cyclically Load R. C. Plane Frames Including Changes in Geometry and Non-Elastic Behaviour of Elements Under Combined Normal Force and Bending*, IABSE Reports, V. 13, pp. 15-22.

Mitchell, D., Paultre, P., (1991). *Assessment of Some Canadian Seismic Code Requirements for Concrete Frame Structures*, Canadian Journal of Civil Engineering, V. 18, No. 3, pp. 343-357.

Monti, G., Nuti, C., (1990). *Numerical Model for Steel Bars Under Cyclic Loading Including Post-Elastic Buckling*, Proceedings of the Ninth European Conference on Earthquake Engineering, Moscow, V. 5, pp. 231-240.

Monti, G., Nuti, C., (1992). *Nonlinear Cyclic Behavior of Reinforcing Bars Including Buckling*, ASCE Journal of Structural Engineering, V. 118, No. 12, December, pp. 3268-3284.

Papia, M., Russo, G., Zingone, G., (1988). *Instability of Longitudinal Bars in RC Columns*, ASCE Journal of Structural Engineering, V. 114, No. 2, February, pp. 445-461.

Park, R., (1977)*Accomplishments and Research and Development Needs in New-Zealand*, Proceedings from the Workshop on Earthquake-Resistant Reinforced Concrete Building Construction, University of California, Berkeley, July 11-15, V. 2, pp. 255-295.

Park, R., Kent, D.C., Sampson, R.A., (1972). *Reinforced Concrete Members with Cyclic Loading*, ASCE Journal of the Structural Division, V. 98, No. ST7, July, pp. 1341-1360.

Park, R., Paulay, T., (1975). *Reinforced Concrete Structures*, John Wiley & Sons, New York, 769 pp.

Park, R., Priestly, N., Gill, W.D., (1982). *Reinforced Concrete Members with Cyclic Loading*, ASCE Journal of the Structural Division, V. 108, No. ST4, April, pp. 929-950.

Park, R., Tanaka, H., (1994). *High Strength Concrete Beam-Column Joints*, Proceeding from Second US-Japan-NewZealand-Canada Multi-Lateral Meeting on Structural Concrete in Seismic Regions, Honolulu, Hawaii, Nov.29-Dec.1.

Paulay, T., (1971). *Coupling Beams of Reinforced Concrete Shear Walls*, Journal of the Structural Division, ASCE, V.97, ST3, March, pp.843-862.

Paulay, T., (1977). *Capacity Design of Reinforced Concrete Ductile Frames*, Proceedings from the Workshop on Earthquake-Resistant Reinforced Concrete Building Construction, University of California, Berkeley, July 11-15, V. 3, pp. 1043-1075.

Paulay, T., (1979). *Capacity Design of Resisting Ductile Multistorey Reinforced Concrete Frames*, Proceedings from the Third Canadian Conference on Earthquake Engineering, Montreal, Quebec, June, V. 2, pp. 917-947.

Paulay, T., Binney, J.R., (1974). *Diagonally Reinforced Coupling Beams of Shear Walls*, Shear in Reinforced Concrete, No. 42, ACI, Detroit, Michigan, pp.579-598.

Paulay, T., Park, R., Priestly, M.J.N., (1978). *Reinforced Concrete Beam-Column Joints Under Seismic Actions*, ACI Journal, V. 75, No. 11, November, pp. 585-593.

Paulay, T., Priestley, M.J.M., (1992). *Seismic Design of Reinforced Concrete and Masonry Buildings*, John Wiley & Sons, New York.

Paultre, P., (1987). *Evaluation of Seismic Performance of Concrete Frame Structures in Canada*, Ph.D. Thesis, Department of Civil Engineering and Applied Mechanics, McGill University, Montreal, Quebec, 213 pp.

Paultre, P., Castele, D., Rattray, S., Mitchell, D., (1989). *Seismic Response of Reinforced Concrete Frame Subassemblages-A Canadian Code Perspective*, Canadian Journal of Civil Engineering, V. 16, No. 5, October, pp. 627-649.

Popovics, S., (1973). *A Numerical Approach to the Complete Stress-Strain Curve of Concrete*, Cement and Concrete Research, V. 3, No. 5, pp. 583-599.

Rattray, S., (1986). *Reversed Cyclic Load Tests on Reinforced Concrete Frame Subassemblages*, M.Eng. Thesis, Department of Civil Engineering and Applied Mechanics, McGill University, May, 143 pp.

Razvi, S., Saatcioglu, M., (1999). *Confinement Model for High-Strength Concrete*, ASCE Journal of Structural Engineering, V. 125, No. 3, March, pp. 281-289.

Richart, F.E., Brandtzaeg, A., Brown, R.L., (1928). *A Study of the Failure of Concrete Under Combined Compressive Stresses*, Bulletin 185, University of Illinois.

Richart, F.E., Brandtzaeg, A., Brown, R.L., (1929). *The Failure of Plain and Spirally Reinforced Concrete in Compression*, Bulletin 190, University of Illinois.

Saatcioglu, M., Razvi, S.R., (1992). *Strength and Ductility of Confined Concrete*, ASCE Journal of Structural Engineering. V. 118, No. 6, June, pp. 1590-1607.

Saatcioglu, M., Razvi, S.R., (1998). *High-Strength Concrete Columns with Square Sections Under Concentric Compression*, ASCE Journal of Structural Engineering, V. 124, No. 12, December, pp. 1438-1447.

Scribner, C.F., (1986). *Reinforcement Buckling in Reinforced Concrete Flexural Members*, ACI Journal, V.83, No. 6, November-December, pp.966-973.

Shah, S.P., Ahmad S.H., (1994). *High Performance Concrete: Properties and Applications*, McGraw-Hill Inc., Great Britain, 403 pp.

Sheikh, S.A., (1982). *A Comparative Study of Confinement Model*, ACI Journal, V. 79, No. 4, July-August, pp. 296-306.

Sheikh, S.A., Uzumeri, S.M., (1980). *Strength and Ductility of Tied Concrete Columns*, ASCE Journal of the Structural Division, V. 106, No. ST5, May, pp. 1079-1102.

Sheikh, S.A., Uzumeri, S.M., (1982). *Analytical Model for Concrete Confined in Tied Columns*, ASCE Journal of the Structural Division, V. 108, No. ST12, pp. 2703-2722.

Shin, S.,Ghosh, S.K., Moreno J., (1989). *Flexural Ductility of Ultra-High-Strength Concrete Members*, ACI Structural Journal, V.86, No.4, July-August, pp. 394-400.

Shin, S.W., Lee, K.S., (1992). *High-Strength Concrete Beam-Column Joints*, Proceedings of the Tenth World Conference on Earthquake Engineering, Madrid, Spain, July 19-24, V. 6, pp.3145-3150.

Shiu, K.N., Barney, G.B., Fiorato, A.E., Corely, W.G., (1978). *Reversed Load Tests of Reinforced Concrete Coupling Beams*, Central American Conference on Earthquake Engineering, El Salvador, January, pp.239-249.

Sinha, B.P., Gerstle, K.H., Tulin, L.G., (1964). *Stress-Strain Relations for Concrete Under Cyclic Loading*, ACI Journal, V. 61, No. 2, February, pp. 195-211.

Singh, A., Gerstle, K.H., Tulin, L.G., (1965). *The Behavior of Reinforcing Steel Under Reversed Loading*, Journal ASTM, Materials Research and Standards, V. 5, No. 1, January, pp 12-17.

Standards Association of New Zealand, (1995). *NZS 3101: 1995, Part 1: Code of Practice for the Design of Concrete Structures and Part 2: Commentary on the Design of Concrete Structures*, Wellington, New Zealand, 127 pp. and 156 pp.

Thorenfeldt, E., Tomaszewicz, A., Jensen, J.J., (1987). *Mechanical Properties of High-Strength Concrete and Application in Design*, Proceedings of the Symposium Utilization of High-Strength Concrete, Stavanger, Norway, June, pp. 149-159.

Tupper, B., (1999). *Seismic Response of Reinforced Concrete Walls with Steel Boundary Elements*, M.Eng. Thesis, Department of Civil Engineering and Applied Mechanics, McGill University, March, 95 pp.

Vallenas, J., Bertero, V.V., Popov, E.P., (1977). *Concrete Confined by Rectangular Hoops Subjected to Axial Load*, UCB/EERC Report No. 77/13, University of California, Berkeley.

Vecchio, F.J., Collins, M.P., (1986). *The Modified Compression Field Theory for Reinforced Concrete Elements Subjected to Shear*, ACI Journal, V. 83, No. 2, March-April, pp. 219-231.

Zhu, J., Wang, L., Chen, Z., (1996). *Experimental Study on Confined HS Columns Under Cyclic Loading*, Proceedings of the Fourth International Symposium on the Utilization of High-Strength/High-Performance Concrete, Paris, France, May 29-31, V. 3, pp. 915-923.

Appendix A

Peak Loads and Axial Deformations of Axially Loaded Specimens

Specimen N1

normal-strength concrete
nominally ductile and ductile beam details

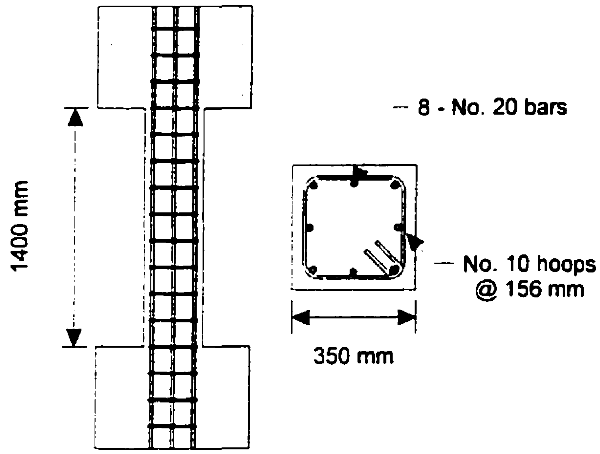

Reinforcement Details

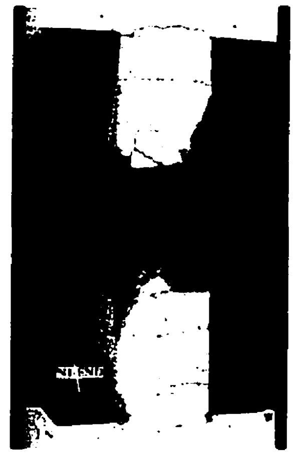

Photograph at Failure

Load Stage	Tensile (A) Cycle		Compressive (B) Cycle		Notes (Δ_y based on tensile cycle) (mcw = max crack width)
	Applied Load (kN)	Axial Deformation (mm)	Applied Load (kN)	Axial Deformation (mm)	
1	241	0.90	-274	0.08	first tensile cracking
2	242	1.04	-276	0.10	
3	232	1.04	-262	-0.16	
4	528	2.14	-1903	-1.28	0.5Δ_y, mcw = 0.1 mm
5	501	2.06	-1893	-1.36	
6	485	2.09	-1899	-1.38	
7	1053	4.77	-2580	-1.84	1.06Δ_y, mcw = 0.3 mm
8	1027	4.83	-2510	-1.81	
9	1021	4.84	-2495	-1.93	
10	1119	8.03	-3258	-2.05	1.78Δ_y, mcw = 1.4 mm
11	1104	11.03	-3817	-2.55	(Load Stage 10 - first splitting cracks)
12	1105	11.13	-3794	-2.60	
13	1145	13.88	-4435	-3.10	3.08Δ_y, mcw = 1.5 mm
14	1149	13.76	-4335	-3.14	
15	1127	13.86	-4239	-3.22	
16	1177	19.81	-4995	-3.81	4.40Δ_y, mcw = 2.0 mm
17	1164	19.88	-4734	-3.89	
18	1158	19.87	-4595	-3.93	
19	1269	31.36	-5599	-4.59	6.97Δ_y, mcw = 3.0 mm
20	1263	31.35	-5204	-4.70	
21	1264	31.21	-5122	-4.69	
22	1318	42.24	-5801	-5.82	9.39Δ_y, cover spalling
23	1322	42.33	-1204	-7.49	severe buckling, core deterioration

Specimen N2

normal-strength concrete
nominally ductile column details

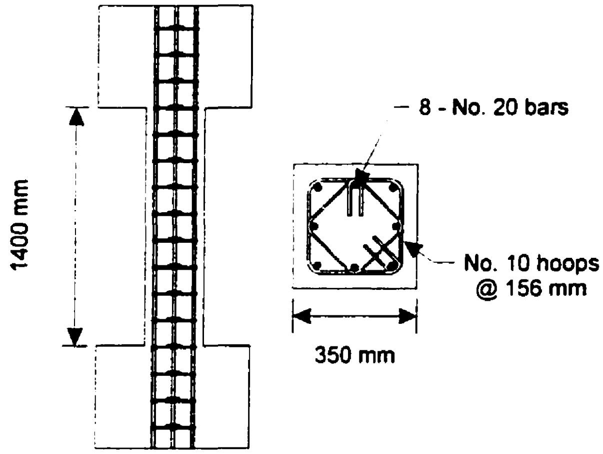

Reinforcement Details

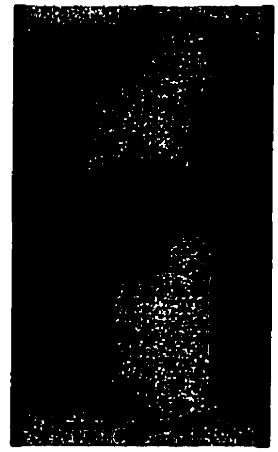

Photograph at Failure

Load Stage	Tensile (A) Cycle		Compressive (B) Cycle		Notes (Δ_y based on tensile cycle) (mcw = max crack width)
	Applied Load (kN)	Axial Deformation (mm)	Applied Load (kN)	Axial Deformation (mm)	
0	-	-	-735	-0.40	$0.2A_gf_c'$ (dead load)
1	-476	-0.31	-1177	-0.67	elastic
2	-475	-0.38	-1183	-0.71	
3	-473	-0.44	-1176	-0.75	
4	147	0.25	-1961	-1.17	first tensile cracking
5	130	0.27	-1941	-1.20	
6	119	0.25	-1936	-1.23	
7	526	2.20	-4071	-2.43	$0.5\Delta_y$, mcw = 0.1 mm
8	540	2.64	-3842	-2.19	
9	516	2.61	-3808	-2.27	
10	1039	4.65	-5385	-3.40	$0.98\Delta_y$, mcw = 0.4 mm
11	1021	4.79	-5086	-3.52	(Load Stage 10 - first splitting cracks)
12	1004	4.75	-5005	-3.56	
13	1094	6.96	-5713	-4.07	$1.47\Delta_y$, mcw = 1.25 mm
14	1095	7.00	-5432	-4.19	
15	1099	7.14	-5255	-3.91	
16	1109	9.01	-5760	-4.40	$1.90\Delta_y$, mcw = 1.1 mm
17	1110	8.81	-5572	-4.70	
18	1104	8.67	-5445	-4.74	
19	1124	10.61	-6437	-5.87	$2.23\Delta_y$, mcw = 1.25 mm
20	1102	10.73	-4216	-6.80	(Load Stage 19 - cover spalling)
21	1107	10.73	-4025	-6.76	

(continued)

Specimen N2 (continued)

normal-strength concrete
nominally ductile column details

Load Stage	Tensile (A) Cycle Applied Load (kN)	Tensile (A) Cycle Axial Deformation (mm)	Compressive (B) Cycle Applied Load (kN)	Compressive (B) Cycle Axial Deformation (mm)	Notes (Δ_y based on tensile cycle) (mcw = max crack width)
22	1102	12.51	-4333	-7.98	$2.63\Delta_y$
23	1116	12.81	-3858	-7.91	
24	1110	12.86	-3635	-7.78	buckling of reinforcement
25	1178	16.47	-3028	-10.43	$3.47\Delta_y$
26	1185	16.41	-2616	-10.64	
27	1174	16.86	-2221	-10.53	severe buckling, core deterioration

Specimen N3

normal-strength concrete
ductile column details

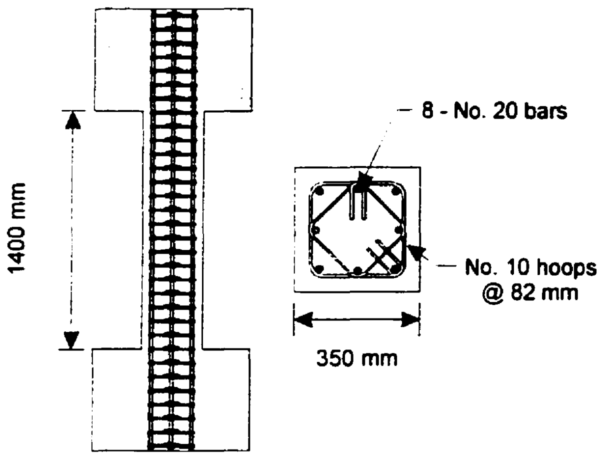

Reinforcement Details

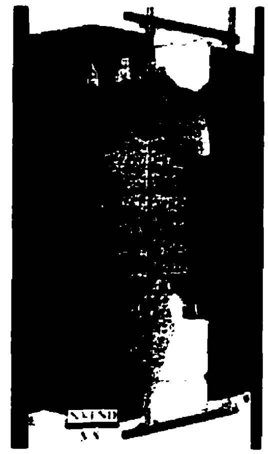

Photograph at Failure

Load Stage	Tensile (A) Cycle Applied Load (kN)	Tensile (A) Cycle Axial Deformation (mm)	Compressive (B) Cycle Applied Load (kN)	Compressive (B) Cycle Axial Deformation (mm)	Notes (Δ_y based on tensile cycle) (mcw = max crack width)
0	-	-	-738	-0.42	$0.2A_g f_c'$ (dead load)
1	-476	-0.34	-1176	-0.68	elastic
2	-477	-0.37	-1180	-0.70	
3	-474	-0.39	-1180	-0.73	
4	142	0.18	-1913	-1.11	first tensile cracking
5	143	0.45	-1942	-1.17	
6	136	0.45	-1927	-1.19	
7	523	2.25	-4070	-2.39	$0.5\Delta_y$, mcw = 0.05 mm
8	515	2.39	-3891	-2.44	
9	530	2.55	-3685	-2.28	
10	1062	4.93	-5358	-3.37	$1.06\Delta_y$, mcw = 0.45 mm
11	1015	4.92	-5055	-3.49	(Load Stage 10 - first splitting cracks)
12	1003	4.78	-4912	-3.53	
13	1102	6.60	-5697	-4.10	$1.45\Delta_y$, mcw = 1.25 mm
14	1080	6.59	-5396	-4.22	
15	1075	6.57	-5283	-4.24	
16	1098	8.25	-5716	-4.64	$1.81\Delta_y$, mcw = 1.25 mm
17	1086	8.22	-5433	-4.71	
18	1088	8.23	-5335	-4.74	
19	1114	10.16	-6407	-5.48	$2.23\Delta_y$, mcw = 1.5 mm
20	1089	10.07	-4659	-6.61	(Load Stage 19 - cover spalling)
21	1095	9.99	-4518	-6.72	

(continued)

Specimen N3 (continued)

normal-strength concrete
ductile column details

Load Stage	Tensile (A) Cycle Applied Load (kN)	Tensile (A) Cycle Axial Deformation (mm)	Compressive (B) Cycle Applied Load (kN)	Compressive (B) Cycle Axial Deformation (mm)	Notes (Δ_y based on tensile cycle) (mcw = max crack width)
22	1109	11.68	-5117	-7.79	$2.57\Delta_y$
23	1100	11.67	-4677	-7.95	
24	1112	11.54	-4403	-7.91	
25	1155	15.22	-5453	-10.27	$3.35\Delta_y$
26	1143	15.20	-4837	-10.41	
27	1140	15.15	-4527	-10.59	
28	1210	18.65	-5261	-12.67	$4.10\Delta_y$
29	1203	18.61	-4689	-12.75	
30	1215	18.56	-4408	-12.82	cover spalled over full height
31	1254	25.71	-4329	-17.71	$5.65\Delta_y$
32	1284	25.62	-3979	-17.45	
33	1286	25.61	-3630	-18.14	
34	1330	32.38	-3406	-23.16	$7.12\Delta_y$
35	1343	32.04	-2735	-23.55	rupture of longitudinal bar : to 36A

Specimen H1

high-strength concrete
nominally ductile and ductile beam details

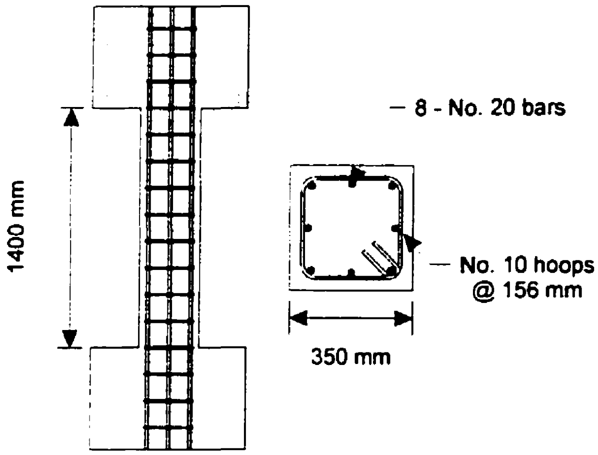

Reinforcement Details

Photograph at Failure

Load Stage	Tensile (A) Cycle: Applied Load (kN)	Tensile (A) Cycle: Axial Deformation (mm)	Compressive (B) Cycle: Applied Load (kN)	Compressive (B) Cycle: Axial Deformation (mm)	Notes (Δ_y based on tensile cycle) (mcw = max crack width)
1	82	0.15	-28	0.14	elastic
2	83	0.20	-27	0.12	
3	85	0.17	-27	0.12	
4	189	0.22	-225	-0.03	first cracking
5	180	0.43	-228	0.00	
6	175	0.33	-226	-0.04	
7	541	2.15	-1603	-0.70	0.5Δ_y, mcw = 0.15 mm
8	512	2.16	-1594	-0.71	
9	505	2.16	-1572	-0.71	
10	1078	4.67	-2726	-1.13	1.08Δ_y, mcw = 0.33 mm
11	1077	4.96	-2548	-0.92	(Load Stage 10 - first splitting cracks)
12	1054	4.97	-2579	-0.94	
13	1126	9.16	-4201	-1.79	2.12Δ_y, mcw = 1.1 mm
14	1126	9.96	-4182	-1.59	
15	1133	10.49	-4226	-1.65	
16	1145	13.73	-5102	-2.00	3.18Δ_y, mcw = 1.4 mm
17	1154	13.90	-5127	-2.03	
18	1146	13.57	-5115	-2.04	
19	1186	19.77	-5890	-2.29	4.58Δ_y, mcw = 2.0 mm
20	1200	19.39	-5713	-2.22	
21	1180	19.99	-5670	-2.27	

(continued)

Specimen H1 (continued)

high-strength concrete
nominally ductile and ductile beam details

Load Stage	Tensile (A) Cycle Applied Load (kN)	Tensile (A) Cycle Axial Deformation (mm)	Compressive (B) Cycle Applied Load (kN)	Compressive (B) Cycle Axial Deformation (mm)	Notes (Δ_y based on tensile cycle) (mcw = max crack width)
22	1264	28.33	-7221	-2.83	6.56Δ_y, mcw = 3.0 mm
23	1262	28.65	-6973	-2.92	
24	1269	29.21	-6935	-2.94	
25	1329	39.79	-8457	-3.40	9.12Δ_y, mcw = 4.0 mm
26	1325	39.67	-8224	-3.54	
27	1320	38.99	-7175	-3.59	severe buckling, core deterioration

Specimen H2

high-strength concrete
nominally ductile column details

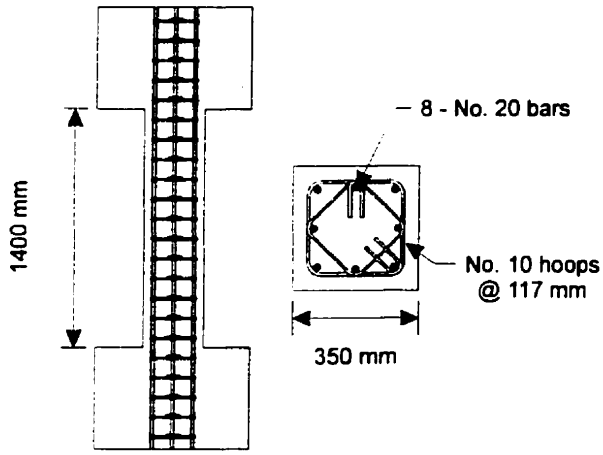

Reinforcement Details

Photograph at Failure

Load Stage	Tensile (A) Cycle Applied Load (kN)	Tensile (A) Cycle Axial Deformation (mm)	Compressive (B) Cycle Applied Load (kN)	Compressive (B) Cycle Axial Deformation (mm)	Notes (Δ_y based on tensile cycle) (mcw = max crack width)
0	-	-	-1658	-0.92	$0.2A_g f_c'$ (dead load)
1	-1399	-0.87	-3384	-1.65	elastic
2	-1396	-1.00	-3382	-1.64	
3	-1399	-0.96	-3393	-1.61	
4	206	0.63	-4041	-1.89	first tensile cracking
5	193	0.66	-4040	-1.93	
6	153	0.69	-4011	-1.97	
7	546	2.29	-7206	-3.16	$0.5\Delta_y$, mcw = 0.1 mm
8	517	2.30	-7014	-3.19	
9	513	2.31	-6901	-3.19	
10	1056	4.75	-9424	-4.38	$1.07\Delta_y$, mcw = 0.33 mm
11	1014	4.85	-9104	-4.42	
12	1011	4.85	-8866	-4.43	
13	1092	5.80	-9763	-4.76	$1.30\Delta_y$, mcw = 0.7 mm
14	1053	6.25	-9508	-4.85	(Load Stage 13 - first splitting cracks)
15	1048	6.20	-9375	-4.89	
16	1082	7.45	-10066	-5.28	$1.67\Delta_y$, mcw = 0.8 mm
17	1083	7.37	-9771	-5.37	
18	1058	7.48	-9555	-5.46	
19	1100	8.13	-9772	-5.54	$1.83\Delta_y$, mcw = 0.8 mm
20	1108	8.30	-3252	-8.90	(LS 19 - cover spalling & buckling)
21	1105	8.23	-3114	-8.89	

(continued)

Specimen H2 (continued)

high-strength concrete
nominally ductile column details

Load Stage	Tensile (A) Cycle		Compressive (B) Cycle		Notes
	Applied Load (kN)	Axial Deformation (mm)	Applied Load (kN)	Axial Deformation (mm)	(Δ_y based on tensile cycle) (mcw = max crack width)
22	1148	9.72	-3225	-9.41	2.18Δ_y
23	1131	9.88	-3054	-9.48	
24	1126	9.96	-2862	-9.56	
25	1149	12.30	-3144	-11.07	2.76Δ_y , severe buckling
26	1158	12.33	-2865	-11.51	core deterioration
27	1170	12.45	-2662	-11.54	

Specimen H3

high-strength concrete
ductile column details

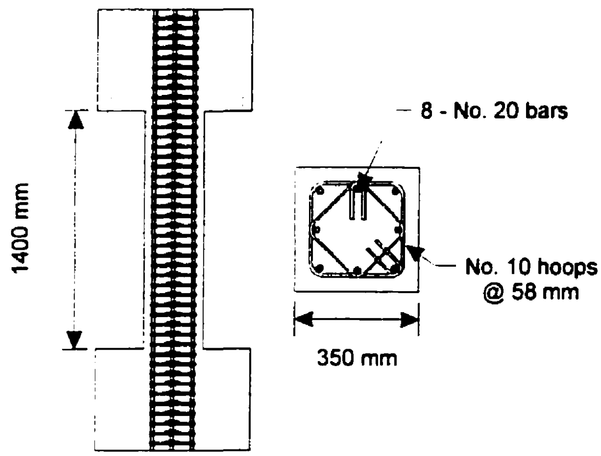

Reinforcement Details

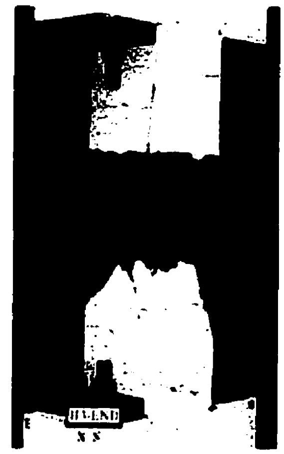

Photograph at Failure

Load Stage	Tensile (A) Cycle Applied Load (kN)	Tensile (A) Cycle Axial Deformation (mm)	Compressive (B) Cycle Applied Load (kN)	Compressive (B) Cycle Axial Deformation (mm)	Notes (Δ_y based on tensile cycle) (mcw = max crack width)
0	-	-	-1710	-0.94	$0.2A_gf_c'$ (dead load)
1	-1404	-0.86	-3389	-1.63	elastic
2	-1414	-1.01	-3391	-1.67	
3	-1413	-1.03	-3391	-1.68	
4	195	0.36	-4041	-1.91	first tensile cracking
5	216	0.98	-3899	-1.53	
6	190	0.98	-3937	-1.57	
7	513	2.50	-7193	-2.95	$0.5\Delta_y$, mcw = 0.15 mm
8	497	2.44	-7069	-3.00	
9	487	2.43	-7011	-3.02	
10	1043	4.72	-9457	-4.20	$1.00\Delta_y$, mcw = 0.4 mm
11	1013	4.89	-9109	-4.34	(Load Stage 10 - first splitting cracks)
12	997	4.89	-8911	-4.38	
13	1072	6.35	-9767	-4.74	$1.35\Delta_y$, mcw = 0.8 mm
14	1060	6.15	-9526	-4.78	
15	1048	6.45	-9411	-4.81	
16	1087	7.28	-10095	-4.92	$1.54\Delta_y$, mcw = 0.9 mm
17	1060	8.01	-9617	-4.86	
18	1043	8.01	-9784	-5.04	
19	1092	9.10	-10235	-5.27	$1.93\Delta_y$, mcw = 0.9 mm
20	1085	8.94	-10089	-5.36	
21	1060	9.14	-9958	-5.39	

(continued)

Specimen H3 (continued)

high-strength concrete
ductile column details

Load Stage	Tensile (A) Cycle Applied Load (kN)	Tensile (A) Cycle Axial Deformation (mm)	Compressive (B) Cycle Applied Load (kN)	Compressive (B) Cycle Axial Deformation (mm)	Notes (Δ_y based on tensile cycle) (mcw = max crack width)
22	1095	10.31	-10471	-5.65	$2.18\Delta_y$, mcw = 1.1 mm
23	1083	10.05	-8010	-6.82	(LS 22 - cover spalling)
24	1091	10.42	-7755	-6.91	
25	1104	13.36	-8460	-7.85	$2.83\Delta_y$
26	1115	13.22	-7821	-8.08	
27	1104	13.26	-7560	-8.27	
28	1164	15.68	-8205	-9.46	$3.32\Delta_y$
29	1152	15.71	-7276	-9.34	
30	1161	15.68	-6030	-9.99	covered spalled over half the length
31	1219	20.81	-5699	-12.87	$4.41\Delta_y$
32	1239	20.83	-5187	-13.18	
33	1239	20.82	-4915	-13.33	buckling of longitudinal bars
34	1273	25.83	-5203	-15.63	$5.47\Delta_y$
35	1284	25.94	-4485	-16.27	
36	1288	25.90	-4062	-16.36	rupture of hoops

Appendix B

Peak Loads and Deflections of Coupling Beam Specimens

Specimen NR2

normal-strength concrete
nominally ductile beam
Δ_y = 14.4 mm

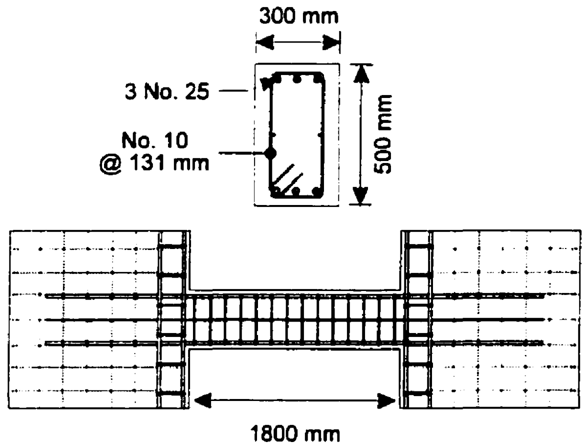

Beam Reinforcement

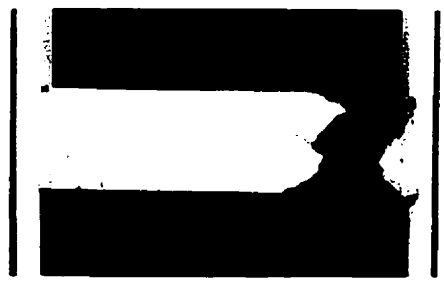

Photograph at Failure

Load Stage	Positive (A) Cycle		Negative (B) Cycle		Notes
	Applied Shear (kN)	Relative Deflection (mm)	Applied Shear (kN)	Relative Deflection (mm)	
1	49.1	0.90	-45.6	-0.63	first cracking
2	46.7	0.91	-40.1	-0.64	
3	49.0	0.93	-38.8	-0.63	
4	141.2	5.68	-139.7	-4.29	0.5M_y
5	123.4	5.02	-144.7	-4.81	
6	121.6	5.06	-146.8	-4.89	
7	294.2	16.34	-312.2	-15.80	+1.13Δ_y, -1.10Δ_y, wall cracking
8	271.0	15.39	-305.2	-16.03	
9	268.5	15.49	-292.8	-15.90	
10	324.1	31.04	-326.0	-31.95	+2.16Δ_y, -2.22Δ_y
11	305.8	31.30	-318.6	-31.74	
12	299.1	31.38	-312.5	-31.98	
13	317.7	47.13	-336.1	-48.15	+3.27Δ_y, -3.34Δ_y, first spalling
14	274.5	47.43	-290.7	-47.99	cover spalling
15	214.9	47.84	-211.6	-47.87	

Specimen NR4

normal-strength concrete
ductile coupling beam
Δ_y = 12.6 mm

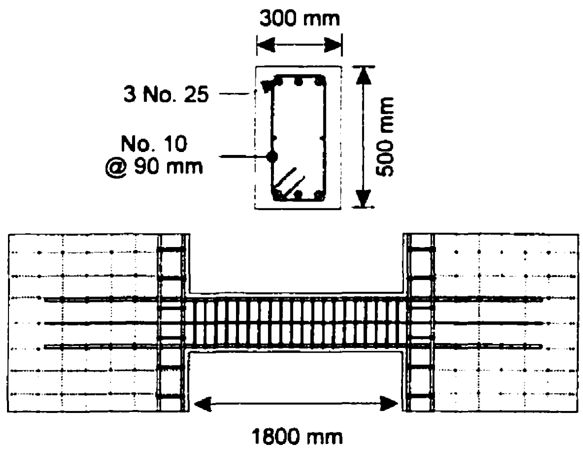

Beam Reinforcement

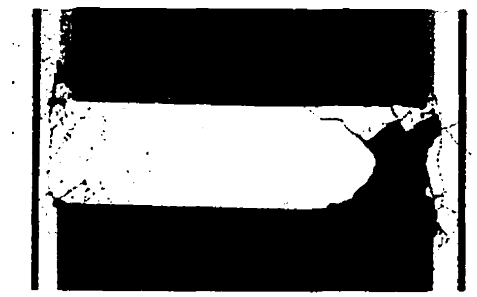

Photograph at Failure

Load Stage	Positive (A) Cycle		Negative (B) Cycle		Notes
	Applied Shear (kN)	Relative Deflection (mm)	Applied Shear (kN)	Relative Deflection (mm)	
1	49.3	0.78	-72.1	-1.00	first cracking
2	43.9	0.72	-41.8	-0.80	
3	36.5	0.70	-38.7	-0.81	
4	136.4	5.12	-164.2	-5.04	$0.5M_y$
5	132.5	5.00	-159.0	-5.05	
6	135.5	5.16	-153.4	-5.13	
7	283.6	15.11	-320.0	-14.57	$+1.20\Delta_y$, $-1.16\Delta_y$, wall cracking
8	268.7	14.32	-311.4	-15.32	
9	263.4	14.40	-305.2	-15.22	
10	321.1	28.97	-331.1	-30.60	$+2.30\Delta_y$, $-2.43\Delta_y$
11	300.7	29.15	-329.1	-30.18	
12	288.9	29.32	-325.0	-30.07	
13	320.2	44.13	-344.3	-45.14	$+3.50\Delta_y$, $-3.58\Delta_y$
14	313.2	44.18	-324.5	-45.15	
15	304.3	44.20	-274.1	-45.02	first spalling
16	293.4	59.07	-209.8	-60.32	$+4.69\Delta_y$, $-4.79\Delta_y$, cover spalling
17	122.9	59.69	-104.4	-60.20	

Specimen MR2

high-strength concrete
nominally ductile beam
Δ_y = 13.0 mm

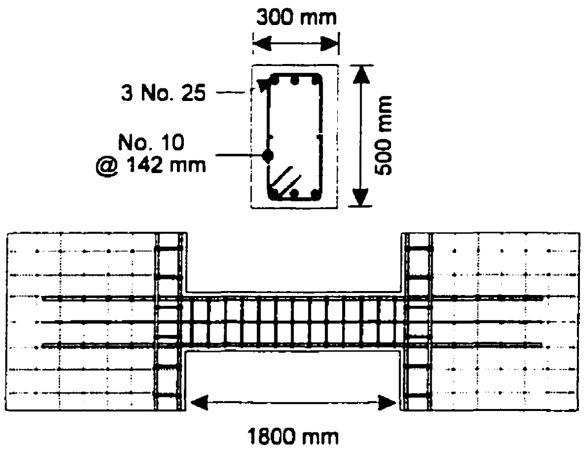

Beam Reinforcement

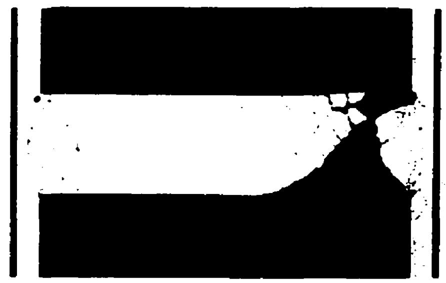

Photograph at Failure

Load Stage	Positive (A) Cycle Applied Shear (kN)	Positive (A) Cycle Relative Deflection (mm)	Negative (B) Cycle Applied Shear (kN)	Negative (B) Cycle Relative Deflection (mm)	Notes
1	49.7	0.75	-51.4	-0.41	elastic
2	41.2	0.73	-54.2	-0.46	first cracking (shrinkage)
3	53.3	0.90	-48.1	-0.47	
4	144.7	5.97	-150.5	-3.59	$0.5M_y$
5	140.4	5.92	-146.2	-3.62	
6	134.7	5.91	-150.1	-3.72	
7	273.5	14.90	-301.6	-12.87	$+1.15\Delta_y$, $-0.99\Delta_y$, wall cracking
8	249.6	13.52	-305.9	-13.99	
9	245.1	13.57	-299.5	-13.95	
10	330.3	25.88	-343.3	-28.15	$+1.99\Delta_y$, $-2.17\Delta_y$
11	302.4	27.14	-335.4	-28.18	
12	299.5	27.07	-332.5	-28.16	
13	320.6	40.96	-354.0	-42.10	$+3.15\Delta_y$, $-3.24\Delta_y$
14	298.0	41.13	-339.8	-41.12	
15	274.2	41.30	-325.7	-42.06	
16	277.5	55.37	-334.2	-56.02	$+4.25\Delta_y$, $-4.31\Delta_y$, first spalling
17	177.5	56.10	-189.1	-55.80	

Specimen MR4

high-strength concrete
ductile coupling beam
Δ_y = 12.2 mm

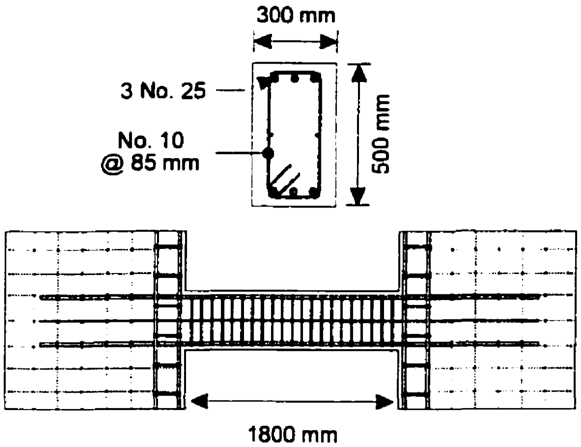

Beam Reinforcement

Photograph at Failure

Load Stage	Positive (A) Cycle Applied Shear (kN)	Positive (A) Cycle Relative Deflection (mm)	Negative (B) Cycle Applied Shear (kN)	Negative (B) Cycle Relative Deflection (mm)	Notes
1	45.3	0.56	-51.9	-0.60	elastic
2	46.6	0.56	-51.2	-0.54	
3	46.2	0.66	-50.2	-0.61	
4	145.5	5.43	-154.5	-4.27	0.5M_y, first cracking
5	146.2	5.31	-155.5	-4.54	
6	143.2	5.28	-147.4	-4.48	
7	280.4	13.84	-290.8	-12.05	+1.13Δ_y, -0.99Δ_y, wall cracking
8	274.7	13.35	-281.3	-12.09	
9	273.1	13.45	-285.0	-12.15	
10	329.1	24.88	-336.5	-26.39	+2.04Δ_y, -2.16Δ_y
11	315.8	25.28	-327.5	-26.57	
12	307.0	25.43	-309.0	-26 28	
13	338.3	37.89	-350.9	-38.68	+3.10Δ_y, -3.17Δ_y
14	333.6	37.67	-332.8	-39.64	
15	323.8	37.79	-327.5	-39.44	
16	340.1	50.78	-356.4	-52.38	+4.16Δ_y, -4.29Δ_y
17	344.8	50.75	-349.1	-52.30	
18	337.1	50.87	-339.9	-52.58	
19	348.4	63.72	-347.1	-65.47	+5.22Δ_y, -5.37Δ_y, first spalling
20	291.0	64.06	-303.9	-65.46	cover spalling
21	200.6	64.83	-193.2	-65.34	

Appendix C

Data Input File and Program Source Code

Data Input File

Input File

Sample						
Q2	Q3					
F0	S0	F1	ESP	Q1		(unconfined concrete)
Z1						
F0	S0	F1	Q1	X1	X2	(confined concrete)
Z2						
E3	Y0	U3				(reinforcing steel)
A3	B3	C3	AB	BB	CB	
H	Y9	C9				
K9	Y1	B1	H1	T1		(concrete layer)
N2						
Y2	A2	T2				(steel layer)
N5						
DVDM						
P2						
PEAK						

Definition of Terms

Sample	=	name of specimen (up to 20 characters)
Q2	=	ϕ_c, concrete phi factor
Q3	=	ϕ_s, steel phi factor
F0	=	peak compressive stress in MPa (positive number)
S0	=	corresponding compressive strain in millistrain (negative number)
F1	=	cracking stress in MPa (positive number)
ESP	=	spalling strain in millistrain (negative number)
Q1	=	$\alpha_1\alpha_2$, tension stiffening factor
Z1	=	number of types of confined concrete (positive integer ≤ 5)
X1	=	k_1, parameter as defined by Cusson and Paultre (1995)
X2	=	k_2, parameter as defined by Cusson and Paultre (1995)
Z2	=	number of types of reinforcing steel (positive integer ≤ 10)
E3	=	elastic stiffness in GPa (positive number)
Y0	=	yield stress in MPa (positive number)
U3	=	ultimate stress in MPa (positive number)
A3, AB	=	parameter A, before and after buckling, respectively
B3, BB	=	parameter B, before and after buckling, respectively
C3, CB	=	parameter C, before and after buckling, respectively
H	=	height of cross-section in mm
Y9	=	distance from reference axis to the centroid of the cross-section in mm
C9	=	number of concrete layers (positive integer ≤ 30)
K9	=	layer shape index (positive integer either 1, 2 or 3)
Y1	=	distance from reference axis to the bottom of the layer in mm
B1	=	width of the layer in mm
H1	=	height of the layer in mm
T1	=	type of concrete in the layer (positive integer, 1=unconfined; 2=1st confined, etc.)
N2	=	number of steel layers (positive integer ≤ 10)
Y2	=	distance from the reference axis to the steel location in mm
A2	=	area of steel at that location in mm^2
T2	=	type of reinforcing steel (positive integer between 1 and Z2)
N5	=	constant applied axial load (either sign, negative is compressive)
DVDM	=	shear-to-moment ratio
P2	=	number of half peaks to be included in response (positive integer ≤ 20)
PEAK	=	peak curvature

```
PROGRAM MOMENT_CURVATURE_RESPONSE
IMPLICIT REAL*8 (A-H,O-Z)
CHARACTER NAME*20
INTEGER I,Z1,Z2,C9,N2,P2,NUM,SIGN, T1(30), T2(10), Q,K9(30)
REAL*8 F0(6),S0(6),F1(6),ESP(6),Q1(6),X1(6),X2(6), L
REAL*8 E1(6),E2(6),R1(6),R2(6),E3(5),Y0(5),A3(5),B3(5),C3(5),U3(5)
REAL*8 AB(5),BB(5),CB(5),Y1(30),B1(30),H1(30),K(30,3),K1(30)
REAL*8 Y2(10),A2(10),PEAK(20),MPREV,INC,M,N,N5,NPLUS
REAL*8 M1,N1,ML,MR,M3,N3
REAL*8 BCSTRAIN(30,10),MCSTRAIN(30,10),TCSTRAIN(30,10)
REAL*8 BCSTRESS(30,5), MCSTRESS(30,5), TCSTRESS(30,5)
COMMON CONMAT(11),CSTRAIN(10),CSTRESS(5)
COMMON STEMAT(9),SSTRAIN(10,6),SSTRESS(10,3) YIELD(10)
COMMON US0,UE1,UF0,UR1,UESP
OPEN (UNIT=10,FILE='DATA',STATUS='OLD')
OPEN (UNIT=11,FILE='OUTPUT',STATUS='UNKNOWN')
READ (10,*) NAME
WRITE (11,*) '********************'
WRITE (11,*) NAME
WRITE (11,*) '********************'
!
!       INPUT MATERIAL PROPERTIES
!
READ (10,*) Q2,Q3
WRITE (11,*) 'MATERIAL RESISTANCE FACTORS'
WRITE (11,500) 'Phi Concrete = ',Q2,'  Phi Steel = ',Q3
500 FORMAT (' ',A,F4 2,A,F4 2)
READ (10,*) F0(1),S0(1),F1(1),ESP(1),Q1(1)
WRITE (11,*) 'UNCONFINED CONCRETE'
WRITE (11,505) 'fc = ',F0(1),'  ec = ',S0(1),'  fcr = ',F1(1)
505 FORMAT (' ',A,F6 2,A,F6 2,A,F6 2)
WRITE (11,506) 'espall = ',ESP(1),'  alphas = ',Q1(1)
506 FORMAT (' ',A,F6 2,A,F3 2)
READ (10,*) Z1
WRITE (11,*) 'CONFINED CONCRETE'
DO 10 I = 2, Z1+1
       READ (10,*) F0(I),S0(I),F1(I),Q1(I),X1(I),X2(I)
       WRITE (11,510) 'I = ',I,'  fc = ',F0(I),'  ec = ',S0(I),'  fcr = ',F1(I)
510    FORMAT (' ',A,I2,A,F6 2,A,F6 2,A,F6 2)
       WRITE (11,520) 'alphas = ',Q1(I),'  k1 = ',X1(I),'  k2 = ',X2(I)
520    FORMAT (' ',A,F3 2,A,F10 2,A,F8 4)
10 CONTINUE
DO 15 I = 1, Z1+1
       E1(I)=(3320*SQRT(F0(I))+6900)/1000
       R2(I)=0 67+(F0(I)/62)
       F0(I)=-F0(I)
       E2(I)=F0(I)/S0(I)
       R1(I)=E1(I)/(E1(I)-E2(I))
15 CONTINUE
UF0=F0(1), US0=S0(1), UE1=E1(1), UR1=R1(1), UESP=ESP(I)
WRITE (11,*) 'REINFORCEMENT PROPERTIES'
READ (10,*) Z2
DO 20 I=1,Z2
       READ (10,*) E3(I),Y0(I),U3(I)
       WRITE (11,530) 'I = ',I,'  E/1000 = ',E3(I),'  fy = ',Y0(I),'  fult = ',U3(I)
530    FORMAT (' ',A,I2,A,F6 2,A,F6 2,A,F6 2,A,F6 2)
       READ (10,*) A3(I),B3(I),C3(I),AB(I),BB(I),CB(I)
       WRITE (11,540) 'A  = ',A3(I),'  B  = ',B3(I),'  C  = ',C3(I)
       WRITE (11,540) 'Ab = ',AB(I),'  Bb = ',BB(I),'  Cb = ',CB(I)
540    FORMAT (' ',A,F6 3,A,F8 2,A,F6 3)
       YIELD(I)=0
20 CONTINUE
!
!       INPUT SECTION COMPONENTS
!
WRITE (11,*) '********************'
WRITE (11,*) 'SECTION COMPONENTS'
WRITE (11,*) '********************'
READ (10,*) H,Y9,C9
WRITE (11,550) 'Height = ',H,'  Moment axis = ',Y9
550 FORMAT (' ',A,F8 2,A,F8 2)
A1=0
DO 30 I=1,C9
       READ (10,*) K9(I),Y1(I),B1(I),H1(I),T1(I)
       WRITE (11,560) 'I = ',I,'  Shape = ',K9(I),'  Y = ',Y1(I),'  B = ',B1(I),'  H = ',H1(I),'  Type = ',T1(I)
560    FORMAT (' ',A,I2,A,I2,A,F8 2,A,F8 2,A,F8 2,A,I2)
       IF (K9(I)  EQ  1) THEN
              K(I,1)=1,K(I,2)=4,K(I,3)=1,K1(I)=1
       ELSEIF (K9(I)  EQ  2) THEN
              K(I,1)=0,K(I,2)=2,K(I,3)=1,K1(I)=0 5
       ELSE
              K(I,1)=1,K(I,2)=2,K(I,3)=0,K1(I)=0 5
       ENDIF
       A1=A1+K1(I)*B1(I)*H1(I)
30 CONTINUE
WRITE (11,*)
WRITE (11,570) 'Concrete Area = ',A1
570 FORMAT (' ',A,F15 2)
WRITE (11,*)
READ (10,*) N2
DO 40 I=1,N2
       READ (10,*) Y2(I),A2(I),T2(I)
       WRITE (11,580) 'I = ',I,'  Y = ',Y2(I),'  Area = ',A2(I),'  Type = ',T2(I)
580    FORMAT (' ',A,I2,A,F8 2,A,F8 2,A,I2)
40 CONTINUE
!
!       DEFINE PROBLEM
!
WRITE (11,*) '********************'
READ (10,*) N5
READ (10,*) DVDM
WRITE (11,590) 'CONSTANT AXIAL LOAD = ',N5
WRITE (11,590) 'dV / dM RATIO = ',DVDM
590 FORMAT(' ',A,F8 2)
WRITE (11,*) '********************'
WRITE (11,*) 'PEAK CURVATURES'
READ (10,*) P2
DO 50 I=1,P2
       READ (10,*) PEAK(I)
       WRITE (11,600)'I = ',I,'  Max Curvature = ',PEAK(I)
600    FORMAT (' ',A,I2,A,F8 1)
50 CONTINUE
CLOSE (UNIT=10)
!
! SOLVE PROBLEM
!
WRITE (11,*)
WRITE (11,*) '****************************************************************'
WRITE (11,*)
WRITE (11,*) '    N       M       CV      ECT      ECM      ECB'
WRITE (11,*)
WRITE (11,*) '****************************************************************'
NUM=0, CURV=0, CEN=0, MPREV=0, SIGN=0, N=31, M=0, NPLUS=0
DO 60 I=1,C9
       BCSTRAIN(I,2)=0, BCSTRAIN(I,3)=0, BCSTRAIN(I,4)=0, BCSTRAIN(I,5)=0
       BCSTRAIN(I,6)=0, BCSTRAIN(I,7)=0, BCSTRAIN(I,8)=0, BCSTRAIN(I,9)=0
       BCSTRAIN(I,10)=0
       MCSTRAIN(I,2)=0, MCSTRAIN(I,3)=0, MCSTRAIN(I,4)=0, MCSTRAIN(I,5)=0
       MCSTRAIN(I,6)=0, MCSTRAIN(I,7)=0, MCSTRAIN(I,8)=0, MCSTRAIN(I,9)=0
       MCSTRAIN(I,10)=0
```

```
        TCSTRAIN(I,2)=0, TCSTRAIN(I,3)=0, TCSTRAIN(I,4)=0, TCSTRAIN(I,5)=0
        TCSTRAIN(I,6)=0, TCSTRAIN(I,7)=0, TCSTRAIN(I,8)=0, TCSTRAIN(I,9)=0
        TCSTRAIN(I,10)=0
60 CONTINUE
DO 70 I=1,N2
        SSTRAIN(I,2)=0, SSTRAIN(I,3)=0, SSTRAIN(I,4)=0
        SSTRAIN(I,5)=0, SSTRAIN(I,6)=0
70 CONTINUE
DO WHILE (NUM LT P2)
        Q=1; L=1
        INC=MIN(ABS(PEAK(NUM+1)/10), 5 0)
        IF (PEAK(NUM+1) LT 0 0) THEN
                INC=-INC
        ENDIF
        IF (ABS(PEAK(NUM+1)-CURV) LE ABS(INC/2)) THEN
                SIGN=1
        ENDIF
        IF (SIGN EQ 1) THEN
                INC=-INC
        ENDIF
        CURV=CURV+INC
        DO WHILE (ABS(N-(N5+NPLUS)) GT MAX(ABS(0 01*(N5+NPLUS)), 25 0) AND L LT 500 AND Q LT 700)
                PN=N, PM=M
                IF (CURV GT 0) THEN
                        S1=CEN+H/2*CURV/1000
                        S2=CEN-H/2*CURV/1000
                ELSE
                        S1=CEN-H/2*ABS(CURV)/1000
                        S2=CEN+H/2*ABS(CURV)/1000
                ENDIF
!
!       CALCULATION OF CONCRETE CONTRIBUTION
!
                M1=0, N1=0, ML=1
                IF (ABS(UF0) GT 50) THEN
                        MR=0 95
                ELSE
                        MR=0 9
                ENDIF
                DO 100 I=1,C9
                        BCSTRAIN(I,1)=S2+(S1-S2)*Y1(I)/H
                        MCSTRAIN(I,1)=S2+(S1-S2)*(Y1(I)+H1(I)/2)/H
                        TCSTRAIN(I,1)=S2+(S1-S2)*(Y1(I)+H1(I))/H
                        CONMAT(1)=F0(T1(I)), CONMAT(2)=S0(T1(I)), CONMAT(3)=F1(T1(I))
                        CONMAT(4)=ESP(T1(I)), CONMAT(5)=Q1(T1(I)), CONMAT(6)=E1(T1(I))
                        CONMAT(7)=E2(T1(I)), CONMAT(8)=R1(T1(I)), CONMAT(9)=R2(T1(I))
                        CONMAT(10)=X1(I), CONMAT(11)=X2(I)
                        CSTRAIN(1)=BCSTRAIN(I,1)
                        CSTRAIN(2)=BCSTRAIN(I,2), CSTRAIN(3)=BCSTRAIN(I,3)
                        CSTRAIN(4)=BCSTRAIN(I,4), CSTRAIN(5)=BCSTRAIN(I,5)
                        CSTRAIN(6)=BCSTRAIN(I,6), CSTRAIN(7)=BCSTRAIN(I,7)
                        CSTRAIN(8)=BCSTRAIN(I,8), CSTRAIN(9)=BCSTRAIN(I,9)
                        CSTRAIN(10)=BCSTRAIN(I,10)
                        CSTRESS(2)=BCSTRESS(I,2), CSTRESS(3)=BCSTRESS(I,3)
                        CSTRESS(4)=BCSTRESS(I,4), CSTRESS(5)=BCSTRESS(I,5)
                        CALL CONSTRS(STRESS,ML,MR)
                        F3=STRESS*Q2
                        BCSTRAIN(I,2)=CSTRAIN(2), BCSTRAIN(I,3)=CSTRAIN(3)
                        BCSTRAIN(I,4)=CSTRAIN(4)
                        BCSTRESS(I,1)=CSTRESS(1)
                        CSTRAIN(1)=MCSTRAIN(I,1)
                        CSTRAIN(2)=MCSTRAIN(I,2), CSTRAIN(3)=MCSTRAIN(I,3)
                        CSTRAIN(4)=MCSTRAIN(I,4), CSTRAIN(5)=MCSTRAIN(I,5)
                        CSTRAIN(6)=MCSTRAIN(I,6), CSTRAIN(7)=MCSTRAIN(I,7)
                        CSTRAIN(8)=MCSTRAIN(I,8), CSTRAIN(9)=MCSTRAIN(I,9)
                        CSTRAIN(10)=MCSTRAIN(I,10)
                        CSTRESS(2)=MCSTRESS(I,2), CSTRESS(3)=MCSTRESS(I,3)
                        CSTRESS(4)=MCSTRESS(I,4), CSTRESS(5)=MCSTRESS(I,5)
                        CALL CONSTRS(STRESS,ML,MR)
                        F4=STRESS*Q2
                        MCSTRAIN(I,2)=CSTRAIN(2), MCSTRAIN(I,3)=CSTRAIN(3)
                        MCSTRAIN(I,4)=CSTRAIN(4)
                        MCSTRESS(I,1)=CSTRESS(1)
                        CSTRAIN(1)=TCSTRAIN(I,1)
                        CSTRAIN(2)=TCSTRAIN(I,2), CSTRAIN(3)=TCSTRAIN(I,3)
                        CSTRAIN(4)=TCSTRAIN(I,4), CSTRAIN(5)=TCSTRAIN(I,5)
                        CSTRAIN(6)=TCSTRAIN(I,6), CSTRAIN(7)=TCSTRAIN(I,7)
                        CSTRAIN(8)=TCSTRAIN(I,8), CSTRAIN(9)=TCSTRAIN(I,9)
                        CSTRAIN(10)=TCSTRAIN(I,10)
                        CSTRESS(2)=TCSTRESS(I,2), CSTRESS(3)=TCSTRESS(I,3)
                        CSTRESS(4)=TCSTRESS(I,4), CSTRESS(5)=TCSTRESS(I,5)
                        CALL CONSTRS(STRESS,ML,MR)
                        F5=STRESS*Q2
                        TCSTRAIN(I,2)=CSTRAIN(2), TCSTRAIN(I,3)=CSTRAIN(3)
                        TCSTRAIN(I,4)=CSTRAIN(4)
                        TCSTRESS(I,1)=CSTRESS(1)
                        Y3=Y1(I)
                        Y5=Y3+H1(I)
                        Y4=(Y3+Y5)/2
                        F6=(K(I,1)*F3+K(I,2)*F4+K(I,3)*F5)/6
                        Y6=(K(I,1)*F3*Y3+K(I,2)*F4*Y4+K(I,3)*F5*Y5)/6
                        N1=N1+F6*B1(I)*H1(I)
                        M1=M1+Y6*B1(I)*H1(I)
100             CONTINUE
!
!       CALCULATION OF STEEL CONTRIBUTION
!
                M3=0, N3=0
                DO 110 I=1,N2
                        SSTRAIN(I,1)=S2+(S1-S2)*Y2(I)/H
                        STEMAT(1)=E3(T2(I)), STEMAT(2)=Y0(T2(I)), STEMAT(3)=U3(T2(I))
                        STEMAT(4)=A3(T2(I)), STEMAT(5)=B3(T2(I)), STEMAT(6)=C3(T2(I))
                        STEMAT(7)=AB(T2(I)), STEMAT(8)=BB(T2(I)), STEMAT(9)=CB(T2(I))
                        CALL STESTRS(I, STRESS)
                        SSTRESS(I,1)=STRESS
                        N3=N3+STRESS*Q2*A2(I)
                        M3=M3+STRESS*Q2*A2(I)*Y2(I)
110             CONTINUE
                N=(N1+N3)/1000
                M=(M1+M3)/1000000-(N*Y9)/1000
                NPLUS=ABS(M*DVDM)
                IF (N NE PN) THEN
                        IF (Q LT 200) THEN
                                DCEN=((N5+NPLUS)-N)*(CEN-PCEN)/(N-PN)
                                IF (ABS(DCEN) GT 2) THEN
                                        IF (DCEN LT 0) THEN
                                                DCEN=-2
                                        ELSE
                                                DCEN=2
                                        ENDIF
                                ENDIF
                                IF (Q LT 20) THEN
                                        EST=CEN+DCEN
                                ELSEIF (Q EQ 20) THEN
                                        BIT=DCEN/200
                                        EST=CEN+BIT
                                ELSE
                                        EST=CEN+BIT
                                ENDIF
                        ENDIF
```

```
                IF (Q GE 200) THEN
                    IF (Q EQ 200) THEN
                        EST=ACEN
                    ELSEIF (Q EQ 201) THEN
                        EST=ACEN+0 005
                    ELSEIF (Q EQ 202) THEN
                        IF (N LT (N5+NPLUS)) THEN
                            STEP=0 005
                        ELSE
                            STEP=-0 005
                        ENDIF
                        EST=EST+STEP
                    ELSE
                        EST=EST+STEP
                    ENDIF
                    L=L+1
                    IF (Q GT 204) THEN
                        IF (ABS(PN-N5-ABS(PM*DVDM)) LT ABS(N-N5-ABS(M*DVDM))-5) THEN
                            N=PN, M=PM
                            L=501
                        ENDIF
                    ENDIF
                ENDIF
            ELSE
                EST=CEN+0 01
            ENDIF
            PCEN=CEN
            CEN=EST
            Q=Q+1
        ENDDO
        WRITE (11,200) N,M,CURV,S1,PCEN,S2
200     FORMAT (*,F10 2,F10 2,F10 2,F10 2,F10 2,F10 2)
        ACEN=PCEN
        N=-31
        DO 300 I=1,C9
            US0=-US0
            BCSTRAIN(I,5)=BCSTRAIN(I,1)
            IF (BCSTRAIN(I,1) LT BCSTRAIN(I,3)) THEN
                BCSTRAIN(I,3)=BCSTRAIN(I,1)
                BCSTRESS(I,3)=BCSTRESS(I,1)
                IF (BCSTRAIN(I,7) GT 0 35*US0) THEN
                    BCSTRAIN(I,1)=-BCSTRAIN(I,1)
                    BCSTRESS(I,1)=-BCSTRESS(I,1)
                    BCSTRAIN(I,4)=BCSTRAIN(I,1)-(BCSTRESS(I,1)/UE1)
                    BCSTRAIN(I,4)=-BCSTRAIN(I,4)
                ELSE
                    IF (BCSTRESS(I,1) NE 0) THEN
                        BCSTRAIN(I,1)=-BCSTRAIN(I,1)
                        BCSTRESS(I,1)=-BCSTRESS(I,1)
                        PART=MAX(US0/(US0+BCSTRAIN(I,1)), 0 09*BCSTRAIN(I,1)/US0)
                        PART1=PART*SQRT(BCSTRAIN(I,1)*US0)
                        TOP=(BCSTRAIN(I,1)+PART1)*BCSTRESS(I,1)
                        BOTTOM=(BCSTRESS(I,1)+UE1*PART1)
                        BCSTRAIN(I,4)=BCSTRAIN(I,1)-TOP/BOTTOM
                        BCSTRAIN(I,4)=-BCSTRAIN(I,4)
                    ENDIF
                ENDIF
            ELSEIF (BCSTRAIN(I,1) GT BCSTRAIN(I,2)) THEN
                BCSTRAIN(I,2)=BCSTRAIN(I,1)
                BCSTRESS(I,2)=BCSTRESS(I,1)
            ENDIF
            IF (BCSTRAIN(I,1) GT BCSTRAIN(I,10)) THEN
                BCSTRAIN(I,10)=BCSTRAIN(I,1)
            ENDIF
            MCSTRAIN(I,5)=MCSTRAIN(I,1)
            IF (MCSTRAIN(I,1) LT MCSTRAIN(I,3)) THEN
                MCSTRAIN(I,3)=MCSTRAIN(I,1)
                MCSTRESS(I,3)=MCSTRESS(I,1)
                IF (MCSTRAIN(I,7) GT 0 35*US0) THEN
                    MCSTRAIN(I,1)=-MCSTRAIN(I,1)
                    MCSTRESS(I,1)=-MCSTRESS(I,1)
                    MCSTRAIN(I,4)=MCSTRAIN(I,1)-(MCSTRESS(I,1)/UE1)
                    MCSTRAIN(I,4)=-MCSTRAIN(I,4)
                ELSE
                    IF (MCSTRESS(I,1) NE 0) THEN
                        MCSTRAIN(I,1)=-MCSTRAIN(I,1)
                        MCSTRESS(I,1)=-MCSTRESS(I,1)
                        PART=MAX(US0/(US0+MCSTRAIN(I,1)), 0 09*MCSTRAIN(I,1)/US0)
                        PART1=PART*SQRT(MCSTRAIN(I,1)*US0)
                        TOP=(MCSTRAIN(I,1)+PART1)*MCSTRESS(I,1)
                        BOTTOM=(MCSTRESS(I,1)+UE1*PART1)
                        MCSTRAIN(I,4)=MCSTRAIN(I,1)-TOP/BOTTOM
                        MCSTRAIN(I,4)=-MCSTRAIN(I,4)
                    ENDIF
                ENDIF
            ELSEIF (MCSTRAIN(I,1) GT MCSTRAIN(I,2)) THEN
                MCSTRAIN(I,2)=MCSTRAIN(I,1)
                MCSTRESS(I,2)=MCSTRESS(I,1)
            ENDIF
            IF (MCSTRAIN(I,1) GT MCSTRAIN(I,10)) THEN
                MCSTRAIN(I,10)=MCSTRAIN(I,1)
            ENDIF
            TCSTRAIN(I,5)=TCSTRAIN(I,1)
            IF (TCSTRAIN(I,1) LT TCSTRAIN(I,3)) THEN
                TCSTRAIN(I,3)=TCSTRAIN(I,1)
                TCSTRESS(I,3)=TCSTRESS(I,1)
                IF (TCSTRAIN(I,7) GT 0 35*US0) THEN
                    TCSTRAIN(I,1)=-TCSTRAIN(I,1)
                    TCSTRESS(I,1)=-TCSTRESS(I,1)
                    TCSTRAIN(I,4)=TCSTRAIN(I,1)-(TCSTRESS(I,1)/UE1)
                    TCSTRAIN(I,4)=-TCSTRAIN(I,4)
                ELSE
                    IF (TCSTRESS(I,1) NE 0) THEN
                        TCSTRAIN(I,1)=-TCSTRAIN(I,1)
                        TCSTRESS(I,1)=-TCSTRESS(I,1)
                        PART=MAX(US0/(US0+TCSTRAIN(I,1)), 0 09*TCSTRAIN(I,1)/US0)
                        PART1=PART*SQRT(TCSTRAIN(I,1)*US0)
                        TOP=(TCSTRAIN(I,1)+PART1)*TCSTRESS(I,1)
                        BOTTOM=(TCSTRESS(I,1)+UE1*PART1)
                        TCSTRAIN(I,4)=TCSTRAIN(I,1)-TOP/BOTTOM
                        TCSTRAIN(I,4)=-TCSTRAIN(I,4)
                    ENDIF
                ENDIF
            ELSEIF (TCSTRAIN(I,1) GT TCSTRAIN(I,2)) THEN
                TCSTRAIN(I,2)=TCSTRAIN(I,1)
                TCSTRESS(I,2)=TCSTRESS(I,1)
            ENDIF
            IF (TCSTRAIN(I,1) GT TCSTRAIN(I,10)) THEN
                TCSTRAIN(I,10)=TCSTRAIN(I,1)
            ENDIF
            IF (BCSTRAIN(I,3) LT BCSTRAIN(I,7)) THEN
                BCSTRAIN(I,7)=BCSTRAIN(I,3)
                BCSTRAIN(I,8)=BCSTRAIN(I,4)
                BCSTRAIN(I,9)=BCSTRAIN(I,6)
                BCSTRESS(I,5)=BCSTRESS(I,3)
                BCSTRAIN(I,3)=0
            ELSEIF (BCSTRAIN(I,2) GT BCSTRAIN(I,6)) THEN
                BCSTRAIN(I,6)=BCSTRAIN(I,2)
                BCSTRESS(I,4)=BCSTRESS(I,2)
                BCSTRAIN(I,2)=0
```

```
        ENDIF
        IF (MCSTRAIN(I,3) LT MCSTRAIN(I,7)) THEN
            MCSTRAIN(I,7)=MCSTRAIN(I,3)
            MCSTRAIN(I,8)=MCSTRAIN(I,4)
            MCSTRAIN(I,9)=MCSTRAIN(I,6)
            MCSTRESS(I,5)=MCSTRESS(I,3)
            MCSTRAIN(I,3)=0
        ELSEIF (MCSTRAIN(I,2) GT MCSTRAIN(I,6)) THEN
            MCSTRAIN(I,6)=MCSTRAIN(I,2)
            MCSTRESS(I,4)=MCSTRESS(I,2)
            MCSTRAIN(I,2)=0
        ENDIF
        IF (TCSTRAIN(I,3) LT TCSTRAIN(I,7)) THEN
            TCSTRAIN(I,7)=TCSTRAIN(I,3)
            TCSTRAIN(I,8)=TCSTRAIN(I,4)
            TCSTRAIN(I,9)=TCSTRAIN(I,6)
            TCSTRESS(I,5)=TCSTRESS(I,3)
            TCSTRAIN(I,3)=0
        ELSEIF (TCSTRAIN(I,2) GT TCSTRAIN(I,6)) THEN
            TCSTRAIN(I,6)=TCSTRAIN(I,2)
            TCSTRESS(I,4)=TCSTRESS(I,2)
            TCSTRAIN(I,2)=0
        ENDIF
        US0=-US0
300  CONTINUE
     DO 310 I=1,N2
        STRESS(I,2)=SSTRESS(I,1)
        IF (ABS(SSTRAIN(I,1)) GT 3 5*Y0(T2(I))/E3(T2(I))) THEN
            YIELD(I)=1
        ENDIF
        IF (ABS(PEAK(NUM+1)-CURV) LE ABS(INC/2)) THEN
            SSTRESS(I,3)=SSTRESS(I,1)
            IF (SSTRAIN(I,1) LT SSTRAIN(I,4)) THEN
                SSTRAIN(I,6)=SSTRAIN(I,1)
                SSTRAIN(I,3)=0
            ELSE
                SSTRAIN(I,5)=SSTRAIN(I,1)
                SSTRAIN(I,2)=0
            ENDIF
            IF (ABS(SSTRAIN(I,1)) GE 1 1*Y0(T2(I))/E3(T2(I))) THEN
                YIELD(I)=1
            ENDIF
        ENDIF
        SSTRAIN(I,4)=SSTRAIN(I,1)
310  CONTINUE
     IF (MPREV*M LT 0) THEN
        NUM=NUM+1
        SIGN=0
     ENDIF
     MPREV=M
ENDDO
CLOSE (UNIT=11)
STOP
END
!
SUBROUTINE CONSTRS(STRESS,ML,MR)
IMPLICIT REAL*8 (A-H,O-Z)
REAL*8 MR,ML
COMMON CONMAT(11),CSTRAIN(10),CSTRESS(5)
COMMON STEMAT(9),SSTRAIN(10,6),SSTRESS(10,3),YIELD(10)
COMMON US0,UE1,UF0,UR1,UESP
IF (CSTRAIN(1) LE CSTRAIN(5)) THEN
    IF (CSTRAIN(1) LE CSTRAIN(8)) THEN
        IF (CSTRAIN(7) EQ 0) THEN
            STRAIN=CSTRAIN(1)
            CALL CONFORM(ML,STRAIN,STRESS)
        ELSEIF (CSTRAIN(1) GE CSTRAIN(7)) THEN
            STRAIN=CSTRAIN(7)
            CALL CONFORM(MR,STRAIN,FNEW)
            SLOPE=FNEW/(CSTRAIN(7)-CSTRAIN(8))
            STRESS=SLOPE*(CSTRAIN(1)-CSTRAIN(8))
        ELSE
            STRAIN=CSTRAIN(7)
            CALL CONFORM(MR,STRAIN,FNEW)
            SLOPE=FNEW/(CSTRAIN(7)-CSTRAIN(8))
            TRIAL1=SLOPE*(CSTRAIN(1)-CSTRAIN(8))
            STRAIN=CSTRAIN(1)
            CALL CONFORM(ML,STRAIN,TRIAL2)
            STRESS=MAX(TRIAL1, TRIAL2)
        ENDIF
    ELSE
        IF (CSTRAIN(9) EQ 0) THEN
            SLOPE=UE1
        ELSEIF (CSTRAIN(9) LT 4) THEN
            FUNPREV=CONMAT(5)*CONMAT(3)/(1+SQRT(0 5*CSTRAIN(9)))
            SLOPE=(FUNPREV)/(CSTRAIN(9)-CSTRAIN(8))
        ELSE
            SLOPE=0
        ENDIF
        IF (SLOPE NE 0) THEN
            FUN=CONMAT(5)*CONMAT(3)/(1+SQRT(0 5*CSTRAIN(6)))
            STRESS=FUN+SLOPE*(CSTRAIN(1)-CSTRAIN(6))
            IF (STRESS LT 0) THEN
                STRESS=0
            ENDIF
        ELSE
            STRESS=0
        ENDIF
    ENDIF
ELSE
    IF (CSTRAIN(1) LE CSTRAIN(8)) THEN
        STRESS=CSTRESS(5)*((CSTRAIN(1)+CSTRAIN(8))/(CSTRAIN(7)+CSTRAIN(8)))**2
    ELSE
        IF (CSTRAIN(10) LT 4 AND CSTRAIN(6) LE CONMAT(3)/UE1) THEN
            ESF=CSTRAIN(1)-CSTRAIN(8)
            STRESS=UE1*ESF
            IF (STRESS GT CONMAT(3)) THEN
                STRESS=CONMAT(5)*CONMAT(3)/(1+SQRT(0 5*ESF))
            ENDIF
        ELSEIF (CSTRAIN(10) LT 4) THEN
            ESF=CSTRAIN(1)-CSTRAIN(8)
            STRESS=CONMAT(5)*CONMAT(3)/(1+SQRT(0 5*ESF))
        ELSE
            STRESS=0
        ENDIF
    ENDIF
ENDIF
CSTRESS(1)=STRESS
RETURN
END
!
SUBROUTINE STESTRS(I,STRESS)
IMPLICIT REAL*8 (A-H,O-Z)
INTEGER I
COMMON CONMAT(11),CSTRAIN(10),CSTRESS(5)
COMMON STEMAT(9),SSTRAIN(10,6),SSTRESS(10,3),YIELD(10)
COMMON US0,UE1,UF0,UR1,UESP
IF (YIELD(I) EQ 1) THEN
    IF (SSTRAIN(I,1) GE SSTRAIN(I,4)) THEN
        IF (ABS(SSTRESS(I,3)) LT STEMAT(2)) THEN
```

```
                OFFSET=SSTRAIN(I,6)+ABS(SSTRESS(I,3))/STEMAT(1)
            ELSE
                OFFSET=SSTRAIN(I,6)+STEMAT(2)/STEMAT(1)
            ENDIF
            ESF=SSTRAIN(I,1)-OFFSET
            IF (ESF .GE. 0) THEN
                CALL STEFORM(ESF,STRESS)
            ELSE
                STRESS=MAX(ESF*STEMAT(1),SSTRESS(I,2)+(SSTRAIN(I,1)-SSTRAIN(I,4))*STEMAT(1))
            ENDIF
        ELSE
            IF (ABS(SSTRESS(I,3)) .LT. STEMAT(2)) THEN
                OFFSET=SSTRAIN(I,5)-ABS(SSTRESS(I,3))/STEMAT(1)
            ELSE
                OFFSET=SSTRAIN(I,5)-STEMAT(2)/STEMAT(1)
            ENDIF
            ESF=SSTRAIN(I,1)-OFFSET
            IF (ESF .LE. 0) THEN
                IF (SSTRAIN(I,1) .LT. UESP) THEN
                    STEMAT(4)=STEMAT(7),STEMAT(5)=STEMAT(8),STEMAT(6)=STEMAT(9)
                ENDIF
                ESF=-ESF
                CALL STEFORM(ESF,STRESS)
                STRESS=-STRESS
            ELSE
                STRESS=MIN(ESF*STEMAT(1),SSTRESS(I,2)+(SSTRAIN(I,1)-SSTRAIN(I,4))*STEMAT(1))
            ENDIF
        ENDIF
    ELSE
        IF (SSTRAIN(I,1) .GT. 0) THEN
            STRESS=MIN(STEMAT(1)*SSTRAIN(I,1),STEMAT(2))
        ELSE
            STRESS=MAX(STEMAT(1)*SSTRAIN(I,1),-STEMAT(2))
        ENDIF
    ENDIF
    RETURN
    END
    !
    SUBROUTINE CONFORM(M,STRAIN,STRESS)
    IMPLICIT REAL*8 (A-H,O-Z)
    REAL*8 M
    COMMON CONMAT(11),CSTRAIN(10),CSTRESS(5)
    COMMON STEMAT(9),SSTRAIN(10,6),SSTRESS(10,3),YIELD(10)
    COMMON US0,UE1,UF0,UR1,UESP
    IF (UF0 .LT. -50) THEN
        FACTOR=1.5
    ELSE
        FACTOR=2
    ENDIF
    IF (CONMAT(1) .EQ. UF0) THEN
        IF (CSTRAIN(7) .GT. CONMAT(4) .OR. STRAIN .GT. CONMAT(4)) THEN
            IF (STRAIN .LT. US0) THEN
                IF (STRAIN .GT. FACTOR*CONMAT(2)) THEN
                    TOP=M*CONMAT(1)*(STRAIN/(M*CONMAT(2)))*CONMAT(8)
                    BOTTOM=CONMAT(8)-1+(STRAIN/(M*CONMAT(2)))**(CONMAT(8)*CONMAT(9))
                    STRESS=TOP/BOTTOM
                ELSEIF (STRAIN .GT. CONMAT(4)) THEN
                    ELIM=FACTOR*CONMAT(2)
                    TOP=CONMAT(1)*FACTOR*CONMAT(8)
                    BOTTOM=CONMAT(8)-1+FACTOR**(CONMAT(8)*CONMAT(9))
                    FLIM=TOP/BOTTOM
                    SLOPE=(-FLIM)/(CONMAT(4)-ELIM)
                    STRESS=FLIM+SLOPE*(STRAIN-ELIM)
                ELSE
                    STRESS=0
                ENDIF
            ELSE
                TOP=M*UF0*(STRAIN/(M*US0))*UR1
                BOTTOM=UR1-1+(STRAIN/(M*US0))**UR1
                STRESS=TOP/BOTTOM
            ENDIF
        ELSE
            STRESS=0
        ENDIF
    ELSE
        IF (STRAIN .LT. US0) THEN
            IF (UF0 .LT. -50) THEN
                STRESS=M*CONMAT(1)*EXP(CONMAT(10)*((STRAIN-M*CONMAT(2))**CONMAT(11)))
            ELSE
                TOP=M*CONMAT(1)*(STRAIN/(M*CONMAT(2)))*CONMAT(8)
                BOTTOM=CONMAT(8)-1+(STRAIN/(M*CONMAT(2)))**(CONMAT(8)*CONMAT(9))
                STRESS=TOP/BOTTOM
            ENDIF
        ELSE
            TOP=M*UF0*(STRAIN/(M*US0))*UR1
            BOTTOM=UR1-1+(STRAIN/(M*US0))**UR1
            STRESS=TOP/BOTTOM
        ENDIF
    ENDIF
    RETURN
    END
    !
    SUBROUTINE STEFORM(ESF,STRESS)
    IMPLICIT REAL*8 (A-H,O-Z)
    COMMON CONMAT(11),CSTRAIN(10),CSTRESS(5)
    COMMON STEMAT(9),SSTRAIN(10,6),SSTRESS(10,3),YIELD(10)
    COMMON US0,UE1,UF0,UR1,UESP
    PART=(1+(STEMAT(5)*ESF)**STEMAT(6))**(1/STEMAT(6))
    STRESS=STEMAT(1)*ESF*(STEMAT(4)+(1-STEMAT(4))/PART)
    IF (STRESS .GT. STEMAT(3)) THEN
        STRESS=STEMAT(3)
    ENDIF
    RETURN
    END
```